TECHNISCHE UNIVERSITÄT MÜNCHEN

Max-Planck-Institut für Biochemie

Quantitative Proteomics Strategies to Reveal Cellular Mechanisms of Kinase Inhibitor Drug Action

Christoph Alfred Willibald Weber

Vollständiger Abdruck der von der Fakultät für Chemie der Technischen Universität München zur Erlangung des akademischen Grades eines Doktors der Naturwissenschaften genehmigten Dissertation.

Vorsitzender: Univ.-Prof. Dr. Michael Groll

Prüfer der Dissertation: 1. Priv.-Doz. Dr. Henrik Daub

                             2. Univ.-Prof. Dr. Johannes Buchner

Die Dissertation wurde am 07.05.2013 bei der Technischen Universität München eingereicht und durch die Fakultät für Chemie am 19.08.2013 angenommen.

Meinen Eltern

Table of contents

I   Introduction

1. Cellular signal transduction via posttranslational modifications

The orchestration of events in a eukaryotic cell, which is maintained by a large array of diverse proteins, can be allegorized as a herculean task. More than 20,500 protein-coding genes give rise to an incomparably higher number of protein species present in a proteome considering, for instance, covalent modifications, proteolytical processing or splicing[1,2]. These individual protein forms exert specific functions within the complex cellular physiology. In assemblies of multilayered and interconnected signal transduction networks protein species elicit a large array of different cellular responses in a highly dynamic, logical and distinctive fashion. Thus, cells can react to cues from inside or outside of the cell, for instance, through cell-cycle checkpoints, changes in oxygen and nutrient supply, DNA damage, ligand binding to extra- or intracellular receptors, electrical excitation or mechanical stress. Regulation of these processes is achieved in a defined manner concerning the spatial distribution, temporal occurrence of protein species and their dynamic interactions among each other. The generation of particular protein species is accomplished on the one hand by selective protein expression in combination with mRNA synthesis, splicing, nuclear export and stability control, on the other hand by their proteolytic depletion to provide a quantitatively defined pool. However, this way of constituting different "types" of proteins is of rather low dynamics and can be therefore observed mostly as an ultimate cellular response of relatively large persistence. In contrast, more rapid adaption to signaling cues requires fast responses through signal transducers already available within the cell. In this regard, the most important regulatory way employed in cellular signaling networks is the mostly reversible covalent enzymatic modification of existing protein molecules. In that process, either a chemical functional group or another small protein is attached to distinct amino acid moieties within the polypeptide chain. A eukaryotic cell draws upon a large variety of these so-called posttranslational modifications (PTMs). More than 300 different types of PTMs have been identified so far and this number is still growing[3]. The biological significance as well as the chemical and structural properties are greatly diverse. A frequently used way to modify proteins is via the covalent

addition of defined tags. For instance, serine, threonine or tyrosine residues can be modified by the enzymatic attachment of phosphate groups through protein kinases, which is denoted as (protein) phosphorylation. Phosphorylation is rather uniform in a sense that always one single phosphate group is transferred to a particular amino acid. In case of methylation, for example, up to two or three methyl moieties are coupled to arginines and lysines, respectively, by methyl transferases. PTMs do not merely describe the covalent attachment of rather small (in)organic residues, including also acetlyation of lysines, sulfation of tyrosines and hydroxylation of prolines or lysines. A more complex and heterogenous PTM is for instance glycosylation where a branched carbohydrate chain is linked to one specific amino acid residue, followed by protein and modification site-specific processing steps. In addition, even small proteins such as ubiquitin or ubiquitin-like modifiers (SUMO, NEDD8) can be conjugated onto proteins via lysine moieties[3]. This class of modification becomes even more multifaceted due to the fact that either one single or multiple units, either in linear or branched fashion, can be attached.

What all these diverse molecular alterations have in common is that they function as flexible regulatory switches leading to alterations in the biological phenotype. In the context of signal transduction dynamics the reversibility of PTMs is of particular relevance. In order to modulate or terminate signaling processes, the functional counterparts of modifying enzymes come into play, such as phosphatases that catalyze hydrolysis of the phosphoester bond between the modified protein and the attached phosphate group. Likewise, deubiquinating enzymes have the ability to remove ubiquitin modifiers, whereas protein demethylases take away methyl residues of modified arginine and lysine residues.

The cellular translation and interpretation of PTMs is primarily provided by imposing additional features on the configuration of the 20 naturally occurring amino acids. Thereby, PTMs have a large impact on physico-chemical properties, such as protein structure and hydrophobicity[4]. For instance, the addition of an acetyl group to an ε amino group of lysine neutralizes the positive charge present under physiological conditions. Likewise, each phosphorylation on serine, threonine or tyrosine residues introduces two negative charges into the protein sequence. Altering the charge state or other site-specific accompaniments influences the prevalent thermodynamic situation in the microenvironment of that modification (Figure 1). Unstructured regions can, for example, be converted into helical regions and these rearrangements can be passed on to adjacent or even, through allosteric communication, to distal regions of that protein[5]. Moreover, to take the phosphorylation example, those dianionic charges can be recognized and neutralized by cationic amino acid residues like arginines or lysines to induce and stabilize conformational changes of a target protein. As a result, PTMs can increase the catalytic ability of a modified protein, as exemplified by autophosphorylation of various protein kinases or by phosphorylation and sumoylation of histone deactetylases, as evident from SIRT1, where these modifications augment catalytic activity[6-8]. In

such a way, PTMs can be considered as an equivalent to a "gain of function" for the target protein, which can manifest itself through structural rearrangements at the intramolecular level[4,9].
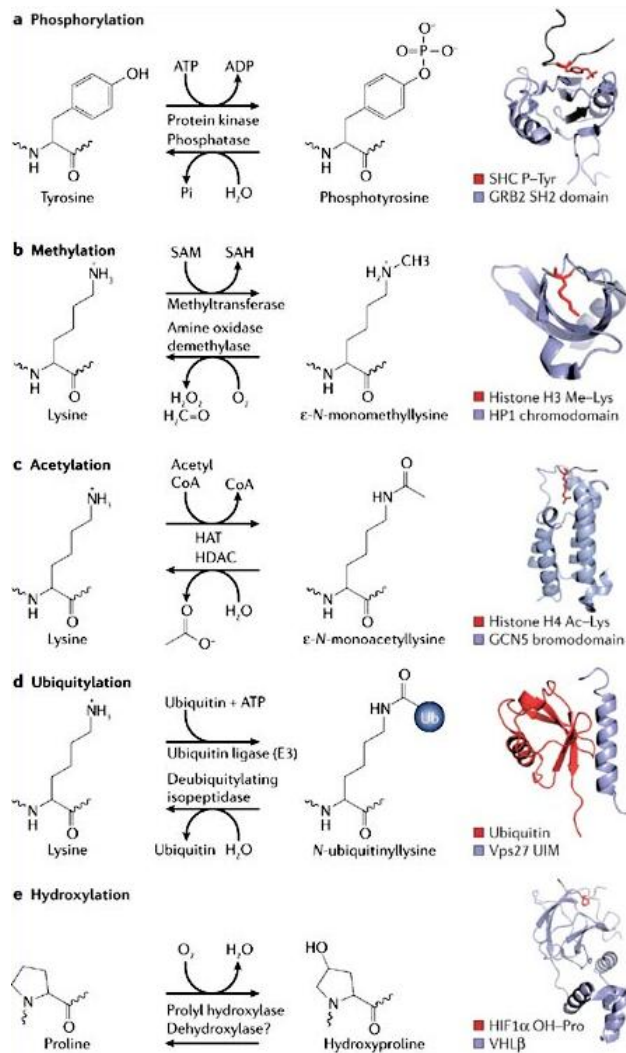
Figure 1: Selected amino acid side chains and possible PTMs. Depicted are phosphorylation (a), methylation (b), acetylation (c), ubiquitylation (d), and hydroxylation (e). Enzymes performing addition and removal modifiers as well as molecules participating are shown on the reaction arrows. The structures on the far right show examples of protein-interaction domains (pale purple) in complex with their respective ligands (red). (Illustration from *Seet et al.*[10]**)**

Structural rearrangements of target proteins are only one vital aspect conferred by PTMs. An alternative way to translate such site specific substitutions on proteins is mostly not on an intramolecular but on a rather intermolecular level. Accordingly, PTMs can constitute docking sites for other proteins. Interestingly, the recognition of such interfaces generated by the PTMs and its molecular surroundings occurs via evolutionary conserved modules as an integral part of the partnering protein[11]. Such recognition domains usually bear conserved binding pockets selective for the modified residue in the context of flanking amino

acid residues. Thus, binding occurs via peptide motifs in which the presence of a PTM plays a crucial role. In case of spatially more extended PTMs, such as ubiquitin modifiers, those domains dock on specific patches on its surface[10]. Figure 1 illustrates selected PTM-dependent binding domains being heavily implicated in cellular signaling. The mutual affinity of such modular interaction domains and its modified counterparts represents a key instrument of signal transmission and regulation. For instance, the occurrence of a PTM can affect the subcellular localization of a protein. A typical example is signaling originating from epidermal growth factor receptor (EGFR), a prototypical receptor tyrosine kinase (RTK). Ligand-activated EGFR becomes phosphorylated at multiple tyrosine sites in the cytoplasmic domain leading to the recruitment of proteins containing SRC homology 2 (SH2) or phosphotyrosine-binding (PTB) domains, such as SHC and casitas B-lineage lymphoma (CBL), respectively. Both events mark the initial steps of two entirely different pathways emanating from EGFR signaling: On the one hand, binding of SHC followed by SHC phosphorylation through EGFR represents an early step signal of EGFR-dependent transmission ultimately leading to activation the mitogen-activated protein kinase (MAPK) signal cascade via the sequential recruitment of other adaptors and factors, such as growth factor receptor-bound protein 2 (GRB2) via its SH2 domain and Son Of Sevenless homolog 1 (SOS1) (Figure 1). The guanin nucleotide exchnage factor SOS1 activates RAS, a small GTPase, which then binds and activates RAF kinase, a MAPK kinase kinase (MAPKKK)[12]. In turn, activated RAF kinase phosphorylates downstream MAPK kinases (MAPKKs), thereby elevating their activity leading to phosphorylation and activation of MAPKs. MAPKs, e.g. ERK, in turn induce phosphorylation and stimulation of an array of substrates, like additional kinases, and, upon nuclear translocation, of several transcription factors causing profound changes in cellular gene expression[13,14]. On the other hand, signal termination via CBL-mediated EGFR ubiquitination prior to recruitment of additional proteins containing ubiquitin binding domains facilitating lysosomal degradation of the RTK[15].

In summary, this example demonstrates that the occurrence one single PTM is capable of setting off a whole cascade on the basis of targeted relocations and the involvement of ordered series of phosphorylations of participating signaling proteins. However, concepts of such discrete linear pathways have turned out as being dramatically simplified and fall short in covering intracellular signaling. Scientific progress has given way to a picture of more interconnected signaling pathways not just simply transmitting, but also processing, encoding and integrating internal and external signals[16]. As described for RAS-MAPK signaling and any other (receptor) pathway, there is no single protein or gene that is responsible for signaling specificity but rather an array of participating components. In this regard, it has become apparent that the integration of diverse inputs modulates decisively the cellular decision about the physiological response. In that context PTMs play a crucial role as evidenced by methylation of RAF kinase in PC12 cells[17]. If, as a result of EGFR-mediated signaling, activated RAF is methylated by

PRMT5, it becomes prone to proteasomal degradation restricting the activation period of RAF. Ultimately, cells undergo enhanced proliferation, while the absence of methylation leads to cellular differentiation. Thus, on the example of the well understood MAPK cascade it becomes obvious how and why the regulation of cellular signaling operates on multiple layers to elicit a distinct cellular response. Moreover, the use of PTMs is not only utilized for plain signal transmission, PTMs also realize its fine-tuning dramatically affecting the overall cellular decision. In fact, while many signaling pathways share a similar protein complement that mediates signal transduction, signal specificity is eventually achieved by means of PTMs determining the temporal (when and for how long a signal input is lasting) and spatial (where within the cell) dynamics of components involved[16].

2. Protein phosphorylation

Protein phosphorylation is the best studied PTM as it decisively controls most processes in cellular signaling[18]. Until today, more than 100 years of research work has been invested from the discovery of phosphorylated proteins in eukaryotes, which was first mapped to serine and threonines in the third decade of the last century[19-21]. Later, in 1979, the existence of phosphotyrosines was published as well[22]. Already in between of these significant discoveries of site-specific phosphomodifications of amino acids, their role as key regulatory element in cellular physiology was recognized by the description of an enzymatically-mediated process behind that phenomenon. A casein kinase was the first protein kinase described carrying out that process termed "phosphorylation" in 1954[23]. Subsequently, it could be demonstrated that the activity of glycogen phosphorylase, an enzyme involved in glycogen metabolism, was under control of phosphorylation, suggesting an underlying reversibility[24]. Since then, phosphorylation has been revealed to be a very frequently occuring PTM with more than 500,000 potential phosphorylation sites in the human proteome, and more than 30,000 phosphorylation events that have been described for 8,500 human proteins so far[25]. These figures considerably outnumber all other classes of PTMs discovered until now. The reason for that wealth of data available is because phosphorylation is well amenable to analysis by mass spectrometry and protein biochemistry (see section I4.5). On the other hand, it incited (and still does) cell biological and medical interest due to is extensive utilization as a 'molecular currency' that is used to transmit information[26].

2.1   Applicability of phosphorylation in a biological system

An important factor making the phosphate transfer universally available within a cell is the ubiquitous presence of adenosine-5'-triphosphate (ATP) at concentrations between 1 and up to 12 mM, being not only the cellular storage of energy but also the dominant co-substrate in phosphorylation reactions in acting as phosphate group donor[27,28]. This role of ATP is largely supported by the fact that the underlying hydrolysis of ATP to adenosine diphosphate (ADP) is thermodynamically favored with a negative change of Gibbs free energy. In essence, that driving force is based on the exothermic hydrolysis of anhydride bond in the course of cleaving the γ-phosphate moiety. Additional Gibbs free energy is "stored" due to the fact that in a cellular system ATP concentrations are uphold at a large excess over the product ADP, which is far from equilibrium conditions[29,30]. Further reasons for the common usage of phosphorylation lie in the physicochemical properties of the phosphate moiety. For instance, at physiological pH phosphate groups are predominantly dianionic conferring an exclusive feature not found in any naturally occurring amino acid. In addition, the attachment of a phosphate group by monoester bond formation is very stable, i.e. its hydrolysis is unfavored due to slow kinetics with a half life of 1.1×10^{12} years at 25°C for spontaneous hydrolysis in water[31,32]. The basis for that outstanding stability lies presumably in the presence of two negative charges repelling anionic nucleophiles. Conversely, enzymatic dephosphorylation of phosphoproteins by phosphatases can be quite facile with 17 orders of magnitude rate acceleration[32,33]. Collectively, these features associated with the attachment of phosphate groups on protein molecules provide important clues about its biophysical applicability as a regulatory switch for critical biological functions. In this manner it can influence complex signaling networks through flexible, rapid and transient phosphorylation events steering cellular signal transduction (see section I1)[33].

2.2   Protein kinase classification structural properties

As mentioned earlier, the attachment of terminal phosphate of ATP on hydroxyl groups of serine, threonine or tyrosine residues is carried out by protein kinases. Since the beginnings with the discovery of casein kinase until today, the human protein kinase superfamily turned out to be one of the largest gene families encoded in the human genome[23,34]. That complement referred as the "kinome" in literature was described to consist of 518 members 478 of which had catalytic domains with similar sequence as a primary classifier[34]. The residual 40 genes were attributed to atypical kinases with deviant sequence, yet with reported kinase activity stemming from partial structural resemblance. In the meantime, the line-up of protein kinases has undergone revision, some kinases were added to the kinome, whereas others were excluded, e.g. if experimental approval of decisive criteria, such as kinase activity of certain atypical ki-

nases has failed[33]. Thus, the number of human protein kinases identified grew up to 538 which corresponds to nearly 2% of the entire genome already pointing at the exceptional significance of that superfamily in regulating biological processes[34,35]. The human kinome can be subdivided into more than 400 serine/threonine-specific kinases, which represent the vast majority, and about 90 tyrosine kinases. Moreover, specificity is not necessarily restricted to either amino acid as there is a small number of so-called dual specific kinases that can modify serines, threonines as well as tyrosines[36]. A rather unexplored field is N-phosphorylation in eukaryotes occurring on histidine, arginine and lysines. Due to the extremely low chemical stability N-phosphorylation is hardly detectable and therefore much less understood, but the development of new approaches to detect that kind of modification is currently in progress[37-39]. Strategies to assemble the human kinome were based on modern DNA-sequencing techniques in combination with sophisticated bioinformatics tools, which enabled the extraction of sequence information on a genome-wide scale and the inference of sequence similarities and conservation. In parallel, a wealth of structural and functional data was generated and made available, especially with regard to kinase domains to dramatically improve the understanding of kinase regulation[40].

The first solved 3D-structure of a kinase catalytic domain was that of Protein Kinase A (PKA) in 1991[41]. In order to resolve not only the plain architecture of the kinase core but also to assign functional attributes of certain residues, PKA was co-crystallized with a substrate analogue inhibitor peptide and magnesium-ATP[41]. Magnesium-ATP is a complex comprised of one Mg^{2+} cation and an ATP molecule representing the biologically active form of ATP. The subsequent X-ray structure analysis revealed and confirmed distinct sequence motifs within the catalytic domain of the kinase superfamily in part being recognized as subdomains in earlier studies based on sequence analyses[24]. The kinase fold of PKA is comprised by two structurally and functionally distinct lobes, an N-terminal and a C-terminal lobe (Figure 2a). While the smaller N-terminal lobe is normally composed of β-strands and an α-helix (αC-helix), the C-terminal lobe is mostly helical. The two subdomains are connected via a short peptide stretch (the hinge) and mold a cleft in their intermediate space which functions as the active site of the enzyme. As protein kinases act in a tightly regulated manner, i.e. they are mostly transiently activated as highly dynamic switches, rather complex regulatory mechanisms are involved in toggling between activated and inactive states[42]. In the active conformation, a highly ordered network of interactions is formed, which is required for correct substrate placements to enable the catalytic phosphotransfer. In that fashion, in the activated state a flexible glycine-rich loop (G-loop) folds over the ATP and positions the γ-phosphate of ATP for catalysis via binding α- and β-phosphate groups and the base via a highly conserved valine. Moreover, the adenine is fastened by the amide backbone of the hinge region. Another structural arrangement which is indicative of the activated state is the positioning of the αC-helix. In inactive kinases this helix is either partially disordered or rotated away from the ATP binding site. In the activated state, the helix in rotated inwards

the catalytic core facilitating the ionic interaction of a conserved glutamate with a conserved lysine to form another bridge with the α-phosphate group of ATP. In the enzymatically competent conformation the αC-helix interacts with the phenylalanine residue of the DFG-motif. DFG is an essential part of the so-called activation segment, which also includes the activation loop and P+1 loop. Its structural orientation influences both substrate binding and catalytic efficiency. The aspartate of DFG is a critical element of the magnesium binding loop that positions the γ-phosphate of ATP indirectly via the Mg^{2+} cofactor for the transfer to the peptide substrate. The contiguous part downstream of the magnesium binding loop is the activation loop. This loop is less conserved and encloses a serine/threonine or tyrosine residue which can be phosphorylated in trans, i.e. via other protein kinases or relatively rarely via autophosphorylation by a cis-mechanism[43]. Phosphorylation of that site is critical to catalytic activity as it creates an interface for an interaction network comprised of strong hydrogen bonds enabling the organization of catalytic active site residues and the phosphoacceptor binding site. More precisely, in the so-called catalytic loop, a positively charged arginine residue of another conserved amino acid triad, namely the HRD motif, interacts with the negatively charged phosphate group. This leads to the interaction of the adjacent aspartate with the OH-group to be modified, thereby driving the phosphotransfer event. Rather variably defined structural elements are represented by two hydrophobic pockets flanking the active site: Next to the hinge region lies a solvent-exposed front pocket and adjacent to the ATP binding site the so-called back pocket[44]. Notably, access to the latter is controlled by the conserved lysine of the αC-helix mentioned above and the "gatekeeper" residue.

With the availability of more and more structural data on various kinases, the architecture of PKA kinase domain turned out to be a model generally valid for all human kinases. Several significant deviations exist within the kinome, e.g. some kinases lack activation loop (auto)phosphorylation sites or the HRG-arginine (non RD-kinases)[42,45]. In such cases, alternative residues, sequence motifs or even binding proteins replace missing components of the canonical protein kinase domain architecture, thus often introducing additionally activity-regulating means[46]. In the course of ongoing structural kinase research, additional substructures providing "networks of connectivity" inside protein kinase molecules were discovered, e.g. hydrophobic spines, which represent integral elements regulating kinase activity[47].
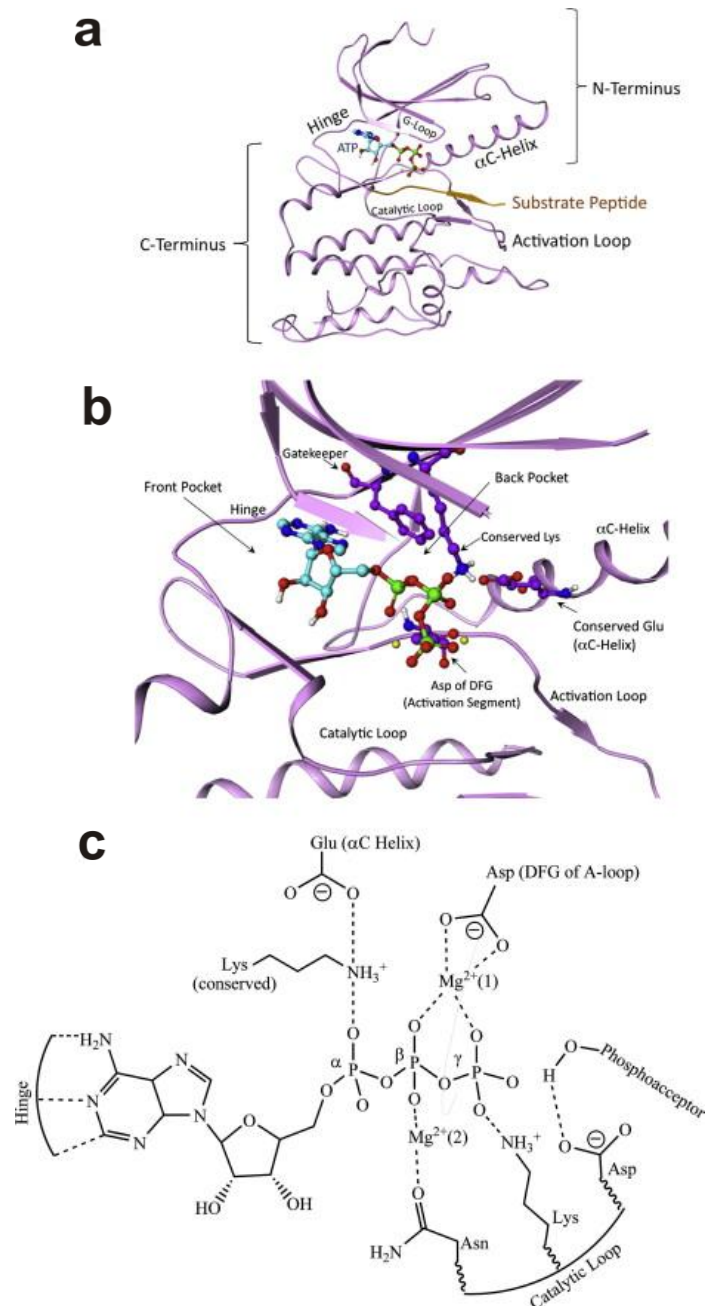
Figure 2: Structure of the phosphorylase kinase peptide substrate complex(Protein Data Bank ID code 2PHK). Ribbon representation of the catalytic domain (magenta), bound with an ATP analog (AMP–PNP), two Mn^{2+} ions (yellow) and peptide substrate (orange) (a). Magnification of the catalytic region in complex with ATP analog and Mn^{2+} ions (yellow). Key residues and binding pockets are highlighted (b). Simplified illustration of the molecular contacts between the substrates and conserved active site residues and cofactors (c). (Illustration adopted from *Schwartz&Murray*[33])

3. Protein kinases and cancer

3.1 The connection between kinases and malignant phenotypes

As indicated above, protein kinases play an important role as key regulators in putatively any cellular signaling pathway thereby processing extra and intracellular stimuli leading to a defined outcome. These decisions can comprise cellular fates, such as differentiation state, capability to migrate, programmed cell death (apoptosis) or proliferation status. Obviously, perturbation of such finely tuned processes may lead to aberrant signal transmission which can ultimately manifest itself into an array of diseases, such as metabolic and immunological disorders, e.g. diabetes or severe combined immunodeficiency (SCID), and particularly cancer[48-51]. Therefore unsurprisingly, very often a direct link between disease phenotype and defective signaling as a consequence of deregulated kinase activity could be established for malignant neoplasms. In 1978, not until 24 years after discovery of the first protein kinase, Erikson and coworkers identified the transforming potential of the Rous sarcoma virus and they were able demonstrate that it originates from a protein kinase[52]. Only four years later, a study identified protein kinase C (PKC) as being activated by tumor-promoting phorbol esters[53]. Since then, researchers' interest on the nexus between abnormal protein phosphorylation and malignancy boosted, consequently leading to the discovery of further numerous examples of protein kinases playing a decisive role in cancer pathogenesis[54-58]. In fact, of all known proto-oncogenes, i.e. genes which in its altered form or quantity contribute to the malignant phenotype, protein kinases represent a significant fraction[57]. Alterations responsible for the transformation towards an oncogene include mutations, gene amplifications as well as chromosomal rearrangements[59]. Thus, oncogenic mutations of protein kinase genes can lead to their constitutive activation. For instance, exchange of one single thymine to guanine in exon 21 of the EGFR gene results in the substitution of Leu858 to arginine in its gene product[60]. The L858R missense mutation is prevalent in many lung cancer patients and is associated with permanent kinase activity not present in wild type EGFR. On the other hand, in gliobastomas EGFR is frequently amplified thereby enforcing EGFR activation. A further mechanism is based on chromosome inversions and translocations which are cytogenetic abnormalities commonly found in cancer cells[59]. These chromosomal rearrangements can increase or deregulate transcription of the oncogene or generate constitutively active kinases. For instance, the genetical characteristic of CML is the Philadelphia chromosome, which is the product of a translocation between chromosomes 9 and 22 that fuses the *ABL* tyrosine kinase gene on chromosome 9 and *BCR* gene on chromosome 22. The *BCR-ABL* fusion gene encodes a constitutively active BCR-ABL tyrosine kinase that plays a causal role in CML[61].

The fact that deregulated kinase activity frequently drives malignant transformation and progression and the discovery of further kinases and their designation as (proto-)oncogenes generated a strong impetus to develop selective small molecule inhibitors against these critical class of proteins. Such a new and intuitive concept seemed to be promising for cancer therapy in combination with or as an alternative to traditional cytotoxic chemotherapy, which is often afflicted by severe side effects as a result of a nonspecific mode of action.

3.2   Protein kinase inhibition

The pioneering work around the mid-1980s with regard to the successful development of the first synthetic (serine/threonine) kinase inhibitors crucially paved the way to implement the concept of small-molecule kinase inhibition on the oncology field[62]. At the same time and before that, several natural products were identified to act as tyrosine kinase inhibitors proving the "druggability" of these enzymes[63-65]. Levitzki and coworkers were the first to successfully apply rational design to generate tyrosine kinase inhibitors from a large number of compounds originally patterned after a natural product called erbstatin[66,67]. These molecules were designated as tyrphostins (tyrosine phosphorylation inhibitors)[68].The first tyrphostins were generated in a target-centric manner to inhibit EGFR *in vitro* and EGFR-dependent proliferation in epidermoid carcinoma cells[68]. Interestingly, a certain emphasis was placed on selectivity and that was why researchers initially focused on substrate-competitive inhibitors and not on ATP-competitive compounds, since previous studies with natural compounds, such as staurosporine (originally considered as a serine/threonine kinase inhibitor against PKC) or quercetin, demonstrated cytotoxicity in conjunction with poor selectivity[69,70]. The prevailing dogma at that time that it would be hard to identify selective ATP-competitive inhibitors due to sequence conservation of the of the ATP binding domain among (tyrosine) kinases was questioning their clinical usefulness[71]. Other doubts were raised regarding the very high potency of an inhibitor molecule required to compete sufficiently with high intracellular ATP concentrations between 2 and 12 mM[27,28]. However, in the early 1990s several findings contradicted these misconceptions: First, investigators succeeded in designing of highly selective and potent ATP-competitive inhibitors[72]. Secondly, the solution of kinase domain 3D-structure also with a co-crystallized inhibitor molecule (SB203580) represented an important turning point[41,73]. In combination with sequence alignment studies among members of the MAPK family, a distinct nonconserved residue, the gatekeeper, was identified as being a critical determinant of inhibitor selectivity[74]. The finding supported the notion that specificity and potency of small-molecule kinase inhibitors are mainly given by additional binding pockets and sites, respectively, which lie adjacent to the conserved ATP-binding site. Thus, the main trust

shifted towards the development of ATP-competitive inhibitor molecules, also because the ATP-binding fold is more structurally defined, whereas the substrate-binding domain is more open and is less easy to use for the rational design of low-molecular-weight inhibitors[75].

Increasing knowledge about kinase inhibition evoked interest among pharmaceutical companies which led to the initiation of several research programs. For instance, Zeneca (now AstraZeneca) and Pfizer generated a lead series of 4-anilinoquinazoline compounds directed against EGFR using pharmacophore modeling of the binding of compounds in the ATP pocket. Upon chemical refinement, from those series emerged erlotinib (OSI774, Tarceva[®]) and gefitinib (ZD1839, Iressa[®]) as selective and potent EGFR-tyrosine kinas inhibitors[76,77]. With these structures clinical trials have been successfully conducted leading to the accelerated FDA approval of gefitinib in 2003 (since 2005 FDA approval is restricted) and erlotinib in 2004 for the third and second line treatment, respectively, of non-small-cell lung cancer (NSCLC)[78-80]. Yet, it was another program carried out contemporaneously by Ciba-Geigy (now Novartis) that heralded the start of small molecule-mediated kinase inhibition for therapeutic intervention in malignant diseases by demonstrating the proof-of-principle[81,82]. In search of ABL tyrosine kinase inhibitors, a compound evolved from a 2-phenylaminopyrimidine backbone: Imatinib (STI571; Gleevec[®] or Glivec[®]). With that molecule in hands, Druker and colleagues were able to demonstrate that in CML cells inhibition of tyrosine kinase activity of the oncogenic BCR-ABL is accompanied by a substantial inhibition of cell growth and induction of apoptosis[61]. In the clinic, this strategy of therapeutic intervention could be validated together with a low side effect burden due to remarkable target selectivity. In 2001, after a dramatically accelerated FDA approval, imatinib reached the market as the first kinase small molecule kinase inhibitor. Imatinib was originally developed as an ATP-competitive inhibitor, which was revised when the cocrystal structure of the inhibitor bound ABL was published[83]. In that complex the kinase was found in its inactive conformation wherein the DFG motif is 180° shifted relative to the active state conformation. While imatinib is occupying the adenosine pocket like "regular" ATP competitive inhibitors, it also extends with its benzamide portion into a contiguous "allosteric pocket", which is accessible due to the aforementioned DFG-out conformation. Kinase inhibitors that exploit the "allosteric pocket" and stabilizeg the inactive DFG-out conformer are termed type II inhibitors. In contrast, type I inhibitors "only" compete with ATP for the nucleotide binding site mimicking the interactions of the adenine moiety and binding to the kinase through the formation of one to three hydrogen bonds with the hinge region[84]. Generally, type II inhibitors exhibit a higher selectivity and affinity than type I inhibitors as a consequence of taking advantage of additional (allosteric) interactions with the kinase domain in its inactive state[46]. In contrast to the active state, these conformations are rather diverse among protein kinases. That explains why binding of an inactive conformation relying on determinants characteristic for the targeted kinase gives rise to high degree of selectivity. Accordingly, imatinib exhibits substantial selectivity for ABL over SRC although these
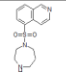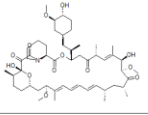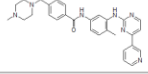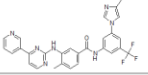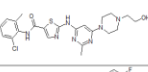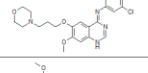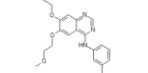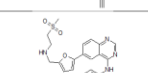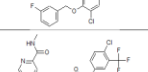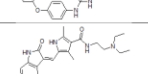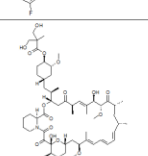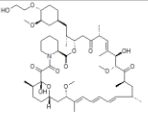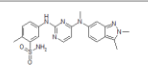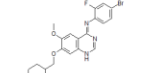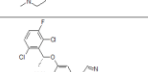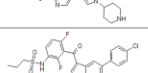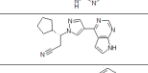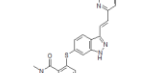
kinases have very similar nucleotide binding pockets[85]. Furthermore, type II inhibitors receive considerable affinity through further interactions stabilizing the inhibitor-target complex. Hence, it is not surprising that a significant proportion of 4 of the meanwhile 18 FDA approved SMKIs are type II inhibitors (Table 1).

Interference with kinase activity is not solely restricted to the ATP-binding pocket. Two additional (reversible) small molecule kinase inhibitor types have been categorized, both of which modulate kinase activity allosterically: Type III inhibitors exclusively bind to the allosteric pocket formed by the binding cleft separating both lobes of the kinase domain, type IV bind outside the nucleotide binding region[46,86]. As these molecules do not bind to the conserved ATP binding pocket, but to regulatory and substrate binding sites significantly differing from kinase to kinase, they are expected to have better target selectivity and therefore exhibit less off-target related toxicities[86]. In particular, type IV inhibitors could be useful to surmount the intrinsically occurring drug resistance against type I and type II kinase inhibitors[87]. Frequently, development of resistance was observed as a result of single amino acid mutations in the catalytic domain of oncogenic kinases, such as BCR-ABL, KIT, FLT3 or EGFR[88]. The most common point mutation affects the gatekeeper residue of the kinase, whose size and shape regulates the access to the allosteric pocket for type II kinase inhibitors. Binding of type I inhibitors often critically relies on the interaction with the gatekeeper, in contrast to ATP[73]. This is the reason why gatekeeper mutations such as T790M in EGFR and T315I in BCR–ABL, respectively, do not negatively affect kinase activity, but confer resistance to a wide spectrum of kinase inhibitors[89]. Therefore, targeting the kinase with inhibitors that bind to alternative binding sites can be a therapeutic option in such cases[90,91].

Another type of kinase inhibitors also with potential in overcoming resistance are covalent inhibitors. These bind covalently to nucleophilic cysteines in the active site and irreversibly inhibit ATP-binding or activity. As approximately 200 human protein kinases contain cysteins close to their ATP-pockets, the potential of covalent kinase inhibitors appears to be promising[92]. Examples for that class have been developed recently to target NSCLC cells resistant to gefitinib and erlotinib due to EGFR gatekeeper mutations[93]. However, for covalent or type III kinase inhibitors no approval is currently granted, but clinical trials are ongoing[94]. In case of type IV inhibitors, three macrolidic molecules targeting mammalian Target Of Rapamycin protein kinase (mTOR) have been approved so far (Table 1).

Table 1: Protein kinase inhibitor drugs in chronological order of their approval.

Generic name	Brand name	Number	Inhibitor Type	Structure	Year of approval	Primary Targets	Indications
Fasudil	-	HA-1077	Type I		1999	ROCK	Cerebral vasospasm
Sirolismus	Rapamune	Rapamycin	Type IV		2000	mTOR	Transplant rejection, restenosis
Imatinib	Gleevec, Glivec	STI-571 (CGP57148B)	Type II		2001	ABL, ARG, KIT, FMS, PDGFR, EFGR, DDR1	CML, GIST, ALL, HES, MDS/MPD, ASM, CEL
Nilotinib	Tasigna	AMN107	Type II		2007	ABL, ARG, KIT, PDGFR and others	CML
Dasatinib	Sprycel	BMS-354825	Type I		2007	ABL, ARG, KIT, PDGFR, SFKs and others	CML, ALL (Ph+)
Gefitinib	Iressa	ZD1839	Type I		2004	EGFR	NSCLC
Erlotinib	Tarceva	OSI-774	Type I		2004	EGFR	NSCLC, PC (in combination with gemicitabine)
Lapatinib	Tykerb	GW572016	Type I		2007	EGFR; ERBB2	BC (HER2+)
Sorafenib	Nexavar	BAY 43-9006	Type II		2006	B-RAF, VEGFR, PDGFR, FLT3, KIT	RCC, HCC
Sunitinib	Sutent	SU11248	Type I		2006	VEGFR, PDGFR, FLT3, KIT and others	RCC, GIST, HCC, pancreatic NET
Temsirolimus	Torisel	CCI-779	Type IV		2007	mTOR	RCC
Everolimus	Afinitor	RAD001	Type IV		2009	mTOR	RCC, pancreatic NET, SEGA, Organ rejection prophylaxis
Pazopanib	Votrient	GW786034	Type I		2009	VEGFR, PDGFR, KIT	RCC, STS
Vandetanib	Zactima, Caprelsa	ZD6474	Type I		2011	RET, VEGFR, EGFR	TC
Crizotinib	Xalkori	PF2341066	Type I		2011	ALK, MET, ROS	NSCLC (ALK+)
Vemurafenib	Zelboraf	PLX4032 (RG7204)	Type I		2011	BRAF(V600E), CRAF, BRAF(wt)	metastatic melanoma
Ruxolitinib	Jakafi	INCB018424	Type I		2011	JAK1, JAK2	Myelofibrosis
Axitinib	Inlyta	AG013736	Type II		2012	VEGFR, KIT, PDGFR	RCC

4. MS-based proteomics

4.1 Proteomics

The expression "proteomics" defines a relatively recent research field in biology covering the entire complement of proteins expressed in a specific state of a biological system[95,96]. As outlined above, proteins function as "cellular executives" of most biological functions, and out of that circumstance arises the ultimate goal of proteomics to identify and analyze their expression and modification depending on a defined cellular state. In contrast to its older sibling transcriptomics, which allows a global view on gene expression on the mRNA level by means of microarrays, and therefore the changes of the intermediate between DNA blueprint and protein, proteomics covers the final product, the active mature protein. This is of particular importance as mRNA levels possess an only limited conclusiveness about the actually amount of protein present in a cell, as translation of mRNA into proteins is tightly regulated just as protein degradation[97]. Furthermore, while the proteome is highly complementary to the genome or transcriptome, a broader diversity is imposed by e.g. PTMs of proteins, which is critical for their functional role within the cellular system. In that way, it is desirable apart from detecting cellular proteins as such, to have advanced technical implementations at hand allowing the in-depth investigation of the proteome. Thus, examining sub-proteomes, which are, for instance, derived from certain cellular organelles, a particular enzyme class, or distinguishing oneself by PTMs, is highly valuable and offers a wealth of functional information[98]. On the other hand, in contrast to transcriptomics or genomics, such examinations pose challenges due to the inconceivable complexity of the (sub-)proteome, as each protein may be present in different amounts, splice variants forms and PTM states at different times and possibly at very low abundance[99]. The development of powerful mass spectrometric technologies has decisively contributed to overcome these issues in a robust and reproducible manner[99,100].

4.2 Mass spectrometric analysis of proteins

Mass spectrometry (MS) is a technique used to measure ionized analyte molecules in the form of mass-to-charge (m/z) ratios. Normally, a mass spectrometer is composed of an ion source for sample introduction, ionization and transfer into the gas phase. The mass analyzer then separates the ions according to their m/z ratios and the detector registers the signal intensities of the resolved ions in a mass spectrum.

It was from the beginning of the 19th century when the first mass spectrometers were developed until 1958 when MS was utilized for the first analysis of small biomolecules, namely amino acids and simple peptide derivates[101]. Despite being the entry point for MS in biochemistry, the use of mass spectrometry was confined to the analysis of small molecules. This was largely due to difficulties with transforming macromolecules into gas-phase ions without extensive decomposition by conventional ionization methods. Towards the end of the 1980s groundbreaking progress was made with the development of softer ionization methods for the establishment of MS as tool for biosciences and as a cornerstone for proteomics. The most commonly used approaches to volatize and ionize proteins and peptides for MS are matrix-assisted laser desorption/ionization (MALDI) and electrospray ionization (ESI)[102,103]. MALDI sublimates and ionizes the samples out of a dry, crystalline matrix via laser pulses. For MALDI-MS, peptides or proteins are homogenously mixed with an organic crystalline matrix (e.g. 2,5-dihydroxybenzoic acid) and the analytes are sublimed and ionized by laser pulses. This process is driven by the absorption of the laser energy by the matrix which transfers charges to the biomolecules avoiding their destruction by laser irradiation. MALDI predominantly produces singly charged ions. For application in proteomics MALDI is normally used to analyze relatively simple peptide mixtures therefore requiring prefractionation steps of complex analyte samples ahead of MS analysis.

ESI is based on the ionization of analyte out of a liquid phase by desolvation of charged solvent droplets in an electric field. Typically, the analyte solution is sprayed via an orifice of very small diameter into the mass spectrometer (Figure 3). The electric potential of several thousand volts applied between the orifice and the inlet of the mass spectrometer accelerates the charged analyte/solvent droplets and directs those via a heated capillary into a vacuum chamber. Subsequently, the aerosols are electrostatically dispersed into smaller, highly charged droplets containing the analytes. With proceeding solvent evaporation, the droplet size decreases while the charge density increases. As soon as the coulombic repulsion is larger than the droplets' surface tension, the droplets burst, producing smaller and less highly charged droplets. Upon several cycles of that process charged analyte molecules either begin to desorb as a consequence of the high electric field on the droplet surface (Ion Evaporation Model) or undergo complete desolvation due to ongoing solvent evaporation (Charge Residue Model)[104,105]. In contrast to MALDI, ESI is implemented as a continuous method to produce gas-phase ions. Therefore, in order to analyze complex analyte mixtures, e.g. protein digests, ESI proved to be advantageous over MALDI when coupled to (high-performance) liquid-based chromatography on a nano flow scale (nano (HP)LC-MS) and as this ionization technique typically generates ions in multiply charged states[99,103].
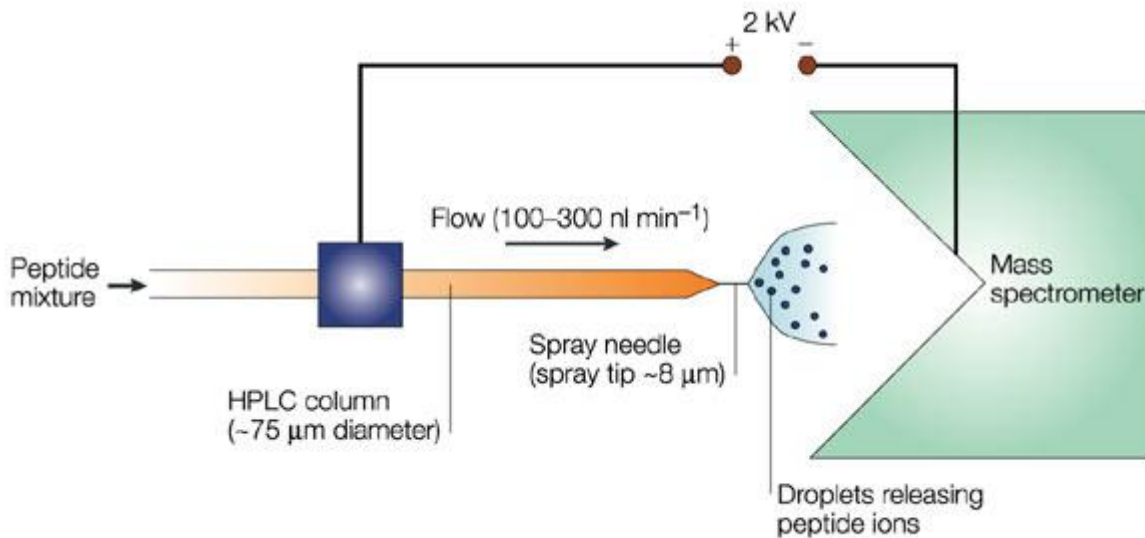
Figure 3: Schematic depiction of electrospray ionization device for LC-MS analysis. Analyte molecules, such as peptides, are separated on a high-performance liquid chromatography (HPLC) column. At the tip of the spray needle the eluting molecules are sprayed in an electric field where they become desolvated and ionized with a positive charge leading to the transfer into the negatively charged entrance of the mass spectrometer for further analysis. (Illustration from *Steen&Mann*[106])

Before the implementation of LC-MS, proteomics research relied on protein and peptide analysis on the individual level and often on the rather small scale, such as one-dimensional (1D) gel electrophoresis prior to antibody-based immunoblot analysis. Technical and methodological advancements made in diverse scientific areas established MS-based proteomics as the leading proteomics technology. For instance, the availability of whole-genome sequence databases ultimately provided amino acid sequences for protein databases against which information from mass spectra can be matched. In addition, the above mentioned soft ionization methods made biological samples compatible with MS. Apart from ionization itself, also novel MS instrumentation formats specially tailored for proteomics analysis as well as innovative database search algorithms and strategies for automated quantification gave rise for a quantum leap of resolution, mass accuracy, dynamic detection range and throughput. In that way, the unbiased analysis of complex protein mixtures of unknown composition is possible, considerably outcompeting traditional protein-chemical approaches. The typical format for MS-based proteomics fulfilling these standards is the combination of liquid chromatography and tandem mass spectrometry (LC-MS/MS) in a so-called bottom-up shotgun experiment.

The workflow in bottom-up proteomics normally starts with an initial fractionation, enrichment or purification step which is conducted with the protein sample of interest, e.g. a cell lysate (Figure 4). Very often, a cell lysate is separated by gel electrophoresis and further processing takes place with single bands or band segments not only to purify the lysate sample but also to reduce complexity by restricting to a certain protein size range. In addition, generation of several independent samples associated with individual LC-MS runs boosts database identifications and the dynamic range of the measurements[107]. Characteristic

for the bottom-up analysis is the subsequent proteolytic cleavage to convert proteins to peptides. Very often trypsin is employed in this step as it features high activity, stability and the specificity to generate cleavage products with arginines or lysines on the carboxy-terminus. Another protease commonly used is Lys-C cleaving C-terminally of lysine residues. Utilizing protein digests instead of intact proteins produces several benefits[108]. Full-length proteins often possess varying degrees of solubility and stability under identical conditions, whereas the substantially shorter proteolytic peptides between 1-3 kDa regularly unwind solubility and stability issues, thus offering at least partial amenability of the proteins for MS-analysis[106]. Thus, even membrane proteins, which are generally difficult to handle in biochemical assays, become quite susceptible to LC-MS. Moreover, the measurement of whole proteins is afflicted with poorer sensitivity of the mass spectrometer in a way that the combinatorial effect resulting from various modifications and processing species of one protein makes determining the masses of the numerous resulting isoforms impossible[106].

For the sake of (additional) reduction of sample complexity and/or targeted enrichment of certain peptide species, e.g. phosphorylated peptides, distinct separation techniques are frequently used. Usually, in that context diverse chromatographic methods are being applied. These can be based on the analytes' charge state, such as ion exchange chromatography or based on the peptides' hydrophobicity by reversed phase liquid chromatography (RPLC) (Figure 4). The purpose of that step is to extract as much information, i.e. attain a comprehensiveness as large as possible of the existing sample, which is referred to as (phospho)proteome coverage.
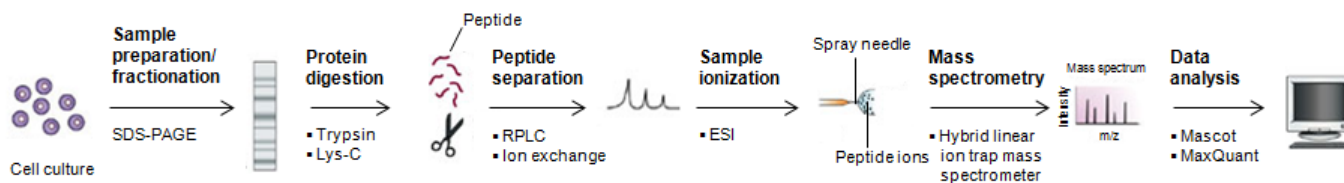
Figure 4: Schematic workflow of a bottom-up shotgun experiment. A protein sample, e.g. cell lysate or chromatography eluate, is often separated by SDS-PAGE. In that case, the gel lane that is obtained is cut into several slices, which are then in-gel digested. Normally, trypsin and/or Lys-C are used for that step. The generated peptide mixture is usually further purified by chromatographic methods before ionization by electrospray ionization subsequent to online- reversed phase liquid chromatography. After mass spectrometric analyisis, data are searched against protein databases using database-searching programmes, such as Mascot, to assign peptide/protein identifications. (Illustration adapted from *Steen&Mann*[106])

As mentioned above, using nano LC-MS includes the direct (online) coupling of nano-flow high-performance liquid chromatography to the mass spectrometer. Before entering the MS device, peptides are separated by an analytical column with a very small inner diameter between 50 and 150 µM packed with reversed phase material, such as C18. This enables very low flow rates (250-500 nl/min) and continuously high peptide concentrations. A starting material of few micrograms peptide are injected with an autosampler into the nano-LC device and sequentially eluted from the reversed phase columns applying a

solvent gradient with increasing organic content, thereby separating the peptides in order of their hydrophobicity. As peptides elute from the chromatographic column, they are vaporized and subsequently ionized as outlined above. Subsequently, they are carried off through a small heated capillary inlet in a vacuum system where they are further passed on. The mass spectrometric device that is often used in that context is the hybrid linear ion trap (LTQ)-Orbitrap mass spectrometer[109]. Figure 5 illustrates the schematic layout of this mass spectrometer, where peptide ions are directed by means of electric fields into a linear ion trap of the LTQ and stored. Upon axial transfer into the C-trap, where the ion population is compacted into a small cloud, follows the injection onto the orbitrap. The orbitrap is a spindle-like mass analyzer consisting of two types of electrodes, outer and central electrodes. Trapped ions start to rotate radially and oscillate harmonically along the central electrode where the attraction is counterbalanced by centrifugal forces. The frequency of these harmonic oscillations is only dependent on the mass-to-charge (m/z) value and independent of rotational motion. More precisely, the oscillating ions induce an image current into the two outer electrodes, which can be detected using a differential amplifier. Signal impositions generated through the presence of different ions species can be converted into individual oscillation frequencies by Fourier Transformation. The high performance of the Orbitrap mass spectrometer in terms of resolution (>100.000 (FWHM) at m/z 400) and mass accuracy of 1-3 ppm (<1 ppm is possible through internal calibration) is a consequence of the harmonic nature of the oscillations[109,110]. Thus, the MS spectrum acquired in the orbitrap assigns each peptide ion an m/z and an intensity value. Yet, this information is not sufficiently informative for a confident identification. Therefore, the most abundant peptide ions are selected to obtain sequence information. This combination of peptide isolation and successive sequence determination is characteristic of tandem MS. The selected peptide ions, also called precursor ions, are subjected to collisions with inert helium gas in the linear ion trap. In the course of that process called collision-induced dissociation (CID) peptide ions break apart and form the of so-called product ions. Their m/z ratios are then recorded in a tandem MS, MS/MS or MS² spectrum. Thereby, only ions of a defined m/z interval are stably oscillating on trajectories in an alternating electric field applied by the four rods of the linear ion trap prior to reaching the detector[111]. Compared to the orbitrap mass analyzer, the linear ion trap has lower mass resolution and accuracy, but considerably higher sensitivity as well as operation speed[106]. The LTQ Oribtrap is normally working in the data dependent mode enabling automatic switching between orbitrap-MS and LTQ ion trap-MS/MS acquisition. Collectively, while peptides are continuously eluted from the nano-LC column the mass spectrometer cycles through a sequence comprised of obtaining high resolution/mass accuracy MS spectra in the orbitrap followed by fast recording of cleavage products in tandem MS/MS spectra upon CID of the precursor ions.
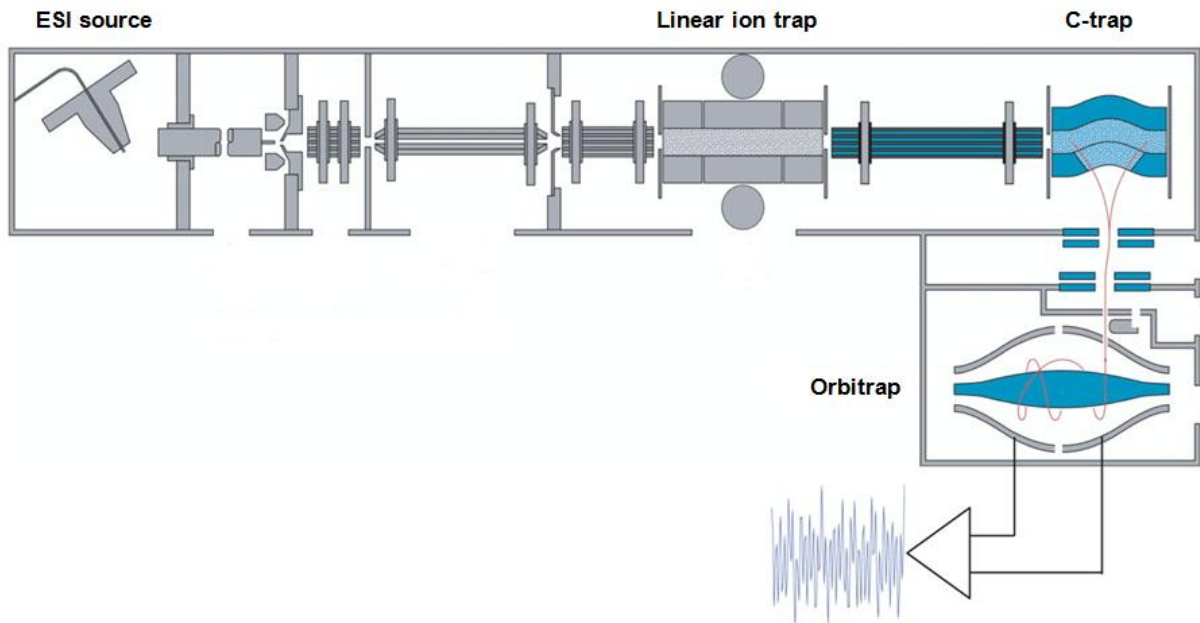
Figure 5: Schematic of the LTQ Orbitrap hybrid instrument. Typically, is operates in a parallel fashion, i.e. precursor ions are selected and accumulated in the C-trap before injection in the orbitrap to generate high-resolution MS spectra. At the same time, the LTQ performs fragmentation reactions simultaneously recording MS/MS spectra of lower resolution, yet with higher speed and sensitivity than the orbitrap mass analyzer. (Illustration adapted from *Olsen et al.*[110])

In shotgun proteomics experiments it is both a benefit but also a remarkable challenge to identify a plethora of peptides for subsequent reconstruction of proteins. The automated assignment of peptide sequences is usually accomplished by means of database searching[112,113]. Peptide ion masses from both MS and MS/MS spectra are scanned through an amino acid sequence database search engine such as Mascot[114]. Those masses can be inferred through the charge state of a peptide which is spotted from the m/z signal of a peptide being present as isotopic clusters of known isotopic element variants[106]. The Mascot algorithm includes matching of measured spectra with theoretically predicted candidate spectra according to protein sequences digested *in silico*. For each candidate spectrum the mass of the precursor and fragment ions are calculated and thus also theoretical fragment spectra are acquired. In case the measured precursor mass corresponds to the mass of the candidate (within defined mass deviation constraints), its theoretical fragmentation patterns are matched against the acquired MS/MS spectrum. For each fragmentation spectrum recorded, the engine compiles a list of peptide sequences and calculates an identification score according to the quality of the match based on the probability of being random. The peptide with highest score assigned to the MS/MS spectrum is used for further analysis. However, matches between observed and expected spectra are not always ideal or partially random leading to some degree of ambiguity associated with each peptide identification[115]. Thus, the Mascot score alone is not sufficient to discriminate true from

false positive as it is reflects the quality of individual matching events while not considering factors influencing the entire population, such as the size of the database or the performance of the mass spectrometer[116]. To overcome these drawbacks a robust and high-throughput compatible target-decoy search strategy has prevailed enabling a tight control of data quality[115]. For that purpose, a target-decoy database is created, which is obtained by concatenating the original database with a variant that is obtained by reversing and/or scrambling protein sequences. Searching a concatenated database needs doubling of the number of decoy hits to enable estimation of false-positive hits because a random match is equally likely to occur in the target and decoy half. So in order to apply a user-defined false discovery rate (FDR), one calculates the fraction of decoy matches and adjusts the Mascot score threshold fulfilling that FDR. By this means, the FDR is an estimate of the proportion of false positives in the whole population.

4.3 Fundamentals of quantitative mass spectrometry

Since mass spectrometry records peptide signals together with intensities several approaches were developed to quantitatively assess relative protein abundances on that basis or on protein identification scores[117-121]. However, parameters utilized such as peptide counts and intensities as well as confidence of protein identification correlate only roughly with analyte concentrations. Generally, the absence of a peptide signal in a MS spectrum does not necessarily mean that it was not present in the sample. Several other factors can be responsible for that circumstance, for instance varying degrees of sample introduction, ionization and of detection efficiency in the mass spectrometer. Moreover, certain unevenness introduced during sample preparation can compromise accurate quantification of relative protein abundance. Very complex samples are particularly affected by these nonsystematic errors[117]. Nevertheless, there are approaches allowing robust and highly accurate quantification of individual peptide and protein intensities, respectively, to turn MS quantitative, which are largely untouched of this shortcomings [96]. For these isotope-based methods heavy isotopic variants of either atoms or amino acids are incorporated into the proteome either metabolically or chemically via molecular tags. By this means, two or more peptide populations are created being qualitatively, e.g. physicochemically identical except for a small mass offset introduced. This allows pooling of differentially labeled protein or peptide samples prior to nano-LC separation and introduction into the mass spectrometer. Peptide species mostly coelute irrespective of their label and subsequently arrive at the detection devices simultaneously leading to their common appearance in mass spectra. Therein, the mass offset manifests itself as m/z shift and the intensity ratio of the two peaks or peak clusters directly indicates the relative amounts of a peptide that is present in the two populations. The recent advent of high-resolution and accuracy MS instrumentation was crucial for accurate quantifi-

cation based on small mass-unit shifts between 4 and 10 Da typically introduced in such labeling experiments[117].

Metabolic labeling can be applied to microorganisms, such as bacteria, plants and mammalian tissue culture cells. For instance, one can use culturing media wherein the naturally occurring hydrogen (^{1}H), carbon (^{12}C), nitrogen (^{14}N) and oxygen (^{16}O) atoms are replaced by ^{2}H (deuterium), ^{13}C, ^{15}N and ^{18}O, respectively, all of which are stable and non-radioactive isotopes. Upon complete metabolic incorporation the proteome can be compared with the proteome of another population grown in a medium with normal amino acids. Each of the heavy isotopes causes a one-mass-unit difference per substituted atom with the exception of ^{18}O that shifts mass by two units. For lower organisms ^{15}N labeling with ammonium salts as nitrogen source has been applied, but its usage is problematic[122,123]. The relatively high cost of the culturing media is one detrimental issue. In addition, mass spectrometric quantification is adversely affected by the additional layer of data complexity introduced, especially if labeling is not complete[124,125]. For metabolic labeling of mammalian cell lines the stable isotope labeling by amino acids in cell culture (SILAC) approach has proven successful in a plenty of quantitative proteomics studies[126,127]. In SILAC culture, media contain stably labeled amino acids, which are directly integrated into the proteome of a cell population. One medium contains a "heavy" form(s) the other medium the "light" form(s) of usually one or two amino acids of choice. While for the light form amino acids are composed of the normal isotopic elements, in the heavy form(s) these are replaced by the aforementioned heavy versions. In order to compel cells to directly incorporate that label only essential amino acids are used which are non-synthesizable by the cell line itself. Upon five or more cell doublings, almost 100% of the respective amino acid has been replaced by the labeled variant within the proteome through cellular protein turnover and growth[117]. For SILAC labeling, normally arginine and lysine enriched in stable nitrogen, hydrogen and carbon isotopes are selected resulting in defined mass differences amenable to MS. In a so-called triple-SILAC experiment up to three cellular states or, respectively, conditions can be compared by differential labeling with either natural lysine and arginine (Arg^0 and Lys^0, light label), with ^{2}H$_4$-lysine and ^{13}C$_6$-arginine (Lys^4 and Arg^6, medium label) or with ^{15}N$_2$^{13}C$_6$-lysine and ^{15}N$_4$^{13}C$_6$-arginine (Lys^8 and Arg^{10}, heavy label) (Figure 6). The combination with tryptic protein digestion ensures labeling of each peptide apart from the very C-terminal ones. In such an experimental variant coeluting peptides are detected in a MS spectrum as triplets with a distinct mass shift of 4 and 8 Da in case of lysine and 6 and 10 Da in case of arginine relative to the light label, respectively (Figure 6). The relative quantification of peptides is achieved via integration and subsequent comparison of the respective isotope cluster intensities of the precursor ions. It is worth of note that the spectral complexity is tripled in such a SILAC experiment and doubled with introduction of two labels leading to a reduction in the number of identified proteins[127].

Due to the limited repertoire of useful heavy labeled arginines and lysines, SILAC is restricted to duplex and triplex experiments[128]. Additional versions of labeled arginines and lysines are only possible at the expense of additional deuterium atoms, which can lead to retention time differences during LC hence hampering accurate quantification[129]. However, further multiplexing is possible by combing separate SILAC experiments each including an identical condition serving as common reference[130].
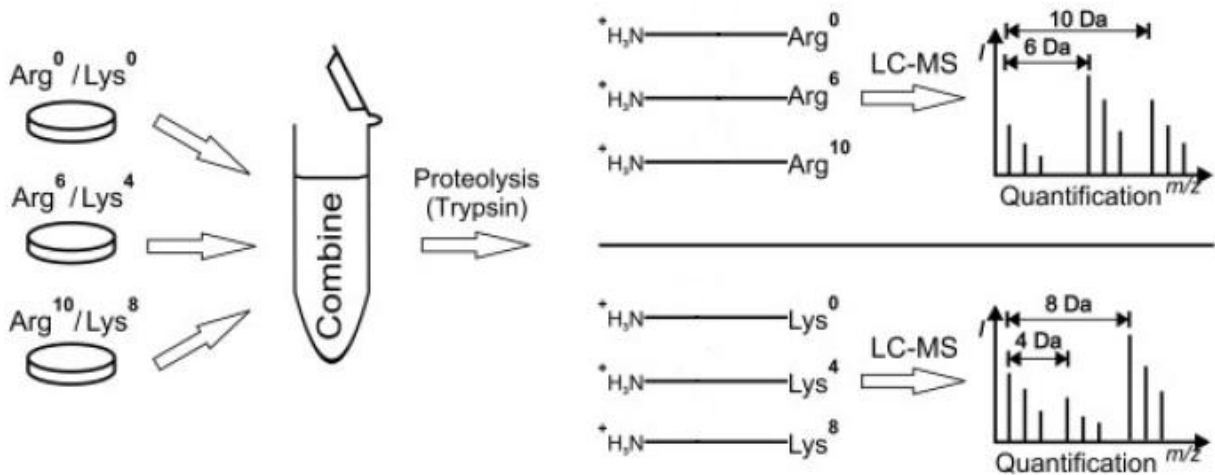
Figure 6: Principle of stable-isotope labeling with amino acids in cell culture (SILAC)-based quantification. For SILAC labeling different cell populations are maintained for several generations in growth media in which the naturally occurring 'light' arginines and lysines have been replaced by their isotopically 'medium' and 'heavy'. Heavy-, medium and light-labeled samples are combined prior to further MS sample preparation steps including proteolysis by trypsin. The isotopic peptide variants can be distinguished and quantified in MS spectra due to their defined mass offsets (+4/+8 Da for lysine, +6/+10 Da for arginine). (Illustration adapted from *Schreiber et al.*[131])

A major benefit of metabolic labeling is that the label is present in live cells and differentially labeled states are normally mixed directly upon cell lysis prior to fractionation or purification. Thus, the accuracy of quantitation is not affected by errors introduced by these subsequent sample preparation steps[117]. The classical SILAC experiment can only be performed with cultured cells of mammalian origin, with yeast strains auxotrophic to arginine and lysine and even with bacteria, all of which exhibiting extensive protein synthesis and turn over[132,133]. In theory, SILAC culture media recipes can be adapted provided that the labeled amino acids are the only available source to growing cells. For this reason, in mammalian cell culture dialyzed serum devoid of low molecular components such as amino acids is used instead of the regular form[117]. However, proliferation of some cell lines depends on growth factors that are removed during dialysis, which can complicate cultivation. Care must also been taken that cells to do not metabolically convert arginine to proline, because this leads to the introduction of labeled proline in the proteome impeding accurate quantification[134]. Meanwhile, several solutions to that problem are available, such as

mathematical or experimental correction strategies[133,135,136]. A limitation of SILAC labeling is that it is not generally applicable for quantifying changes in protein or peptide abundances in tissue samples. Although SILAC has been successfully used to label mice, this is associated with huge time, cost and effort far from becoming a standard approach[137]. However, the idea of using a labeled tissue proteome to compare with other mouse proteomes paved the way for recent innovations utilizing SILAC labeled internal standards to allow tissue proteome quantification in an indirect fashion[138].

Parallel to the development of metabolic labeling strategies, various chemical labeling approaches have been developed and are also being widely used in MS-based proteomics[128]. In contrast to metabolic labeling, an isotope-coded mass tag is attached to a reactive group of an amino acid, such as amino or thiol groups. A general caveat of chemical labeling for shotgun proteomics is that the label is introduced on the peptides level upon proteolytic digestion, and only after that step the differentially labeled samples can be combined. In case of an extensive sample preparation procedure preceding digestion, later quantitation may be negatively affected due to experimental variation[117]. An obvious advantage over metabolic labeling techniques is its usability for tissue or patient samples, whose quantitative characterization is particularly relevant, for example, in biomarker discovery[139,140]. Another benefit accompanied by chemical but not metabolic labeling is its ability for multiplexed analysis of different biological samples. While SILAC enables a direct quantitative comparison of up to three samples, so-called isobaric labeling reagents, such as time tandem mass tags (TMTs) and isobaric tags for absolute and relative quantification (iTRAQ), are available in up to eight different versions[141,142]. These tags are composed of multiple nitrogen and carbon atoms available to substitution with stable isotope while avoiding deuterium labeling. Moreover, these reagents are built in a way that peptides from differentially labeled samples are isobaric, i.e. possess identical masses. By that means, the complexity of MS spectra is not increased compared to non-quantitative runs leading to better protein identification rate. The quantitative analysis takes place using MS/MS spectra upon peptide fragmentation wherein reporter ions with defined mass offsets in the low mass range (below a m/z value of 150) are quantified. Whereas identification rates are higher with isobaric labeling strategies, a general problem associated with it is the occurrence of interfering signals from near-isobaric precursor ions in the MS/MS isolation window affecting accuracy of peptide quantification[143]. Particularly complex samples can lead to simultaneous isolation of multiple precursor species and, thus, measured ratios tend toward the median ratio of 1:1, a phenomenon termed "ratio compression effect"[144].

4.4   Affinity chromatography-based proteomics

A common approach for understanding biomolecular signal networks and the role of their components involved is to discover the underlying protein-protein interactions. The goal is to gain essential infor-

mation about the topology of such networks, the participating protein complexes and their functional roles. In that context, the usage of small molecule tool compounds can contribute to this with the provison that previous knowledge about targeted proteins is available. In addition, these specifications can also be utilized to bring in mechanistic insight into a compound's mode of action, which is particularly relevant in drug discovery and development. A classical way to address these subjects in biochemical studies is by affinity chromatography. In combination with modern MS instrumentation and its highly sensitive protein identification capability, affinity chromatography with cellular extracts offers the potential to characterize protein-protein (interaction proteomics) as well as target protein-compound (chemical proteomics) interactions on a whole-proteome scale.

4.4.1   Principles of chemical proteomics

The term "chemical proteomics" implies the profiling of small molecules immobilized on a solid support and the enrichment of their protein targets prior to mass spectrometric detection. Chemical proteomics can be subdivided into two distinct methodologies, one is called Activity-Based Probe Profiling (ABPP), which enriches enzymatic activity of a particular protein family, and affinity-based Compound-Centric Chemical Proteomic (CCCP) approaches[145,146]. In the following the focus will be laid on CCCP, because of its relevance in the context of this thesis.

For immobilization of a small molecule of interest on a matrix - such as Sepharose or agarose beads - prior knowledge of structure-activity relationship (SAR) data are required to localize positions within the compound qualifying for the attachment of functional groups like amino, hydroxyl or carboxyl groups or affinity tags, e.g. biotin. In general, eligible positions have to be dispensable for the compound's cellular activity and are accessible from the outside solvent when in complex with its target(s). That is why careful monitoring of whether activity of modified molecules is preserved, through biochemical or cell-based assays, is essential[146,147]. The compound or the modified compound analog can then be conjugated to a chromatography resin via these functional groups or affinity tags to create an affinity matrix. Extracts prepared from cells or tissues containing the proteome in its native state are then incubated with the affinity matrix. Generally, a rather large amount of cellular material is required for that assays, and not all protein will be available in its active form, depending on the method of cell lysis. Membrane proteins in particular, which are notoriously difficult to handle, may lose their structural integrity required for ligand biding upon solubilization. In such a case, these targets will escape capturing by the affinity matrix.

The elution of bound proteins takes place after extensive washing and normally under highly denaturing conditions or, in a more specific fashion, by adding an excess of soluble compound. Sample preparation

for mass spectrometric analysis of retained target proteins is then usually continued with tryptic in-gel digestion procedures (Figure 4)[147,148].

4.4.2   Chemical proteomics for characterizing kinase inhibitors

The chemical proteomics methodology has its origins in the pioneering work on affinity chromatography with the scope of enriching and purifying proteins by means of small molecules[149-151]. Shortly after, its potential to identify direct targets for mechanistic studies on drug action was recognized[152,153]. Initially, the identification of bound protein was the major bottleneck, which is now overcome with state-of-the-art mass spectrometry and the availability of protein databases facilitating a fast and sensitive detection and identification of proteins[154]. With these advances, chemical proteomics matured to a versatile tool for drug target deconvolution. Accordingly, concerning a forward chemical proteomics approach, it can be used during drug discovery processes to identify target spectra of drug candidates in search of the molecular basis of drug phenotypes. Moreover, despite the fact that drugs are usually optimized against a single target, their specificity is often broader as initially anticipated. Binding such "off-targets" can be associated with an increase of therapeutic potential, but also with toxic side effects being the main reason for failing in clinical development[147]. By that means, it would be feasible to recognize possible side effects in early stages of drug development avoiding significant costs associated with subsequent failure in clinical trials. On the other hand, the finding of alternative cellular targets can be utilized to discover new drug-induced phenotypes, e.g. in alternative disease models to reveal an additional therapeutic benefit of a drug, or in basic research to study modulation of cellular signaling.

Applying chemical proteomics in combination with complex and disease-relevant biological systems, such as cell lines, offers an unbiased way to validate and identify drug targets on a proteome-wide scale. In the past years, drug target deconvolution mainly, but not exclusively, focused on ATP-competitive kinase inhibitors. Several factors made these molecules to ideal utensils for their use as affinity ligands in the context of chemical proteomics: For instance, there is and was a general interest in understanding the mode of action of a promising drug class. Additional factors are the scientific experience so far due to the widespread use as research tools, practical aspects like the high potency and availability of SAR information and, as a result, the efficient tethering on solid matrixes predestined small-molecule kinase inhibitors as workhorses in the development of chemical proteomics.

In early studies, it was possible to demonstrate that the true selectivity of kinase inhibitors, which is crucial for interpretation of biological effects, was actually considerably broader that anticipated. For instance, the compound SB203580 (Figure 15) was believed to be a specific p38 kinase inhibitor. However,

by means of chemical proteomics with a linker derivative and subsequent validation experiments, it could be demonstrated that it also targets additional kinases with similar potency[155]. Another study employed the linkable gefitinib derivative AX14596 (Figure 8) to uncover more than 20 previously unknown gefitinib targets[148]. Due to the unbiased nature of that approach, also non-kinase targets were identifiable, which would have escaped detection using hypothesis-driven strategies[156]. This is because alternative target deconvolution techniques are generally restricted to a defined panel of putative targets, as it is the case for recombinant assay systems, protein microarrays or expression-cloning-based methods[157-159]. The concept of chemical proteomics on the basis of affinity chromatography has so far the inherent limitation of addressing molecule-target interaction in a qualitative fashion, which is not the case in activity assays with recombinant target candidates whose enzymatic action is affected through small-molecule binding[147]. Ranking of these interactions, however, would be important to identify the strongest molecular associations that are likely the most relevant in physiological conditions. Another critical issue is the discrimination between specific and background binders, which is not straightforwardly assessable in affinity chromatography-based approaches[146]. A recently developed kinase inhibitor chemical proteomics profiling technique enabled the quantitative monitoring of dose-dependent inhibitor effects on target protein binding to a mixture of immobilized kinase-selective ligands[160]. About 140 protein kinases have been quantitatively assessed for their interactions with clinical BCR-ABL kinase inhibitors in leukemia cell extracts[160]. Despite these advances, quantitative data obtained with this approach considerably vary from the half maximal inhibition (IC_{50}) values measured *in vitro* for a subset of kinase targets. Moreover, no inherent controls on the individual target level had been implemented to monitor experimental factors that are potentially critical for IC_{50} determinations.

4.4.3 Proteomic examination of protein-protein interactions

Traditionally, large-scale protein-protein interaction data are based on the yeast two-hybrid system and phage display technologies[161]. Later on, with the advent of lab automation, binary interaction testing was feasible with a higher throughput using protein chips[162]. However, both methods bear significant drawbacks such as the difficulty to denote false negatives and positives in yeast two-hybrid system, e.g. arising from the overexpression of bait and prey proteins and their intracellular mislocalization[163]. Moreover, *in-vitro*-based methods using recombinant proteins do not resemble the intracellular milieu and are limited to a defined panel of putative prey proteins spotted on a chip of fused to phage particles. By means of affinity chromatography with cellular extracts these limitations can be circumvented. [164]. In combination with state-of-the-art mass spectrometry, affinity chromatography-based approaches for measuring protein-

protein interactions are feasible on a large scale. However, there are a number of challenges, such as the identification of specific targets and their differentiation from unspecific binders. Notably, substoichiometric and weak interactions can run the risk of being not detected. Analogously to chemical proteomics techniques, the immobilization of bait protein and bait complexes, respectively, also relies on conjugation to a solid matrix. This can be addressed via antibody-mediated immobilization very much like co-immunoprecipitation (co-IP) with cell lysates or by expression of recombinant fusion proteins bearing an epitope or an affinity ligand directly in the organism to be studied. Upon cell lysis, fusion proteins can be pulled out in complex with its interactors by immunoprecipitation or beads containing suitable high-affinity interactors, such as protein domains. Previous knowledge about the interface in charge of mediating contact with target proteins is advantageous. Furthermore, if placing fusion tags on the protein is desired, it is critical to know whether protein functions are affected by tagging in general and if not, to specify the right end of the protein (C- or N-terminal). Likewise, in case of co-IP approaches, the epitope should not overlap with the binding interface to evade competition of the used antibody with putative interactors of the bait. To guarantee formation of fusion protein complexes mirroring the physiological situation, expression should be close to the level of its endogenous counterpart[161]. Numerous experimental implementations have been developed such as the tandem affinity purification (TAP) tag as one of the most successful techniques[165]. TAP tags are comprised of two different affinity tags which are combined in succession to perform two consecutive affinity purification steps. Between the first and second enrichment steps, the first half of the tag is released by protease action. TAP tag enrichments and its methodological variants enable a very stringent and clean purification of interacting proteins and their detection is easily combinable with MS detection[166,167]. However, the highly stringent discrimination between specific and background binders adversely affects sensitivity at the expense of losing low affinity binders[164]. In that context, quantitative proteomics implementations offer a possibility to distinguish true from unspecific protein-protein interactions without losing sensitivity. In practice, two different affinity purifications are performed in parallel with lower stringency compared with TAP tag approaches, one with the protein bait of interest and the other one with a non-specific bait acting as a control. In contrast to specific binders, background binders will be detected in equal quantities and therefore exhibit a ratio of one when comparing relative signal intensities of differentially labeled peptides[164]. The only criterion for being identified as true binder is based on the intensity ratio of binding to bait protein versus control incubation, which should be considerably higher than one. Thus, compared to TAP tag approaches, even lower affinity or rarely occurring interactions are amenable to detection. In addition, higher stringency can be reached simply by specifying higher binding ratio thresholds. In the past, several quantitative proteomics-based protein-protein interaction studies were carried out successfully, either by means of chemical or metabolic labeling[168-170]. A recent advancement of that principle called QUICK (quantitative immunoprecipitation

combined with knockdown) was developed in the group of Matthias Mann and combines SILAC with RNA interference (RNAi) to elegantly assign protein-protein interactions with high confidence, thereby overcoming the need to tag proteins[170]. A more specific application of quantitative interaction proteomics is devised on the basis of PTMs. In numerous cases, phosphorylations, acetylations, methylations or combinations thereof are prerequisite to arbitrate protein-protein interactions (see section I1). For that purpose, peptide pull-downs on the basis short synthetic peptide stretches immobilized on a resin are performed with cellular extracts. Binding to a modified versus unmodified peptide version can then quantitatively compared - due to prior introduction of isotopic labels - for filtering out background proteins. By that means it was possible to identify phosphotyrosine dependent interactions in the EGF signaling pathway or to systematically screen for novel interactors of histone PTMs[171,172].

4.5   Phosphoproteomics

As indicated earlier, reversible attachment of phosphate groups to proteins by kinases and phosphatases represents one of the most significant regulatory mechanisms in eukaryotic cells. With respect to phosphorylation, previous biochemical efforts and genetic approaches, such as *in vivo* labeling, peptide mapping, phosphoamino acid analysis and purification of kinase activities have laid the foundation to a better understanding on individual components in linear signaling cascades, albeit at a rather small scale[173,174]. With a growing number of signaling components identified and the progressive deciphering of their potential to integrate, potentiate or terminate signal transduction processes, more powerful techniques with the ability to paint a more comprehensive picture of complex highly dynamic phosphorylation-based signaling networks are required[16,175]. In addition, a better insight into kinase signaling at the systems level bears extensive opportunities for biological as well as medical research, e.g. by comparing disease states or by monitoring cellular responses upon kinase inhibitor treatment. For that purpose, sensitive and robust MS-based methods have been developed recently addressing the substoichiometric presence of phosphorylations for an unbiased identification and quantification in a site-specific way[176]. In order to harness the potential of MS for phosphoproteomics, a general workflow has been established where progress in each of the individual steps of sample preparation, MS itself, bioinformatics processing and data evaluation has been made in recent years[176].
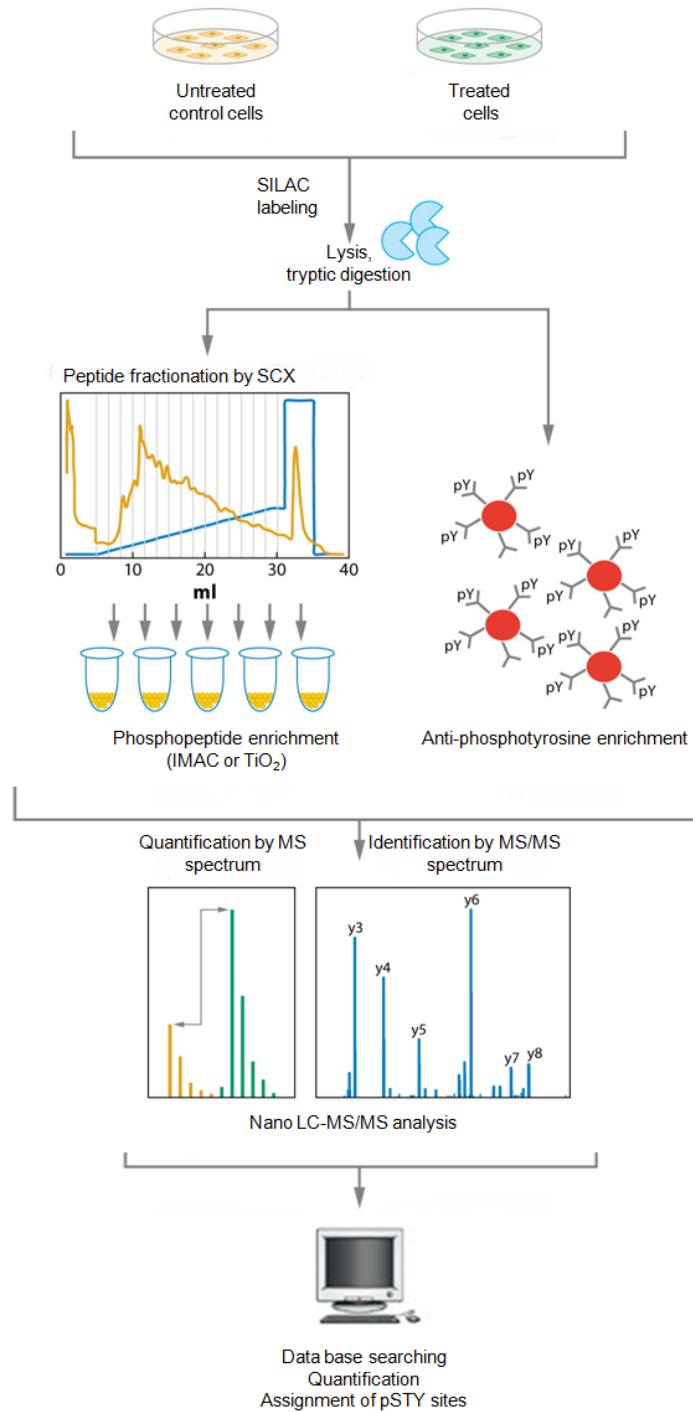
Figure 7: Typical procedure for phosphopeptide enrichment and analysis. Control and treated cells are differentially labeled with SILAC, lysed, and pooled at equal protein amounts. Protein extracts are digested by trypsin, and phosphopeptides are enriched by a combination of SCX chromatography and IMAC, or by immunoprecipitation with phospho-specific antibodies. Phosphopeptides are then separated on nano-LC and directly measured in a mass spectrometer. Relative peptide quantitation is usually based on the precursor ion spectra (MS) and peptide identification is achieved by means of associated fragmentation spectra (MS/MS). These raw data are finally analyzed for peptide identification and quantification by database searching, such as Mascot, quantification software, such as MaxQuant. That examination includes the probability-based localization of pSTY sites, which is also implemented in MaxQuant. (Illustration adapted from *Macek et al.*[176])

4.5.1 Enrichment of phosphorylated peptides

For an efficient recovery of the phosphoproteome one must consider the low abundance of many site-specific phosphorylations as well as their short-lived nature due to impaired stability at basic pH and to the presence of phosphatases. That subject is commonly addressed by the introduction of broadly-selective phosphatase inhibitors during initial sample preparation steps[177]. The classical approach suitable for tyrosine phosphorylation analysis is antibody-based (Figure 7). Scientific relevance for investigating phosphotyrosine-based signaling specificity arises from its impact on the regulation of fundamental cellular processes, which, in case of their deregulation, can lead to pathological outcomes like cancer[57]. The very low abundance of phosphorylated tyrosines necessitates antibodies with high affinity and selectivity[178]. Thus, an enrichment strategy is implemented either on the whole-protein level prior to or on the peptide level subsequent to proteolytic digestion. By this means, recent optimization enabled mapping up to thousands of phosphotyrosine sites[178-181]. Compared against the protein phosphorylation in its entirety, phosphorylation on tyrosines is of rather low proportion. To gain a more comprehensive picture of cellular phosphorylation, including modification of serine and threonine residues, chromatographic methods, such as immobilized metal affinity chromatography (IMAC), are utilized. IMAC enables enrichment of peptides based on the high-affinity coordination of phosphates to trivalent metal ions, such as Fe^{3+}, Ga^{3+}, Al^{3+} and Zr^{3+}[176,182-184]. Alternatively, phosphate group-containing peptides can be adsorbed by metal oxide affinity chromatography using titanium dioxide (TiO_2) microspheres through Lewis acid-base interactions[185,186]. However, for both materials nonspecific binding of non-phosphopeptides might occur when operating outside of the appropriate pH range, or in case the ratio of capturing reagent to peptide mixture is not optimal [176,185,187]. In such cases, increasing proportions of acidic peptides rich in glutamic and aspartic acid residues become prevalent. 2,5-dihydroxy benzoic acid (DHB) can be added for TiO_2 enrichment where it acts as a competitive binder for circumventing this problem[185]. A surplus of DHB outcompetes other carboxylic acids from TiO_2 binding while binding to phosphopeptides is not affected, thus considerably improving the selectivity of TiO_2 for phosphopeptides[185]. However, the usage of DHB at high concentrations interferes with the chromatographic separation and ionization in the mass spectrometer[188]. That is why it has to be handeled with caution. In the literature the selectivity issue of IMAC was addressed by materials on the basis of tetravalent metal ions (Ti^{4+}- or Zr^{4+}-IMAC), which seem to show an improved enrichment performance over conventional trivalent metal ions[184,189]. In addition, selective protonation of carboxylic acids through low TFA appears to impede their binding to IMAC materials[188].

4.5.2 Phosphopeptide fractionation

Apart from the classical fractionation strategies based on 1D-gel electrophoresis, which are characterized by high robustness, liquid chromatography methods to reduce sample complexity subsequent to in-solution digestion of protein extracts became widely popular in MS-based phosphoproteomics applications[190]. Their high potential lies in their ability to not only fractionate but also to simultaneously enrich for phosphorylated peptides. Ion exchange chromatography and particularly strong cation exchange chromatography (SCX) fulfils that criterion. SCX allows separation of peptides according to their solution charge states. Prior to loading on the column, peptides are acidified to a pH of 2.7 and bound peptides are eluted with increasing salt and pH. At pH 2.7 lysine, arginine, histidine residues and the N-termini of peptides are positively charged. As tryptic proteolysis produces peptides with an arginine or lysine on the C-terminus, they carry a solution charge of +2 if unmodified[108]. Phosphate groups retain their negative charge at this pH due their lower pK_a and the net charge state of singly phosphorylated peptides in solution should be +1. That is why the phosphopeptides tend to elute earlier from the SCX column[191]. Peptides with two or three phosphate groups posses a net charge which is neutral and -1, respectively, preventing adsorption to the resin material and leading to their occurrence within the flow-through fraction. Thus, mostly the first SCX fractions exhibit a considerable enrichment of phosphopeptides. For highest phosphopeptide recovery SCX is arranged upstream of IMAC or TiO_2 enrichment prior to mass spectrometric detection[130,133,192].

4.5.3 Quantitative mass spectrometry analysis of phosphorylated peptides

MS-based analysis of phosphopeptides imposes additional technical challenges compared to the examination of unmodified peptides. Although modern tandem MS instrumentation is easily capable of resolving the mass shift of 98 Da introduced by each additional phosphate group, the correct placement within the peptide sequence remains difficult. When using CID for MS/MS experiments often a significant neutral loss of the phosphate group from the precursor ion is observed due to the relatively labile phosphoester bond. As a result, uninformative fragment ions are generated, which greatly compromise peptide sequence delineation and accurate assignment of phosphosite positions. Conversely, these neutral loss ions can be exploited as a diagnostic marker of phosphopeptides and further isolation of the neutral loss precursor followed by its fragmentation and analysis in ion traps yields fragment-rich mass spectra[133]. This data-dependent MS/MS/MS (MS^3) strategy is now well-established in a way that the selected precursor ions undergo a process known as multistage activation (MSA)[193]. Thereby, neutral loss ions produced and

isolated in an MS/MS CID step are subjected to an additional CID to generate a MS^3 spectrum. MSA significantly saves analysis time by avoiding the detection of separate MS/MS and MS/MS/MS spectra. Nevertheless is such a collective pseudo MS^n spectrum rich in information boosting the identification of phosphopeptides and assignment of phosphorylation sites. A recent development in tandem-MS is called higher-energy C-trap dissociation (HCD) which is able to overcome some limitations of CID, such as the low mass cut-off for fragment detection and the production of partially less informative product ions[194]. With this fragmentation technique at hand, more informative MS/MS spectra covering low-mass fragment ions as well as immonium ions indicative of phosphotyrosine modifications can be recorded. Advanced orbitrap-based instruments with improved ion optics and detection frequencies further established HCD as tool for phosphopeptide analysis as these can compensate for the generally slower and less sensitive re-cording of MS/MS spectra in the orbitrap mass analyzer[195,196]. Electron transfer dissociation (ETD) and electron capture dissociation (ECD) are alternative fragmentation modes for the identification of phosphopeptides[197,198]. In both methods electrons are transferred to peptides with multiple positive charg-es in the gas phase. Upon formation of these radical cations, decomposition of the peptide occurs while the phosphoester bond remains intact generally allowing more confident phosphorylation site assignment[199]. ETD, which is suitable for ion trap spectrometers, bears potential in global analyses of phosphorylation, in particular for multiply charged (3+ and higher) and multiply phosphorylated peptides[176]. In contrast to the quantitative comparison of protein abundances, the quantitative assessment of phosphorylation sites relies on single-peptide analysis. Thus, quantitation is based on a significantly lower number of mass spectrometric detection events to the detriment of precision. In order to guarantee a quantitation as accurate as possible, variation already introduced during sample preparation should be avoided. That is why metabolic labeling strategies for quantitative MS such as SILAC have attracted sig-nificant attention in that context and chemical labeling approaches seem to be inferior even more if quan-titation is dependent on MS/MS spectra like TMT or iTRAQ being also afflicted with reduced quantifica-tion efficiency (see section I4.3) [130,200,201]. Nevertheless, chemical labeling can be an appropriate alterna-tive especially if metabolic labeling is not possible in tissue or patient samples[176]. The correct assignment of the actual phosphorylation site is another challenging issue associated. Especially if the phosphopeptide is composed of more than one (consecutive) serine, threonine or tyrosine residue, the presence of an indicative mass increment alone is not sufficient to position the phosphate group to the corresponding residue. Similarly, unambiguous pinpointing the positions of multiple phosphorylation sites on one peptide is not trivial. To resolve this issue particularly for large scale data sets, where manual inspection is not an option, sophisticated algorithms have been developed based on database matching and subsequent calculation of probability scores, which, upon normalization, are further divided into dif-ferent classes of localization probability[130,176,202].

5. Acute myeloid leukemia

Acute myeloid leukemia (AML) is an aggressive neoplastic disorder in which progenitor cells of the myeloid lineage turn through genetic alterations into so-called leukemic stem cells (LSC)[203]. Despite the various epi- and cytogenetic alterations involved in driving this transformation process and the existence of different AML subclasses reflecting the branches of the myeloid lineage, AML shares a common pattern of pathogenesis. This is described by the so-called two-hit model hypothesis of leukemogenesis: The first hit alters pathways involved in regulating proliferation and cell death, for example by mutations of receptor tyrosine kinases leading to their constitutive activation. The second hit results in an inability to differentiate normally and, thus, cells bear the capability of self-renewal[204-206]. This is enabled by either an overexpression of *HOX* genes or cytogenetetic instabilities in terms of, for example, chromosome translocations[204,207]. Only if both hits occur, AML will develop[204]. The outcome is an abnormal clonal amplification of LSCs turning the scales against the development of normal hemopoietic cells. The consequences are lethal infections and organ infiltrations due to the resulting cytopenias. AML progresses rapidly and is fatal within one year without treatment[208]. The advancements that have been made during the recent years in understanding the molecular pathogenesis of AML are remarkable, nevertheless, current standardized cytotoxic therapies are still rather inefficient and do not comply with the individual variances[205,209,210]. Although complete remission is achieved in many cases, the disease is often not fully eradicated resulting in relapse later on, in particular in elderly patients[211]. Accordingly, the patients' overall survival remains poor in addition to a significant burden related to chemotherapeutic intervention or radiation therapy[208,212]. For this reason, the necessity for targeted therapies intervening in a well-defined target or in a biologic pathway emerges, chiefly owing to the vast genotypic heterogeneity of that disorder[213-215]. Ideally, as a consequence of such interference, the malignancy becomes attenuated or disrupted, respectively, with only limited side effects for the patient. Therefore, patient stratification is considered as essential to ensure presence of the genetic alteration from which the molecularly targeted oncoprotein emerges. An impressive proof of the targeted therapy concept is selective tyrosine kinase inhibition (see section I3.2), as aberrant regulation of phosphorylation-based signaling notably contributes in malignant transformation processes[57]. The receptor tyrosine kinase FLT3 is intensely pursued as a molecular target and is mutationally activated in about 30% of patients, in most cases due to an internal tandem duplication that disrupts negative regulation by the juxtamembrane region of the receptor[216]. However, even in the subset of patients bearing FLT3 mutations, clinical responses have been rather modest when available FLT3 inhibitors were tested. However, second generation FLT3 inhibitors of higher selectivity and *in vivo* potency, such as AC220, have recently shown promising clinical activity as single agent and likely bear

potential for more effective combination therapies[217,218]. As shown earlier, a growing number of small molecule protein kinase inhibitors have received FDA approval as cancer treatments for other indications (Table 1). In NSCLC, activating mutations were found in the epidermal growth factor receptor (EGFR) and shown to drive tumorigenesis in a subset of cases. These NSCLC patients are often highly responsive to the clinical EGFR inhibitors gefitinib and erlotinib[219]. Both drugs have been evaluated in AML cell lines and patient-derived AML blasts. They exhibited antineoplastic effects by promoting myeloid differentiation and/or inhibiting cell viability *in vitro*[220-224]. Potent anti-AML activity has been observed for erlotinib *in vivo* and even complete remissions were reported in two cases in erlotinib-treated patients suffering from AML and concomitant NSCLC[225,226].

Strikingly, antileukemic effects were detected despite the absence of measurable EGFR expression, implying that gefitinib and erlotinib act through interference with other molecular targets. Previous studies showed cellular phosphoregulation of the cytoplasmic tyrosine kinases JAK2 and SYK upon erlotinib or gefitinib treatment, respectively[221,222]. There is no experimental proof yet that these kinases are directly targeted by EGFR inhibitors in AML cells. Neither JAK2 nor SYK was identified as a target by *in vitro* selectivity testing against a recombinant kinase panel or by chemical proteomics using immobilized gefitinib for affinity capture in combination with mass spectrometry identification[148,158]. However, these studies identified several proteins in addition to the EGFR that interacted with considerable affinity and could therefore be involved in cellular responses to with erlotinib and gefitinib.

II Materials and Methods

1. Materials

1.1 Laboratory chemicals and biochemicals

2-Butanol ($C_4H_{10}O$)	Sigma-Aldrich
Acetic acid ($C_2H_4O_2$)	Sigma-Aldrich
Acetonitrile for HPLC (ACN; C_2H_3N)	Sigma-Aldrich
Adenosine-5'-triphosphate (ATP; $C_{10}H_{16}N_5O_{13}P_3$)	Sigma-Aldrich
Ammonium bicarbonate (ABC; NH_4HCO_3)	Sigma-Aldrich
Ammonium peroxodisulfate (APS; $(NH_4)_2S_2O_8$)	Bio-Rad
Aprotinin	Alexis Biochemicals
Bromophenol blue ($C_{19}H_{10}Br_4O_5S$)	Sigma-Aldrich
Calcium chloride ($CaCl_2$)	Sigma-Aldrich
Calyculin A	Alexis Biochemicals
Dimethylsulfoxide (DMSO; C_2H_6OS)	Sigma-Aldrich
Dimethylthiazolyldiphenyltetrazolium bromide (MTT; $C_{18}H_{16}BrN_5S$)	Sigma-Aldrich
Dipotassium phosphate (K_2HPO_4)	Roth
Dithiothreitol (DTT; $C_4H_{10}O_2S_2$)	Sigma-Aldrich
Ethanol p.a. (C_2H_6O)	Riedel
Ethanolamin (C_2H_7NO)	Sigma-Aldrich
Ethylene glycol tetraacetic acid (EGTA; $C_{14}H_{24}N_2O_{10}$)	Sigma-Aldrich
Ethylenediaminetetraacetic acid (EDTA; $C_{10}H_{16}N_2O_8$)	Merck
Formic acid (FA; CH_2O_2)	Sigma-Aldrich
Gelatine	Sigma-Aldrich
Glycerol ($C_3H_8O_3$)	Sigma-Aldrich
Glycine ($C_2H_5NO_2$)	Sigma-Aldrich
Hydrochloric acid (HCl)	Sigma-Aldrich
Hydroxyethyl piperazineethanesulfonic acid (HEPES; $C_8H_{18}N_2O_4S$)	Roth
Iodoacetamide (IAA; C_2H_4INO)	Sigma-Aldrich
Leupeptin	Alexis Biochemicals
Magnesium chloride ($MgCl_2$)	Sigma-Aldrich
Manganese(II) chloride ($MnCl_2$)	Sigma-Aldrich

Methanol p.a. (CH$_4$O)	Fisher
Monopotassium phosphate (KH$_2$PO$_4$)	Roth
N,N,N',N'-tetramethylethylenediamine (TEMED; (NH$_4$)$_2$S$_2$O$_8$)	Serva
Nitrogen (l) (N$_2$)	Linde
Phenylmethanesulfonyl fluoride (PMSF; C$_7$H$_7$FO$_2$S)	Sigma-Aldrich
Phosphatase Inhibitor Cocktail 1	Sigma-Aldrich
Phosphatase Inhibitor Cocktail 2	Sigma-Aldrich
Phosphoric acid (H$_3$PO$_4$)	Sigma-Aldrich
Polysorbate 20 (Tween 20; C$_{58}$H$_{114}$O$_{26}$)	Sigma-Aldrich
Ponceau S (C$_{22}$H$_{16}$N$_4$Na$_4$O$_{13}$S$_4$)	Sigma-Aldrich
Potassium chloride (KCl)	Sigma-Aldrich
Sodium azide (NaN$_3$)	Serva
Sodium chloride (NaCl)	Sigma-Aldrich
Sodium dodecyl sulfate (SDS; NaC$_{12}$H$_{25}$SO$_4$)	Roth
Sodium fluoride (NaF)	Merck
Sodium hydroxide (NaOH)	Merck
Sodium orthovanadate (Na$_3$VO$_4$)	Sigma-Aldrich
ß-Mercaptoethanol (C$_2$H$_6$SO)	Sigma-Aldrich
Thio urea (CH$_4$N$_2$S)	Invitrogen
Trifluoroacetic acid(TFA; C$_2$HF$_3$O$_2$)	Fluka
Tris/HCl (C$_4$H$_{11}$NO$_3$/HCl)	Sigma-Aldrich
Triton X-100 (C$_{14}$H$_{22}$O(C$_2$H$_4$O)$_n$)	Serva
Urea (CH$_4$N$_2$O)	Merck

1.2   Small molecules

AX14596	Vichem
Erlotinib	LC Laboratories
Gefitinib	LC Laboratories
SB203580	Vichem
VI16742	Vichem

1.3   Biologicals

1.3.1   Ligands

Epidermal growth factor (EGF)	Preprotech

1.3.2   Antibodies

Name/epitope	Origin	Clonality	Supplier/Source
α-pSFK-Tyr(P)-416	rabbit	polyclonal	Cell Signaling Technology
α-LYN	rabbit	polyclonal	Cell Signaling Technology
α-EGFR	mouse	monoclonal	Blencke et al.[227]
α-FITC-CD11b	mouse	monoclonal	Abcam
α-VSV (P5D4) (Isotype control)	mouse	monoclonal	Roche
α-rabbit-HRP	goat	polyclonal	BioRad

1.3.3   Peptides

p914IRS4929 Desthiobiotin-SGSGEADSSSDpYVNMDFTKR   MPI of Biochemistry
914IRS4929 Desthiobiotin-SGSGEADSSSDYVNMDFTKR   MPI of Biochemistry

1.3.4   Enzymes and substrates

Breast tumor kinase (BRK)   ProQinase
Bruton tyrosine kinase (BTK)   Millipore
Casein kinase 1δ (CK1δ)   Millipore
Casein kinase 1ε (CK1ε)   Invitrogen
C-jun NH2 terminal kinase 2α2 (JNK2α2)   Millipore
CK1tide   Upstate
Cyclin G–associated kinase (GAK)   Godl et al.[155]
Ephrin receptor B4 (EphB4)   Millipore
Glycogen synthase kinase 3β (GSK3β)   ProQinase
GSK3β substrate   Calbiochem
GST–c-JUN   Hibi et al.[228]
Hepatocyte growth factor receptor (MET)   ProQinase
Histone mix   Roche
Lys-C   WAKO
Myelin basic protein   Sigma-Aldrich
Poly(Glu$_4$Tyr)   Sigma-Aldrich
Receptor-interacting protein kinase 2 (RIPK2)   Millipore
Spleen tyrosine kinase (SYK)   Millipore
Trypsin (seq. grade modified)   Promega
Tyrosine-protein kinase SYK   Millpore
Tyrosine-protein kinase YES   ProQinase

V-YES-1 Yamaguchi sarcoma viral related oncogene homolog (LYN)   ProQinase

1.3.5   Components of molecular weight standard

Beta-galactosidase   Sigma-Aldrich
Bovine serum albumin (BSA)   Sigma-Aldrich
Carboanhydrase   Sigma-Aldrich
Lysozyme   Sigma-Aldrich
Myosin   Sigma-Aldrich
Ovalbumin   Sigma-Aldrich
Phosphorylase b   Sigma-Aldrich
Trypsin inhibitor   Sigma-Aldrich

1.4   Consumables

C18 SepPac columns 100 mg cartridges   Waters
C18 SepPac columns 500 mg cartridges   Waters
Cell culture dishes 150x25 mm (p15 dishes)   Corning
Cell culture petri dishes 145x20 mm   Greiner
Cell culture plates (6-Well, 12-Well, 96-Well)   Nunc
Cell scraper 24 cm   TPP
Centrifuge tubes (15 ml, 50 ml)   TPP
Cryotube (1.5 ml)   Nunc
Empore Disk C18 47 mm   3M
Epoxy-activated Sepharose 6B   GE Healthcare
FACS tubes   BD Bioscience
Hyperfilm MP   GE Healthcare
Millex Syringe filters 0.22 μm PVDF 33 mm   Millipore
Millex Syringe filters 0.45 μm PVDF 33 mm   Millipore
NuPAGE Novex Bis-Tris gel 10%   Invitrogen
P30 glass fiber filters   Wallac
Parafilm   Dynatech
PHOS-Select™ Iron Affinity Gel (IMAC beads)   Sigma-Aldrich
Pipette Tips (1000 μl, 200 μl, 10 μl)   Eppendorf
Protein G-Sepharose Amersham   Pharmacia
Protran nitrocellulose membrane   Whatman
Scintillation tubes (27 x 58 mm, 20 ml)   Nerbe Plus
Stripette (5 ml, 10 ml, 25 ml)   Corning
Tubes (0.5 ml, 1 ml, 2 ml)   Eppendorf
Whatman paper 3MM   Whatman

1.5   Kits

BCA assay kit	Pierce
Bradford assay kit	Biorad
Colloidal Blue® staining kit	Invitrogen
Western Lightning ECL kit	PerkinElmer

1.6   Buffers and solutions

1.6.1   Commercial

[γ-^{33}P]ATP	PerkinElmer
Acrylamide/bisacrylamide 37.5:1	Serva
FACS Flow	BD Bioscience
NuPAGE LDS sample buffer 4x	Invitrogen
NuPAGE MOPS SDS running buffer 20x	Invitrogen
NuPAGE®	Antioxidant
Scintillation cocktail Rotiszint®ecoplus	Roth

1.6.2   Home-made

ABC buffer	50 mM ABC

0.01% Bromphenol blue (v/v)

Destaining buffer (In-gel-digestion)	25 mM ABC
	50% Ethanol (v/v)

FACS buffer	0.1% NaN$_3$ (w/w)
	2% FBS (v/v)
	in PBS

45% Glycerol (v/v)

Gel extraction buffer   30% ACN (v/v)
                                                     3% TFA (v/v)

IMAC binding buffer   40% ACN (v/v)
                                                     25 mM FA

IMAC C18 elution buffer   50% ACN (v/v)
                                                     0.5% acetic acid (v/v)

IMAC elution buffer   500 mM K_2HPO_4, pH 7

IMAC washing buffer   1% FA (v/v)

Kinase buffer   60 mM HEPES-NaOH pH 7.5
                                                     3 mM $MgCl_2$
                                                     3 mM $MnCl_2$
                                                     3 μM Na_3VO_4
                                                     1.2 mM DTT

7.5% ß-Mercaptoethanol (v/v)

MS buffer A   0.5% acetid acid (v/v)

MS buffer B   80% ACN (v/v)
                                                     0.5% acetic acid (v/v)

MTT solution 5x   5 mg/ml MTT
                                                     in PBS

Phosphate buffered saline (PBS)   137 mM NaCl
                                                     27 mM KCl
                                                     80 mM Na_2HPO_4
                                                     1.5 mM KH_2PO_4
                                                     pH 7.4

Peptide extraction solution (In-gel-digestion)   30% ACN (v/v)
                                                     3% TFA (v/v)

Ponceau S staining solution   0.2% Ponceau S (w/w)
                                                     2% TCA (w/w)

SCX buffer A   30% ACN (v/v)
                                                     7 mM KH_2PO_4
                                                     pH 2.65

SCX buffer B	30% ACN (v/v) 350 mM KH_2PO_4 pH 2.65
SDS Sample buffer 3x	100 mM Tris/HCl pH 6.8
2% SDS (w/w)	
3% SDS (w/w)	
SD-Transblot buffer	50 mM Tris/HCl pH 7.5 40 mM glycine 20 % methanol (v/v) 0.004 % SDS (w/w)
Sep-Pak C18 elution buffer	50% ACN (v/v) 0.5% acetic acid (v/v)
Sep-Pak C18 washing buffer 1	0.1% TFA (v/v)
Sep-Pak C18 washing buffer 2	0.5% FA (v/v)
Stage tip washing buffer	0.5% acetic acid (v/v) 0.1% TFA (v/v)
StageTip elution buffer	80% ACN (v/v) 0.5% acetic acid (v/v)
StageTip sample buffer	0.2% TFA (v/v) 4% ACN (v/v)
Stop-Solution (MTT)	9.5% SDS (w/w) 5% 2-butanol (v/v) 12 mM HCl
Stripping buffer	62.5 mM Tris/HCl 100 mM β-mercaptoethanol pH 6.8
TBS-T 10x	200 mM Tris/HCl pH 7.5 1.4 M NaCl 50 mM EDTA 0.5% Tween 20

Tris-glycine-SDS buffer	25 mM Tris/HCl pH 7.5
	200 mM glycine
	0.1% SDS (w/w)

Triton X-100 lysis buffer	50 mM HEPES pH 7.5
	150 mM NaCl
	0.5% (v/v) Triton X-100
	1 mM EDTA
	1 mM EGTA
	10 μg/ml Aprotinin
	10 μg/ml Leupeptin
	1 mM PMSF
	10 mM NaF
	2.5 mM Na_3VO_4
	50 ng/ml Calyculin A
	1% Phosphatase Inhibitor Cocktail 1
	1% Phosphatase Inhibitor Cocktail 2

Urea lysis buffer	8 M Urea
	75 mM NaCl
	50 mM Tris pH8.2
	1 mM EDTA
	1 mM EGTA
	10 μg/ml Aprotinin
	10 μg/ml Leupeptin
	1 mM PMSF
	10 mM NaF
	2.5 mM Na_3VO_4
	50 ng/ml Calyculin A
	1% Phosphatase Inhibitor Cocktail 1
	1% Phosphatase Inhibitor Cocktail 2

Western blot blocking solution	5% BSA (w/w)
	in TBS-T

Western blot washing buffer	2% BSA (w/w)
	in TBS-T

1.7   Cell culture media and supplements

DMEM, without arginine and lysine	Gibco
Dulbecco's modified Eagle's medium (DMEM)	Gibco

FBS, dialyzed	SAFC Biosciences
Fetal bovine serum (FBS)	Gibco
Freezing medium	FBS / DMSO 10:1 (v/v)
L-Arginine (Arg^0)	Gibco
L-Arginine: HCl, U-$^{13}C_6$ (Arg^6)	Cambridge Isotope Laboratories
L-Arginine: HCl, U-$^{13}C_6$$^{15}N_4$ (Arg^{10})	Cambridge Isotope Laboratories
L-Glutamine	PAA
L-Lysin (Lys^0)	Gibco
L-Lysine: 2 HCl, $^2H_4$ (Lys^4)	Cambridge Isotope Laboratories
L-Lysine: 2 HCl, U-$^{13}C_6$$^{15}N_2$ (Lys^8)	Cambridge Isotope Laboratories
Penicillin/streptomycin, 100x	PAA
Roswell Park Memorial Institute medium 1640 (RPMI1640)	Invitrogen
RPMI 1640, without arginine and lysine	Invitrogen
Trypsin/EDTA	Invitrogen

1.8   Cell lines

Hela S3	ATCC; Department of molecular cell biology, MPI of Biochemistry
KG-1 (#CCL-246)	ATCC

1.9   Instruments

Agilent HPLC-System 1100	Agilent
ÄKTA Explorer	GE Healthcare
Axiovert 135	Carl Zeiss
Biofuge fresco	Heraeus
Blot apparatus (semi-dry)	Bio-Rad
Centrifuge 5415 R	Eppendorf
Chemie-HYBRID-pump RC 6	Vacuubrand
Compact PAGE system	Atto
Digital camera Visitron System	Visitron Systems
ELISA Reader	MWG Biotech
FACSCalibur	Becton Dickinson
Fuji BAS-2500 Phosphorimager	Fuji
Incubator HeraCell 150	Thermo
LTQ-Orbitrap MS 2.2	Thermo
Lyovac GT2	Leybold-Heraeus
Nanospray ion source	Proxeon
Observer A1	Carl Zeiss
Orbital shaker Polymax 1040	Hydolph

Phosphoimager plates	Fuji
Power supply EV261	PEQLAB
Scintillation counter LS 6500	Beckmann
Thermomixer comfort	Eppendorf
Ultrasonic homogenizer Sonopulus GM70	Brandelin electronic
Vacuum Concentrator 5301	Eppendorf
XCell SureLockTM Mini Cell	Invitrogen
Z1 cell and particle counter	Beckman Coulter

1.10   Software and online Tools

BD CellQuest™ Pro (version 4.0.2)	Beckton Dickinson
Corel Draw (version 12.0)	Corel Corporation
Cytoscape (version 2.6/version 2.7)	www.cytoscape.org
DAVID	www.david.abcc.ncifcrf.gov
Excel 2007	Microsoft
MaxQuant Suite (version 1.0.13.12/version 1.0.12.0)	MPI of Biochemistry dept. Mann
Motif-x	www.motif-x.med.harvard.edu
MultiExperiment Viewer MeV (version 4.4.1)	www.tm4.org/mev/
Phosphosite	www.phosphosite.org
STRING (version 8)	www.string.embl.de
Sigmaplot (version 10)	Systat Software
Unicorn (version 5.1)	Thermo
Uniprot	www.uniprot.org
XCalibur (version 2.0)	Thermo

2. Methods

2.1   Cell culture

2.1.1   Standard Maintenance

Cell culturing conditions were 37°C and 7% CO_2 in a humidified atmosphere. The AML cell line KG-1 was cultured in suspension in RPMI 1640 medium containing 10% FBS and 2 mM l-glutamine. Cells were passaged twice a week at a density of $2x10^5$cell/ml. Hela S3 cells were grown under adherent condi-

tions in DMEM supplemented with 10% FBS and 2 mM l-glutamine and penicillin/streptomycin. For subculturing cells were propagated twice a week at a split ratio of 1:4.

2.1.2 SILAC labeling

For all SILAC experiments, KG-1 and Hela S3 cells were cultured in RPMI 1460 and DMEM media without arginine and lysine supplemented with dialyzed FBS, 2 mM l-glutamine, penicillin/streptomycin (Hela S3 only) and either 42 mg/l Arg^0 and 71 mg/l Lys^0 or equimolar amounts of Arg^6 and Lys^4 or Arg^{10} and Lys^8. After six doublings in SILAC medium to ensure complete proteome labeling cells were ready for treatment or, respectively, harvest.

2.2 Treatment, cell harvest and lysis

2.2.1 Lysis with triton X-100 lysis buffer

SILAC labeled Hela S3 cells confluently grown on p15 plates were washed twice with PBS before adding 600 µl Triton X-100 lysis buffer per plate.

By contrast, KG-1 cells grown in petri dishes were repeatedly washed with PBS by means of centrifugation for 5 min at 500 g and 4°C. Here, 300 µl Triton X-100 lysis buffer were applied per plate containing $4x10^7$ cells. For subsequent immunoblotting, KG-1 cultivation was downscaled to a 6-well-plate format. Upon treatment with different gefitinib and erlotinib concentrations or an isovolume of DMSO (0.05% v/v), cells were treated in the same way as described above. Upon 10 min incubation on ice, lysates were collected, cleared by centrifugation for 20 min at 16,500 g and 4°C. Extracts were then filtered through 0.45 µm Millex syringe filters. Protein concentration was measured using the BCA assay kit.

2.2.2 Lysis with urea lysis buffer

4×10^8 KG-1 cells in a volume of 200 ml per differentially labeled population were treated for 1 h with either 10 µM erlotinib, 10 µM gefitinib or an identical volume of DMSO solvent (0.05% v/v) prior to cell harvest and two washing steps with cold PBS by centrifugation at 500 g and 4 °C. Subsequently, each cell pellet was lysed in 4 ml of urea lysis buffer and sonicated three times for 1 min on ice, pre-cleared as

described above and protein concentrations were determined by Bradford assay. All three SILAC labeled conditions of a replicate experiment were pooled at equal protein amounts to obtain 18 mg in total.

2.3   *In vitro* association experiments

For *in vitro* association with inhibitor affinity beads, differentially labeled Hela S3 (KG-1) cells were lysed in Triton X-100 lysis buffer. After lysis, extracts were adjusted to 1 M NaCl before *in vitro* association samples comprised of 750 µl (375 µl) lysate containing 3 mg (1.5 mg) of protein with either 30 µl (15 µl) of drained inhibitor or control matrix were incubated for 2.5 h at 4°C. Where indicated, supernatant from a first round of incubation with inhibitor beads was subjected to a second *in vitro* association for additional 2.5 h in the presence of the same amount of inhibitor resin. To test whether immobilized inhibitors were present in molar excess over their potential target proteins, differently labeled lysate containing 1 mg (0.5 mg) or 3 mg (1.5 mg) of protein in a volume of 750 µl (375 µl) were incubated with inhibitor resin. Moreover, incubation times of 2.5 h and 5 h were compared to analyze whether the binding reactions had reached the equilibrium after 2.5 h. For competition experiments, SILAC-encoded cell lysates were treated with different concentrations of gefitinib, erlotinib or SB203580 for 30 min before the addition of AX14596 or VI16742 beads, respectively. Alternatively, lysates were incubated with the inhibitor beads for 30 min before addition of the free inhibitors. Subsequently, *in vitro* associations were performed for additional 2.5 h at 4 °C. Extracts of Hela S3 cells were thereby treated with 0 nM, 10 nM, 100 nM, 1 µM and 10 µM gefitinib or 0 nM, 100 nM, 1 µM, 10 µM and 100 µM SB203580. KG-1 lysates were incubated with 0 nM, 20 nM, 100 nM, 2 µM and 20 µM gefitinib and erlotinib, respectively. In all *in vitro* association experiments, three washing steps (two with lysis buffer containing 1 M NaCl and one with regular lysis buffer) were performed before elution of resin-bound material with 30 µl of 1.5x LDS sample buffer at 70°C for 10 min.

For binding experiments involving peptide baits, N-terminally desthiobiotin-conjugated IRS4 peptide encompassing amino acids 914 to 929 was synthesized as tyrosine-phosphorylated (pTyr921) and non-phosphorylated version as described[171,229]. Immobilization on streptavidin agarose beads was monitored at 215 nm to determine the amount of resin-bound peptides. For immunoprecipitation experiments with monoclonal antibody directed against EGFR, mAb108.1, Hela S3 cells were stimulated for 5 min with 100 ng/ml EGF before lysis[227]. The monoclonal EGFR antibody was bound for 30 min to protein G–Sepharose before addition of lysate. *In vitro* association experiments with peptide baits and EGFR antibody were performed as described for kinase inhibitor beads except that 150 mM NaCl was included in all buffers.

2.4 SDS-polyacrylamide-gelelectrophoresis (SDS-PAGE)

Prior to western blotting, lysates were loaded on home-made 10% SDS gels with a 4% stacking gel[230]. In parallel, a molecular weight standard mixture consisting of myosin (205 kDa), beta-galactosidase (116.25 kDa), phosphorylase b (97.4 kDa), BSA (66.2 kDa), ovalbumin (42.7 kDa), carboanhydrase (29 kDa), trypsin inhibitor (21.5 kDa) and lysozym (14.4 kDa) was electrophoretically separated in Tris-glycine-SDS buffer at an electric current of 25 mA until loading dye reached the phase boundary.

For subsequent in-gel disgestion, *in vitro* association eluates were combined and resolved on a NuPAGE 10% Bis-Tris gel. Proteins were separated over half of the gel in 1x NuPAGE MOPS SDS running buffer supplemented with 0.1% NuPAGE antioxidant at a constant voltage of 200 V.

2.5 Western Blotting

For immunoblot analysis proteins were transferred to a nitrocellulose membrane for 2 h at a current $0.8mA/cm^2$ using a semi-dry blotting system and SD-transblot buffer[231]. Upon transfer, the membrane was stained with Ponceau S staining solution to monitor protein transfer and to mark standard protein bands followed by several washes with dH_2O for destaining. The subsequent incubation steps were performed at constant agitation on an orbital shaker. To avoid unspecific protein binding, the membrane was "blocked" with western blot blocking solution for 1 h at RT. Thereafter, the epitope-specific primary antibody diluted in western blot washing buffer according to the manufacturer's instructions was added over night at 4°C. The membrane was then washed three times for 10 min with western blot washing buffer before probing with α-rabbit-HRP antibody diluted 1:50,000 in western blot washing buffer for 1 h at RT. Again, the membrane was washed three times for 10 min and antibody-antigen complexes were visualized by ECL and detected by X-ray films according to the manufacturer's instructions. To enable re-probing with a different primary antibody, membranes were stripped of bound antibody by shaking in stripping-buffer for 1 h at 52°C. After several washing steps, stripped membranes were blocked and ready for incubation with another primary antibody.

2.6   Sample preparation for (phosphoproteomics) analysis

2.6.1   In-gel digestion

Resolved proteins were visualized in gel by Colloidal Blue staining kit according the supplier's instructions and gel lanes were cut into three slices. In the following sample preparation steps, each slice was processed separately as described earlier[190]. Unless otherwise indicated, the following incubations were performed at 25°C in an Eppendorf shaker at 1000 rpm. In brief, gel slices were cut into small 1 mm x 1 mm cubes and washed with destaining buffer until being decolored. Gel pieces were then dehydrated with ethanol and after that rehydrated with ABC buffer containing 10 mM DTT. To facilitate efficient brake-up of disulfide bonds by means of chemical reduction, samples were incubated at 56°C for 1 h. In the next step, reduced thiol groups were alkylated by adding 55 mM IAA diluted in ABC buffer for 1 h in the dark. Thereafter, gel pieces were washed with ABC buffer, dehydrated with ethanol, rehydrated ABC buffer and dehydrated again. Gel cubes were then fully dried in a vacuum concentrator and incubated over night at 37°C with ABC containing modified trypsin corresponding to 1% (w/w) of the estimated protein content in the gel slice. To stop digestion, TFA at a final concentration of 0.5% (v/v) was added and liquids were transferred to fresh Eppendorf tubes. For further peptide extraction, gel pieces were incubated twice with gel extraction buffer and ACN, respectively. All extraction liquids obtained from a sample were combined including the acidified trypsin solution and subjected to vacuum concentration to completely remove the ACN fraction prior to StageTip desalting.

2.6.2   In-solution digestion

After pooling of equal protein amounts of 6 mg per SILAC labeling and treatment condition, the combined lysate was adjusted to 6 M urea and 1.5 M thiourea. Unless otherwise indicated, the following incubations took place at 25°C on an Eppendorf shaker at 1000 rpm or on a rotation wheel for sample volumes exceeding a volume of 2 ml. In a reduction step, pooled lysates were reduced in a final concentration of 1 mM DTT for 45 min followed by alkylation by adding 5.5 mM IAA for 30 min in the dark. Afterwards, proteins were digested with Lys-C for 4 h at an enzyme/substrate ratio (w/w) of 1:150 followed by 1:4 (v/v) dilution with ddH2O to add trypsin at an identical proportion. Trypsin digestion was stopped after 16 h by acidification with TFA which was added at a final concentration of 0.5% (v/v). The resulting

peptide sample was filtered through a 0.45 μm Millex syringe filter and desalted on reversed-phase C18 Sep-Pak cartridges (500 mg sorbent weight).

2.6.3   Desalting of peptide mixtures

2.6.3.1   C18 Sep-Pak cartridges

In order to remove salt species from in-solution peptide digests prior to SCX-based peptide separation or phosphopeptide enrichment, reversed-phase C18 Sep-Pak columns containing 500 mg or 100 mg sorbent material were used as described earlier[192]. In brief, columns were washed and conditioned with 9 ml or 2 ml ACN and 3 ml or 1 ml Sep-Pak C18 elution buffer. Subsequent to cartridge equilibration with 9 ml or 2 ml Sep-Pak C18 washing buffer 1, acidified peptide mixture was loaded. Upon successive washing with 9 ml or 2 ml Sep-Pak C18 washing buffer 1 and 2 ml or 1 ml Sep-Pak C18 washing buffer 2, bound peptides were eluted with 3 ml or 0.6 ml Sep-Pak C18 elution buffer. Desalted peptides were then snap-frozen in liquid N_2, lyophilized and stored at -20°C.

2.6.3.2   StageTips

Smaller peptide amounts extracted from in-gel digests were desalted by means of home-made StageTips immediately before mass spectrometric analysis[232]. From an Empore Disk C18 small discs were punched out and placed into a 200 μl pipette tip. Tips were then conditioned with 50 μl methanol, washed with 100 μl StageTip elution buffer and further conditioned two times with 100 μl MS buffer A. Subsequently, acidified peptide samples were loaded on StageTips and thereafter, these were washed with 200 μl MS buffer A. With two consecutive additions of 20 μl StageTip elution buffer peptides were eluted and the volumes of combined eluates were reduced using a vacuum concentrator. As soon as the volume reached approximately 3 μl, an isovolume of StageTip sample buffer was added to reach TFA and ACN concentration of 0.1% (v/v) and 2% (v/v), respectively, prior to loading onto the LC-MS device.

2.6.4   Strong cation exchange chromatography

For SCX chromatography on an ÄKTA explorer system, the total peptide sample was dissolved in 600 μl SCX buffer A and upon pH adjustment with FA to a value of 2.65, loaded onto a Polysulfoethyl A column with a flow rate of 3 ml/min. The flow-through was collected and retained peptides were gradually

eluted by a 30 min linear gradient ranging from 0% to 30% SCX buffer B, followed by washing with 100% buffer B as described[192]. Collected SCX fractions were pooled to twelve samples of similar peptide contents according to the UV absorption measured at 215 nm. Upon evaporation of ACN through a vacuum concentrator, the resulting peptide samples were desalted with reversed-phase C18 Sep-Pak cartridges (100 mg sorbent weight).

2.6.5   Immobilized metal affinity chromatography enrichment of phosphopeptides (IMAC)

In order to enhance the percentage of phosphorylated peptides within samples designated for phosphoproteomic analysis, IMAC was performed. Each enrichment batch consisted of 5 µl equilibrated IMAC beads, which were washed four times with IMAC binding buffer in advance, and 200 µl pooled SCX fractions reconstituted in 400 µl IMAC binding buffer. Thus, each peptide sample was subjected to two parallel incubations with PHOS-Select Iron Affinity Gel. After 1 h incubation at RT on an Eppendorf shaker at 1400 rpm, the slurry was loaded C18-StageTips conditioned and washed in advance with 50 µl methanol, 70 µl IMAC C18 elution buffer and twice with 70 µl IMAC washing buffer. After washing twice with 70 µl IMAC binding buffer and another 70 µl of IMAC washing buffer, phosphopeptides were eluted from IMAC beads by adding three times 70 µl IMAC elution buffer. Thereby, peptides are retained by the C18 disk. Salt remnants were subsequently removed by washing two times with 70 µl IMAC washing buffer and peptides were eluted from the C18 material with 30 µl IMAC C18 elution buffer. In order the remove the ACN fraction and to reduce the overall sample size a vacuum concentrator was used. As soon as the volume reached approximately 3 µl, an isovolume of StageTip sample buffer was added to reach TFA and ACN concentration of 0.1% and 2% (v/v), respectively, prior to loading onto the LC-MS device.

2.7   Kinase assays

In vitro kinase assays of RIPK2, JNK2α2, CK1δ, EphB4, CK1ε, GSK3β, BRK, LYN, YES, MET, GAK, SYK and BTK were performed in kinase buffer containing 60 mM HEPES-NaOH (pH 7.5), 3 mM MgCl$_2$, 3 mM MnCl$_2$, 3 µM Na$_3$VO$_4$ and 1.2 mM DTT. The substrates used were 0.33 mg/ml myelin basic protein for RIPK2 and BRK, 200 µM CK1tide for CK1δ and CK1ε, 0.2 mg/ml histone mix for GAK, 0.2 mg/ml poly(Glu$_4$Tyr) for EphB4, LYN, YES, SYK, BTK and MET, 80 µg/ml GST-c-jun2 for JNK2α2 and 50 µM GSK3β substrate for GSK3β. All kinases were assayed in a total volume of 25 µl in the presence of 0.1 µM ATP, 0.5 µCi [γ-^{33}P]ATP and different SB203580, AX14596, erlotinib or gefitinib

concentrations. After a 30 min preincubation step on ice, the kinase reactions were started by the addition of ATP and performed for 7 min at 30°C. Kinase reactions were linear over the incubation time. In case of GAK and RIPK2, the reaction was stopped by the addition of 3× SDS sample buffer. After SDS-PAGE separation, phosphorylated substrate proteins were quantified by phosphoimaging. For all other kinases the reactions were terminated by addition of 6 μl 3% (v/v) phosphoric acid and phosphorylated substrates were bound to P30 glass fiber filters to measure ^{33}P incorporation. For EGFR *in vitro* kinase assays, Hela S3 cells were grown to confluence on p15 dishes. Lysates were prepared with 750 μl Triton X-100 lysis buffer and precleared by centrifugation[227]. Aliquots of 350 μl of lysate were immunoprecipitated with mAb108.1 and protein G-Sepharose beads for 3 h at 4°C[227]. Beads were washed twice with 300 μl of lysis buffer without additives and twice with 200 μl of kinase buffer. Precipitated EGFRs were then preincubated on ice for 30 min in kinase buffer supplemented with 0.2 mg/ml poly(Glu$_4$Tyr) and different gefitinib concentrations. Kinase reactions were started by the addition of 0.1 μM ATP and 1 μCi [γ-^{33}P]ATP and performed for 10 min at 30°C in a total volume of 50 μl before the addition of 12 μl 3% (v/v) phosphoric acid and measuring ^{33}P incorporation into filter-bound substrate. For all kinases, the IC$_{50}$ values were then determined using SigmaPlot. IC$_{50} \cong K_d$ for the analyzed kinases, as the ATP concentration used in all assays (0.1 μM) was considerably lower than the K$_M$ values of the analyzed kinases for ATP[233].

2.8   Cellular CD11b staining for FACS analysis

To assess myelocytic differentiation upon kinase inhibitor treatment, KG-1 cells were seeded in 12-well plates at a density of 10^5 cells/ml in regular medium and treated with 1 μM, 5 μM and 10 μM erlotinib or gefitinib or an identical volume of DMSO solvent (0.05% v/v) as control. After four days cultivation, cells were washed (5 min centrifugation with 400 g at 4°C, resuspension in 200 μl ice cold FACS buffer) and thereby transferred to 96-well plates. Cells were centrifuged and the pellet was resuspended in 100 μl FACS buffer containing 0.1% α-FITC-CD11b antibody (v/v). In parallel, a DMSO control was incubated with 100 μl 0.4% α-VSV isotype control antibody in FACS buffer (v/v). After 1 h incubation, stained cells were washed three times witch FACS buffer and immediately measured by flow cytometry. Measurements of the FITC signal were performed on live cells, which were gated on the basis of forward and side scatter patterns, using excitation at 488 nm and detection of fluorescence emission at 518 nm (FL-1 channel). Data were further analyzed BD CellQuest Pro software.

2.9   Cell viability assay

The effect of kinase inhibitor treatment on cellular viability was measured with the colorimetric MTT assay. In that assay, cellular metabolic activity is evaluated on the basis of NAD(P)H-dependent oxidoreductase activity[234]. For that purpose, 10^5 cells/ml KG-1 cells were seeded in 12-well plates in regular medium and treated with 1 μM, 5 μM and 10 μM erlotinib, gefitinib or an identical volume of DMSO solvent (0.05% v/v) as control. After 72 h of cultivation, MTT solution at a final concentration of 1 mg/ml was added to each well. The plates were incubated for 2 h in an incubator at 37°C and during that period yellowish MTT dye is reduced to a purple formazan, which was subsequently solubilized by adding stop-solution and absorbance was recorded with an ELISA reader at 570 nm.

2.10   Mass spectrometric analysis

LC-MS analyses were conducted on a LTQ-Orbitrap hybrid mass spectrometer connected to an Agilent 1100 nanoscale capillary liquid chromatography system by a nanoelectrospray ion source as described previously[130,235]. In brief, samples were loaded on a 15 cm reversed-phase, fused silica capillary column with 75 μm inner diameter, packed in-house with 3 μm ReproSil-AQ Pur C18 beads. Peptides were separated in 140 min LC-MS runs using a gradient ranging from 5% to 40% ACN in 0.5% acetic acid at a flow rate of 250 nl/min. Eluting peptides were directly electrosprayed into the LTQ-Orbitrap mass spectrometer, which was operated with Xcalibur 2.0 in the data-dependent mode to automatically switch between full scan MS and MS/MS acquisition in the positive ion mode essentially as described[235]. Survey MS spectra (from m/z 300–2000) were acquired in the orbitrap mass analyzer with resolution of 60,000 at m/z 400 after accumulation to a target value of 1,000,000 charges in the linear ion trap. The 10 (phosphoproteomics analysis) or 5 (chemical proteomics analysis) most intense peptide ions were isolated, fragmented and analyzed in the LTQ part of the instrument. For phosphoproteomics experiments multi-stage activation was enabled to trigger further fragmentation of phosphopeptide-derived neutral loss species at 97.97, 48.99, or 32.66 m/z below the precursor ion[130,193]. For all measurements with the orbitrap detector, a lock-mass strategy was used for internal calibration as described[110]. Selected mass spectrometric conditions were: spray voltage 2.4 kV; no sheath and auxiliary gas flow; heated capillary temperature 150 °C; normalized collision energy 35% for multistage activation (MSA) in LTQ. The ion selection threshold was 500 counts for MS/MS. An activation parameter q of 0.25 and an activation time of 30 ms were used for MS/MS acquisitions in the LTQ.

2.11 Processing of MS data

2.11.1 MaxQuant

MS raw files were collectively processed with the MaxQuant software suite, which extracts peak lists, performs SILAC-based quantification, estimates false positive rates, assembles peptides to protein groups and performs phosphorylation site assignment as described before[236]. For the phosphoproteomics raw data version 1.0.13.12 was used and for the chemical proteomics files version 1.0.12.0. Using the Mascot search engine (Matrix Science, version 2.2.04) peak lists were searched against a concatenated forward and reverse version of the human International Protein Index (IPI) database version 3.37 with 69,141 protein entries as well as frequently appearing contaminants such as porcine trypsin, human keratins and Lys-C. Carbamidomethyl cysteine was set as fixed modification, oxidized methionine, N-pyroglutamate, N-pyrocysteine, N-terminal acetylation of proteins were permitted as variable modifications. In case of the phosphoproteomics study also phosphorylation of serine, threonine, and tyrosine were included. In SILAC-based triplets detected by the MaxQuant pre-search routine Arg^6, Arg^{10}, Lys^4, and Lys^8 were searched as additional fixed modifications. If the SILAC state of the precursor ion could not be determined spectra were searched with Arg^6, Arg^{10}, Lys^4, and Lys^8 as variable modifications. The mass tolerances of the precursor were set to 7 ppm for phosphoproteomic analyses and 5 ppm chemical proteomics. For fragment ions peaks in MS/MS mass deviations of 0.5 Da were allowed. The minimum required peptide length was set to six amino acids with up to three missed cleavages (enzyme specificity was set to trypsin) and three isotopically labeled amino acids were allowed per peptide. Searches against the aforementioned database were filtered for an estimated false-discovery rate of less than 1% (protein and peptide identifications) and an individual posterior error probability (PEP) of peptides of less than 0.1[236]. Peptide PEPs were determined by generating Mascot score and peptide-length-dependent histograms for both the forward and the reverse hits and then deriving the probability of a false identification for a given top-scoring peptide using Bayes' theorem. The PEPs of peptides belonging to the same proteins were then multiplied. Each peptide sequence was considered only once with the lowest PEP determined in case of multiple sequencing of the same isotopic pattern or of peptide species with different SILAC, charge or modification states.

2.11.2 Data analysis

2.11.2.1 Phosphoproteomics

For site-specific phosphorylation analysis only serine, threonine or tyrosine assignments with a localization probability of at least 0.75 (class I sites) were considered. For further quantitative analysis, phosphorylation site SILAC ratios (gefitinib versus control treatment and erlotinib versus control treatment) normalized by MaxQuant were averaged for each biological replicate experiment in case of quantification in both technical replicate analyses. Subsequently, phosphorylation sites for which SILAC ratios were measured in at least two out of the three biological replicate experiments were analyzed with the unpaired rank product algorithm implemented in the MultiExperiment Viewer software to identify statistically significant and biologically reproducible phosphorylation changes upon kinase inhibitor treatment[237]. The global rank algorithm performs probability-based determinations of so-called rank products that further permit the application of an FDR threshold, which was set to 5% in our quantitative analysis and filtered for phosphosites up to the corresponding q values of 0.05 in the reported list of significant phosphorylation changes.

Enrichment analysis for Gene Ontology (GO) biological process terms in identified phosphoproteins was carried out with the DAVID gene classification tool applying an expression analysis systematic explorer (EASE) score set to $P < 0.05$[238,239].

For network visualization, IPI identifiers of proteins harboring significantly downregulated phosphosites upon either gefitinib and/or and erlotinib treatment were converted into Ensembl entries using BioMart and subsequently uploaded to the web-based search tool for the retrieval of interacting genes/proteins (STRING)[240]. Only interactions with a confidence score of at least 0.5 and exclusively based on experimental or database information were considered for protein network visualization with the Cytoscape software (version 2.7)[240].

Phosphorylation motifs that were significantly overrepresented among the identified class I sites from KG-1 cells were identified with the Motif-X algorithm[241]. Modified serine, threonine and tyrosine residues were centered and extended 6 amino acids on each side, fed into the online-algorithm (foreground dataset) and therein compared with all identified motifs of the respective modified residue as background. The minimal number of occurrences and significance were set to 20 and 10^{-6} respectively.

2.11.2.2 Chemical proteomics

In addition to the FDR threshold applied for protein identification, proteins were only included if they were identified with at least two peptides (of which one was required to be unique for the protein) and

quantified if at least one quantifiable SILAC pair was associated with them. Outliers were not removed as protein ratios were calculated as the median instead of the average of all peptide ratios. For peptides shared among different identified proteins, SILAC ratios were only considered for the ratio of the protein identified with the highest number of unique peptides. Protein ratios for the different *in vitro* association experiments were corrected for the initial SILAC pooling ratio, which was determined from the median of protein ratios in pooled SILAC-encoded cell extracts. Quantified proteins were first sorted according to the averaged ratio of protein bound to control beads without inhibitor versus protein bound to inhibitor beads. Only proteins with a background ratio of less than 0.2 were considered further. Subsequently, proteins for which the ratios of binding in the second versus the first round of incubation with inhibitor beads were available as duplicates were taken with their averaged values for further data evaluation (in case this averaged value was less than one). Likely contaminants exhibiting an inverted ratio in the replicate experiments were excluded from further analysis. The ratio r of target protein binding in the second versus the first round of *in vitro* association was used to calculate the respective dissociation constants $K_d(inhibitor_{im})$ for the immobilized inhibitor according to the equation

$$K_d(inhibitor_{im}) = [inhibitor_{im}] \times r / (1-r)$$

in which $[inhibitor_{im}]$ was the concentration of immobilized inhibitor in the final volume of the binding assay. Moreover, ratios of resin bound targets after 5 h versus 2.5 h and for binding from 1 mg compared to 3 mg of starting extracts were determined to evaluate to which extent equilibrium binding conditions were satisfied in the *in vitro* association experiments.

For *in vitro* association experiments involving immobilized peptide baits, data processing and K_d determination was performed in the same way as described for small-molecule inhibitor resins.

In parallel, the pooling error-corrected ratios from the competition experiments using AX14596 (VI16742) resin and different gefitinib (SB203580) concentrations were used to determine IC_{50} values for half maximal inhibition of binding for targets, for which K_d values for immobilized ligand was available. The corresponding ratios from duplicate experiments were averaged.

Using the equation for one site saturation with maximum binding in the absence of inhibitor set to 100%, target-specific IC_{50} values were determined with the ligand binding module of SigmaPlot. Only target proteins were considered with ratios of 0.6 or less at the highest concentration of free inhibitor compared to the control incubation. Subsequently, target K_d values for free inhibitors were calculated according to the Cheng-Prusoff equation[242]:

$$K_d(inhibitor_{free}) = K_d(inhibitor_{im}) / ([inhibitor_{im}] + K_d(inhibitor_{im})) \times IC_{50}(inhibitor_{free})$$

For enrichment analysis of GO categories, BiNGO together with the Cytoscape plugin was used to identify statistically overrepresented GO molecular function terms compared to a reference dataset consisting of all IPI database entries and their respective GO identifiers essentially as described[243-245].

III   Results

1. Proteomics strategy for quantitative protein interaction profiling

As mentioned earlier, target profiling of small organic molecule drugs is of particular interest for basic research as well as for drug discovery efforts. For the former application it can be informative to unveil how these molecules give rise to a specific phenotype by targeting distinct protein activities in complex biological systems. Moreover, in the context of drug discovery and development, it is of great importance to ideally identify the complete array of targets to promote drug efficacy, reduce off-target-related side effects and to overcome drug resistance[246,247]. A comprehensively identified target spectrum might also reveal additional therapeutic potential for clinically approved drugs as well as for drug candidates. The significance of such profiling methods emerges especially when working with small molecules directed against a structurally conserved catalytic domain shared within a large enzyme superfamily such as protein kinases. The advent of high-resolution MS-based proteomics in combination with isotopic labeling of entire proteomes paved the way for large-scale detection of target proteins in chemical proteomics approaches (see section I4.4.2). Exploiting quantitative information not only for discriminating between specific and background binding, but also for deducing binding parameters would enhance chemical proteomics to an even more powerful technique superior to conventional *in vitro*-based methodologies with their inherent limitations.

Low-molecular-weight antagonists of protein kinases are of particular interest for the detailed qualitative and quantitative characterization of their interactomes[148,160]. Moreover, the rather strong affinity for their target protein class confers applicability for affinity chromatography-based approaches. For the concepts established in this work, the clinically approved kinase inhibitor gefitinib was employed. This drug has been developed as an epidermal growth factor receptor (EGFR) antagonist for the treatment of non-small cell lung cancer (Figure 8)[248,249]. Furthermore, AX14596, a derivative of gefitinib, was used for the purpose of immobilization to Sepharose beads (Figure 8)[148].
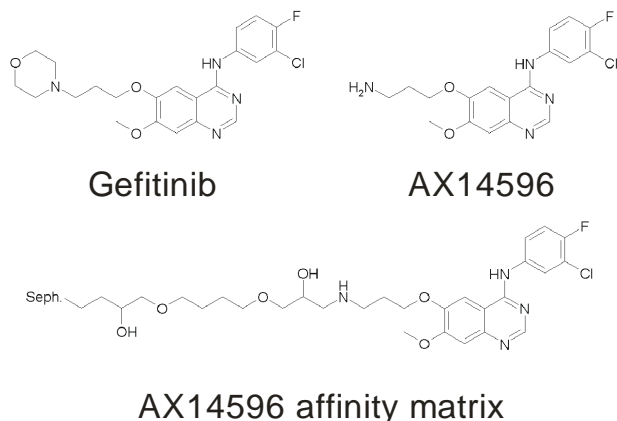
Figure 8: Structural formula of gefitinib, its derivative AX14596 and the immobilized form of AX14596 on Sepharose beads (Seph.)[148].

The replacement of the morpholino group at the gefitinib molecule by a primary amine yields the AX14596 molecule. Via this amino group AX14696 can be coupled on epoxy-activated Sepharose beads, while keeping the correct spatial orientation that enables, together with a long hydrophilic spacer arm, binding within the ATP binding pocket of the kinase target (Figure 8)[148]. In order to quantify the density of the immobilized ligand on the surface of the beads an indirect Uv/Vis spectrometric method was used. Thereby, an aliquot of the AX14596 solution (here 2.5 mM) that was exposed later to the epoxy-activated Sepharose beads was diluted on a $\log_2$ series to generate five dilutions. Each of the dilutions was measured in duplicates with a Uv/Vis photometer on a defined wavelength of 336 nm at which the substance exhibits an absorption maximum. The obtained data were plotted and the corresponding regression line was fitted using the equation $y = 0.9837x + 0.0073$, with a determination coefficient of $r^2 = 0.99$ (Figure 9). After overnight incubation of the beads with the coupling solution, an aliquot of the supernatant was taken and the absorption was measured at 336 nm. By insertion of the absorption value $0.95 \pm 4.25*10^{-4}$ into the equation obtained after linear regression, the concentration of AX14596 could be calculated. The difference between the AX14596 concentrations before and after the coupling reactions was assumed to result from covalent binding to the beads. In this example it was 0.97 mM. Considering that in this batch two volumes of solution were used for one volume of beads, the concentration of ligand on the undiluted beads was 3.06 mM, according to following calculation (2.5 mM - 0.97 mM)*2.
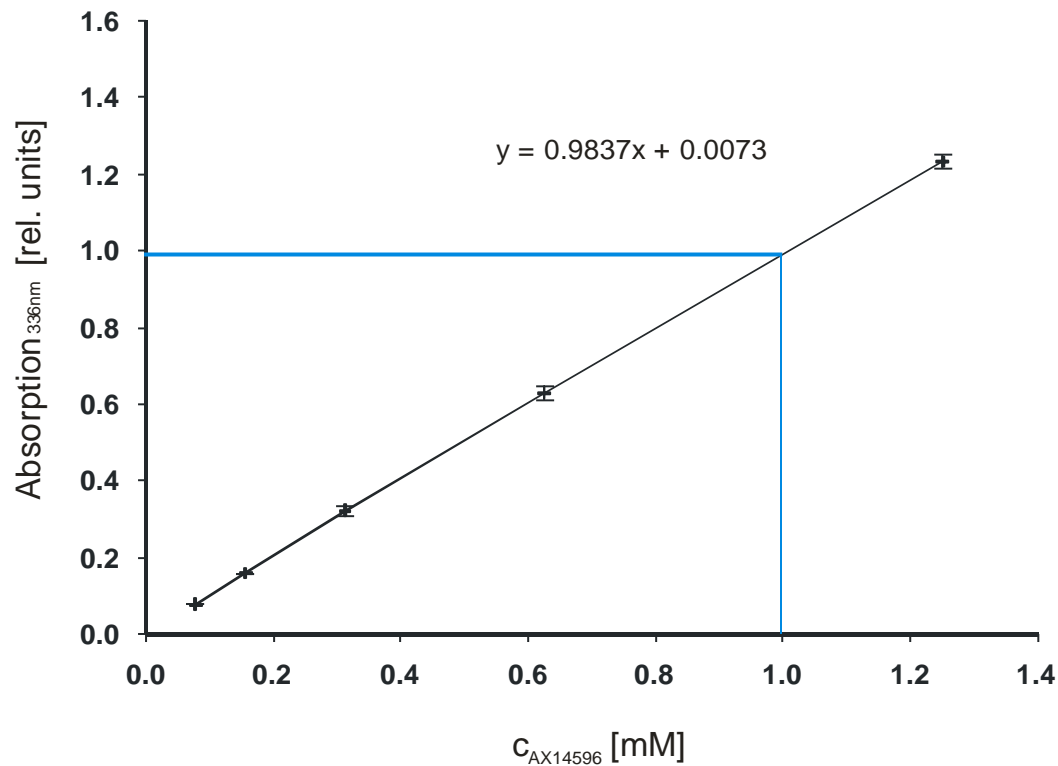
Figure 9: Concentration series of AX14596 with their absorption values. The equation of the regression line is indicated as well as concentration of the corresponding absorption (see text) measured after the coupling reaction (blue lines).

1.1   Conceptual outline of the quantitative *in vitro* association strategy for target affinity determinations

The assessment of cellular protein target affinities was based on two successive batch enrichments from whole cell lysates with affinity ligands immobilized on an insoluble resin. Cell lysate was incubated with AX14596-coupled beads and, after this first round, the same lysate was exposed to a fresh batch of these beads. The protein eluates of both incubations were subsequently compared in terms of bound target proportions to directly evaluate their affinities. This was possible due to the circumstance that the relative amount of AX14596-bound target of the second incubation round versus the first round, expressed as ratio *r*, is equivalent to the proportion of target that is not attached to the resin. The rationale behind these two consecutive *in vitro* association experiments is as follows (Figure 10): After the first incubation round the amount of a target protein in the lysate is reduced by the resin-bound portion according to its affinity.

In a second round of incubation, the remnant of that particular protein in the supernatant is depleted to the identical proportion as in the previous round. The quantitative comparison of the resin-bound protein fractions of both rounds, namely r, provides the share of a target that is not attached to the inhibitor beads. This context is exemplified by two interactors in Figure 10. One of them, target B, exhibits high binding affinity to the resin with 90% binding in the first incubation round, the other, target A, with moderate binding affinity and 50% binding. As a consequence, 10% and 50%, respectively, of the target quantities are left in the lysate. These information is, however, not accessible, because the portion in the supernatant cannot be determined. The reason for that lies in the high complexity of the lysate that makes a comprehensive quantitative analysis nearly impossible. Yet, a second *in vitro* association experiment with the target-depleted supernatant can provide this information. Thereby, of the remaining target quantities, again 90% of the residual 10% of target B are bound, i.e. 9% of the initial quantity of target B. For target A, 50% of the residual 50% bind to the AX14596 beads, i.e. 25% of the initial quantity of target A. If one compares the relative quantities bound to the beads in each round of the *in vitro* association, one will get ratios of 0.1, 9% of divided by 90%, and 0.5, 25% divided by 50%, respectively. These ratios r match, however, exactly the target proportions that are left in the supernatant after each *in vitro* association (Figure 10). Thus, an r of 0.1 for target B indicates that 10% of this target is left in the supernatant after such an *in vitro* association experiment. An r of 0.5, like for target A indicates that 50% do not bind to the inhibitor beads.
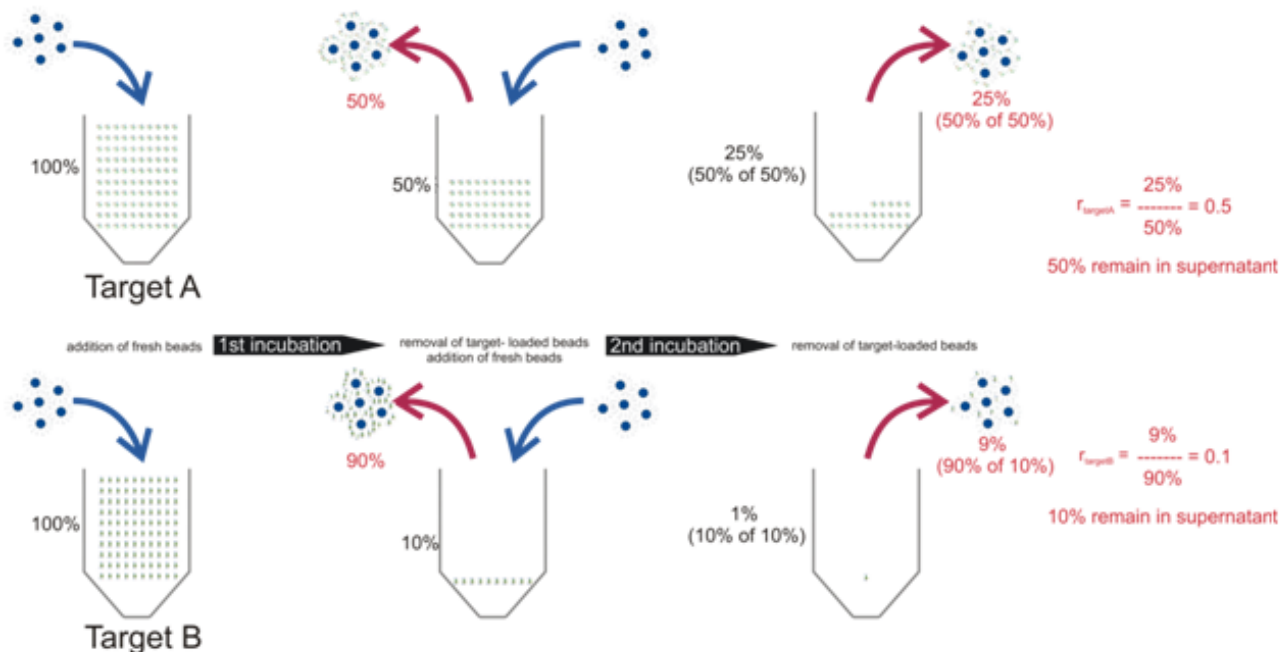
Figure 10: Idea behind the concept of quantitative proteomic profiling with immobilized small molecule inhibitors. The principle is exemplified on the basis of a moderate affinity target (above) and a high affinity target (below).

1.2 Quantitative chemical proteomics profiling of gefitinib

1.2.1 Affinity chromatography with immobilized AX14596 as capturing molecule

In order to bring these considerations into effect, quantitative mass spectrometry on the basis of stable isotope labeling by amino acids ins cell culture (SILAC) was employed (see section I4.3)[126]. This metabolic labeling approach represents the starting point for the work flow as depicted in Figure 11a. Hela S3 cells were either grown in media containing normal arginine and lysine (Arg^0, Lys^0; "light" labeling) or combinations of heavier isotopic variants of the two amino acids (Arg^6, Lys^4; "medium" labeling, Arg^{10}, Lys^8; "heavy" labeling). Upon labeling, the light labeled lysate was incubated with beads coupled with AX14596, the medium extract was added to control resin devoid of ligand. The third sample was obtained in two steps: Upon incubation of heavy lysate with AX14596 resin, the supernatant was subjected to a second incubation with the same amount of inhibitor beads. Bound proteins obtained by these *in vitro* association experiments were eluted from each batch with Laemmli buffer and thereafter eluates were combined. Upon separation by gel electrophoresis, an in-gel digestion with trypsin was carried out and

the resulting peptides were extracted. After further processing, the peptide intensities were measured with the LTQ-Orbitrap mass spectrometer (see section I4.2)[110]. Due to their equal physicochemical properties, differently labeled peptides with identical sequence and charge coelute from the nano-LC column and their ion intensities appear in triplets with distinct mass shifts. Each part of the triplet originates from one of the previous batches and it differs only by its mass-to-charge (m/z) ratio due to the incorporation of diverse arginine and lysine variants[126,134]. Peptides were identified by database searching and quantitatively assigned to with the aid of the MaxQuant software for protein identification and quantification[236]. In the course of data processing, ratios of the retained proteins were calculated by the ratios of underlying SILAC peptide ion intensities.

Out of the three intensities obtained here, one can extract important information about the resin-bound proteins in two different ways: One crucial aspect is about the specificity of the attached protein. This is expressed by the ratio of protein bound on the inhibitor-coupled beads versus the control beads. Proteins for which this ratio was greater or equal than five were considered as specific binders. Accordingly, proteins were considered as background binders in case they were eluted from the ligand-free beads with signal intensities of Arg^6 and/or Lys^4-labeled peptides of more than one fifth of these of identical Arg^0 and/or Lys^0-labeled peptides eluted from AX14596-coupled beads. The second feature that can be deduced from that experiment provides information on target affinities to the inhibitor matrix. Quantitative comparison of target proteins binding to inhibitor beads during the second against first incubation round generated the above described ratio r (see section III1.1). To be exact, r is obtained by division of peptide intensities labeled with the heavy Arg^{10} and/or Lys^8 by intensities of the corresponding peptides with light isotopic Arg^0 and/or Lys^0 variants. The ratio r for specific binders was used to directly calculate the target-specific dissociation constants for the immobilized AX14596, $K_d(AX_{im})$. To do this, one has to consider that - as mentioned above (Figure 10) - r corresponds to the portion of unbound, and thus $1-r$ to bound target portion. Together with the apparent concentration of immobilized AX14596, $[AX_{im}]$ which is inferred from the photometrical analysis upon the coupling reaction, this value is inserted into the equation of the law of mass action for the target binding reaction (Figure 9, Figure 11).
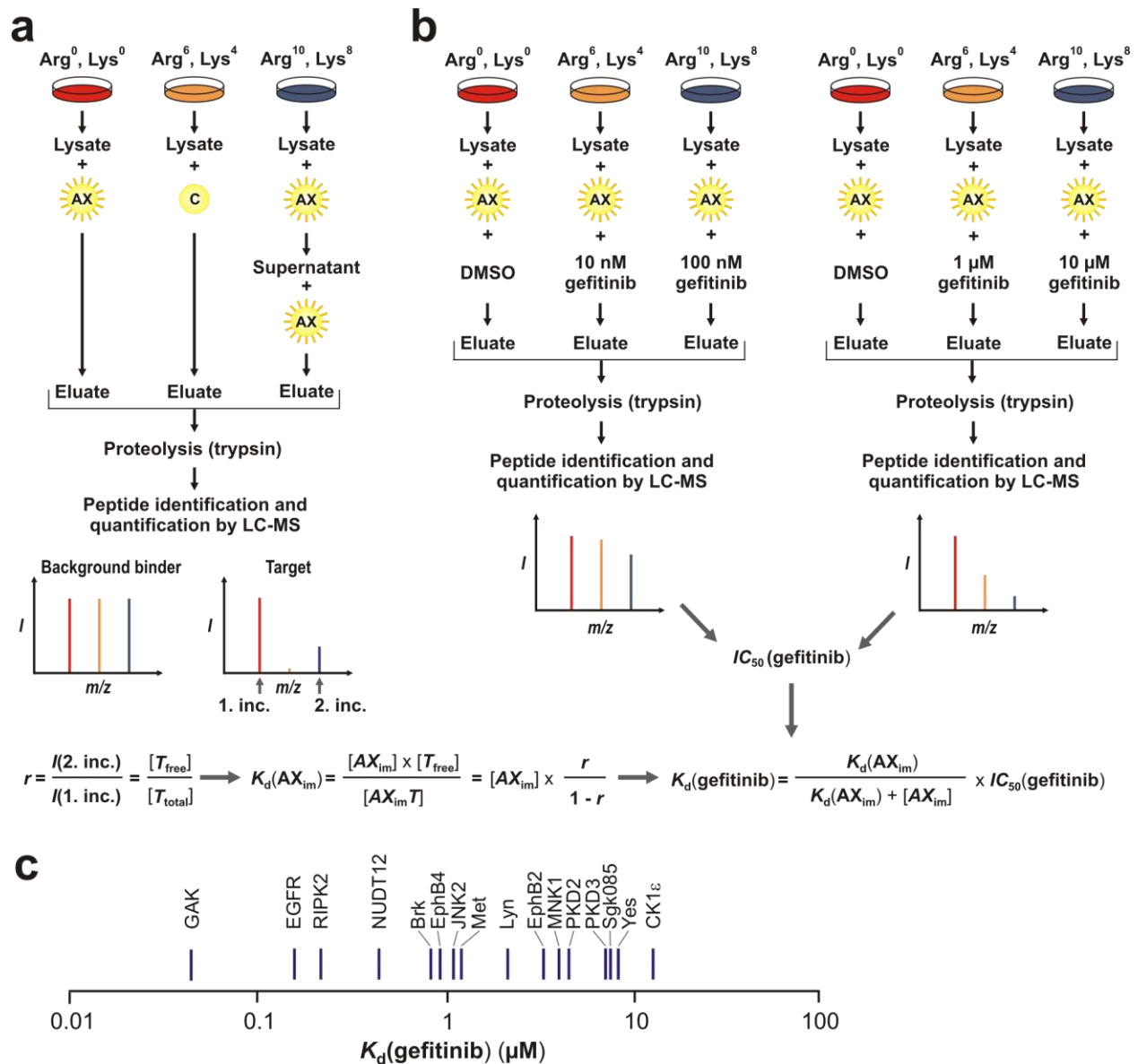
Figure 11: Overview of the chemical proteomics strategy with immobilized AX14596. Depicted are the sequential enrichment (a) and the competition with increasing concentrations of gefitinib (b). The target-specific data obtained from both modules as well as the knowledge of the concentration of immobilized AX14596 sufficed to calculate dissociation constants for free gefitinib K_d(gefitinib) according to the equation of Cheng and Prusoff[242](c).

Theoretically, contamination by proteins coming from outside the cell lysate can occur during sample preparation and might be recognized as bound protein. Such proteins exclusively appear as light labeled proteins comprised of normal arginines and lysines. To be able to sort out such contaminants and to generate more accurate affinity values, the experiments were performed in duplicates with an inverted labeling scheme. For the replicate, the light labeled lysate was incubated twice with AX14596 beads, the medium with control beads as before, and the heavy lysate was added to AX14596 beads for one incubation round (Figure 12a). Both the specificity ratios as well as the determination of r were averaged and used

for further calculations or deliberations (Figure 12b). Indeed, the data produced with the AX14596 were consistent over both replicates in case of specific and more affine interactors (Figure 12c).
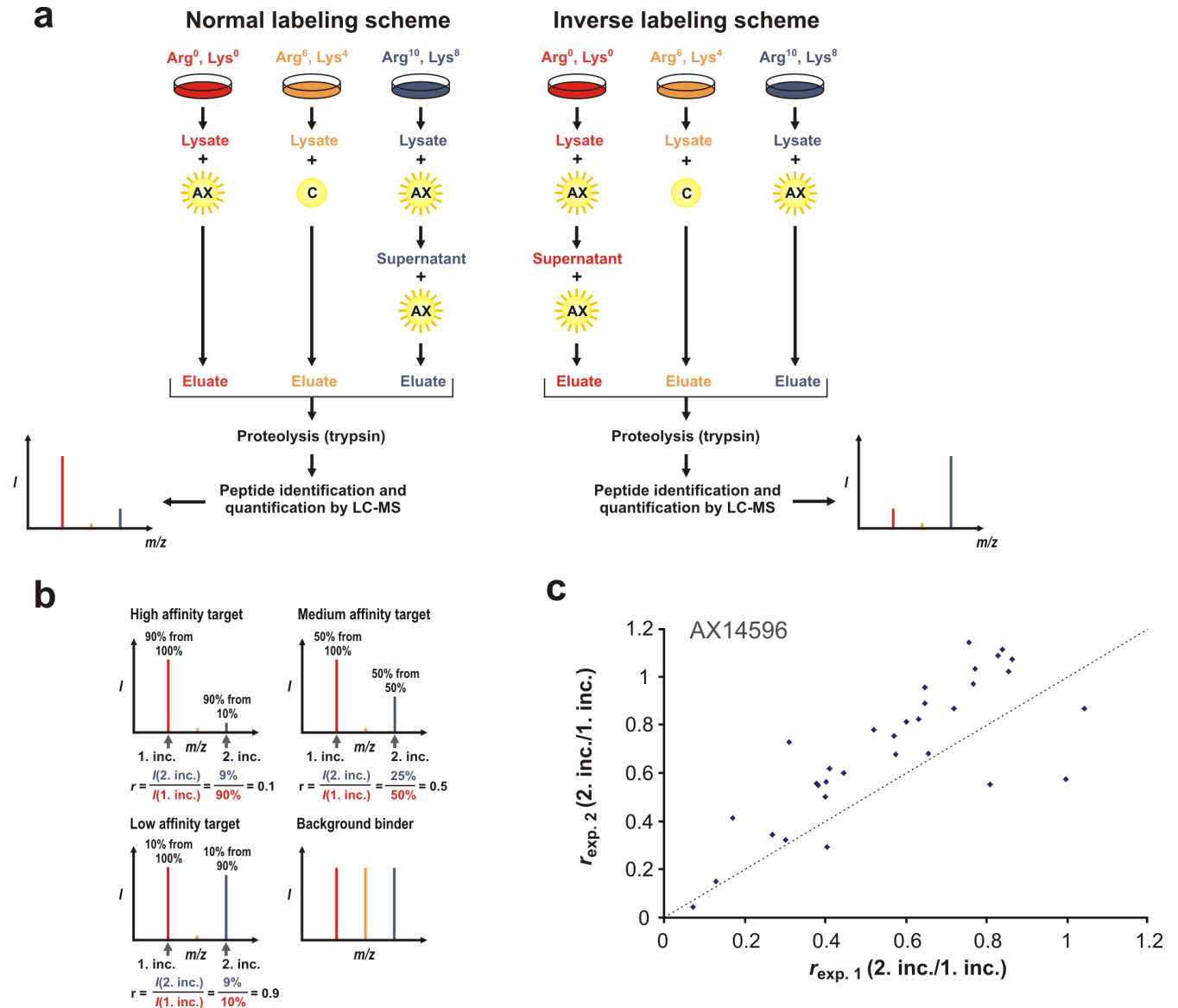
Figure 12: Schematic overview of quantitative target binding data for reproducibility analyses. SILAC-based experiments to determine the specificity and affinity of target proteins from Hela S3 cell extracts to immobilized AX14596 were conducted in duplicates in a crossed-over manner in order to verify reproducibility and to eliminate false-positive target identifications (a). Examples of protein binding with varying degrees of affinity and specificity are shown (b). These characteristics are expressed by SILAC target ratios (*see text*) as an implementation of the gedankenexperiment in Figure 10.   Ratios of target protein amounts retained in the second versus the first round of binding to AX14596 beads are compared for the SILAC experiments done according to the inverse (experiment 1, x-axis) and normal (experiment 2, y-axis) labeling scheme (c). The dotted line indicates identical ratios in replicate experiments.

Additional quality controlling was necessary to deduce valid affinity parameters. As the calculation of dissociation constants was based on the assumption of equilibrium conditions with regard to target binding, monitoring on the individual target level was facilitated by the implementation of a supplementary experimental setup, which was also SILAC-based (Figure 13). In this control experiment light labeled

lysate was incubated together with AX14596 beads for 2.5 h, which was the standard incubation time, likewise heavy labeled lysate, yet twice as long for 5 h (Figure 13a). The combined eluates of this double SILAC experiment were treated and analyzed in an analogous manner as described before. If the standard incubation time already sufficed to reach the binding equilibrium, it was assumed that the target ratio of 5 h (Arg^{10} and/or Lys^8-labeled peptides) versus 2.5 h (Arg^0 and/or Lys^0-labeled peptides) incubation time is close to 1. This filtering criterion was complemented with another important supposition that had to be fulfilled to ensure full validity of determineddissociation constants. Only if the ligand is present in molar excess over its cellular target proteins the formula for the dissociation constant remains valid. In that case, the capture reagent was not saturated by is binding proteins. To address that issue in an additional experiment, Arg^0 and Lys^0-labeled lysate of the standard protein content of 3 mg per batch was incubated with AX14596 resin and, in parallel, one third of that, namely 1 mg, with the heavy Arg^{10}/Lys^8-labeled extract. Under non-saturation conditions the ratio of specifically binding targets of light- versus heavy-label origin approached three (Figure 13b). Specific binders that complied with equilibrium binding and exhibited attachment beneath saturation were considered as appropriate for K_d calculations.

a
Control equilibrium binding

b
Control ligand concentration
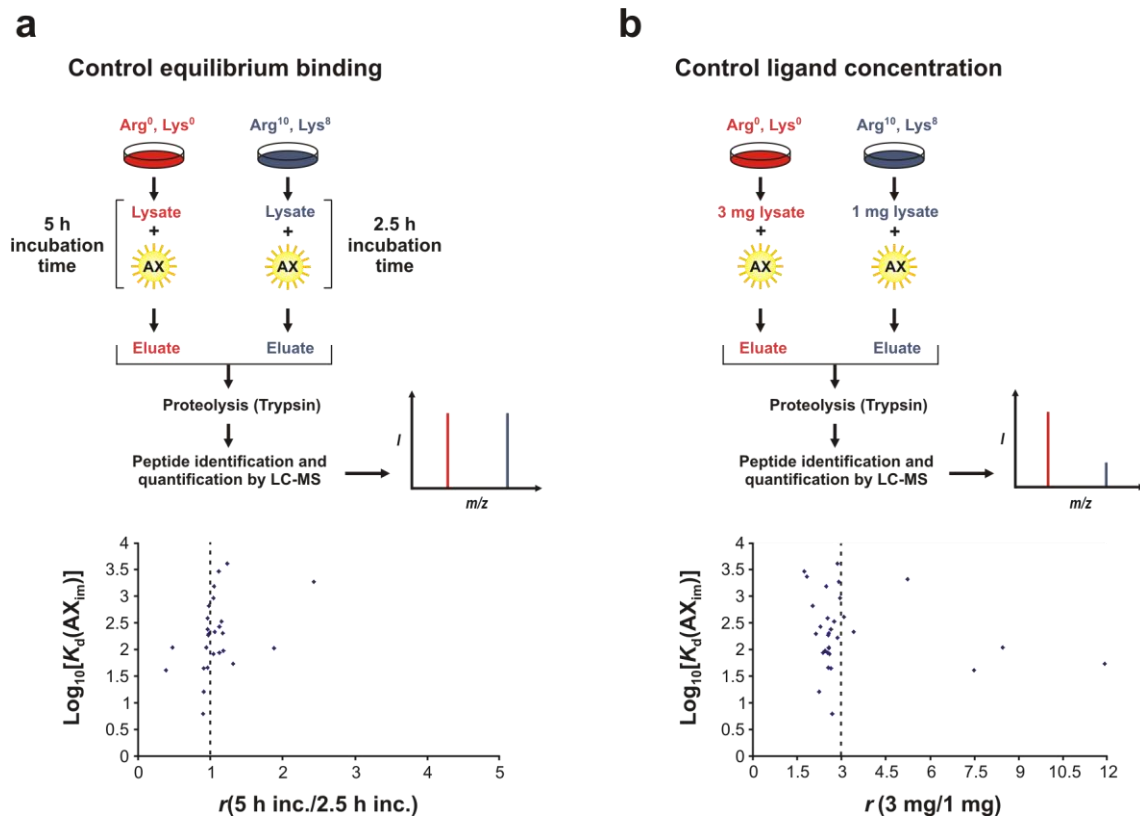
Figure 13: Control experiments for K_d measurements for AX14596 resin. For specific targets binding on immobilized AX14596 after standardized 2.5 h incubation versus 5 h in a SILAC based experiment was compared in order to assess whether binding equilibria have been reached after 2.5 h (upper panel of (a)). These ratios were plotted against $\log_{10}$ transformed values of the $K_d(AX_{im})$. The majority of targets showed equal binding behavior irrespective of the intervals lengths, indicating that binding equilibria had been reached after 2.5 h (lower panel of (a)). The SILAC based control experiment to determine whether immobilized AX14596 is present in molar excess over its cellular target proteins is depicted (upper panel of (b)). The use of 3 mg protein lysate per *in vitro* association, as standard, is compared with 1 mg. Most of the specific binders of AX14596 exhibit a ratio close to three, reflecting the ligand not being saturated by its binders.

In total, 1027 proteins were identified of which 76 showed specific binding according to our criteria (data not shown). In order to provide substantial data, only those targets came into consideration for affinity calculations where the average of two specificity and affinity ratios were below the thresholds. In addition, the individual values had to be in consistence with each other. Thus, these 76 targets were characterized by in average fivefold higher intensities of AX14596-bound proteins against those derived from proteins attached to control resin. Moreover, target affinity ratios for AX14596 were examined for their repeatability as mentioned above and, indeed, for specific targets a good agreement among each other was seen (Figure 12c). Of these 76, 32 exhibited an average affinity ratio *r* clearly less than one, and out of those meaningful values for $K_d(AX_{im})$ could be calculated. In Table 2 the specific interactors with AX14596 showing considerable affinity towards the resin are listed. The micromolar value range of the binding constants lies between one-digit and four-digit figures. The majority, to be precise 20, were protein kinases, both serine/threonine as well as tyrosine kinases. In agreement with earlier findings, most of

them have been reported as interactors with AX14596, which underscores the pertinence of our conception[148,158]. RIPK2 exhibited the lowest K_d for AX14596 of about 6 µM and has been identified together with GAK ($K_d(AX_{im}) = 82.05$ µM) to be rather promiscuous binders to several structurally divergent classes of kinase inhibitors[148,155,250]. Another top target was the EGF receptor. The EGFR demonstrated proof of principle, though it does not bind with highest affinity within the target spectrum. Moreover, other protein kinases showed significant binding towards AX14596 confirming the overall ranking obtained in a previous proteomics study, e.g. YES ($K_d(AX_{im}) = 658.37$ µM), BRK ($K_d(AX_{im}) = 45.43$ µM) and JNK2 ($K_d(AX_{im}) = 109.65$ µM), although the affinities were not categorized therein[148]. Other kinase targets, which have not been reported as specific interactors of AX14596 yet, were the uncharacterized serine/threonine kinase SgK085, the serine/threonine kinase haspin homolog ALK2 and serine/threonine kinase D3 PKD3. Apart from the identified protein kinases, another 12 targets were found to interact with the AX14596 matrix. All of which, with the exception of the aminopeptidase bleomycin hydrolase BLMH, share reported nucleotide-binding properties[251]. These proteins were shown to either use nucleotides catalytically with regard to their enzyme function, e.g. the peroxisomal NADH pyrophosphatase NUDT12 and the Nicotinamide phosphoribosyltransferase NAMPT, or toat least bind to these molecules, such as Small nuclear ribonucleoprotein G SNRPG[248,252,253]. Notably, NUDT12, an enzyme involved in the cellular oxidative metabolism, showed a particularly low $K_d(AX_{im})$ of 16.14 µM, which, in terms of affinity, surpassed all of the genuine protein kinase targets with the only exception of RIPK2.

Remarkably, the presence of a molar excess of the immobilized ligand over its cellular target proteins could be substantiated by the control experiment. In fact, when plotting SILAC ratios of target proteins that originated from the incubation of 3 mg versus 1 mg lysate against their $\log_{10}$ transformed $K_d(AX_{im})$ values, almost all binding ratios originating from specific targets reflected the initial protein amounts (Figure 13b). Under these reaction conditions the immobilized AX14596 ligand obviously outnumbered the target protein quantities and, in effect, the accessible ligand molecules are not fully occupied by its binding proteins, but just slightly reduced. Figure 13a displays the outcome of the second control experiment addressing the presence of binding equilibria between ligands and binding partners. Here, target protein binding was compared for the standard incubation period of 2.5 h with an extended interval of 5 h. For that, the SILAC target protein ratio was generated and plotted against the $\log_{10}$ transformed dissociation constants for immobilized AX14596. In fact, the ratio was always close to one with only scattered exceptions, indicating that binding equilibrium had been reached already after 2.5 h as evidenced by unchanged binding after additional 2.5 h.

The results of both control experiments confirmed the chosen vertices for the *in vitro* association experiments. Apparently, under binding equilibrium conditions, the amount of 3 mg protein lysate gave good

detection sensitivity and nevertheless assures rather low occupancy of binding sites on the inhibitor resin. Still, some outliers were detectable, yet exclusively among the non-kinase targets.

1.2.2 Competition with "free" gefitinib

AX14596 was used to have an immobilizeable gefitinib in hands through which - based on the above described setup - it is possible to directly delineate affinities for protein targets. Nevertheless, this approach harbors limitations. For instance, the chemical modification of gefitinib and the fact that it was used in an immobilized form may exert an effect on its target affinities. For instance, its structural properties were optimized in order to exhibit high affinity against the primary target, the EGF receptor, and in contrast to gefitinib, AX14596 is lacking the morpholine ring. Even though the right orientation of the ligand is ensured to protrude into the ATP-binding pocket of the target kinase, it is possible that the absence of this ring plus the presence of an additional aliphatic linker might affect the binding properties in comparison to the parental drug. In addition, it is just as conceivable that the immobilized compound might not be always exposed properly on the surface of the beads obscuring the actual concentration of functional inhibitor as a determining factor for affinity calculations. Similarly, the lack of flexibility may have an effect upon optimal binding. In terms on binding kinetics, the reduced mobility in comparison to the free ligand may also lead to deviations regarding the association (on-rates) versus their dissociation (off-rates) kinetics and thus lead to changes of the binding constant. To overcome these drawbacks, the concept was expanded with another module. Free gefitinib was used along with the immobilized AX14596 to compete for their targets present in the cellular extract. In order to examine the effect of increasing free inhibitor concentrations directly, SILAC-based competition experiments were performed (Figure 11b). Therein, lysates of differentially labeled Hela S3 cells were exposed to the AX14596 coupled beads and in parallel to each lysate free gefitinib of defined quantities was added. In each experiment four different gefitinib concentrations, 10, 100, 1,000 and 10,000 nM, were used to compete with the beads for the targets. In combination with a DMSO control, which was used as a common reference, in each of the two experiments two inhibitor concentrations could be applied to exploit the triple SILAC setting (Figure 11b). Thus, for each target peptide, ideally two triplets were measured with the mass spectrometer to infer the portion of bound protein dependent on the gefitinib concentration in comparison with DMSO control. The obtained data points could be used to fit binding curves to calculate target-specific IC_{50} values, which are the gefitinib concentrations values at which 50% of target were displaced from AX14596 beads.

To make sure that the measured binding changes were reproducible, this experiment was conducted twice as two distinct variants. The lysate was either exposed to free inhibitor for 30 min followed by the addition of inhibitor beads for a further 2.5 h or with inverted order, i.e. a 30 min preincubation step with inhibitor beads alone followed by the supplementation of soluble compound (Figure 14). Obviously, it turned out that it made barely any difference if the free inhibitor was exposed to the cell lysate prior to the immobilized AX14596 or *vice versa* (Figure 14). Consistent with binding equilibrium that has been reached under these conditions the order of the added competitor had no impact for specific target proteins. The average over the values obtained from both differentially arranged experiments, first "free" gefitinib plus AX14596 beads and the other way round, were then calculated. On that basis, a binding curve for each target over the different gefitinib concentrations was fitted by regression line calculations in order to determine IC_{50} values for gefitinib, IC_{50}(gefitinib).
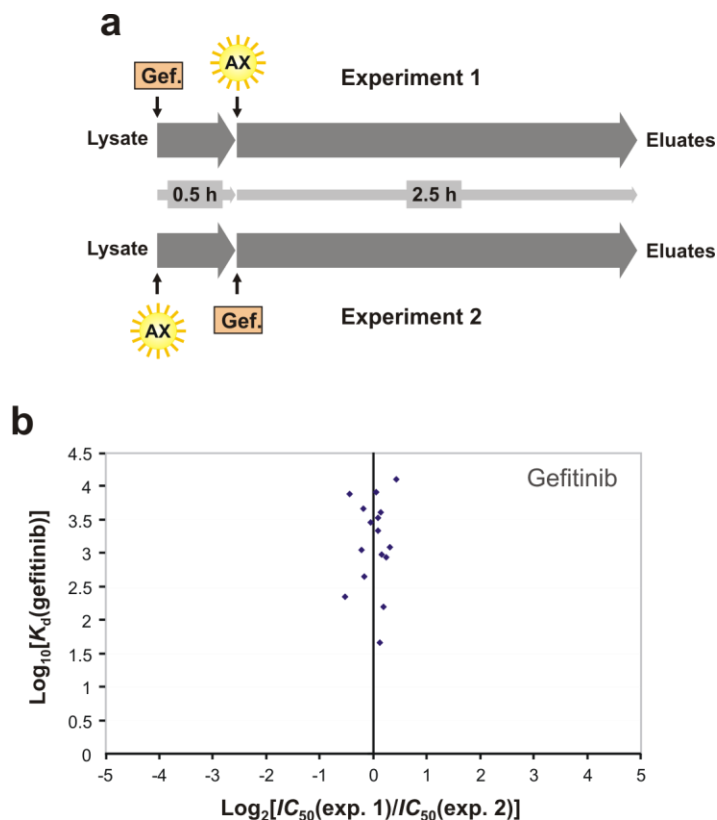
Figure 14: Correlation of target binding data in replicate competition experiments with gefitinib. Competition experiments with different concentrations of "free" gefitinib and immobilized AX14596 were performed in duplicates. Lysate was pre-incubated for 30 min with gefitinib followed the addition of AX14596 beads and further 2.5 h incubation or *vice versa* starting with AX14596 beads for 30 min and subsequent addition of gefitinib for another 2.5 h (a). For each of the replicates, target-specific IC_{50} values were determined, the ratios between both values were $\log_2$ transformed and plotted against the $\log_{10}$ transformed ratios of the calculated target affinities for gefitinib K_d(gefitinib). Equilibrium binding was obvious from the $\log_2$ transformed IC_{50} ratios being close to zero across the whole target affinity range.

These values resembled a relative measure which depends on the concentration of the coupled competitor AX14596 in a modified competitive binding assay. Moreover, together with $K_d(AX_{im})$ determined before,

as well as the concentration of the ligand AX14596 [AX_{im}] it was possible to calculate an absolute target-specific dissociation constant K_d(gefintib) for "free" gefitinib according to Cheng and Prusoff as outlined in Figure 11b[242]. The immobilized inhibitor functions as capture reagent and thus as a reference system with a specific affinity to the target proteins. This affinity is, as seen above, dependent on the concentration of the ligand molecule AX14596. However, this apparent affinity may be shifted due to non-functional and inaccessible ligand molecules. The K_d-calculation for gefitinib evens these limitations out due to the identical capture reference system used in competition experiments.

Table 2: Quantitative chemical proteomic analysis of gefitinib's cellular targets.

Protein Names	Protein Kinase	r (2. inc/1. inc)	$K_d(AX_{im})$ [μM]	Specificity ratio (control/1. incubation)	Ratio 3 mg/1 mg lysate	Ratio 5 h/2.5 h incubation time	IC$_{50}$ (gefitinib) [nM]	K_d (gefitinib) [nM]	IC$_{50}$ ~ K$_d$ [nM], kinase assay (Gefitinib)
Cyclin G-associated kinase	GAK	0.45	82.05	0.04	2.59	1.05	101.2	45.59	35.24
Bleomycin hydrolase		0.35	53.58	0.08	11.91	1.31	223.4	77.89	
Epidermal growth factor receptor precursor	EGFR	0.31	44.48	0.03	2.65	0.90	512.3	157.61	5.58
Receptor-interacting serine/threonine-protein kinase 2	RIPK2	0.06	6.19	0.02	2.68	0.90	3757	218.91	46.12
Peroxisomal NADH pyrophosphatase NUDT12		0.14	16.14	0.04	2.24	0.91	3221	447.35	
Tyrosine-protein kinase 6	BRK	0.31	45.43	0.02	2.56	0.96	2760	861.60	279.50
Ephrin type-B receptor 4 precursor	EphB4	0.71	241.53	0.05	2.65	0.96	1351	955.15	424.30
Mitogen-activated protein kinase 9	JNK2	0.52	109.65	0.03	2.58	0.95	2130	1113.49	5964.67
Hepatocyte growth factor receptor precursor	MET	0.73	266.54	0.06	2.30	1.12	1661	1207.51	5462.33
LYN protein	LYN	0.66	195.32	0.07	2.14	0.98	3237	2140.18	406.85
Acyl-CoA dehydrogenase family member 10		0.52	107.62	0.08	8.45	0.48	5531	2865.59	
Ephrin type-B receptor 2 precursor	EphB2	0.68	213.19	0.04	3.41	1.06	4980	3388.83	
MAP kinase-interacting serine/threonine-protein kinase 1	MNK1	0.90	921.63	0.04	2.94	1.05	4429	3995.09	
Serine/threonine-protein kinase D2	PKD2	0.79	385.13	0.08	2.53	0.96	5883	4669.36	
Serine/threonine-protein kinase D3	PKD3	0.94	1508.12	0.08	2.49	1.05	8213	7701.80	
Putative myosin light chain kinase 3	SgK085	0.65	185.78	0.00	2.56	0.97	11960	7772.27	
Proto-oncogene tyrosine-protein kinase Yes	YES	0.87	658.37	0.05	2.03	0.98	9385	8146.40	1343.30
Casein kinase I isoform epsilon	CK1e	0.98	4082.93	0.09	2.87	1.23	13050	12737.71	
Nicotinamide phosphoribosyltransferase		0.29	41.20	0.04	7.48	0.39			
Calcium/calmodulin-dependent protein kinase type II delta chain	CaMK2d	0.47	87.22	0.07	2.39	1.13			
Small nuclear ribonucleoprotein G		0.47	87.62	0.16	2.54	-			

Calcium/calmodulin-dependent protein kinase (CaM kinase) II gamma	CaMK2g	0.48	93.37	0.04	2.45	1.17
Small nuclear ribonucleoprotein E		0.51	105.76	0.07	2.57	1.88
Mitogen-activated protein kinase 14[a]	p38a	0.63	167.83	0.03	2.87	-
Activin receptor type-1 precursor	ALK2	0.67	201.86	0.15	2.57	1.17
Mitogen-activated protein kinase 14[b]	p38a	0.77	331.74	0.06	2.74	1.15
Insulin-like growth factor 2 mRNA-binding protein 1		0.79	367.24	0.19	-	-
Cytidine deaminase		0.80	402.28	0.09	3.09	-
Sepiapterin reductase		0.95	1858.55	0.02	2.91	2.43
60S ribosomal protein L7a		0.95	2103.58	0.17	5.23	-
RPL7 protein		0.96	2313.35	0.19	1.82	-
60S ribosomal protein L27a		0.97	2929.01	0.06	1.75	1.12

[a] CSBP1
[b] CSBP2

In order to fit meaningful binding curves for IC_{50} determinations, at least 40% of the bound target had to be displaced by soluble gefitinib. In total, 15 kinase targets as well as 3 non-kinase targets were identified to fulfill the all set criteria according to which appropriate K_d(gefitinib) values by means of the above described competition experiments could be calculated. The remainder, although showing specific binding to the AX14596 matrix, was not significantly displaced off the AX14596 matrix by free gefitinib, even at its highest concentration. Obviously, AX14596's target-specific binding affinities did not always mirror those of its structurally close relative, since in some cases, gefitinib binds, if at all, considerably weaker.

The kinase target with the lowest dissociation constant for gefitinib was GAK (K_d(gefitinib) = 45.59 nM) followed by EGFR (K_d(gefitinib) = 157.61 nM), RIPK2 (K_d(gefitinib) = 218.91 nM) and 12 others (Table 2). Generally, the K_d(gefitinib) spans a two-digit nanomolar to two-digit micromolar range. Confirming previous findings, binding of gefitinib under conditions which are close to physiology was not restricted to tyrosine kinases like EGFR and SRC family kinases; it also showed significant affinity to serine/threonine kinases like GAK or RIPK2[148]. The K_d(gefitinib) values of the kinase hits were generally found in good correlation with those deduced by *in vitro* kinase assays with recombinant enzymes as a reference system (Figure 19a, Table 2). However, a remarkable divergence existed in case of EGFR in terms of its dissociation constants itself, 5.58 nM versus 157.61 nM, as well as in its overall rank among listed kinase targets. Moreover, several non-kinase targets were identified as well. Among those off-targets three stood out, whose binding to gefitinib was shown to be rather strong, which was the case for BLMH (K_d(gefitinib) = 77.89 nM), NUDT12 (K_d(gefitinib) = 447.35 nM) or intermediate for ACAD10 (K_d(gefitinib) = 2865.59 nM), thereby demonstrating that this method is not restricted to protein kinases

(Table 2). Although not much is known about the biological impact of these proteins, NUDT12 and ACAD10 are proven to bind and turn over purine-based molecules (NUDT12 binds NAD^+, NADH and NADPH; ACAD10 binds FAD^+ and FADH) associated with the enzymatic function accounting for the affinity to the ATP-competitive compounds gefitinib and AX14596[252,254].

1.3   Quantitative chemical proteomics profiling of SB203580

1.3.1   *In vitro* association experiments with immobilized VI16742 as capturing molecule

As a part of the approach, working with an immobilized derivative of the inhibitor of interest most likely ensures the highest possible coverage of the compound's cellular target spectrum, given that the solid-phase bound molecule can capture virtually all the cellular protein targets which are displaced in the course of competition experiments using the "free" inhibitor. Yet, not all molecules destined for target profiling are immobilizeable *per se* and require conversion into a form that allows tethering to a solid resin material as mentioned earlier (see section I4.4.1). This is, in turn, afflicted with additional expenditures in terms of finding the suitable attachment points to retain their protein-binding properties relying on the knowledge about the structure-activity relationship and the spatial interaction with its targets. And, even if that information is available, the implementation of a chemical synthesis strategy is necessary to guarantee efficient affinity purification.

An alternative to bypass such requirements is using the molecule to be profiled in combination with a broadly selective molecule serving as immobilized capture reagent. Ideally, the capture molecule possesses a cellular target spectrum which encloses or largely overlaps with that of the other molecule. Here, the kinase inhibitor VI16742 was used as immobilized affinity ligand in combination with a structurally unrelated kinase inhibitor SB203580 to outline this concept (Figure 15). Previously, several N8-derivatized pyrido[2,3-*d*]pyrimidine-based small molecules have been described as high-affinity and low-selectivity capture reagents for a large subset of the human kinome[255,256]. VI16742, in particular 2-[4-(2-Amino-ethoxy)-phenylamino]-8-isopropyl-8*H*-pyrido[2,3-d]pyrimidin-7-one (Figure 15), belongs to the aforementioned molecule class and is distinguished by a primary amino group for immobilization on epoxy-activated Sepharose beads. Initially, SB203580, 4-(4´-fluorophenyl)-2-(4´-methylsulfinylphenyl)-5-(4´-pyridyl) imidazole (Figure 15), has been developed and described as a competitive and specific p38 kinase inhibitor, while modulating the inflammatory response[257,258]. However, more recent findings suggested a broader target spectrum as previously assumed[155,259].
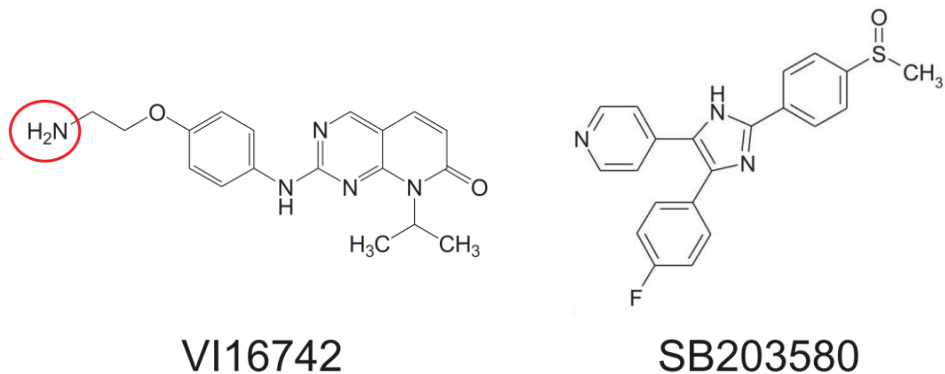
Figure 15: Structural formula of VI16742 and SB203580. Via the red circled amino group, VI16742 is chemically attached to the epoxy-activated Sepharose beads.

In analogy with the quantitative chemical proteomics strategy described in the previous section, protein binding to immobilized VI16742 was examined and characterized according to identical criteria, such as specificity, achievement of equilibrium and non-saturation of the binding matrix to generate $K_d(VI16742_{im})$ values. Additionally, detachment of specific VI16742-binders by soluble SB203580 was quantitatively monitored to obtain half-maximum inhibitory concentrations for SB203580, $IC_{50}(SB203580)$, and in combination with respective $K_d(VI16742_{im})$ values, target-specific $K_d(SB203580)$ values.

Using the same threshold for specific target binding, the affinity ratios indicative for binding to VI16742 were found to be in good correlation between each other and, hence, reproducible (Figure 16a). More than 135 kinases representing all subgroups of the human protein kinase superfamily as well as 25 further nucleotide-binding enzymes could be enriched via the sequential incubation procedure (Figure 18, Table A 1). Figure 16b exemplifies representative peptide MS spectra of selected kinase targets obtained in the SILAC setting with the sequential enrichment approach in addition to lack of binding to control beads. Here, the peptide intensities of control bead-bound proteins, which were labeled with the medium isotopic variants, are utterly underrepresented in comparison with the resin-bound targets, accounting for their high specificity. In line with the higher target affinities expressed as $K_d(VI16742_{im})$, the ratio of first (light label) versus second incubation (heavy SILAC label), was increasing with its affinity. For instance, high affinity targets like GSK3ß ($K_d(VI16742_{im})$= 5.21 μM) or RIPK2 ($K_d(VI16742_{im})$ = 5.06 μM) revealed a very low heavy-to-light ratio. For medium affinity targets, e.g. GAK ($K_d(VI16742_{im})$ = 28.55 μM), this ratio is moderately higher, whereas the ratio for lower affinity targets, e.g. ROCK2 ($K_d(VI16742_{im})$ = 254.87 μM), is nearly equalized.

Additionally, equivalent to binding to immobilized AX14596, the target binding over time as well as the presence of immobilized VI16742 were analyzed in order to assess the validity of this approach. Specific
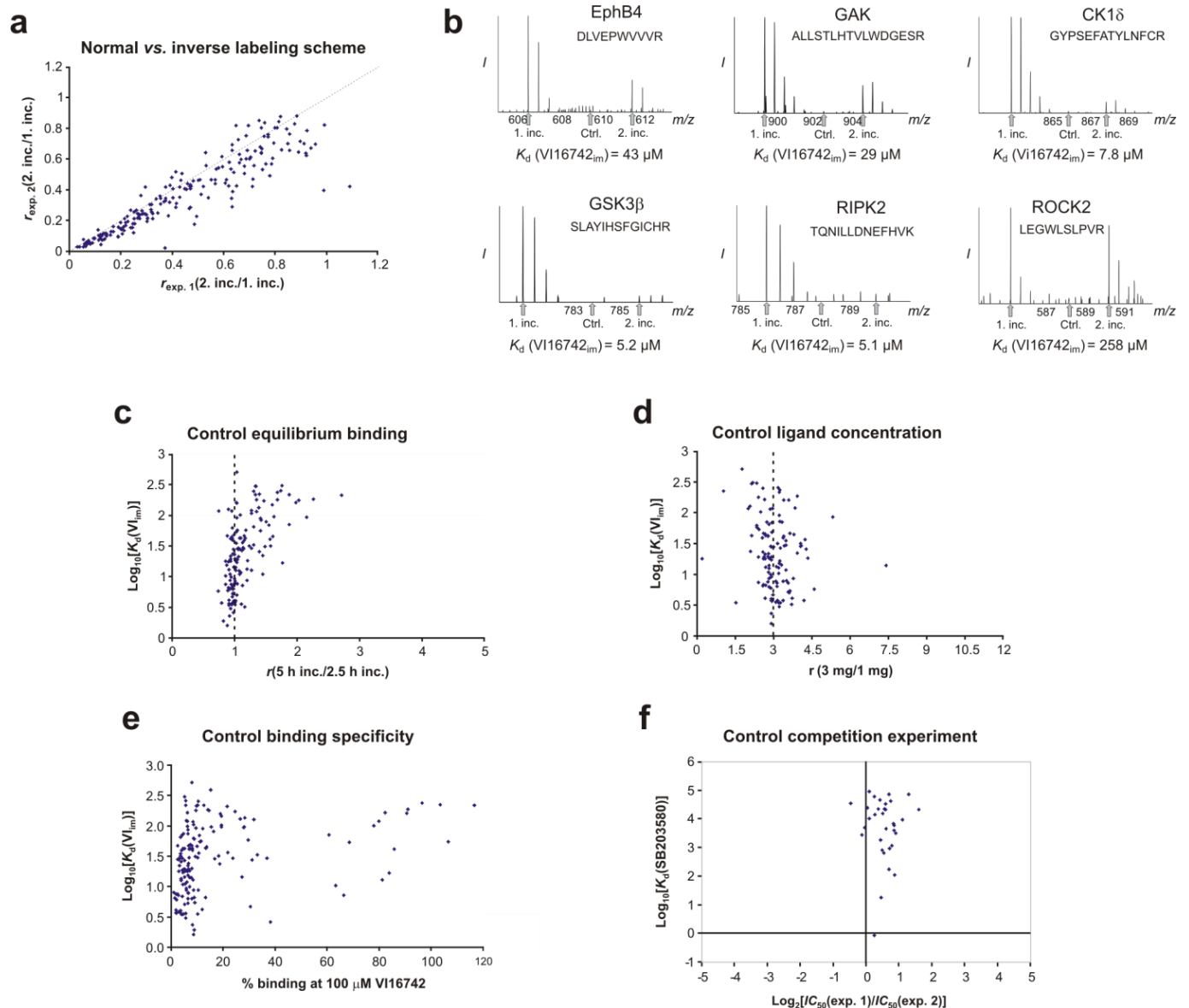
Figure 16: Quantitative chemical proteomics with the VI16742 resin. Ratios of target protein amounts retained in the second versus the first round of binding to VI16742 beads are compared for the normal (experiment 1, x-axis) and the inverse labeling scheme (experiment 2, y-axis). The dotted line indicates identical ratios in replicate experiments (a). MS spectra of representative peptides and the determined K_d values are shown for several kinase targets of immobilized VI16742 (b). Examination whether experimental conditions fulfill requirements to determine K_d values for specific targets of VI16742 (c and d). The influence of a prolonged incubation interval on target protein binding was analyzed by doubling up the standard period to 5 h in order to verify - by relating with exposure of 2.5 h - that target binding reactions had reached equilibrium within 2.5 h as a function of the $\log_{10}$ transformed values of the target dissociation constants for immobilized VI16742 (c). The aim of the second control experiment was to determine whether immobilized VI16742 was present in molar excess over its cellular target proteins. The use of 3 mg protein lysate per *in vitro* association, as standard, is compared with 1 mg. When plotting against the $\log_{10}$ transformed values of K_d(VI16742$_{im}$) most of the specific binders exhibit a ratio close to three, indicating the ligand concentration not being limited in its availability (d). Specific and reversibility of binding to the VI16742 matrix were additionally verified by a competition experiment in which lysates were pre-incubated for 30 min with either 10 μM or 100 μM of free VI16742 prior to incubation with VI16742 resin for a further 2.5 h. Percentage of residual target binding in the presence of 100 μM VI16742 is plotted against the $\log_{10}$ transformed values of the target dissociation constants for immobilized VI16742. With the exception of a small proportion, most targets were specifically and reversibly detached from the resin (e). Correlation of target binding data in replicate competition experiments with SB203580 and VI16742 beads (f). The IC_{50} values for SB203580 targets were determined separately for two experiments in which SB203580 was added either before or after VI16742 resin to lysates. The ratio of these IC_{50}s was $\log_2$ transformed and is plotted against the $\log_{10}$ transformed ratios of the calculated target affinities K_d(SB203580) (f).

binders of VI16742 were found to have reached binding equilibrium after 2.5 h. For almost all targets, in comparison to 5 h incubation, target binding had not changed significantly, particularly in case of higher affinities (Figure 16c). The amount of inhibitor affinity resin was not limiting the binding assay and it could be demonstrated to be in molar surplus over its cellular target proteins (Figure 16d). For this experimental setup an additional instance was introduced in order to verify the specificity of target binding to immobilized VI16742 (Figure 16e). Since this resin was capturing more than ostensibly 200 specific targets according to the above explained criterion, it was worth investigating the specificity of binding by concurrent competition of "free" ligand. For this purpose, lysates were preincubated with 100 μM VI16742 for 30 min following addition of VI16742 beads for another 2.5 h and, in a SILAC based approach, compared with lysates pretreated with DMSO instead of "free" VI16742. The vast majority (80% of all identified targets) of all apparently specific targets was replaced and thus only 20% or less of the target was retained on the resin. Even with highly concentrated soluble VI16742 these proteins were hardly replaceable due to unspecific binding or as a result of to tight attachment to immobilized VI16742 with a low off-rate constant (Figure 16e).

1.3.1.1 Gene ontology analysis of VI16742 binders

To enable an in-depth inspection and categorization in terms of overrepresented functional categories emerging with the identified target proteins, Gene Ontolgy (GO) analysis was performed (Figure 17)[260]. These categories describe gene product characteristics and gene product annotation data in fixed vocabulary terms. Terms significantly sticking out in numbers of the population as compared with the identical terms in a reference population encompassing all existing terms are considered as overrepresented. For the dataset here, "molecular functions" was chosen as category because it includes biochemical activity of proteins, which also involves binding to ligands or structures[260]. Figure 17 depicts GO terms (p < 0.001) for all specific targets that are statistically significantly overrepresented in comparison to the reference population. In addition, the occurrence of those terms within all quantified proteins is shown. It became obvious that, for instance, terms like protein kinase activity or lipid kinase activity were much more pronounced in the specific target fraction compared to all entries and even more to all quantified resin-bound proteins. However, as expected, the ability of the VI16742 resin, virtually resembling the ATP-like binding behavior, was not solely restricted to binding to the kinase group among purine nucleotide binders. (Purine) nucleotide-binding was overrepresented in the specific targets and all quantified proteins, whereas the difference among each other was considerably smaller compared to protein kinase activity. Thus, the specifically resin-retained targets showed a stronger enrichment of the more specialized kinase activity terms than the less-specialized molecule binding terms among all proteins quantified. With that prefer-

ence the original purpose of that molecule for which it was optimized was reflected. In line with its binding to kinases as signal modulators, redundant in addition to more specialized terms such as "proteins involved in receptor signaling" were overrepresented as well.

1.3.2   Competition with "free" SB203580

With immobilized VI16742 employed as capturing molecule, a broad screening panel against about 130 kinases as well as 70 other cellular proteins was provided. With an analogous SILAC approach as described above (see section III1.2.2) and applying a concentration range between 100 nM to 100 μM SB203580 as a 'free' competitor, nearly 40 proteins could be significantly replaced from the VI16742 matrix. Again, great importance was attached to reproducibility of the inhibitor versus control (DMSO) ratios and an appropriate fit of the regression curve over the whole concentration span of SB203580.
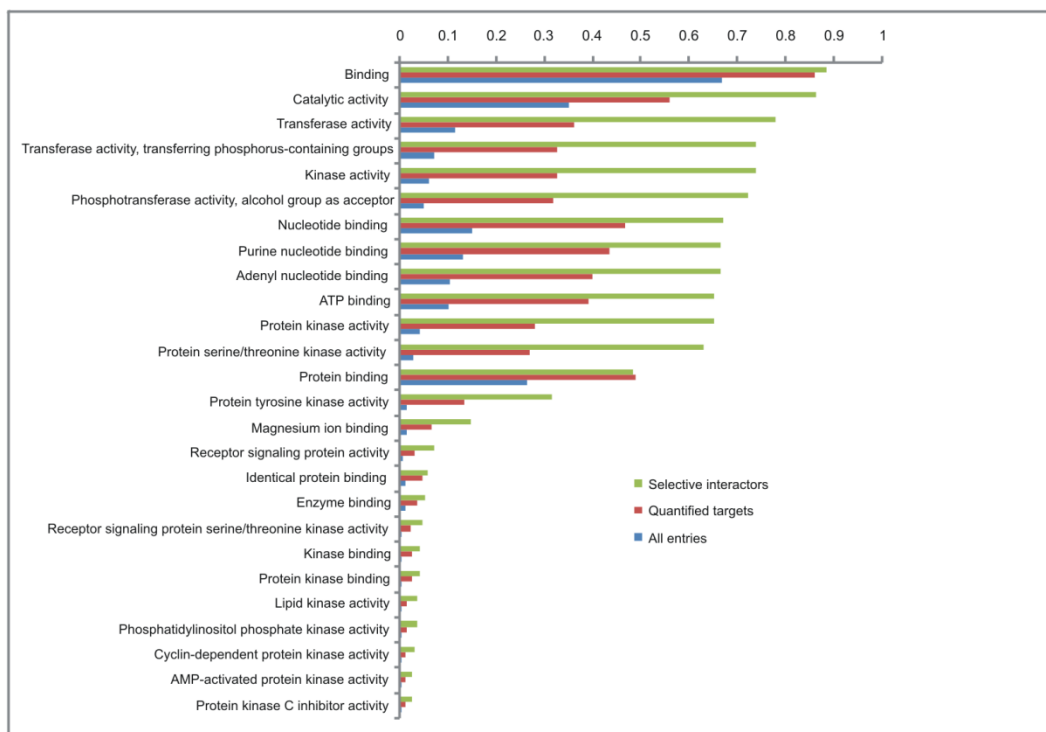
Figure 17: Gene Ontology (GO) analysis of VI16742 resin-bound proteins. Significantly overrepresented GO molecular function terms (P < 0.001) for all quantified proteins retained by VI16742 affinity beads and the subset of proteins characterized as specific inhibitor targets.

In addition to these requirements, a protein was only then considered as target, if it was displaced by more than 40% at the highest concentration of free inhibitor in comparison to DMSO only. Consequently, for

interactors meeting the criteria, IC_{50}s were determined and found in good accordance irrespective whether SB203580 or VI16742 beads were added first to lysates, being indicative for the achievement of equilibrium binding in both sequences (Figure 16f). The averaged IC_{50} values were used for calculations of target-specific dissociation constants, K_d(SB203580), according to Cheng and Prusoff (Figure 18)[242]. SB203580 was found to compete with 39 specific binders of VI16742, most of which, 36, were protein kinases. Yet, the selectivity was not restricted to protein kinases. SB203508 supplanted also a nucleotide kinase (adenosine kinase) and two nucleotide-binding enzymes (cAMP-specific 3',5'-cyclic phosphodiesterase 4D and 5'-nucleotidase domain-containing protein 1). However, all of which with fairly low affinity to SB203580 (Table A 1). The essentially low selectivity of the capturing ligand in the first place enabled the identification of not only serine/threonine kinases as SB203580 targets, but also tyrosine kinases, one of which, DDR1 with rather high affinity (K_d(SB203580) = 804.64 nM). Figure 18 depicts the concentration-dependent inhibition of binding to the VI16742 resin by SB203580 for additional protein kinases. Here again, GAK and RIPK2 were found with low K_d(SB203580) values. Also for previously identified targets across all subgroups of the human kinome, binding curves resulting in a wide range of IC_{50} values that could be fitted (Figure 18, Table A 1)[155]. Additionally, *in vitro* kinase assays with selected recombinant kinase targets provided K_d values for SB203580 in very good conformance (Figure 19a). In that particular case, all these features confirm the rebuttal of the initially assumed specificity of SB203580 concomitantly assessing the respective target-specific affinities[155,158].
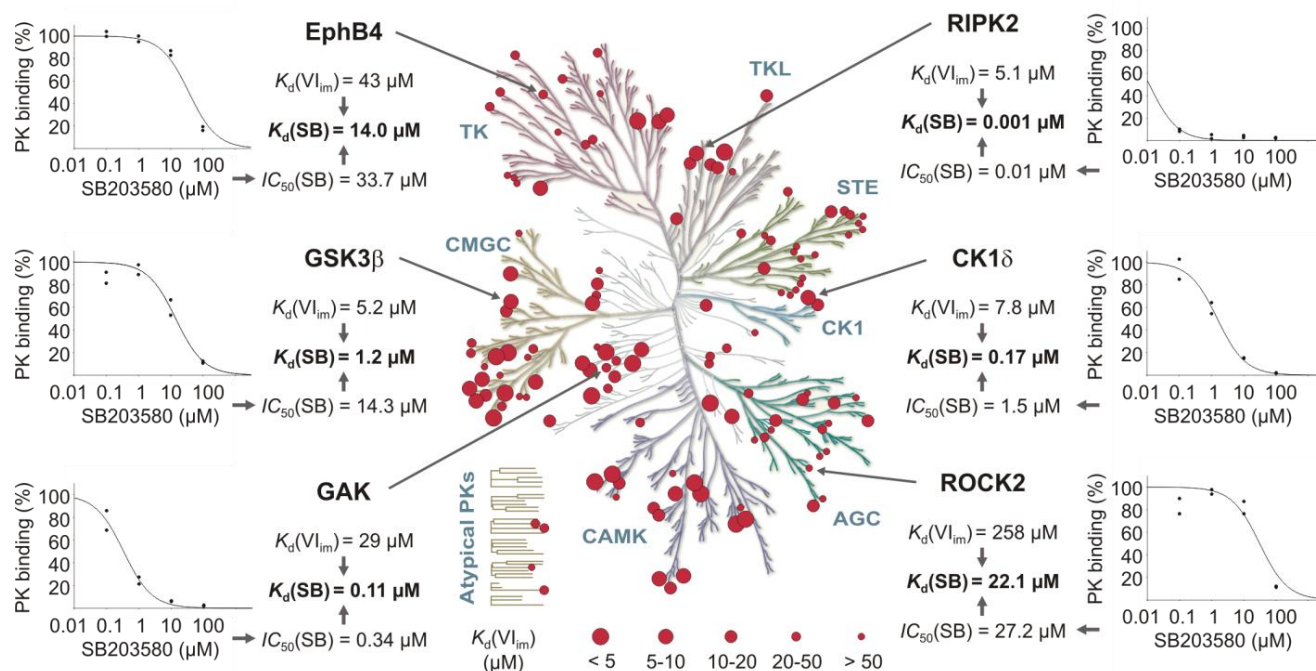
Figure 18: Analysis of binding affinities of cellular targets of immobilized VI16742 and "free" SB203580 according to the principle shown in Figure 10. VI16742-interacting protein kinases from Hela S3 cells are marked in the dendrogram of the human kinome. The size of the red circles indicates their binding affinities for immobilized VI16742, specified by the dissociation constant K_d(VI16742$_{im}$). For selected kinases concentration-dependent inhibition of binding to the VI16742 resin by SB203580 is depicted laterally. Additionally, the dissociation constants for SB203580 K_d(SB203580) as an outcome of the obtained IC_{50} values and respective K_d(VI16742$_{im}$)s are specified. The kinase dendrogram was adapted from *Manning et al.*[34].

1.4   Comparison with another quantitative chemical proteomics technique

A number of previous studies were already focused at MS-based proteomic profiling of immobilized kinase inhibitors, with the majority offering qualitative data about specifically bound interactors originating from cellular proteomes[148,155,261,262]. Yet, another report went one step further and described quantitative drug-protein binding parameters with a mixed broad-specificity kinase inhibitor matrix ('kinobeads') in combination with free kinase inhibitor drug elution[160]. Here, Bantscheff and colleagues were able to enrich about 140 protein kinase targets as well as other non-kinase proteins with a combination of seven kinase inhibitors from whole-cell lysates. The replacement of a bound target dependent on increasing concentration of free inhibitor was monitored with each of the four isoforms of the iTRAQ reagent, isobaric tags that covalently bind to lysine side-chains and the N-terminal group of each peptide[141]. After

mixing, the intensities of tag-derived reporter ions were measured by LC-MS/MS and were related to the control sample without inhibitor. Thus, binding curves of hundreds of proteins retained on the kinobeads were fitted by quantification of iTRAQ marker ion intensities for multiple inhibitor concentrations. This strategy was implemented with the clinical BCR-ABL kinase inhibitors imanitinib, dasatinib and bosutinib in combination with whole-cell lysates from K562 leukemic cells and the kinobeads as capture resin. The target-specific IC_{50} values, the inhibitor concentration at which half maximal target binding was observed, was considered as a quantitative measure of drug target affinity. By this means, for instance the receptor tyrosine kinase DDR1 and the quinone reductase were identified as high affinity targets for imatinib. *In vitro* enzyme activity assays were also performed in this study in order to confirm the IC_{50} values. However, as depicted in Figure 19, these IC_{50} values diverged by up to three orders of magnitude compared to the *in vitro* data. Such significant deviations are most likely the result of very high target affinities to at least one of the immobilized kinase inhibitor components of the kinobeads. If the assumption of Bantscheff et al. that only a small fraction of the kinobeads' cellular targets is bound does not apply, target-specific IC_{50} concentrations are shifted to higher values. By contrast, target-specific dissociation constants obtained by the above mentioned approach deliver for both gefitinib and SB203580 values in good agreement with the *in vitro* data (Figure 19). This is a result of stringently controlling the binding characteristics (binding equilibrium, molar excess of the capturing ligand over the target) on an individual target level set up for the experimental conditions. The study of Bantscheff et al. does not monitor these critical issues systematically across the target spectrum of the kinobeads. Thus, it cannot be excluded that in their approach inherent and unexamined difficulties are causal for the huge difference between their data and those obtained by *in vitro* assays.
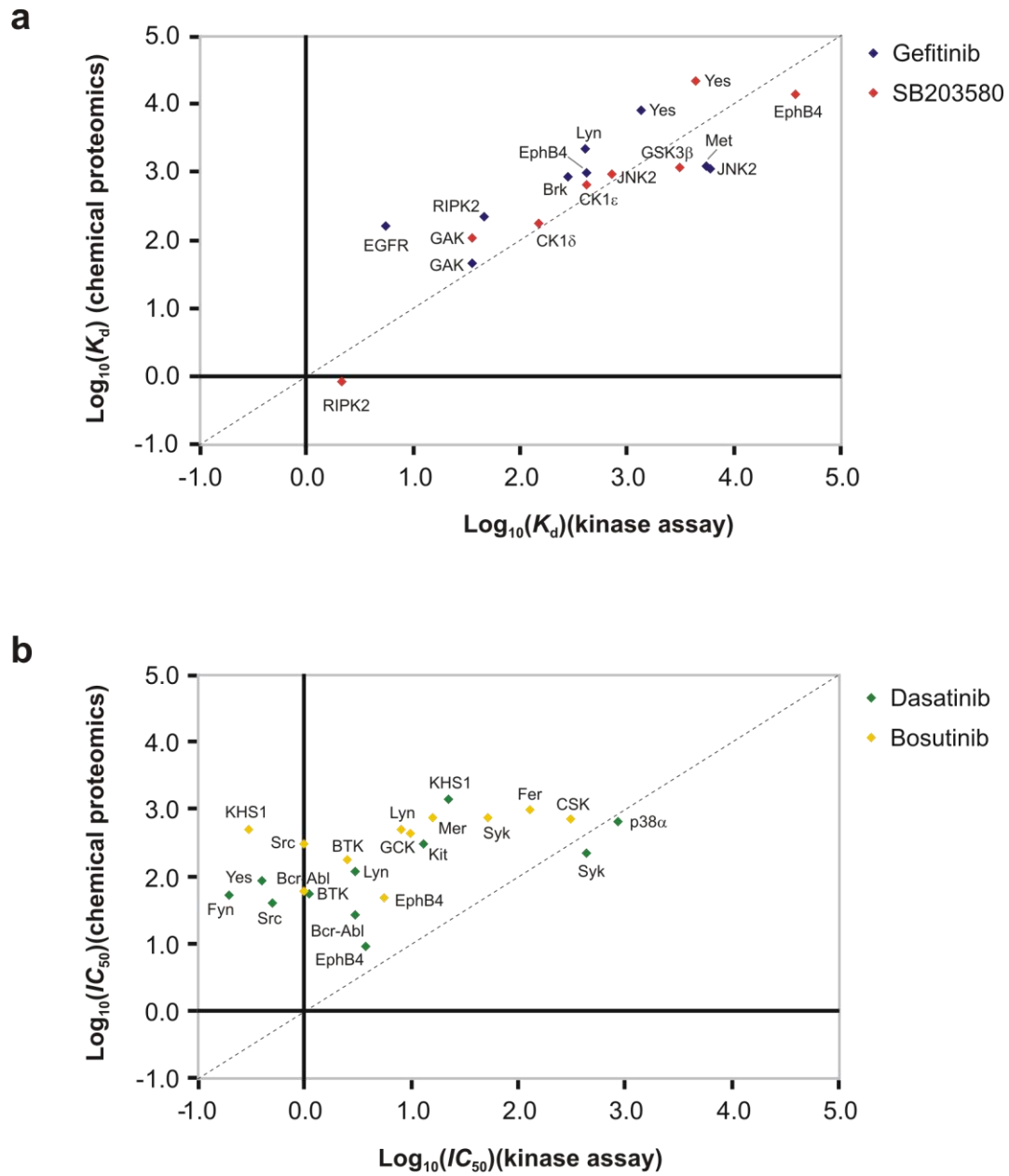
Figure 19: Correlation of target-specific dissociation constants. IC_{50} values determined by means of *in vitro* kinase assays are compared with K_d values according to the approach presented here for gefitinib (blue dots) and SB203580 (red dots) (a). The correlation of IC_{50} values obtained by Banscheff et al.[160] for dasatinib (green dots) and bosutinib (yellow dots) with those from *in vitro* kinase assays is shown in (b). The respective parameters were plotted as $\log_{10}$ transformed figures and the dotted line indicates identical ratios in both assays (a and b).

1.5   Quantitative profiling of peptide-protein interactions

In a next step it was assessed whether the potential of the approach presented above goes beyond quantitative profiling of small-molecule kinase inhibitors. Accordingly, it was tested if the principle of consecutive affinity purifications is applicable to determine affinity constants between proteins and a short interaction motif harboring a PTM since many protein-protein interactions are mediated through specialized domains recognizing posttranslationally modified peptide sequences of on their binding partners(Figure 1)[229,263]. With the method described here, the cellular interactome of a small phosphorylated peptide sequence (see II1.3.3) originating from the Insulin Receptor Substrate 4 (IRS4) was investigated with the focus on deducing binding affinities. IRS4 plays an important role in FGF2-induced FGFR-1 signaling, wherein it becomes phosphorylated on Tyr921 upon FGFR-1 activation turning into a docking interface for downstream signaling molecules[229]. The short synthetic IRS4 peptide used here corresponds to amino acids 914–929 containing this phosphorylated Tyr921 ($p^{914}IRS4^{929}$). In addition, it was fused to a desthiobiotin linker enabling stable coupling to streptavidin-coated beads. The identical peptide, yet non-phosphorylated ($^{914}IRS4^{929}$), attached to the beads served as a control resin. In order to assign affinities of specific binders, the previously described concept was realized with this immobilized affinity ligand (Figure 20). In combination with differentially labeled Hela S3 cell extracts the aforementioned affinity ratio r was measured in duplicates, i.e. in a 'normal' order and in a cross-over experiment, where the incubation scheme was swapped, resulting in inverted SILAC ratios (Figure 20a). Specific protein attachment was inspected by assessing binding to $p^{914}IRS4^{929}$-coupled beads compared to $^{914}IRS4^{929}$-coupled control beads. The binding ratios of both replicate experiments were plotted in Figure 20c. The majority of the identified proteins did not show a consistent binding preference for the modified peptide over both experiments. However, a distinct population comprised of 31 hits showed an enhanced attachment to the peptide harboring the phosphorylated tyrosine residue. This group was considered as specific for $p^{914}IRS4^{929}$ (Figure 20c). The preference of these proteins to bind the phosphorylated peptide in contrast to its unphosphorylated counterpart corresponded numerically to an average factor of more than 14 (Table 3). GRB2, phospholipase Cγ (PLCG), the p85 regulatory subunits of phosphatidylinositol 3 kinase (PIK3R) and SHC1 were identified as specific interactors in accordance with previous findings[229]. In addition, many other proteins were found in this group, for instance Signal Transducer and Activator of Transcription 5A (STAT5A) and B (STAT5B), Suppressor of Cytokine Signaling 6 (SOCS6), GRB7, the tyrosine kinase FER or the p110 catalytical subunits of PI3K (PIK3Cs). Notably, the vast majority of the proteins therein possess at least one phosphotyrosine-binding SH2 domain indicative of direct interactions with $p^{914}IRS4^{929}$.

Table 3: Quantitative chemical proteomic target analysis of tyrosine phosphorylated IRS4 peptide.

Protein Names	SH2 or other pY binding domain	r (2. inc/1. inc)	K_d(pY-921) [µM]	Specificity ratio (control/1. incubation)	Ratio 3 mg/1 mg lysate	Ratio 5 h/2.5 h incubation time
Phosphatidylinositol 3-kinase regulatory subunit beta	+	0.06	1.40	108.02	2.14	1.20
Phosphatidylinositol 3-kinase regulatory subunit gamma	+	0.06	1.60	40.90	2.28	1.09
Putative uncharacterized protein DKFZp434N101	+	0.12	3.22	345.73	2.21	1.17
1-phosphatidylinositol-4,5-bisphosphate phosphodiesterase gamma-1	+	0.12	3.38	73.15	2.16	1.17
Growth factor receptor-bound protein 2	+	0.22	6.74	115.17	2.39	1.07
SH2B adaptor protein 1	+	0.26	8.44	41.68	4.86	0.58
55 kDa protein	+	0.29	9.86	26.50	3.56	0.48
1-phosphatidylinositol-4,5-bisphosphate phosphodiesterase gamma-2	+	0.29	9.93	38.42	1.87	1.15
Tyrosine-protein phosphatase non-receptor type 11	+	0.30	10.08	42.28	2.34	0.99
Suppressor of cytokine signaling 6	+	0.30	10.27	26.23	1.84	1.18
Vav 2 guanine nucleotide exchange factor	+	0.32	11.18	40.74	2.47	0.95
Growth factor receptor-bound protein 7	+	0.44	19.08	27.51	1.77	1.15
Protein MEMO1	+	0.47	21.19	20.86	2.52	0.84
Proto-oncogene tyrosine-protein kinase Fyn	+	0.48	21.93	16.69	2.35	1.04
Signal transducer and activator of transcription 5B	+	0.49	23.16	53.03	2.26	1.04
Signal transducer and activator of transcription 5A	+	0.51	24.66	48.70	2.11	0.96
Tyrosine-protein kinase 6	+	0.56	30.57	18.48	2.22	0.85
Proto-oncogene tyrosine-protein kinase FER	+	0.59	34.44	25.95	2.00	0.84
SH3 domain-binding protein 2	+	0.66	46.45	19.62	2.68	0.65
Cytoplasmic protein NCK1	+	0.72	62.21	17.58	3.06	0.42
Growth factor receptor-bound protein 10	+	0.86	n.d.	14.14	2.76	0.61
SHC-transforming protein 1	+	0.92	n.d.	27.79	2.42	0.66
Ras GTPase-activating protein 1	+	0.92	n.d.	28.78	2.03	0.77
Tensin-3	+	0.99	n.d.	16.53	2.82	0.70
Phosphatidylinositol-4,5-bisphosphate 3-kinase catalytic subunit beta isoform		0.03	n.d.	60.37	2.37	1.08
Phosphatidylinositol-4-phosphate 3-kinase C2 domain-containing beta polypeptide		0.04	n.d.	66.80	n.a.	n.a.
Son of sevenless homolog 1		0.05	n.d.	72.62	8.14	1.00
Phosphatidylinositol-4,5-bisphosphate 3-kinase catalytic subunit delta isoform		0.06	n.d.	24.53	2.29	0.96
Phosphatidylinositol-4,5-bisphosphate 3-kinase catalytic subunit alpha isoform		0.06	n.d.	52.27	2.12	1.22

Son of sevenless homolog 2	0.06	n.d.	27.70	5.75	1.00
Uncharacterized protein ARHGEF5	0.10	n.d.	109.53	5.55	1.15

Others like SOS1 or the PIK3Cs are lacking a SH2 or any other phosphotyrosine-binding domain and therefore, this interaction was most likely indirectly mediated through GRB2 and PI3KR, respectively. Analogously to the chemical proteomics strategy devised above, the enrichment ratios of the specific interactors together with the concentrations of immobilized IRS4 peptide, which were also determined photometrically, were sufficient to determine dissociation constants K_d(pY-921) for the individual binders. However, to be able to fully apply that principle, here as well the above described control experiments had to be performed to verify reached binding equilibria and molar excess of the immobilized peptide over its targets (Figure 20b). For most of the specific targets the requirements were fulfilled and K_d(pY-921) determinations were facilitated (Table 3). Figure 20d illustrates the specific binders with their respective enrichment ratios. For K_d(pY-921) calculations only targets with a phosphotyrosine binding domain were considered in order to provide sound values. By the same token, proteins were only included if they possess a phosphotyrosine domain, because only for those can be assumed to interact directly with the phosphorylated IRS4 peptide. Finally, in order to provide substantial K_d(pY-921) values, more than 20% of the specifically interacting protein in the lysate must be bound to the $p^{914}IRS4^{929}$-beads, i.e. the value for r was smaller than 0.8. Under these conditions for 20 binders dissociation constants could be delineated. The PIK3Rs ß (p85) and γ (p110) headed the list in terms of high affinity with K_d(pY-921) of around 1.5 μM (Figure 20e). Many other factors involved in growth factor receptor signaling were also identified with considerable affinity to phosphorylated IRS4 peptide, such as adaptor proteins, e.g. GRB2 (K_d(pY-921) = 6.74 μM) or GRB7 (K_d(pY-921) = 19.08 μM), PLCG1 (K_d(pY-921) = 3.38 μM), the adaptor protein NCK1 (K_d(pY-921) = 62.21 μM) or the guanine nucleotide exchange factor VAV2 (K_d(pY-921) = 11.18 μM) (Figure 20e). With the data provided here, it was not only possible to confirm previously identified interactions of GBR2, p85 and PLCG1, but also to identify and rank so far unknown interactors according to their individual dissociation constants, having measured values up to approximately 60 μM.
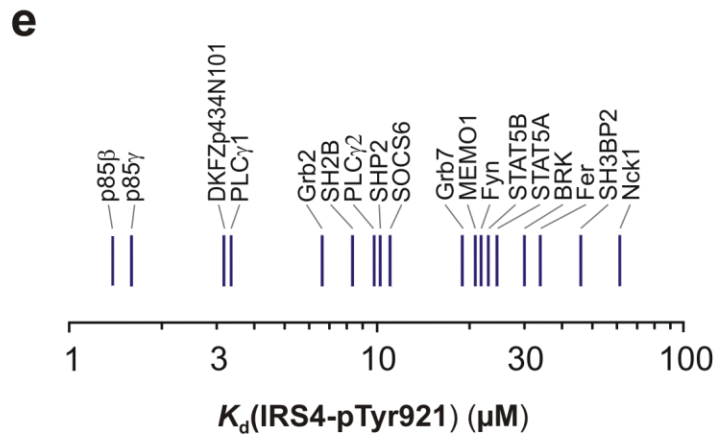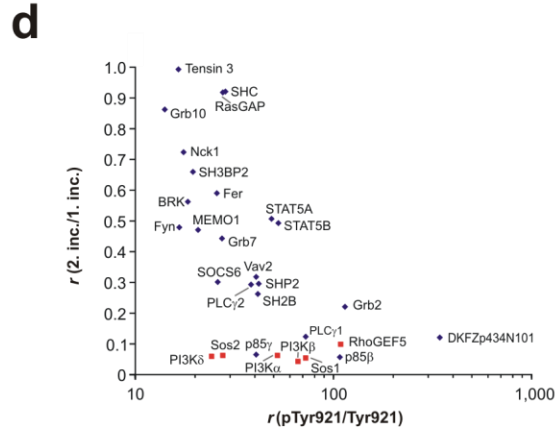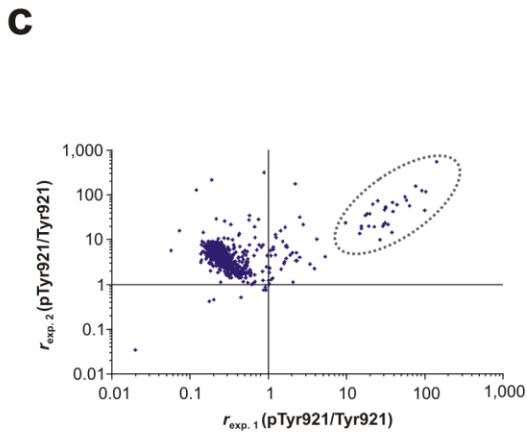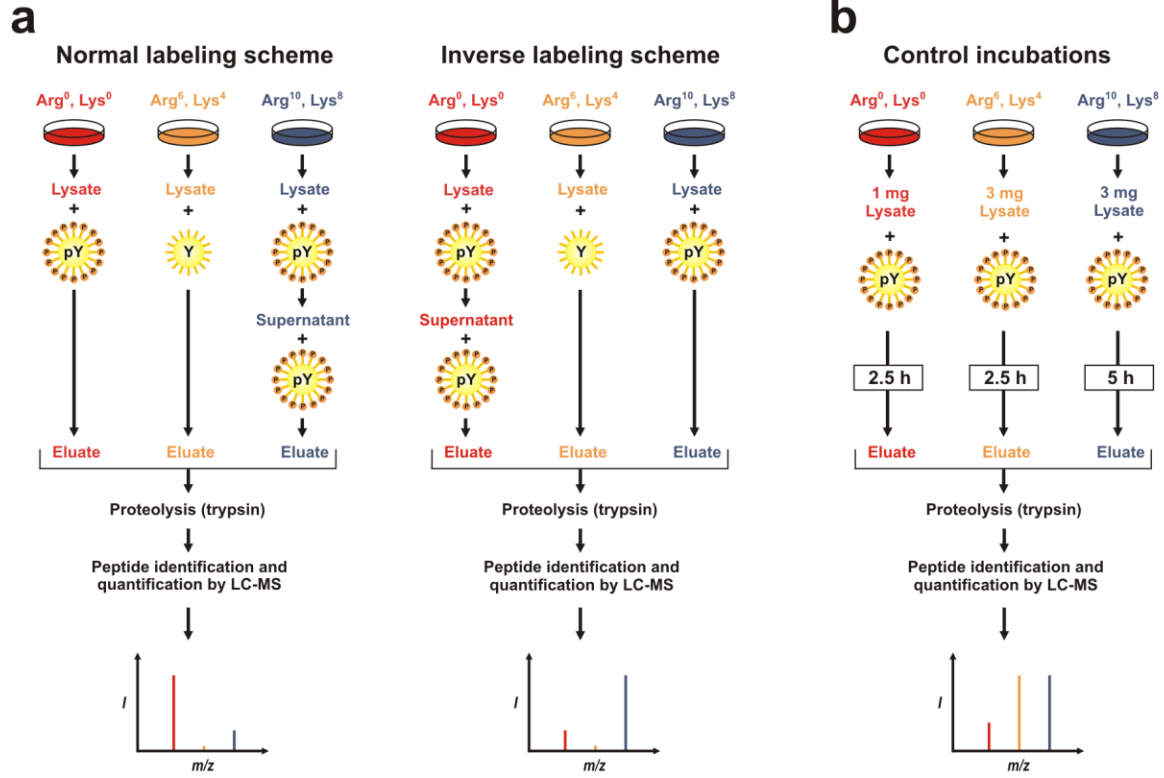
Figure 20: Quantitative proteomics analysis of phosphotyrosine-dependent peptide interactions. Analogous to the strategy outlined in Figure 12a, affinities and specific binding to immobilized and phosphorylated IRS4 peptide was assessed by two SILAC-based cross-over experiments in order to verify reproducibility and to eliminate false-positive target identifications (a). In a third SILAC experiment, analogous to the strategy depicted in Figure 13, it was assessed whether the immobilized ligand is present in molar excess over its cellular target proteins and whether binding equilibria have been reached under these experimental conditions (b). Notably, only one single control experiment was set up, which enabled the monitoring of both binding parameters. Scatter blot showing protein binding ratios to phosphorylated IRS4 peptide (pTyr921) versus the non-phosphorylated version (Tyr921) in both replicate experiments. Specifically bound proteins (encircled) were found in reproducibly high ratios, which discriminated them from background binders exhibiting ratio variability in the replicate analyses (c). Specific binders obtained from (c) were plotted along with their protein names against their averaged affinity ratio r (2.inc/1.inc.), which expresses binding in a consecutive second versus the first incubation with tyrosine-phosphorylated IRS4 peptide. Proteins with known phosphotyrosine-binding domains are depicted as red dots. (d). K_d values for protein binding to $p^{914}IRS4^{929}$ peptide were calculated for specific interactors with known phosphotyrosine-binding domains (e).

1.6   Profiling of protein-protein interactions

A consequent expansion of the concept presented in the preceding sections is the profiling of protein-protein interactions. According to the previously described approach with the phosphorylated IRS4-peptide bait, proteins co-purify indirectly in complex with direct protein targets. With the use of the sequential incubation procedure, these secondary interactors enrich in similar ratios as the primary target, provided that its interaction with of the affinity ligand is of adequate strength (Figure 20d). An experimental setup that is feasible to be translated into practice is the use of immunopurified protein in a cellular extract as protein bait. Antibody-antigen interactions are reported as being extremely strong and also qualify by their broad availability[264]. In the implementation presented here, a monoclonal antibody directed against EGFR was used in combination with differentially SILAC labeled Hela S3 cell lysates. The cells were treated with EGF prior to lysis in order to activate EGFR-mediated signal cascades being associated with the induction of several molecular interactions with the receptor. Analogous to the experiments described above (Figure 20a), the lysate was incubated either once or twice with EGFR antibody (mAb108.1) dependent on their label and each incubation step was followed by capture via protein G Sepharose beads. In parallel, to discriminate between specific and unspecific binding, cell extracts were incubated without antibodies. Again, the experiment was performed in two replicates including an inverted labeling arrangement. When plotting the individual affinity ratios, i.e. intensities of second divided by first incubation, against the specificity ratio, i.e. intensities of first incubation divided by control incubation, a distinct group of proteins around EGFR emerged characterized by high specificity - the underlying rations were larger than eight - and substantial enrichment or high affinity (Figure 21).

r (1. inc./control)
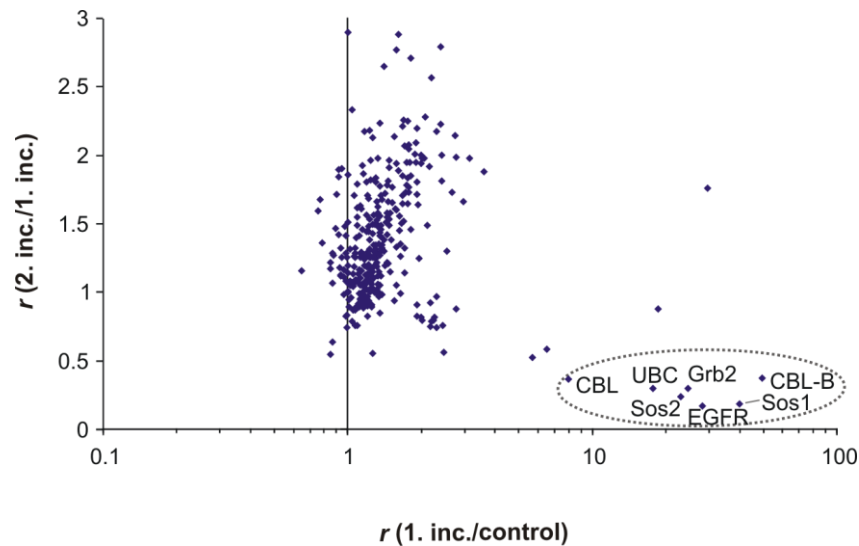
Figure 21: Analysis of protein interactions with immunoprecipitated EGF receptor by means of quantitative proteomics. EGF receptor was precipitated with monoclonal antibody out of lysates stemming from EGF-stimulated Hela S3 cells and its binders were analyzed according to the principle outlined in Figure 12a. Average attachment of both experiments to the anti-EGFR antibody versus the control without antibody is proportional to its specificity and plotted along the abscissa. Average ratios describing the binding to precipitated EGFR in the second versus the first incubation round are indicative of target affinity and plotted as ordinate. EGFR and its identified association partners are encircled.

To this group, which distinguished itself from 600 other identified proteins, belonged SOS1, SOS2, GRB2, UBC, CBL and CBL-B, all of which showing similar low enrichment ratios r between 0.18 and 0.38, similar to that of the bait protein EGFR. All these proteins were previously reported to be either involved in signaling downstream of activated EGFR or in its signal modulation, highlighting the validity of that concept[265-267].

Table 4: Quantitative proteomic analysis of co-precipitated EGFR interactors.

Protein Names	r (2. inc/1. inc)	Specificity ratio (control/1. inc)
Epidermal growth factor receptor precursor	0.17	28.45
Son of sevenless homolog 1	0.18	40.13
Son of sevenless homolog 2	0.23	23.08
Growth factor receptor-bound protein 2	0.29	24.82
cDNA FLJ75516, highly similar to Xenopus tropicalis ubiquitin C, mRNA	0.30	17.83
E3 ubiquitin-protein ligase CBL	0.36	8.03
E3 ubiquitin-protein ligase CBL-B	0.37	49.90

2. Quantitative proteomic analysis of gefitinib's and erlotinib's effects in AML cells

In previous observations several groups were able to demonstrate that the kinase inhibitors gefitinib and erlotinib exert antineoplastic effects in AML cells including proapoptotic activity, induction of differentiation, anti-proliferative activity and cell cycle arrest[220,221,223,225,226]. Despite considerable scientific efforts, the detailed mechanisms underlying the described consequences was not clarified yet and remained elusive, particular because those come about by an "off-target" [220,222]. The expression "off-target" effect refers to the fact that AML cells generally lack expression of EGFR, which represents the *bona fide* target of both tyrosine kinase inhibitors[220,223]. To shed light on the molecular basis of antagonistic effects leading to the overall outcome in AML cells, perturbation of phosphorylation-based signaling upon gefitinib and erlotinib treatment is investigated in the following section. In order to obtain a comprehensive overview over significant phosphorylation changes high-resolution mass spectrometry was used in addition to the quantitative chemical proteomics approach portrayed above to identify direct kinase targets whose inhibition may account for the observed consequences in AML cells. As outlined earlier, within a cell, kinases are crucial key controllers of phosphorylation based signal transmission in a partially strongly interwoven signal networks (see section I1). Consequently, a dispersed interference with these control points may to lead to an extensive overall outcome on the phosphoproteome ultimately representing the basis of the observed phenotype. Hence, in that context it is of enormous advantage to enable monitoring phosphorylation levels on a system-wide level, which is enabled by MS-based phosphoproteomics.

An earlier study with a similar objective suggested an association of altered tyrosine phosphorylation with the effect of gefitinib as this drug and its structural relative erlotinib were originally designed to target the tyrosine kinase EGFR[222]. However, it has been demonstrated before that both drugs' target spectrum is not only restricted to tyrosine kinases but also includes an array of serine/threonine kinases[148,158]. That fact by itself therefore allows alternative scenarios to be closely examined potentially being causal for the inhibitors' antineoplastic effects in AML.
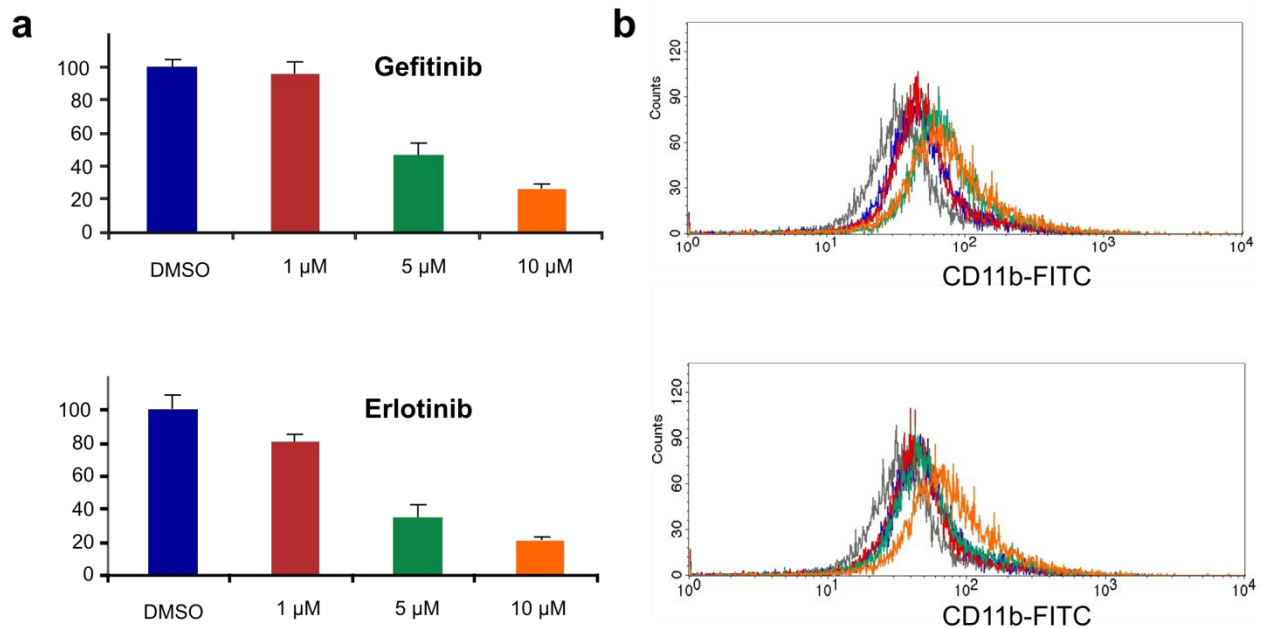
Figure 22: Gefitinib- and erlotinib-induced effects on viability and differentiation in KG-1 cells. To study viability, KG-1 cells were treated with the indicated inhibitor concentration for three days followed by live incubation in MTT reagent prior to lysis and read out. Viability decreases in a dose-dependent manner (n=2) (a). For assessment of differentiation the same concentrations (note identical color coding) of gefitinib and erlotinib were used for KG-1 cells (b). After four days of differentiation was quantified by immunofluorocytometric measurement of surface CD11b on day four. These representative diagrams point toward a concentration-dependent induction of cellular differentiation.

In order to assess the phosphorylation changes the AML cell line KG-1 was used due to its high susceptibility to gefitinib as well as erlotinib in terms of induction of apoptosis and differentiation (Figure 22)[220,221]. Indeed, with increasing inhibitor concentrations a clear shift in expression of the myelocytic differentiation antigen CD11b was visible, accompanied by significantly reduced cell viability (Figure 22).

2.1   Experimental strategy

To allow for quantitative examination of phosphorylation changes upon gefitinib and erlotinib treatment on a proteome-wide scale, KG-1 cells were labeled with either light (Arg^0, Lys^0), medium (Arg^6, Lys^4) or heavy (Arg^{10}, Lys^8) arginine and lysine variants. This metabolic SILAC labeling of growing cells leads to the total replacement of both essential amino acids by the presented variants in the entire cellular proteome, creating measurable differences of peptide masses enabling the quantitative comparison of three cell populations on the individual phosphopeptide level. After six doublings to enable complete incorporation of arginine and lysine into the cellular proteome, cells were discriminatively treated as follows: KG-1

cells containing the light label were treated with DMSO and cells with medium and heavy label were treated for 1 h with 10 μM erlotinib and 10 μM gefitinib, respectively (Figure 23). The relatively high inhibitor dosage, being markedly beyond the IC_{50} of both drugs in terms of KG-1 cell viability, was chosen to elicit a prominent perturbation in cellular phosphorylation- based signal transduction. The incubation for 1 h was selected to enable propagation the interference with the primary kinase target(s) as well as to allow for a marked imbalance in favor of phosphatase-mediated dephosphorylation events eventually leading to observable phosphorylation changes. In addition, drug-induced changes in protein level via protein expression or degradation are rather unlikely to occur within that short period. Such processes would complicate interpretation of altered phosphorylations as it would not be clear if they are true (de)phosphorylation events or a result of a changed phosphoprotein amount. In order to ensure validity as well as reproducibility for later data analysis, the experiment was repeated two more times with inverted variants of SILAC labels enabling all possible treatments for each label (Figure 23). Subsequent to 1 h incubation, cells were lysed and for each experiment equal protein amounts were pooled. Each lysate pool was digested with trypsin and Lys-C and the resulting peptide mixture was separated into 12 fractions by SCX chromatography according their charge states in solution under acidic conditions. To enrich for phosphorylated peptides each fraction was incubated with IMAC beads in technical duplicates. After elution from the beads phosphopeptides were analyzed by LC-MS on a high-resolution LTQ-Orbitrap hybrid mass spectrometer. In summary, three biological replicate experiments were performed differing by the label arrangement and each of the 12 fractions derived from one biological replicate was further analyzed in two technical replicates.
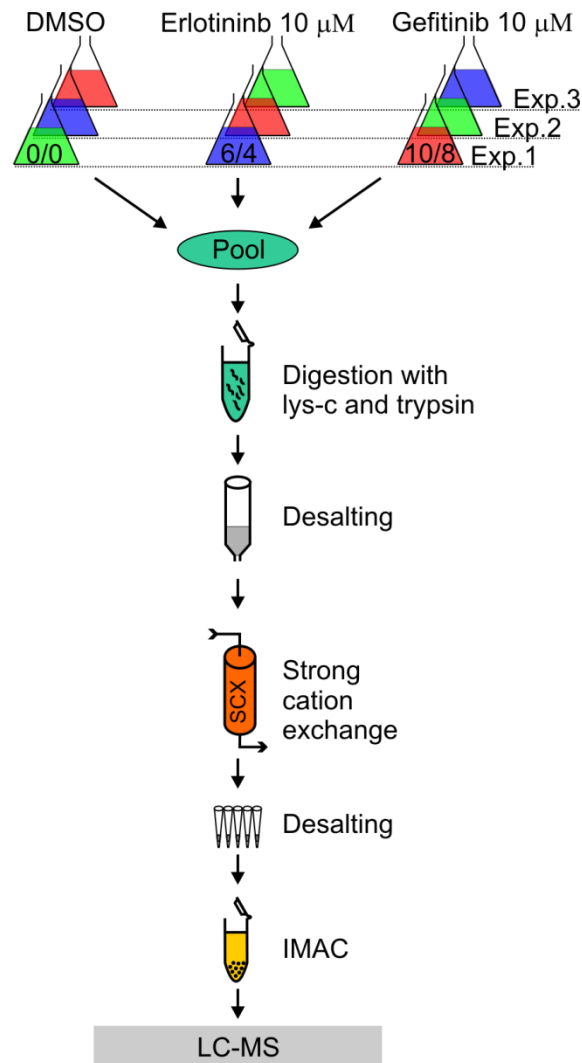
Figure 23: Experimental workflow for quantitative phosphorylation analysis of KG-1 whole-cell extracts by means of mass spectrometry.

2.2   Qualitative phosphoproteomics analysis of KG-1 cells

The raw data files obtained by mass spectrometer were further processed with the MaxQuant software bundle to allocate identification and SILAC-based quantification of (phospho)peptides and proteins[236]. Over all experiments, from 97,081 independent peptide-to-spectrum assignments 11,867 unique phosphopeptides were identified arising from 3,458 different proteins at an accepted false-discovery rate of 1%. Of these 3,458 proteins 2,960 were found phosphorylated and further identified from 11,867 unique phosphopeptides across biological replicate experiments. Moreover, post-translational modification scoring of phosphopeptides localized as many as 10,975 distinct phosphorylation sites to specific residues (class I phosphosites with a localization probability of at least 0.75). The distribution of serine,

threonine and tyrosine sites was 83%, 15% and 2%, respectively, with the latter accounting for 209 distinct modification sites. Until now, this amount represents the highest number of reliably identified phosphorylation sites in a leukemic cell line with an overall comprehensiveness of phosphoproteomic coverage as obtained in an earlier phosphoproteomics study[268].

2.2.1   Gene ontology analysis

In order to study phosphorylated proteins emerging from the whole dataset for overrepresented functional categories, GO analysis was carried out. In contrast to section III1.3.1.1, the focus was layed on "biological processes" as functional category[260]. In these terms a series of several molecular functions are assembled to defined cellular physiological processes. Those are indicative of a pronounced relevance when found overrepresented[260]. For proteins bearing phosphorylation sites, highly significant enrichments of biological processes dealing with RNA localization, processing and transport were found (Figure 24).
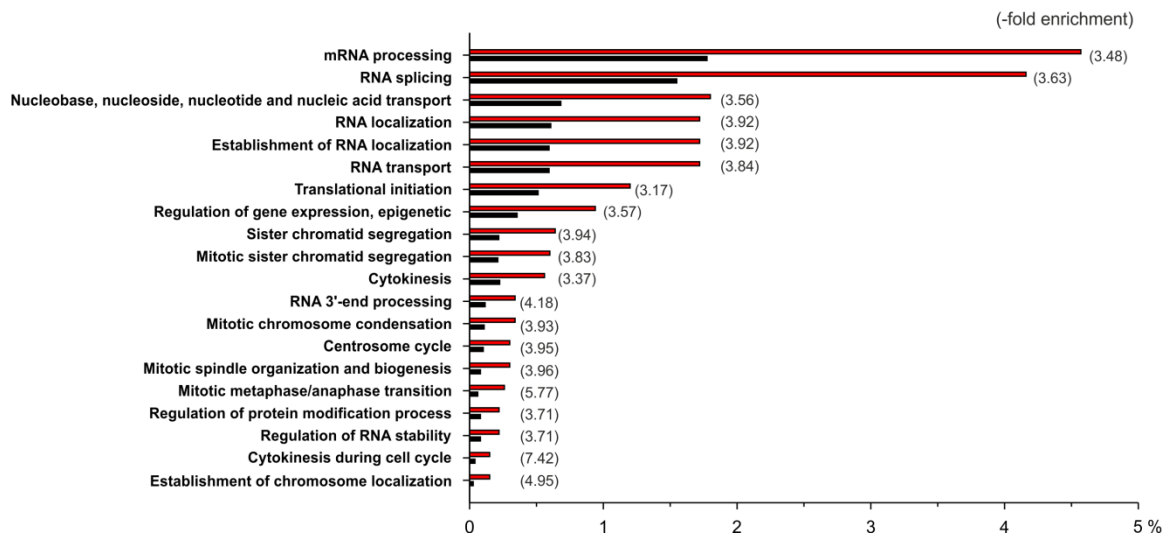
Figure 24: GO analysis of identified KG-1 cell phosphoproteins. Significantly overrepresented GO biological process terms (P<0.05) are shown for the set of phosphoproteins identified in KG-1 cells compared to all human proteins used as reference by the bioinformatics tool DAVID. Percentage values shown as red bars indicate the number of KG-1 cell phosphoproteins annotated to the respective GO biological process term divided by the number of all phosphoproteins with GO biological process annotation. The black bars indicate the corresponding ratios for the reference data set. The figures in brackets specify the -fold enrichment of KG-1 cell phosphoproteins compared to all reference proteins for the significantly overrepresented GO terms.

In this context, also phosphoproteins showing involvement in cell division, i.e. mitosis, centrosome cycle and cytokinesis, were noticeably overrepresented in comparison to the reference population. Obviously, AML KG-1 cells use phosphorylation-based signaling for protein expression as well as proliferation very extensively and both processes play a central role in cell viability. This behavior underscores the potential

of (targeted) inhibition of phosphorylation for interference with processes indispensably for cellular prosperity, particularly in AML cells.

2.2.2 Analysis of phosphorylations within the activation loops of kinases

Next, to gain functional insight in cellular kinase activity behind active biological processes, phosphorylation sites were analyzed in the activation loop of protein kinases. The activation loop of a kinase is polypeptide region whose phosphorylation exerts influence on kinase conformation thereby inducing or preserving its activity (see section I2.2). By this means, kinase activity can be affected by its catalytic rate or by substrate access, both as a result of structural rearrangement. These modification events occur on about 50% of all members of the human protein kinase superfamily[6]. In this dataset several class I sites on 27 different protein kinases were identified as activation loop sites, e.g. on tyrosine kinases of the SRC-family (SFKs), such as LYN, LCK and YES, or BTK. Interestingly, serine/threonine kinases involved in cell cycle progression were detected as being activated, namely the Cyclin-Dependent Kinases (CDK) family (CDK1, CDK2, CDK7). To uncover known physical and functional associations between activated kinases a STRING-based interaction analysis was performed, and indeed, both kinase groups assembled into defined components which are most likely responsible mitogenic activities in KG-1 cells (Figure 25). In line with that oberservation, also mitogen-activated protein kinases such as p38α and p38γ, which are known for their role in cell growth and proliferation, also gathered to that network comprised of activated kinases. Remarkably, kinase activity downstream of p38α was also found connected in terms of the Ribosomal protein S6 Kinases RSK1 and RSK2 known for their involvement, for example, in mRNA translation (Figure 25).
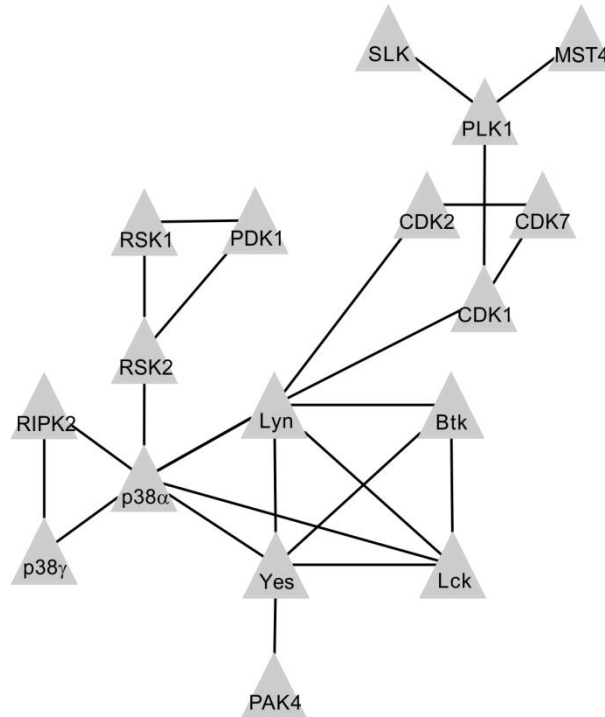
Figure 25: Network of protein kinases for which activation loop phosphorylation was detected in KG-1 cells. Nodes were assembled by STRING database based on known physical and functional interactions and kinase were named after *Manning et al.*[34].

2.2.3 Extraction of overrepresented phosphorylation motifs

Phosphorylation events are, as mentioned in the introductory paragraph, very often directed by short sequence motifs. In this context, the knowledge of preferentially occurring substrate motifs can be indirectly utilized to trace back protein kinases responsible for distinct substrate phosphorylation patterns. In order to apply these principles within this dataset, confidently localized class I phosphorylation sites were subjected to motif analysis to extract overrepresented sequence patterns. This analysis was performed by means of the Motif-X algorithm[241]. Thereby, each class I site was centered on the phosphorylated site and extended six amino acids on each side, fed into the online-algorithm and therein compared with all identified motifs of the respective modified residue as background. Eventually, the occurrence was compared with that in a human reference database[241]. In this way, 77 phosphoserine, 16 phosphothreonine and 2 phosphotyrosine site motifs could be extracted (data not shown). Various serine and threonine phosphorylation site motifs were extracted containing Casein Kinase II (CK2) motifs characterized by up to three acidic glutamic or aspartic acid moieties in '+'-direction (e.g. sDDD and sDxE) as graphically displayed in Figure 26 as logo-like representations. Apart from the centered phosphorylation site on position 0, these logos included adjacent amino acids whose overall occurrence was proportional to depicted letter sizes

(Figure 26). Highly enriched motifs bearing phosphorylated threonines were found to be in combination with proline in the +1 position being preferentially recognized by CDKs (Figure 26). Again, that data emphasize the prevalence of enhanced CDK activity which is known to control together with CK cell cycle progression thereby supporting the findings of GO and STRING analysis in Figure 24 and Figure 25[269]. As one would expect, fewer phosphotyrosine-based motifs were found because of the lower overall number of modified tyrosines identified. Moreover, both identified did not allow for meaningful conclusions in terms of underlying kinase specificity.
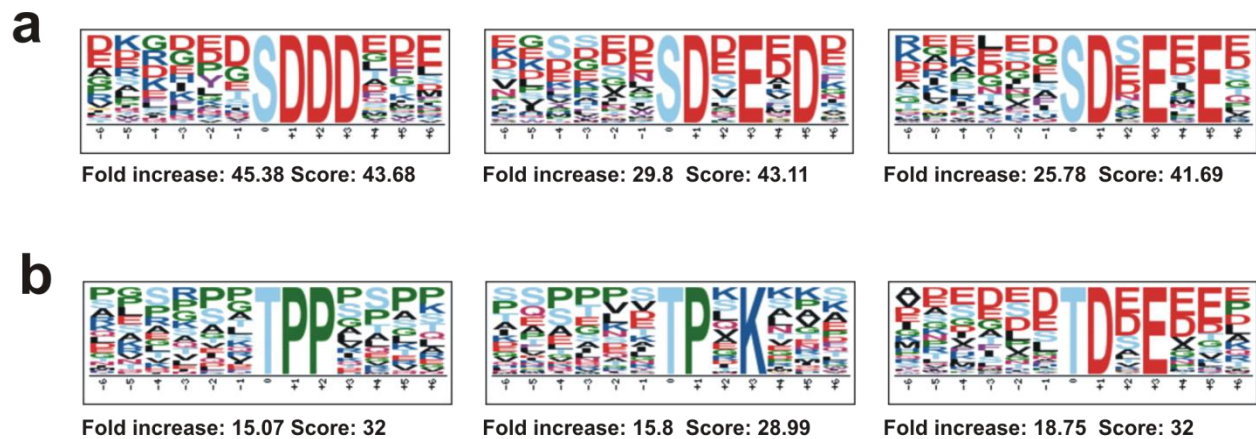
Figure 26: Extracted phosphorylation site motifs using Motif-X algorithm[241]. The motif score (Score) is depicted and motif enrichment is expressed in fold increase of motifs with a frequency of at least 30. Only class I sites were included for motif identifications. Logo-like representations of acidic motifs for phosphoserine are shown in (a) as well as of proline-directed and acidic threonine site motifs, respectively (b)[270].

2.2.4   Phosphorylation of histone deacetylases

Epigenetic regulation of gene expression was one of the highly significant terms found enriched in the GO analysis described above (Figure 24). In order to address a connection between both protein kinase activity and epigenetic regulation of gene expression, phosphorylations on the large enzyme family of histone deacetylases (HDACs) were further explored. That family tightly regulates together with their functional counterparts, called histone acetyltransferases (HATs), not only acetylation of histones, an epigenetic modification that controls chromatin structure and thus, gene expression, but also of other proteins, like transcription factors[271,272]. In that regard, epigenetic alterations induced by HDACs are involved in numerous cellular disease states such as malignant transformation, e.g. by silencing critical tumor suppressive genes[273]. These characteristics confer a considerable therapeutic potential on targeting HDAC activity in disease and, in this context, two HDAC inhibitors are currently clinically approved[274]. However, since HDAC activity is also influenced by phosphorylation, the knowledge of the phosphorylation

status of specific sites can serve as a helpful resource, e.g. in order to describe biological implications within the cell or to facilitate therapeutic intervention against these modifications parallel to direct targeting with HDAC inhibitors.

Table 5: Phosphorylation sites identified on histone deactelyases (HDACs).

Protein	Protein IPI	Postion	Modified Residue	Modified Sequence	Functional role
HDAC1	IPI00013774	393	S	_MLPHAPGVQMQAIPEDAIPEE**pS**GDEDEDDPDKR_	unknown
		421	S	_IACEEEF**pS**DpSEEEGEGGRK_	enzymatic activation, molecular association[275]
		423	S	_IACEEEFpSD**pS**EEEGEGGRK_	enzymatic activation, molecular association[275]
HDAC2	IPI00289601	394	S	_MLPHAPGVQMQAIPEDAVHED**pS**GDEDGEDPDKR_	enzymatic activation, enzymatic inhibition, molecular association[276,277]
		422	S	_RIACDEEF**pS**DpSEDEGEGGRR_	enzymatic inhibition, molecular association[277]
		424	S	_RIACDEEFpSD**pS**EDEGEGGRR_	enzymatic inhibition, molecular association[277]
		331	S	_YYAVNFPMRDGIDDE**pS**YGQIFK_	unknown*
HDAC4	IPI00010088	565	S	_QEPIE**pS**DEEEAEPPREVEPGQR_	unknown
		632	S	_AQ**pS**SPASATFPVSVQEPPTKPR_	molecular association, intracellular location[278,279]
		465	T	_**pT**QSAPLPQNAQALQHLVIQQQHQQFLEK_	unknown
HDAC5	IPI00871583	703	T	_**pT**QSSPAAPGGMK_	unknown*
		705	S	_TQ**pS**SPAAPGGMK_	unknown
HDAC6	IPI00005711	22	S	_QNPQ**pS**PPQDSSVTSK_	unknown
HDAC7	IPI00418482	109	S	_TVHPN**pS**PGIPYR_	unknown
		486	S	_AQ**pS**SPAAPASLSAPEPASQAR_	unknown
		358	S	_TR**pS**EPLPPSATAPPPPGPMQPR_	intracellular location[280 281]

Table 5 summarizes confidently localized serine and threonine sites on different HDAC family members, several of which bear functional roles in terms of enzyme activity, such as Ser421 and Ser423 on HDAC1, molecular association, e.g. Ser331 on HDAC4, and intracellular localization, e.g. Ser358 on HDAC7, as described earlier. Notably, the sites on HDAC1, HDAC2 as well as HDAC7 were found in a highly acidic sequence environment indicative of being CK2 and/or PKD substrate sites[275,276,280,282]. Moreover, further modifications occurred on residues proximal to proline or glutamine residues. Thus,

these results deliver possible targets being relevant in the context of a therapeutic strategy in co-targeting members of both enzyme families.

2.3   Quantitative analysis of gefintib- and erlotinib-induced phosphoregulation

For the assessment of phosphorylation changes in consequence of the treatment with gefitinib and erlotinib only class I sites were taken into consideration. For reasons of precision and robustness, identified and quantified phosphopeptides emerging from at least two of the three independent biological replicate experiments were further studied to detect substantial alterations in phosphorylation. Thus, out of the 10,975 class I phosphorylations sites 10,544 could be quantitatively determined. Per experiment about 8,000 distinct class I phosphosites were on average determined. 7,563 class I sites were repeatedly quantified in at least two independent biological replicate experiments and consequently considered for further analysis, including 5,342 distinct phosphosites quantified in all three experiments (Figure 27). In order to address possible errors introduced by unequal pooling of the differentially labeled lysates, only phosphosite ratios normalized by MaxQuant software were utilized[236]. That operation includes shifting to obtain a logarithmized median of zero on the supposition that the majority of phosphosites show no differential regulation[236]. In case a class I phosphosite was quantified in both technical replicates of a biological experiment, these ratios were averaged.
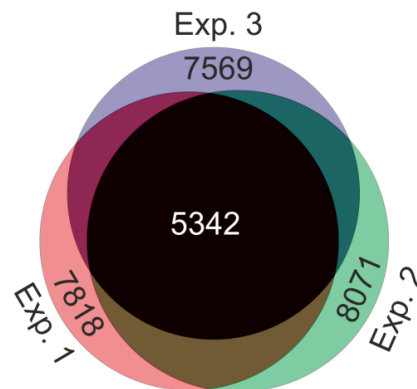
Figure 27: Comparison of class I phosphosites quantified in the three biological replicate experiments. Numbers indicate the quantified phosphosites for each individual phosphoproteomics analysis and in the overlap of all three replicates.

The next step was to discriminate phosphosites which were significantly regulated from non-regulated as a consequence of inhibitor treatment. In this regard, it was of importance to find valid statistical means to

provide reliable significance thresholds to discern truly regulated phosphorylation sites. Therefore, a rank product strategy was applied to this dataset which was implemented in the Multiexperiment Viewer software. This algorithm works as follows: At first, the overall rank of a phosphosite ratio obtained in an individual (biological) replicate is calculated of all ratios obtained for all replicate experiments. The rank is dependent on the order of the fold change ratios, and thus, either decreasing or increasing.
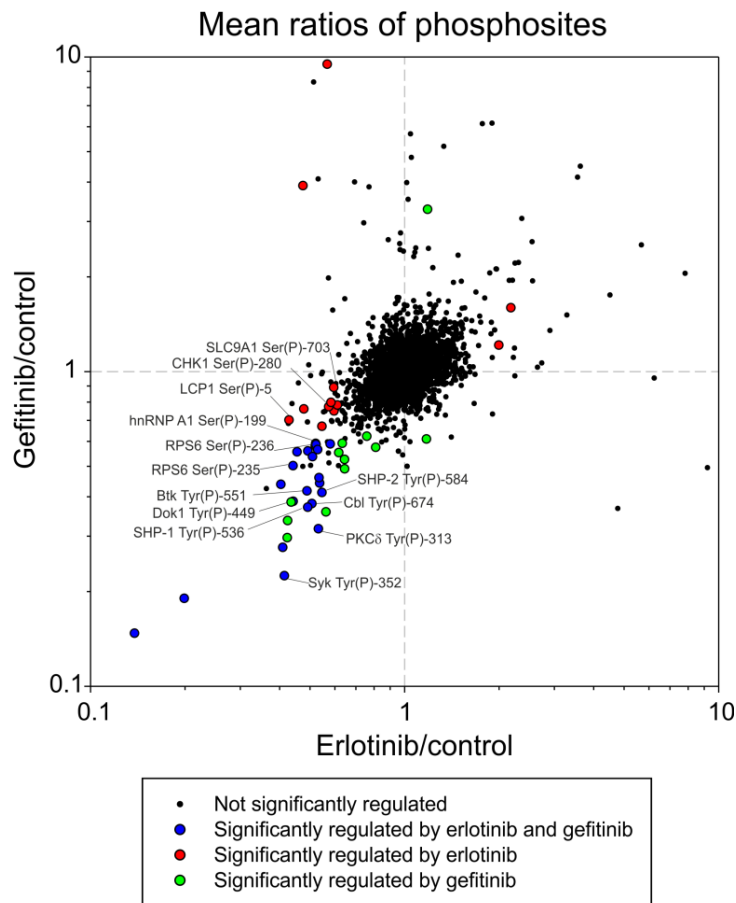
Figure 28: Scatter plot comparison of average phosphosite ratios quantified from gefitinib- versus erlotinib-treated KG-1 cells. Phosphosites exhibiting statistically significant regulation upon kinase inhibitor treatment are highlighted by color-coded dots as indicated.

Subsequently, this rank is transformed into a probability by division by the number of all ratios. Finally, the so-called Rank Product (RP) for a specific phosphopeptide is calculated by multiplication of the respective probabilities of each biological replicate[237]. RPs are considered significant by determining the likelihood by comparison with randomized experiment simulations[237]. Based on this probability, false-positive rate calculations were carried out and here differentially regulated phosphopeptides were estimated being within a FDR of 5%.

Thus, 36 and 35 regulated site-specific phosphorylations upon 1 h treatment with erlotinib and gefitinib, respectively, were identified (Figure 28, Table 6). This small fraction compared to the overall number of

phosphorylation sites points at a rather specific interference by both inhibitors. Only two and one site(s) were upregulated due to incubation with erlotinib and gefitinib, respectively. As expected, the residual peptides were downregulated. Notably, there was a large overlap between sites that showed significantly reduced phosphorylation due to both treatments (Table 6). Nearly all of the phosphosites found to be confidently downregulated by only one of the inhibitors were also influenced in a similar manner by the other inhibitor; however, due to the rigorous statistics applied here, they did not fulfill the necessary confidence level. The scatter plot in Figure 28 illustrates this issue on the basis of the chosen FDR, where all quantified phosphorylation sites are compared for their quantitative changes and significant regulated sites are highlighted. Thus, these results were indicative of similar modes of action for both inhibitors in KG-1 cells, which is also expressed in comparable effects seen in cell viability assays (Figure 22). Notably, compared to the distribution of all sites quantified in which phosphorylated tyrosines are significantly underrepresented, in terms of phosphosites regulation tyrosines account for substantial proportions (Figure 29). Moreover, when looking at the effects of individual inhibitors, the proportion of phosphotyrosine residues comprised about the half of the sites affected gefitinib, whereas this fraction in case erlotinib did not even account for one third.
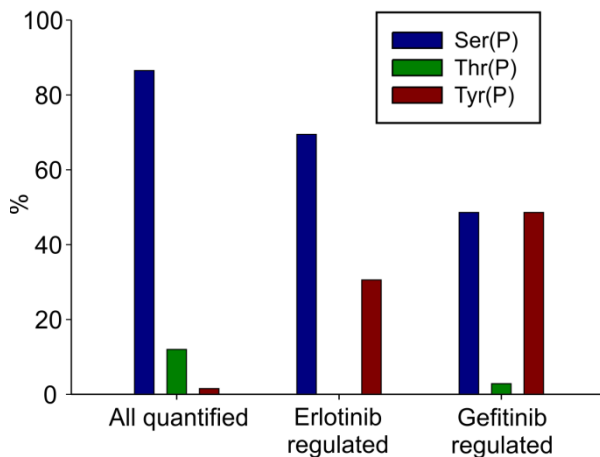
Figure 29: Percentage distribution of phosphorylated serines, threonines and tyrosines. Depicted are all quantified phosphosites as well as gefitinib- and erlotinib-regulated phosphosites in KG-1 cells.

Table 6 summarizes all identified phosphorylation changes upon inhibitor treatment that were significant by the FDR criteria. As a starting point to scrutinize cellular modes-of-action of gefitinib and erlotinib, a tighter focus was set on phosphorylation sites on protein kinases and their substrates. For instance, both inhibitors led to a reduction of phosphorylated tyrosines of SYK (Tyr352), BTK (Tyr551) and PKCδ (Tyr313). Remarkably, all of them are critical for the kinases' activation. Phosphorylated Tyr313 on

PKCδ is reported to stabilize structural arrangements necessary to promote kinase activity[283]. Similarly, Tyr551 lying in the activation loop of BTK and Tyr352 in SYK enhance catalytic activity of both kinases when getting phosphorylated[284,285]. Interestingly, when looking at possible functional relations between these tyrosine kinases, BTK can be turned on via modification of Tyr551 in several ways, either by SYK, alternatively by itself via autophosphorylation and, as a third option, SFKs were reported to phosphorylate this site[284,286-288]. Additionally, Tyr352 in SYK is also known to be phosphorylated in a SFK-dependent fashion[289]. Interestingly, *in vitro* and *in vivo* approaches demonstrated that SFKs can also modify Tyr313 of PKCδ, another site which was suppressed upon both erlotinib and gefitinib treatment[283,290,291]. Collectively, these results suggest a possible involvement of SFKs as common transphosphorylating tyrosine kinases affected by kinase inhibitor interference. When looking at the activity promoting SFK autophosphorylation sites (Tyr397 in LYN and Tyr426 in YES residing in the activation loop region), levels were consistently reduced by about 30% upon either 10 µM erlotinib or gefitinib in KG-1 cells, and thus not yet reaching the statistical confidence required for significant change according to an accepted FDR of 5% (Table 6).

Table 6: Erlotinib- and gefitinib-regulated phosphorylation sites.

Protein Names	Short name‡	IPI	Site	Sequence Window	Ratio erlotinib/ctrl	Ratio gefitinib/ctrl
Significantly downregulated upon erlotinib and gefitinib						
70 kDa SHP-1L protein	SHP-1	IPI00795221	Y536	KGQESE**Y**GNITYP	0.49	0.37
E3 ubiquitin-protein ligase CBL	Cbl	IPI00027269	Y674	SSANAI**Y**SLAARP	0.51	0.38
Hematopoietic progenitor cell antigen CD34	CD34	IPI00006070	Y329	RLGEDP**Y**YTENGG	0.54	0.44
Phosphoprotein associated with glycosphingolipid-enriched microdomains 1	PAG	IPI00020464	Y359	SSCNDL**Y**ATVKDF	0.51	0.54
Protein kinase C delta type	PKCD	IPI00384562	Y313	SEPVGI**Y**QGFEKK	0.53	0.32
Putative uncharacterized protein C1orf150	LOC148823	IPI00152169	Y89	SSNDDG**Y**ENIDSL	0.44	0.39
Transgelin-2	TAGLN2	IPI00647915	Y29	ANRGPA**Y**GLSREV	0.53	0.46
Tyrosine-protein kinase BTK	Btk	IPI00029132	Y551	YVLDDE**Y**TSSVGS	0.49	0.42
Tyrosine-protein kinase SYK	Syk	IPI00018597	Y352	EVYESP**Y**ADPEEI	0.41	0.22
Tyrosine-protein phosphatase non-receptor type 11	SHP-2	IPI00658023	Y584	EDSARV**Y**ENVGLM	0.55	0.41
Forty-two-three domain-containing protein 1	FYTTD1	IPI00289907	S61	RRLLQQ**S**GAQQFR	0.49	0.56
MORC family CW-type zinc finger protein 3	MORC3	IPI00436705	S515	VPRRHL**S**EGTNSY	0.52	0.58
40S ribosomal protein S6	S6	IPI00021840	S235	AKRRRL**S**SLRAST	0.45	0.56
40S ribosomal protein S6	S6	IPI00021840	S236	KRRRLS**S**LRASTS	0.52	0.59
40S ribosomal protein S6	S6	IPI00021840	S240	LSSLRA**S**TSKSES	0.44	0.50

40S ribosomal protein S6	S6	IPI00021840	S242	SLRAST**S**KSESSQ	0.53	0.57
Heterogeneous nuclear ribonucleoprotein A1	hnRNP A1	IPI00215965	S199	QRGRSG**S**GNFGGG	0.52	0.59
Eukaryotic translation initiation factor 4 gamma 1	eIF4G	IPI00552639	S1093	APGGRL**S**WGKGSS	0.40	0.44
Eukaryotic translation initiation factor 4 gamma 1	eIF4G	IPI00552639	S1146	RVVQRS**S**LSRERG	0.41	0.28
Eukaryotic translation initiation factor 4 gamma 1	eIF4G	IPI00552639	S1148	VQRSSL**S**RERGEK	0.58	0.59
Eukaryotic translation initiation factor 4 gamma 1	eIF4G	IPI00552639	S1186	TPATKR**S**FSKEVE	0.14	0.15
Eukaryotic translation initiation factor 4 gamma 1	eIF4G	IPI00552639	S1188	ATKRSF**S**KEVEER	0.10	0.09
Eukaryotic translation initiation factor 4 gamma 3	eIF4G3	IPI00646377	S1131	TLTSRG**S**MGREKN	0.20	0.19

Significantly downregulated upon erlotinib

Phosphoprotein associated with glycosphingolipid-enriched microdomains 1	PAG	IPI00020464	Y341	TVPEST**Y**TSIQGD	0.47	3.90
CTD small phosphatase-like protein 2	CTDSPL2	IPI00033054	S9	LRTRKA**S**QQSNQI	0.55	0.67
Microtubule-actin cross-linking factor 1, isoforms 1/2/3/5	ACF7	IPI00256861	S1376	KRRRML**S**SSDAIT	0.60	0.75
Myc proto-oncogene protein	Myc	IPI00033016	S21	TMPLNV**S**FTNRNY	0.61	0.78
Plastin-2	L-plastin	IPI00010471	S5	__MARG**S**VSDEEM	0.43	0.70
Putative uncharacterized protein DENND1A	DENND1A	IPI00873295	S523	RRTSVP**S**PEQPQP	0.48	0.76
Putative uncharacterized protein GTSE1	GTSE1	IPI00871779	S690	KNVAKP**S**PVVGQL	0.57	9.49
Serine/threonine-protein kinase Chk1	Chk1	IPI00023664	S280	KRPRVT**S**GGVSES	0.58	0.77
Small glutamine-rich tetratricopeptide repeat-containing protein alpha	SGTA	IPI00013949	S301	LRSQIR**S**RTPSAS	0.57	0.77
Small glutamine-rich tetratricopeptide repeat-containing protein alpha	SGTA	IPI00013949	S305	IRSRTP**S**ASNDDQ	0.58	0.80
Sodium/hydrogen exchanger 1	NHE1	IPI00020060	S703	SRARIG**S**DPLAYE	0.59	0.89

Significantly downregulated upon gefitinib

Docking protein 1	Dok1	IPI00015287	Y449	SHNSAL**Y**SQVQKS	0.44	0.39
Intersectin-2	ITSN2	IPI00414027	Y968	EEPEAL**Y**AAVNKK	0.62	0.55
Nuclear transcription factor Y subunit alpha	NF-YA	IPI00333568	Y266	LEEEPL**Y**VNAKQY	0.64	0.49
Phosphoprotein associated with glycosphingolipid-enriched microdomains 1	PAG	IPI00020464	Y163	LGMEGP**Y**EVLKDS	0.63	0.59
Phosphoprotein associated with glycosphingolipid-enriched microdomains 1	PAG	IPI00020464	Y387	EEPEPD**Y**EAIQTL	0.64	0.53
Serine/threonine protein phosphatase	PPP1CA	IPI00027423	Y317	DKNKGK**Y**GQFSGL	0.42	0.34
Vimentin	vimentin	IPI00418471	Y53	STSRSL**Y**ASSPGG	0.42	0.30
COP9 signalosome complex subunit 8	COPS8	IPI00009480	S175	AGALDV**S**FNKFIP	0.56	0.36
Gamma-adducin	ADD3	IPI00004408	S402	EKPRHK**S**DVEIPA	0.76	0.62
Pleckstrin homology domain-containing family G member 3	PLEKHG3	IPI00291711	S433	LKKAWS**S**QDEVST	1.17	0.61

Uncharacterized protein C14orf43	C14orf43	IPI00784739	T715	SVMGEA**T**PVSIEP	0.81	0.57
Other sites						
Proto-oncogene tyrosine-protein kinase Yes	Yes	IPI00013981	Y426	LIEDNE**Y**TARQGA	0.73	0.66
Proto-oncogene tyrosine-protein kinase Lyn	Lyn	IPI00298625	Y397	VIEDNE**Y**TAREGA	0.72	0.76
Tyrosine-protein kinase SYK	Syk	IPI00018597	Y323	TVSFNP**Y**EPELAP	0.62	0.50
Phosphoprotein associated with glycosphingolipid-enriched microdomains 1	PAG	IPI00020464	Y417	VPKENDYESISDL	0.73	0.69
Phospholipase C, gamma 1	PLCG1	IPI00383849	Y783	GRNPGFYVEANPM	0.74	0.75

‡Short protein name according to PhosphoSitePlus database (http://www.phosphosite.org)

Due to the possible role of SFKs in the aforementioned kinase modifications a phosphoepitope-specific antibody was used to assay cellular SFK autophosphorylation levels by immunoblotting. While inhibitor concentrations of 10 μM led to a modest reduction in accordance with the MS data, higher erlotinib and gefitinib doses of 30 μM potently suppressed phosphorylation of the conserved tyrosine residue in the SFK activation loop region (Figure 30).
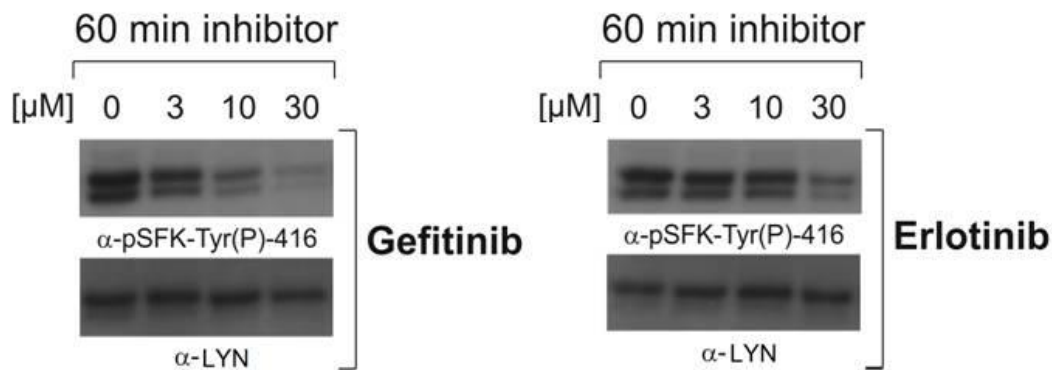
Figure 30: Immunoblot analysis of SFK phosphorylation. KG-1 cells were treated with the indicated concentrations of gefitinib or erlotinib for 1 h before lysis. Total cell lysates were subjected to immunoblotting with anti-phospho-Tyr416 SFK-specific and anti-LYN antibodies.

These results validated cellular inhibition of SFK activity by erlotinib and gefitinib. Therefore, the slight reduction observed at the 10 μM inhibitor dose used in SILAC experiments likely represented a real change that might already translate into lower SFK activity towards potential cellular substrates such as SYK, BTK and PKCδ. Moderately reduced SFK activity towards Tyr352 of SYK and Tyr551 of BTK might further diminish the autophosphorylation of these residues by the tyrosine kinases, which would amplify the overall inhibitory effect on these site-specific phosphorylations.

In order to explore a broader context of individual phosphorylation changes potential connections between regulated sites were examined using the STRING database. In addition, the SFKs LYN and YES were included in that network analysis to highlight their potential role upon inhibitor treatment. Notably, even though only a minor fraction of identified phosphosites were downregulated as a result of gefitinib and erlotinib treatment, small interaction network structures could be assembled. The original STRING output originally delivered two distinct networks, one of which harbored nearly all regulated tyrosine phosphorylated proteins and the other one three proteins being modified at serine and threonine residues. An additional edge between PKCδ and ribosomal S6 protein based on literature evidence enabled the combination of both (Figure 31)[292]. Accordingly, to this unified network belonged the protein kinases BTK, SYK and PKCδ but also its catalytic counterparts, such as the protein tyrosine phosphatases SHP-1 and SHP-2. Moreover, proteins not carrying any enzymatic activity showed substantially reduced phosphorylation upon gefitinib and erlotinib treatment, such as PAG or CD34. Especially those proteins regulated at phosphotyrosine sites have all been reported as important modulators of cellular signaling pathways with an impact in cell proliferation, differentiation and survival in both hematopoietic and non-hematopoietic cells[293-301]. Apart from the significantly downregulated phosphorylated tyrosine sites, at phosphoserine sites only the eukaryotic translation initiation factors 4 γ1 and γ3 together with the ribosomal S6 protein were found repressed and within the network (Figure 31, Table 6). Interestingly, these three proteins are involved in mRNA translation control which applied for most of the other proteins identified with significantly reduced phosphorylations at serine residues, such as Heterogeneous nuclear ribonucleoprotein A1 (hnRNP A1) (Table 6)[302].
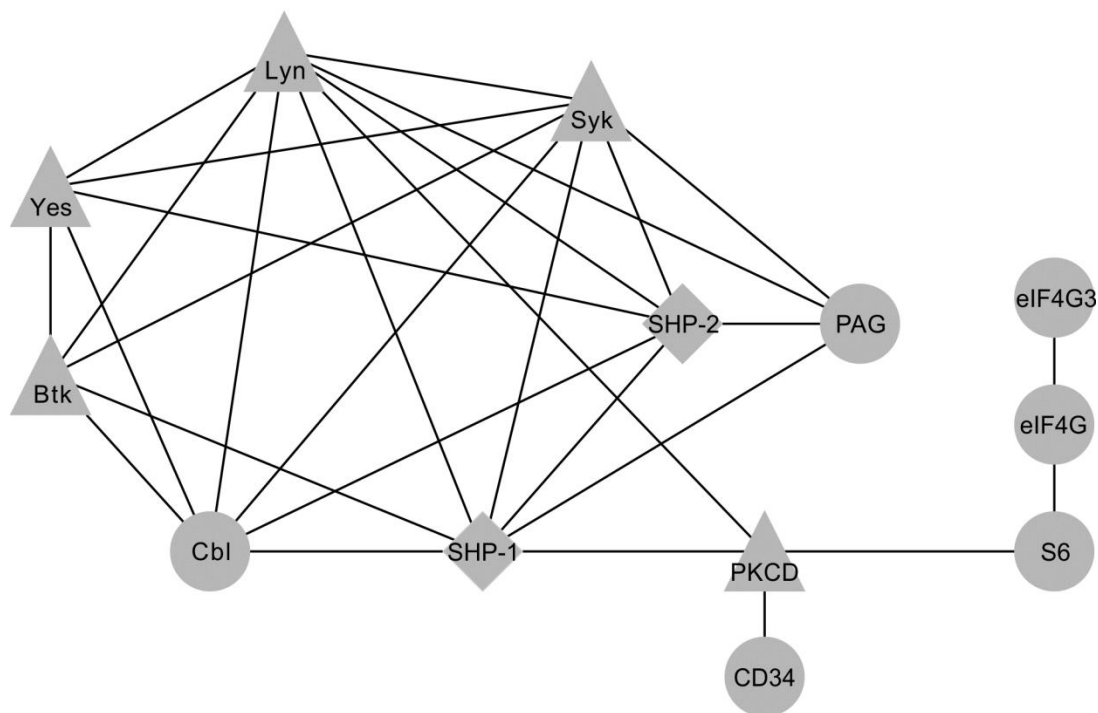
Figure 31: Network showing kinase inhibitor-regulated phosphoproteins including the SFKs LYN and YES based on known physical and functional interactions retrieved by STRING analysis. An additional edge connecting PKCδ and ribosomal S6 protein was added based on literature evidence[292]. Triangle-shaped nodes indicate protein kinases, square-shaped nodes protein phosphatases and all other proteins are represented by circular nodes. Short protein names according to the PhosphoSitePlus database are shown in the network (http://www.phosphosite.org).

2.4   Quantitative chemical proteomic profiling of gefitinib and erlotinib in KG-1 cells

The previous section gave an insight into the target-specific outcome of erlotinib and gefitinib treatment in terms of reduced substrate protein phosphorylations as a result of direct kinase targeting. Among the identified proteins were several kinases, partially showing decreased phosphorylation on sites influential to their enzymatic activity. However, this information itself does not sufficiently support the conclusion that these kinases are directly affected by the inhibitor. Thus, the question raised was which kinases are direct targets of the inhibitor. This information would complement the information derived from the phosphoproteomic approach with regard to a better understanding of the cause of the observed effect. In addition, the knowledge about the actual molecular mode of action of a drug provided a sound basis of further target-directed optimization strategies.

In order to address this issue the chemical proteomic approach delineated in the first part of this thesis was employed, offering quality-controlled screening of the examined inhibitors in a nearly physiological milieu to calculate target-specific dissociation constants. As a capturing agent were used the gefitinib derivative AX14596 (Figure 8) immobilized on Sepharose beads. Using differentially labeled extracts of KG-1 cells from cultivation in SILAC media, experiments were performed in analogy to the scheme depicted in Figure 11a, Figure 12a and Figure 13.
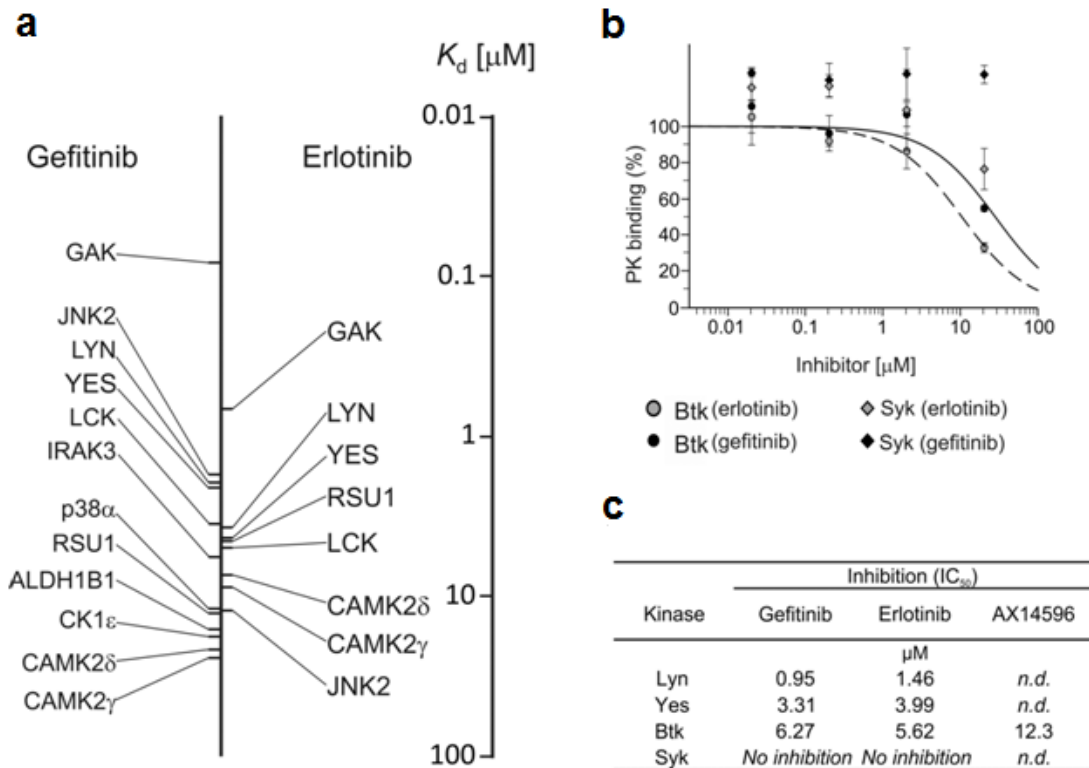
Figure 32: Identification and characterization of direct erlotinib and gefitinib targets in KG-1 cells. Target protein K_d values for erlotinib and gefitinib were determined in quantitative chemical proteomics experiments using the AX14596 resin as capture reagent (a). Binding behavior of cellular BTK and SYK to the VI16742 resin in the presence of different concentrations of erlotinib or gefitinib is depicted. SILAC quantification was done to measure BTK and SYK binding for the different concentration compared to control incubation without inhibitor, which was set as 100% binding (b). *In vitro* kinase assays with recombinant kinases were performed to determine IC_{50} values for gefitinib, erlotinib and AX14596. Reactions were carried out in the presence of sub-micromolar ATP concentrations well below the $K_M(ATP)$ of the tested kinases[233]. Therefore, the measured IC_{50} values provide a close approximation of the respective dissociation constants. SYK kinase activity was not inhibited by up to 30 μM erlotinib or gefitinib.

Thus, lysates were incubated once and twice with AX14596 beads to determine binding affinities of specifically retained target proteins. Those were filtered by comparison of binding to control beads versus inhibitor beads. If both control criteria were met (equilibrium binding and molar excess of immobilized ligand over target quantities), dissociation constants for AX14596 were determined. In parallel, target-specific IC_{50} values for gefitinib and erlotinib were obtained by measuring concentration-dependent dis-

placement of AX14596 resin-bound targets. As described earlier, the IC_{50} values, the dissociation constants for AX14596 and the concentration of immobilized inhibitor were inserted into the Cheng-Prusoff equation to calculate the individual target affinities. Among the kinases whose binding to the AX14596 matrix was inhibited at low micromolar gefitinib or erlotinib concentrations were the serine/threonine kinases GAK and JNK2, as well as several SFKs, namely LYN, LCK and YES (Figure 32a). In addition, an array of other previously reported serine/threonine kinase targets of gefitinib and erlotinib were detected, though with rather low affinities[148,158]. In the phosphoproteomic dataset regulation of phosphotyrosine sites was a prevailing element and this at inhibitor concentrations in the range of the detected tyrosine kinases' IC_{50} values. In addition, the low overall incidence of identified tyrosine phosphorylation argues against an effect that was caused by direct interference with serine/threonine kinases. On that note, in contrast to the SFKs identified by quantitative chemical proteomics, the tyrosine kinases SYK and BTK, both showing a downregulated activation loop phosphorylation in the phosphoproteomics dataset, were not retained by the AX14596 resin. However, SYK and BTK could not be excluded as direct targets merely because not being available for affinity determinations. Accordingly, it is conceivable that both kinases are susceptible to erlotinib and or gefitinib inhibition but were not bound to the gefitinib derivative AX14596 in a sufficiently strong manner. Taking this possibility into consideration an alternative *in vitro* association experiment was set up using the broadly selective kinase inhibitor VI16742 as an immobilized capture matrix to enable affinity determinations harnessing its particular target spectrum (Figure 15). Indeed, SYK and BTK were efficiently retained by the inhibitor resin and subsequent competition experiments laid the ground for affinity evaluations. In contrast to BTK, which was considerably displaced from immobilized VI16742 by more than 40% and 60% with the highest applied concentrations (20 µM) of gefitinib and erlotinib, respectively, SYK binding was not affected at all (Figure 32b). While SYK was excluded as target of erlotinib and gefitinib, K_d value calculations for BTK were feasible. Including its affinity for immobilized VI16742 this competition behavior translated into K_d values of 7 and 18 µM for erlotinib and gefitinib, respectively. In order to validate these affinities and to rule out that displacement of BTK from the matrix takes place in an indirect manner, e.g. via binding of a gefitinib and erlotinib-binding protein, which is conceivable due to the large array of targets of VI16742, *in vitro* kinase assays were performed with recombined BTK enzyme. It turned out that the enzymatic activity of BTK is suppressed by both drugs while AX14596 was less potent, confirming the hypothesis that BTK is a direct target of gefitinib and erlotinib (Figure 32c). Moreover, the small affinity to AX14596 is most likely the reason why it was not enriched by the AX14596 resin. The *in vitro* data also verified the outcome of the quantitative chemical proteomics experiment which implied that SYK is neither a target of gefitinib nor of erlotinib. Moreover, dissociation constants of the SFKs LYN and YES were found in good accordance with those acquired by *in vitro* association experiments. In summary, the chemical pro-

teomics approach in combination with *in vitro* data obtained with recombinant enzymes pointed at SFKs and, to a lesser extent, BTK as direct targets of gefitinib and erlotinib, while SYK could be eliminated as point of inhibitor action. In addition, measured target affinities were in the low micromolar range and comparable for both drugs, thus correlating with the observed dose-dependent effects of erlotinib and gefitinib on KG-1 cell viability. Although the SFKs LYN and YES were somewhat more sensitive than BTK, our *in vitro* target data does not exclude a possible contribution of cellular BTK kinase inhibition to the observed tyrosine phosphorylation changes upon erlotinib and gefitinib treatment. A previous study employing orthogonal pharmacological and genetic approaches claimed that targeted invention in SYK activity bears a large potential for AML therapy[222]. This is not necessarily contradictory to the results obtained here, but rather complementary in that sense that reduced phosphorylation of SYK by SFKs and/or BTK might be impaired upon drug treatment. In that case, SYK can be rather considered as an indirect target of erlotinib and gefitinib treatment.

IV   Discussion

1. Quantitative protein interaction profiling

1.1   Methodical remarks

1.1.1   Quantitative *in vitro* association experiments

An integral part of research aimed at the elucidation of functional aspects of proteins is to study their interactome, preferentially in their native intracellular context. For instance, small organic molecules designed to perturb the cellular signaling machinery often rely on selective protein targeting and are common tools in basic as well as in drug discovery-orientated research. For both disciplines extensive knowledge about their interaction partners is of great importance, on the one hand to comprehend in detail how small-molecule tool compounds elicit the observed effects in order to elucidate associated consequences of specific interventions in cellular signaling; on the other hand, to promote the agent's efficacy and/or to minimize off-target-related side effects in drug discovery efforts. For cell biological research endeavors studying interactions between proteins may be considered as essential business with the purpose of unraveling of cellular processes mostly taking place as a sequence of more or less transient protein complex formations. Therefore, in order to unravel the molecular quality of these cellular processes it is indispensible to precisely decipher the molecular environment of proteins with known functions. The methodology presented within the scope of this study is capable to address these issues for both protein-protein just as for protein-small molecule interactions and, even more importantly, in a quantitative manner.

Moreover, many of the drawbacks of previous *in vitro* approaches can be overcome, as the affinity chromatography-based approach facilitates the exposure of affinity ligands with the entire expressed cellular proteome as potential targets present in cellular extracts. Therein, proteins are available in their full length

form, with their naturally occurring posttranslational modifications and in relative proportions of the individual protein expression levels. On this account, the intracellular conditions are largely resembled and inhere the identification of previously unknown interactions as shown for VAV2 for the phosphorylated IRS4 peptide or BLMH for AX14596 and gefitinib, respectively.

The outlined concept for affinity determinations is not restricted to profile interactions of kinase inhibitors or tyrosine phosphorylated peptides as exemplified here. An implementation with various affinity ligands such as other classes of small molecules, peptides and also proteins should be feasible for any biological extracts. In order to obtain distinctive peptide and ultimately protein ratios to perform accurate affinity measurements across the proteome, SILAC labeled cell lysates were used in combination with a high resolution MS readout. Upon trypsin digestion virtually each peptide contained at least one lysine or arginine residue of a particular isotopic variant due to the preceding SILAC labeling. In turn, this enabled high precision quantitation within a broad dynamic range, which is essential for accurate affinity assignments. Furthermore, SILAC is versatile for many different cell lines and even for mouse tissue enabling a large applicability of the approach for diverse scientific issues linked to a certain cell type[137]. However, metabolic SILAC labeling not always working, e.g. if human tissue is the protein source[303]. For such cases, alternative labeling techniques in combination with quantitative MS are apposite to the *in vitro* association strategy, such as the isobaric peptide tagging with iTRAQ to gain quantitative information from tandem MS spectra[141].

The concept provided here represents a novel and crucial advancement of earlier studies focused on the qualitative discovery of interactions between a cellular proteome and small molecule kinase inhibitor or peptide ligands[148,155,229]. Among these improvements is the capability of direct filtering for specific binders, which is generally a minor fraction of all identified proteins and especially of all proteins in a cellular extract. Moreover, it enables the evaluation of the corresponding strength of the individual target interactions. In extension to an approach employing sequential affinity chromatography to discriminate between background and specific binders, the methodology here is able to yield affinity information provided that the ligand concentration is known (Figure 11)[304]. The complete experimental setup integrated supplementary "checkpoints" to exclude false positives among the identified binders. Whether a protein is attached randomly to the affinity ligand or in a directed manner is under strict supervision by comparison with control bait: Only targets showing a strong average preference for the affinity ligand comprised of two individually reproducible ratios were admitted for further analysis. The next hurdle to pass was the consistency of the affinity ratio *r* itself, to exclude alleged targets exhibiting considerable low affinity ratios in average, particularly in replicates where the light labeled lysate was incubated in the first and the heavy label in the second round with the capture resin. The origin of such ratios can lie in contamination with exogenous protein, which is naturally occurring in the light isotopic form, during sample preparation.

A significant aspect in this quantitative proteomics-based concept lies in the target ranking according their individual dissociation constants as a universal measure for affinity. Dissociations constants describe the stability of a complex in an equilibrium state, which requires accurate monitoring preferably on the individual target level. The incorporated control experiment clearly provided indication of the presence of equilibrium conditions, which has been reached for the vast majority of specific binders within the selected incubation period of 2.5 h by comparison to additional 2.5 h incubation (Figure 13a, Figure 16c). Yet, some outliers showed up sporadically with either lower ratios, e.g. ACAD10, with 0.48 or nicotine phosphoribosyltransferase with of 0.39 (both in Table 2), or with higher ratios than the predicted value of 1, e.g. sepiapterin reductase with 2.43 (Table 2) or 1.87 (Table A 1) or ATP-citrate synthase with 1.98 (Table A 1). A possible explanation for proteins showing decreased binding after 5 h compared to 2.5 h may be the fact that they cannot stably maintain their binding-competent conformation over time which leads to a ratio considerably lower than one. Proteins that show a significantly higher ratio than one might tend to aggregate or precipitate after a certain time. Alternatively, these binders may possess slow binding kinetics, especially slow on-rates, so that the establishment of binding equilibrium is delayed and takes measurably longer than 2.5 h. In line with this hypothesis are observations with VI16742 as affinity ligand. Supported by a number of hits - especially with regard to low-affinity targets - clearly tending to show an imbalance towards higher ratios than one as smaller target affinities often go hand in hand with a protracted establishment of equilibrium (Figure 16).

Another key issue that had to be controlled carefully when working with the above described derivation for target-specific dissociation constants was the quantitative surplus of immobilized ligand molecules over their targets in solution. Indeed, for most of the specifically retained proteins that case has occurred as expressed by a ratio close to three in the immobilized ligand control with 3 mg versus 1 mg protein (Figure 13b, Figure 16d). Again, a number of exceptions appeared that were above the expected ratio of three. For instance, SOS1 with 8.14 (Table 3), ACAD10 with 8.45 and BLMH with 11.91 (both in Table 2) or cell division cycle 2-like protein kinase 5 (CHED) with 5.31 (Table A 1) were among that proteins. Several reasons may account for those cases. For instance, indirect binding could be casual, i.e. if a protein binds weakly to a direct interactor and dissociation from such a complex occurs in the more dilute lysate. This is most likely the case for SOS1 which does not possess a "proprietary" phosphotyrosine-recognizing domain but interacts indirectly via GRB2 that is strongly attached to the phosphorylated peptide via its SH2 domain. Another reason could be concentration-dependent binding kinetics particularly for targets that generally show low on- and off-rates, respectively, for attachment to the affinity ligand. This would lead to markedly increased binding in the 3 mg compared to the 1 mg condition in a mode that is non-linear. A candidate where this may have applied was ACAD10 that missed the equilibrium control. For few cases, deviations from the predicted protein ratios may have occurred due to fact that

precise quantification was disabled since only a low number of peptides were amenable for LC-MS measurements.

A critical aspect for correct affinity determinations is worth of note when dealing with immobilized ligand in molar excess. Per definition, targets that exhibit extremely strong binding would yield an enrichment ratio r coming close to zero. However, for those cases, accurate ratio assignment for dissociation constant calculations becomes more intricate considering the dynamic range of SILAC-based quantification[236]. In order to circumvent that problem adjusting the concentration of immobilized ligand downwards would be helpful resulting in a shift of the quantification range window towards higher affinities. Yet, this was not a crucial in any of the *in vitro* association experiments in the presented study here.

1.1.2 Profiling of soluble small-molecule kinase inhibitors

Picking up the previous section, it is remarkable that outliers for both the equilibrium as well as ligand controls were underrepresented among protein kinase targets yielding meaningful dissociation constants for the immobilized inhibitors. Nevertheless, a strict quality control was a substantial prerequisite for the extension of the concept from determining dissociation constants of immobilized affinity ligands as a reference system to soluble kinase inhibitors by means of competition experiments. Therefore, a closer inspection of target binding to the capturing ligand might be appropriate. As outlined with the results of a supplementary control experiment depicted in Figure 16e, where VI16742 competed for target in the 'free' versus the immobilized form, more in-depth information about apparently specific proteins was provided. Obviously, a small proportion of targets was not detached from the solid inhibitor matrix even at high concentrations of soluble VI16742, which is indicative of largely irreversible or largely unspecific binding. One reason for such binding behavior may be that these proteins did not interact specifically with the ligand in the designated binding manner but rather, yet in a directed way, with an interface formed in consequence of its coupling to the Sepharose beads. Alternatively, slow off-rates for the binding reaction could be casual, which are potentially even more decelerated due to the local surplus of immobilized ligand on the beads compared to the inhibitor concentration in solution. In some cases, this control can be of relevance to attribute putative false negative hits among overlooked soluble compound targets, particularly if the immobilized resin and competing inhibitor used are structurally unrelated.

The general framework chosen for the concentration-dependent competition experiments as the basis for determining target-specific IC_{50} and consequently K_d values for the "free" inhibitors was adequate to monitor the establishment of binding equilibrium since this was indispensible for calculations of affinity constants according to Cheng and Prusoff[242]. Thus, K_d values were only considered meaningful if under-

lying IC_{50} values were in accordance irrespectively of whether potential target proteins were first exposed to soluble or immobilized competitor (Figure 14 and Figure 16f). Otherwise, binding equilibrium would have not been reached in at least one of the approaches and consequently provide inadequate quantitative data for the purpose of K_d value calculation.

Again, the possibility to carefully monitor each critical control parameter that is individually tied to each target is a substantial advance over earlier methods aimed at profiling small molecule's target affinities[160]. With the prerequisite, profiling of gefitinib in combination with its immobilized analogue AX14596 and similarly SB203580 with VI16742 yields affinity data that are in good correlation with dissociation constants obtained by *in vitro* kinase assays (Figure 19a). Generally, small molecule kinase inhibitors are a well characterized molecule class also in terms of their affinity parameters allowing benchmarking of results against data from other assay formats, such as *in vitro* kinase assays. With such reference data at hand, comparisons with other methods having similar aims are feasible. On that note, more pronounced divergences were generated by another technique with an identical purpose, yet a different methodical implementation lacking rigorous monitoring (see section III1.4 and Figure 19b)[160]. In addition, the controllability turns the approach unbiased as well as truly generic. The latter becomes obvious through the realization of the concept with both inhibitor combinations, independent of their structural relationship. This, in turn, is also advantageous by the fact that the methodology can be applied with an array of different kinase inhibitors or other small molecules that qualify for covalent immobilization and affinity capture. Indeed, several studies showed its practicability for kinase inhibitors as well as other small molecule ligands[146,147,160,305,306].

Using a broad-sprectrum affinity ligand of an identical tool compound or drug class, can represent a valid alternative. Especially, in cases where SAR information about the molecule designated for target profiling is not available and therefore an adequate immobilization strategy is rather intricate. Alternatively, if immobilization is generally not feasible without interfering with target binding or one wants to save the effort of compound synthesis. As exemplified by VI16742, competitive small-molecule kinase inhibitors directed against the conserved ATP-binding pocket share a similar pharmacophore model and, therefore, using that molecule class for implementation of that concept was absolutely feasible. With this broadly selective inhibitor a panel of potential targets was exposed to another, soluble inhibitor to be profiled for its target-specific affinities. In that case it was SB203580. However, a possible limitation of that variant is that it can only provide data for targets retained on the affinity resin. Thus, in order to obtain the largest coverage as possible the immobilization of an analogue or, even better, of the compound of interest itself is preferable.

1.2 Cellular targets of gefitinib

On examination, a discrepancy between the individual targets of gefitinib derivative AX14596 and gefitinib was visible. Only 18 of 32 specifically retained targets were significantly replaced from the matrix as a result of concomitant gefitinib incubation at the highest concentration applied. The underlying binding behavior is possibly a consequence of the altered chemical structure of AX14596 compared to the parental molecule and/or of its coupling to the Sepharose beads. It is conceivable that newly created surfaces formed in that process may have accounted for additional attachment points for protein interactions that are are not present within free gefitinib. Consequently, gefitinib is not capable of competing for these binders leading to the persistent attachment to the resin. Among these 14 hits to which that circumstance applied were five protein kinases and other purine nucleotide binders. At least these proteins may support the notion of a specific affinity to the immobilized inhibitor but not to soluble gefitinib. For those targets which were specifically displaced from the inhibitor matrix by increasing concentrations of soluble gefitinib, the ranking of target affinities was in good accordance with results of *in vitro* kinase assays. Among the strongest interactors of gefitinib were GAK, RIPK2 and BRK, whose inhibition bears therapeutic potential as reported earlier (Table 2)[148]. While GAK was the most affine target, EGFR was surprisingly only the third most. In addition, dissociation constants obtained by quantitative chemical proteomics differed from the *in vitro* data by a factor of about 30 (Table 2). This was conspicuous considering data from earlier studies demonstrating that gefitinib - originally developed as a very selective inhibitor of EGFR - possess an IC_{50} of approximately 30 nM as well as a high degree of selectivity along with a high affinity constant in the low nanomolar range[158,307]. However, these findings were made under *in vitro* kinase assay conditions using recombinant enzyme and this might explain why according to our method it is not the top most affine target. It is speculative and needs further investigation to exactly delineate the basis for that difference of data between the *in vitro* and more "*in vivo*" situation. One possible explanation might be that the *in vitro* data were generated with only a fragment of EGFR and not the full length version which is present in cellular lysates used in our method. Thus, intramolecular interactions or dimerization could account for a reduced affinity towards the antagonist. Moreover, the presence of regulatory proteins in the cell lysate could potentially alter the binding strength to gefitinib. This issue emphasizes the general actuality that the comparability of target-specific affinity constants determined by *in vitro* experiments may be limited due to protein-specific cellular factors, e.g. formation of protein complexes, posttranslational modifications and the presence of competing substrates. All of which are not transferable into the test tube because of practical reasons in addition to a lack of detailed knowledge regarding the composition of the individual components. Consequently, the chemical proteomic approach introduced here provides a milieu that closely resembles the native cellular conditions. Other techniques

that measure kinase activity and its inhibition in physiologically relevant environment, e.g. cell-based kinase assays, often require significant experimental efforts[308]. In addition, only one single target can be monitored per experiment and off-target effects are not detecteable. In contrast, the concept presented here is hypothesis-free and allows the measurement of binding affinities and, accordingly, for off-targets as well.

In that context, another remarkable finding was offered by this study. Among the topmost affine targets of gefitinib were the pyrophosphatase NUDT12 and aminopeptidase BLMH. The physiological roles of both enzymes are not understood in its entirety, BLMH is not even reported to bind nucleotides[251,252]. Whether gefitinib binding can also interfere with their biological function is possible, but has to be proven. If that is the case, such off-target effects could be utilized for particular scenarios. For instance, the cysteine protease BLMH was reported to catalyze the inactivation of the glycopeptide and antitumor drug bleomycin by hydrolyzing the carboxamide bond of its B-aminoalaninamide moiety thus protecting normal and malignant cells from bleomycin toxicity[251,309]. It seems to be highly expressed in a variety of tumor cell lines and it has been reported that an allelic variant of BLMH is genetically linked to Alzheimer's disease[309,310]. Assuming that gefitinib is able to inhibit BLMH's enzymatic activity, which is not proven yet, a therapeutic application on the basis of such an off-target effect is imaginable. In that way, the availability of quantitative in contrast to solely qualitative data enables prioritizing of drug target interaction and thus bears a large potential for drug development processes, e.g. in such a way that it enables correlations between effective and maximally tolerated doses[92]. The remaining targets of gefitinib were partially known for their interaction and/or confirmed rather weak affinities[148].

1.3   Cellular targets of SB203580

Utilization of the fairly unselective kinase inhibitor VI16742 facilitates the specific capturing of about 185 proteins from Hela S3 lysates that show predominantly kinase function (135) or at least nucleotide binding properties and enzymatic activity (49), underscoring the applicability of the performed filtering for specific targets (Figure 16, Table A 1, Figure 17). Assuming that in a mammalian cell line approximately 300 different protein kinases are expressed, this target platform covers more than 40% of the cellular kinome distributed over all protein kinase families (Figure 18)[311]. Indeed, due to its promiscuous target binding behavior VI16742 represents a suitable starting material for profiling a large protein kinase panel. Also the fact that it can be immobilized on Sepharose beads without any major efforts is definitely of advantage. Owing to the unbiased nature of affinity chromatography-based methods not only a large array of cellularly expressed protein kinases is at hand for subsequent profiling but also a proportion of other enzymes or binding proteins whose inhibition or interaction might be of therapeutic relevance. With

the coverage of the human kinome as shown here this resin can compete with a mixed-inhibitor resin of a previous study capturing, though affected with the aforementioned limitations, 174 protein kinases out of Hela S3 lysates (see section III1.4)[160]. In accordance with a previous study, profiling of SB203580 yielded almost 40 targets, however, only 7 showed submicromolar dissociation constants (Table A 1). Among these targets were kinases already known to interact with SB20350, namely RIPK2, GAK, CK1δ, CK1ε, DDR1 as well as a newly identified target PKN3, an interesting hit linked with a role in prostate cancer progression[155,312]. These results as well as those for weaker interaction partners were also in good agreement with data from in vitro activity assays in this study and that of Godl et al.[155]. In line with their observations, the lack of selectivity of the actual p38 inhibitor was confirmed and thus supporting the notion that drug-related effects may not be a result of disabling p38 activity alone[155,258]. Since no interaction between p38 and the VI16742 resin was observable, the determination of a dissociation constant for that kinase was not possible, emphasizing the dependency on the affinity ligand for the required target coverage. Nevertheless, SILAC-driven quantification has once more proven the ability of that method to measure target-specific dissociation constants over a wide range up high micromolar figures (Table A 1). Collectively, the strategy outlined here could fulfill requirements for target deconvolution in basic science as well as drug development research, especially for small organic molecules of various classes.

1.4 Interaction partners of phosphorylated IRS4 peptide

The application of the sequential affinity chromatography approach is *per se* not restricted to the use of small molecules as capturing ligand. Instead, with the implementation demonstrated here using a short peptide stretch containing a characteristic interaction site, the concept is substantially extended demonstrating its general versatility. The relevance of this experimental variant is justified due to the fact that many protein-protein interactions occur via modular domains recognizing short peptide motifs in their associated proteins, which is a universal basis of the structure and versatility of signaling networks (Figure 1)[263]. IRS4 plays a role as an interface downstream of multiple growth factor receptors, such as FGFR1, and acquires this role upon site specific tyrosine phosphorylation at Tyr921[229,313,314]. This patch is the crucial motif to be recognized primarily by signaling molecules containing SH2 domains[229]. With a short peptide sequence harboring the phosphorylated residue as a capturing ligand - besides the recently identified interactors p85, GRB2 and PLCG - several unknown interactors could be precisely delimited in comparison to the non-phosphorylated counterpart of IRS4. The vast majority of these interactors possesses a SH2 or other phosphotyrosine-binding domain and were therefore considered as direct binders of the phosphorylated IRS4 peptide (Figure 20, Table 3). These 17 proteins showed significant enrichment ratios hinting at a complex network of intracellular signaling molecules downstream of IRS4 confirming

its assigned role as an important crossing point between growth factor receptors and these molecules. With regard to the methodology, the distinct values for the dissociation constants were found to span a range from 1.5 to about 60 µM, indicative of the wide dynamic range detectable in this SILAC-based method. Remarkably, all three catalytic p110 PI3K subunits were found with similar affinity ratios as the regulatory p85 subunits. However, in contrast to the regulatory subunits, it is very unlikely that the catalytic ones attach directly to the peptide. That fact points at a relative strong interaction between the two different subunit types under the actual assay conditions. This also applies most probably for other specific interactors without phosphotyrosine-binding domain, e.g. SOS1 and SOS2, which can interact with GRB2 and FYN[315,316]. Support for the latter notion comes from the enrichment ratios of both nucleotide exchange factors. Those were found with lower values for the enrichment ratio r compared to GRB2 or FYN. This has most likely been a consequence of depleting of both proteins upon the first incubation round, and upon partial dissociation from the complex with GRB2 and/or FYN over time, its detection is artificially lowered following the second incubation, which is erroneously yielding stronger target affinities. Alternatively, it might be possible that GRB2 and FYN exhibit a stronger affinity for phosphorylated IRS4 if attached to the SOS proteins. This phenomenon is a rather marginal note, however, it suggests once again the potential that lies in working in a physiological milieu also for the detection of indirect targets. In this regard, the quantitative assessment of full-length binding partners of a short peptide is more informative than data derived from quantitative *in vitro* experiments[317]. It can lay the basis for an in-depth (mechanistic) understanding of highly dynamic protein assemblies relevant for any cellular process which depend amongst other factors (e.g. subcellular localization, expression levels) critically on the mutual affinities[318].

1.5   Profiling of EGFR interaction partners

Though pursuing a slightly different objective, namely the stringent discrimination between specific and background binding, the sequential enrichment strategy introduced by this study revealed its high potential for co-immunoprecipitation experiments to pull down protein-protein complexes. As demonstrated in the IRS4 experiment, co-interactors of proteins primarily bound to the affinity ligand were quantitatively characterized by a similar enrichment ratio r, as illustrated by the regulatory subuntits of PI3K and the SOS proteins. By harnessing that observation in the course of co-immunoprecipitation experiments specific EGFR binders could be discriminated through intuitively emerging filtering criteria (Figure 21). Again, this became only possible in combination with the quantitative SILAC methodology which allowed the dual classification of non-random binding by comparison with a control ligand as well as by its affinity. By that means, previously known EGFR interaction partners could be identified, all of which are

involved in the RAS-RAF-MAPK pathway as major downstream signaling route (SOS1, SOS2 and GRB2) or in signal modulation by receptor internalization or degradation (UBC, CBL and CBL-B)[265-267]. All these *bona fide* EGFR-interacting proteins clearly distinguish themselves from almost 600 other un-specific background proteins, which were pulled out of the lysate and identified in parallel proofing the validity of the methodology. Co-immunoprecipitation is among the standard methods of a molecular biologists lab to explore the interplay of distinct protein with their molecular surroundings. If quantitative MS instrumentation is available, the approach can be easily implemented to assign interactions in a large scale, with high confidence and in an unbiased manner without further need of sophisticated bioinformatic and statistical analysis[319]. It is of importance, however, to select an appropriate, ideally monoclonal, antibody which allows unrestricted interaction with co-purifying proteins. An alternative implementation of that concept avoiding immunoprecipitations is the usage of full-length proteins as affinity ligands immobilized by an affinity tag, e.g. the widely used HA- or GST-tags. These expression tags can be easily attached by standard recombinant techniques avoiding laborious and sophisticated chemical coupling[320].

2. Phosphoproteomics and chemical proteomics characterization of erlotinib and gefitinib interference in AML cells

Exploring the molecular origin of effects elicited in targeted therapies includes in the first place the characterization of the cellular effect together with the identification of the target(s) on which the observed outcome is based on. The integrated approach provided here combines large-scale quantitative phosphoproteomics with quantitative chemical proteomics for target deconvolution in order to clarify the cellular mode-of-action of erlotinib and gefitinib in KG-1 AML cells. An essential requirement of the strategy conducted here was its unbiased nature, which enabled the revealing of SFKs and most likely BTK as targets especially in view of the fact that the highly responsive cell line is lacking the prime-target EGFR. The dose-dependent antineoplastic effects evoked by erlotinib and gefitinib treatment were characterized by impaired viability, apoptosis and to a minor extent differentiation (Figure 22)[221]. With a relatively high, though therapeutically achievable concentration of 10 μM of either inhibitor the outcome of in total 49 significantly regulated phosphorylation sites pointed at a fairly selective interference with cel-

lular signaling[321,322]. The coverage of these inhibitor-induced phosphorylation changes was based on the comprehensive and reproducible identification with high confidence and on the quantification by means of SILAC of over 7,500 phosphosites out of three biological replicates. This number was extracted from almost 11,000 class I sites identified in the entire dataset, which represents the highest number of protein phosphorylation sites recorded from a human leukemia cell line thus far. Only a study published previously acquired similar figures for the murine myeloid cell line 32D, transformed by oncogenic FLT3-ITD[268]. Interestingly, even though tyrosine phosphorylation constituted expectably only a minor fraction of all confidentially assigned sites, 2% versus 83% and 15% phosphoserines and threonines, respectively, for the regulated sites, phosphotyrosine sites accounted for approximately 30% of regulation for erlotinib and 50% in case gefitinib treatment (Figure 29). In spite of the absence of EGFR, these data support the notion that the off-target interference of both tyrosine kinase inhibitors is nonetheless a result of attenuated activity among the group of tyrosine kinases in the human kinome[34]. With the assigned downregulated phosphotyrosines it was possible to assemble a highly interconnected network of known functional interactions. Constituents of the network were proteins functioning at nodes in signaling networks controlling signal transmission, many of which playing a role in malignant disorders[301,323-326]. One major branch point was SYK. After erlotinib and gefitinib treatment a significant reduction of phosphorylation at Tyr352 was detectable. The modification of this site is associated with a structural rearrangement of the kinase leading to an increased activity[285]. Notably, the downregulation of this phosphorylation site of SYK was accompanied by a dephosphorylation of Tyr551 within the activation loop of BTK. Tyr551 is also critical for the enhancement of BTK catalytic activity while SYK is being directly involved in that process by trans-phosphorylating BTK at that site[284,286,327]. Both cytosolic nonreceptor tyrosine kinases are expressed in all hematopoietic cells and represent key elements downstream of different activated (immuno)receptor tyrosine kinases, e.g. F_C- and B cell receptors (BCRs). SYK and BTK couple upstream signals to downstream signaling events that regulate proliferation, survival and differentiation in leukocytes such as B lymphocytes, mast cells and macrophages[298,328-331]. Thus, it is plausible that the inhibitory effect of erlotinib and gefitinib on this signaling interface was crucial for the observed effects in KG-1 cells. Earlier findings, primarily in lymphoid tissue, support a notion according to which highly active SYK and BTK were specified to play a role in autoimmune disorders and hematological neoplasms and, consequently, targeting these kinases was reported to bear therapeutic potential in these disorders[326,332-335]. The functional interactions in the described network resemble in some cases putative kinase substrate relationships (Figure 31). For instance, the ubiquitin ligase CBL is considerably less phosphorylated at Tyr674, a site known to be under control of the close relative of SYK, namely ZAP70[336,337]. Phosphorylation of that site is important for the negative regulatory role of CBL, because it enables its interaction with substrates that leads to their proteasomal degradation[338]. Notably, to that group of substrates belongs SYK itself as well as SFKs[338,339].

Another phosphosite reported to be regulated by SYK is Tyr783 of PLCG1[340]. Interestingly, upon its phosphorylation, PLCG1 becomes activated due to an induced intramolecular association between this site and the C-terminal SH2 domain[341]. The activation leads to the generation of two intracellular messengers, diacylglycerol (DAG) and inositol 1,4,5-trisphosphate (IP$_3$). These second messengers in turn promote the activation of PKC and the release of Ca^{2+} from intracellular stores, respectively[342]. Among the various cell type dependent responses associated with of PLCG1 activity are promotion of mitogenic signaling as well as induction of differentiation, which was found in the myeloid cell line U937[343]. Only a slight decrease of phosphorylated Tyr783 of PLCG1 after application of both drugs has been recorded here, thus not meeting the threshold to be significant (Table 6). However, the concomitant reduction of kinase activity may contribute to the observed effects in KG-1 cells, e.g. the induction of differentiation. Moreover, BTK and other TEC family kinases are also described to be involved in PLCG1 activation in hematopoietic cells[344,345]. Yet, according to quantitative chemical proteomics experiments, gefitinib and erlotinib bind BTK only with moderate affinity. Moreover, this analysis revealed that SYK, which was reported as a potential target in AML, could be excluded as an interactor of both drugs[222]. Remarkably, a previously published study suggested the tyrosine kinase JAK2 as direct erlotinib target in AML cells for which no phosphorylation sites could be identified. However, those sites known to be critical for JAK2 activity, namely Tyr1007 and Tyr1008, are located in proximity to two lysine residues and tryptic digestion generates a peptide of only four amino acids in size which escapes mass spectrometric detection due to its low m/z ratio. Moreover, the JAK2 substrate site Tyr694 on STAT5 was not recorded either. Given that erlotinib and gefitinib exert a comparable effect on the cellular phosphoproteome as well as on cell viability and that *in vitro* only erlotinib shows inhibition of JAK2, it is not likely that JAK2 is a shared direct target of both drugs[346]. Results from chemical proteomics further indicate that inhibition of JAK/STAT is, at most, a secondary effect, because neither of the inhibitors was able to compete with the VI16742 matrix for the closely related Janus kinase family members JAK1 and JAK2 (data not shown). On the contrary, SFKs LYN, YES and LCK turned out to be most susceptible to inhibition by erlotinib and gefitinib, respectively (Figure 32). Additional support of that assumption comes from *in vitro* activity assays confirming LYN and YES having dissociation constants in a low micromolar range. Moreover, results from these experiments obtained for SYK and BTK coincided with those obtained by quantitative chemical proteomics validating the missing and restrained affinity, respectively, of both drugs. Besides, it turned out that with regard to BTK, the very high dissociation constant of AX14596 acquired *in vitro* is most likely the reason why it was not efficiently retained by AX14596 coupled on beads and, accordingly, this was most likely the reason why detection by MS was hampered. In summary, the quantitative chemical proteomics and *in vitro* kinase activity data point at SFKs and at least to some degree at BTK as direct erlotinib and gefitinib targets. However, phosphorylation sites in the activation loop of LYN, YES and

LCK were not found downregulated to a significant extent according to the applied criteria. Nonetheless, some reduction in phosphorylation was detectable. Thus, the accompanied small decline of SFK activity was apparently sufficient to affect signal propagation to their cellular substrates, most importantly Tyr551 and Tyr352 on BTK and SYK, respectively[284,289].

LYN possessed the highest affinity for erlotinib and gefitinib among the bound SFK members and its inhibition could conceivably exert a major impact on the observed response in KG-1 cells. Moreover, in line with earlier findings in KG-1 cells, LYN accounts by far for the major fraction among SFKs being phosphorylated at that particular site indicative for their activity[347]. This kinase is expressed in all -with the exception of T-lymphocytes and NK cells- hematopoietic lineages and is activated by various immune receptors. Once switched on through ligand binding, these receptors translate and forward these extracellular signals into the cell eventually leading to modulation of key leukocyte functions, e.g. cell migration, survival and proliferation[348]. More precisely, upon immune receptor activation, SFKs can phosphorylate immunoreceptor tyrosine-based activation and/or inhibition motifs (ITAMs and/or ITIMs). Signaling is further propagated by activation of SYK following phosphorylated ITAM binding and subsequent activation of, for instance, the above described SYK/BTK/PLCG1 axis[349]. In non-malignant hematopoietic cells this cascade underlies tight regulation also including a negative regulatory facet of LYN depending on the cellular context[348]. In AML cells, this cascade often exhibits aberrant activity due to mutations or overexpression of involved genes or gene products offering a rationale for its targeting as a therapeutic option (see section I3.2)[347]. In KG-1 cells and in certain samples of AML patients LYN expression levels were found elevated accompanied by a high activation status, both of which might account for a crucial role of LYN in controlling downstream signaling towards an anti-apoptotic and pro-proliferative effect[347]. In such a scenario, inhibition and depletion of LYN, e.g. by siRNA knockdown, led to a substantial reduction of viability and induction of apoptosis, whereas normal hematopoietic progenitor cells being more independent from LYN were not affected by such treatments[347].

Further indication of reduced SFK activity upon inhibitor treatment was received with regard to downregulation of additional substrate sites. The two phosphotyrosines at positions 387 and 417 of the transmembrane adaptor protein PAG were dephosphorylated after treatment with both drugs, though only the decline of phosphorylated Tyr387 reached the significance level for gefitinib treatment (Table 6). These phosphotyrosines provide docking sites for LYN and enable PAG-mediated attenuation of LYN activity by enabling inhibitory phosphorylation by CSK, dephosphorylation by several cell membrane-associated phosphatases, such as SHP-1 and SHP-2, or degradation by SOCS1[350,351]. Remarkably, Tyr387 and Tyr417 are putative SHP-1 and SHP-2 substrate sites and their rather moderate dephosphorylation might be a consequence of the concurrently reduced activity of both enzymes. For both phosphatases a significant drop of Tyr536 phosphorylation on SHP-1 and Tyr584 on SHP-2 was recorded and both sites,

when phosphorylated, enable activation of the enzymes. The circumstance that Tyr536 on SHP-1 is among the substrate sites of SFKs may explain why upon SFK inhibition only few phosphorylation changes on direct substrates became detectable as phosphate groups do not dissociate spontaneously from modified tyrosines but require enzymatic removal by phosphotyrosine phosphatases[296]. That hypothesis might also apply for Tyr317 of PAG, which is, if phosphorylated, a docking site for CSK[350]. That phosphorylation site was reported to be under control of both LYN together with SHP-1, and, interestingly, at this site a notable phosphorylation change was not detectable[350]. Conceivably, in that case this system-inherent negative feedback mechanism may have attenuated downstream propagation of kinase inhibition effects. Inhibition of SHP-2 might also be an important factor promoting gefitinib's and erlotinib's antineoplastic activity. That phosphatase is considered as a positive mediator of proliferation, differentiation and survival downstream of growth factor receptor tyrosine kinases[352]. Consequently, aberrant SHP-2 activity, e.g. due to mutation or overexpression, has been attributed as a distinguished element in malignant transformation of carcinomas as well as of several leukemias such as AML[353]. The underlying mechanism of how SHP-2 activity contributes to these pathogenic outcomes is not fully understood so far, however, activation of SFKs has been found to be indirectly mediated by SHP-2 due to dephosphorylation of the aforementioned docking sites on PAG for CSK[351]. Like SHP-2, SHP-1 is involved in balancing phosphotyrosine-based signaling though exhibiting a different substrate spectrum[354]. In contrast to SHP-2, SHP-1 expression is reduced in most leukemias and lymphomas being indicative of an important function in maintaining normal cell proliferation by moderating tyrosine kinase activity[355-357]. Further investigations are required to clarify the precise impact of reduced phosphatase activity upon inhibitor treatment. Obviously, several negative feedback loops in phosphotyrosine-based signaling wherein phosphatases occupy a central role, are simultaneously affected by invention with small-molecule kinase inhibitors in cellular signal transduction.

Another example of a negative regulator of phosphotyrosine-based signaling pathways downstream of immunoreceptors found in the network was DOK1 (Table 6)[358]. In a phosphorylated state it is believed to act as a scaffold for recruiting RAS-GTPase-activating protein to lipid rafts and ultimately to a reduction of RAS-mediated signaling[358]. Interestingly, DOK1 is a direct substrate of SFKs substantiating SFK-inhibition as mode of action[300,359]. However, the impairment of this negative feedback loop cannot compensate the antiproliferative effects of SFK inhibition in KG-1 cells. Like DOK1, PPP1CA is only significantly downregulated upon gefitinib treatment at their respective phosphotyrosine sites but also upon erlotinib application, yet not meeting the FDR for being denoted as significant (Table 6). In contrast to the tyrosine specific phosphatases SHP-1 and SHP-2, PPP1CA is the catalytic subunit of the serine/threonine specific protein phosphatase PP1, which is ubiquitously expressed over all tissue types. It is conceivable that the downregulated and previously unknown phosphorylation site on Tyr317 has an impact on enzyme

activity due to the proximity to the negative regulatory site at Thr331. As PPP1CA adapts a critical role in cell division, apoptosis, protein synthesis and metabolism and at least two of such processes were altered upon inhibitor treatment (Figure 24)[221,299]. In addition, impairment of PPP1CA's activity may describe a possible switch from tyrosine kinase inhibition to phosphoserine and -threonine regulation[360]. Another example of changed serine and threonine phosphorylations as a consequence of altered tyrosine kinase activity may have started from the above described dephosphorylation of PLCG1 as a result of reduced SYK activity. As mentioned earlier, activated PLCG1 produces the second messenger molecule DAG which shows high affinity binding to PKCδ. By association with DAG, PKCδ is relocated to the plasma membrane and undergoes a substantial conformational change eventually leading to enhanced enzymatic activity[361]. At the membrane, as a direct impact of SFK activity, PKCδ is phosphorylated at Tyr313, which lies in the hinge region and is reported to enhance kinase activation[283,291]. Upon treatment with erlotinib and gefitinib Tyr313 was dephosphorylated. Thus, it is likely that in KG-1 cells SFK inhibition interferes in two ways with PKCδ induction by cutting the DAG supply as well as by preventing an activating phosphorylation. Apparently, the impairment of cell viability in KG-1 cells is triggered by reduced PKCδ activation which underscores its role as a key regulator of apoptosis[362]. Intriguingly, in a hyperactive state PKCδ can also act in a pro-apoptotic fashion as shown previously for AML cells, suggesting a complex regulation maintaining a precise balance between apoptosis and survival dependent of its activation state[363].

In that context the question arises how perturbation of SFK-driven signaling translates into functional consequences having a relation to the observed effects in an AML. The phosphoproteomics data presented here shed light on that issue providing valuable information in two key respects: In combination with previous findings on the one hand, it enables "tracking" of active signal transduction pathways, on the other hand identified constituents thereof bear a certain potential as targets for pharmaceutical interference with that disease by themselves. For instance, the downregulation of phosphorylated Ser235 and Ser236 of ribosomal S6 protein was most likely a consequence of a PKCδ activity reduction since both sites were shown to be under its control[292]. When phosphorylated, the recognition of the 5'-cap of mRNA, in particular the 7-methylguanosin structure leading to so-called cap-dependent translation, is promoted[364]. Another indication supporting the intervention in that gene expression process with both gefitinib and erlotinib is demonstrated by the dephosphorylation of eIF4γ1 and eIF4γ3. These translation initiation factors are components of the eIF4F complex that is also involved in the recognition of the 5'-cap of mRNA. Both factors bind to the same region of eIF4E as other eIF4E-binding proteins such as 4E-BP1. These binding proteins interfere with cap-dependent translation when dephosphorylated at multiple residues. In contrast, when phosphorylated at those sites by mTOR binding is disabled and the translation blockade is raised[365,366]. While interference in cap-dependent translation has seemingly occurred, evidence

was provided that translation starting from internal ribosomal entry sites (IRES) was fostered by inhibitor treatment. An inhibitory phosphorylation of that process at Ser199 on hnRNP A1 was significantly reduced indicative of an opposing outcome on cap- versus IRES-dependent translation[302,367]. In accordance with previous findings, expression of genes bearing IRES elements is favored under stress conditions when cap-dependent translation is compromised eventually leading to the decrease in KG-1 cell viability as a result of erlotinib or gefitinib treatment[367].

The delineation of the origin of the off-target response in KG-1 AML cells as a result of tyrosine kinase inhibitor application was enabled through the combination of two complementary approaches. On the one hand, large-scale quantitative analysis of lysate from inhibitor treated cells by LC-MS enabled the reproducible detection of a plethora of phosphorylation sites of which only a small proportion was regulated. After all, one third of these hits could be assembled to a functional network providing insight into altered signal transduction modules for which - by itself - it was not able to classify direct and indirect downstream effects of kinase inhibition. This is even more complicated by 1h-treatment leading to the propagation of the interference beyond the point of intervention in a fast-paced phosphorylation-based cellular signal transduction system. Extended incubation periods enable alternatively shedding light on a possible mode-of-action behind the efficacy of a drug which was also possible in that study. Although the data are comprehensive, the recorded phosphorylation changes are presumably not complete. Other phosphopeptides may have escaped detection for several reasons such as their low cellular abundance, low molecular weight leading to an m/z value outside the detection range of a LTQ-Orbitrap analyzer or their positioning within the protein at the C-terminus that is not amenable for SILAC-based quantification due to the lack of an arginine or lysine residue. Moreover, for reaching statistical significance it is essential that efficient dephosphorylation occurs within the timeframe of inhibitor treatment by cellular protein phosphatase action. This would not be the case if it is delayed or only small changes are detectable, which was the case for SFKs. Using higher inhibitor concentrations than the 10 μM used in the phosphoproteomics analysis substantiated that SFKs represent common erlotinib and gefitinib targets (Figure 30). Obviously, in KG-1 cells an only incomplete activity reduction - equivalent to a decreased phosphorylation of a particular site in the activation loop - was sufficient to evoke a remarkable outcome on various cellular substrates eventually leading to the observed phenotype. However, evidence providing the basis for the identification of SFKs and potentially BTK as direct targets was finally inferred from quantitative assessment by means of a chemical proteomics strategy established in the first part of this thesis. Combining that strategy with quantitative phosphoproteomics analysis enabled a universal comprehension of cellular mechanisms of signaling interference with the observed outcome on cellular physiology. Remarkably, antineoplastic effects of varying degree were also evident upon incubation with pri-

mary, patient-derived malignant myeloblasts[220,221]. These effects were characterized by various cellular processes, such as induction of apoptosis, differentiation or growth arrest resembling observations among different AML or MDS cell lines. The existence of common targets appears likely as these cells exhibit an increased activation status of SFKs[347]. Together with previous findings according to which neither erlotinib nor gefitinib treatment affected viability of hematopoietic progenitor cells of healthy donors, it appears that AML can display dependence on pathways emerging from SFK or probably BTK activity to facilitate sustained proliferation and/or survival depending on the individual cellular context[220,221]. It will be tempting to reveal to what actual extent in AML such an oncogene-addiction to SFK- and/or BTK-dependent signaling is actually existent or not[368].

In an application context, one could take advantage of that knowledge by identifying suitable biomarkers for response prediction enabling patient stratification to provide individualized therapeutic intervention by means of targeted therapies. In that picture fits that drug discovery efforts aimed at inhibition of SFKs and BTK for the treatment of various neoplastic disorders has currently made considerable advancements[369-371]. However, in order to discover that molecular determinants underlying the therapeutic potential of erlotinib and gefitinib, additional extended analysis of signal transduction perturbation across AML cell panels or patient isolates will be necessary.

V   Summary

The identification and characterization of interactions between proteins and exogenous ligands such as small molecules constitutes a considerable challenge not only for drug discovery efforts but also in basic research to functionally explore individual targets and their role within distinct cellular processes. To approach that matter, a chemical proteomics strategy based on kinase inhibitor affinity resins was implemented in the first part of this thesis. Its applicability was first demonstrated by means of two different kinase inhibitor matrices consisting of the selective immobilized gefitinib derivative AX14596 and the nonselective pyrido[2,3-d]pyrimidine compound VI16742. These affinity resins were employed in combination with metabolically labeled Hela S3 extracts to provide an unbiased and comprehensive source of potential cellular targets under physiological conditions. Together with high-resolution mass spectrometric identification and quantification, dissociation constants for target proteins became accessible. To account for potentially altered target affinities due to modification and immobilization of parental drug molecules, competition experiments were demonstrated as an appropriate strategy to measure target affinities of "free" kinase inhibitors, here gefitinib in combination with AX14596 and SB203580 with VI16742, respectively. What clearly distinguished the methodology from previous chemical proteomics applications was the high level of quantification accurateness as a result of extensive quality control measures. Remarkably, the general practicability of that approach in interactome profiling was further underscored with dissimilar affinity ligands, namely tyrosine-phosphorylated peptide from insulin receptor substrate 4 (IRS4) and an antibody directed against epidermal growth factor receptor (EGFR).

The objective of the second part of this thesis was to unravel the cellular mode of action of the EGFR kinase inhibitors erlotinib and gefitinib in acute myeloid leukemia (AML) cells. Pursuing that issue required an unbiased and large-scale quantitative protein analysis as the previously described antineoplastic effect is based on off-target activity since AML cells do not express the drugs' primary target EGFR. Therefore, an experimental setup was implemented consisting of a recently developed quantitative phosphoproteomics workflow employing mass spectrometry in the first place, providing insight into cellular phosphoregulation occurring upon inhibitor treatment in KG-1 AML cells. Data obtained from that pointed at a very selective interference of both drugs, which was largely overlapping and comprised of less than 50 significant site-specific phosphorylations changes among 7,563 repeatedly quantified sites.

Subsequent bioinformatics analyses assembled a network of regulated phosphotyrosines including SRC family kinases (SFKs) and the tyrosine kinases BTK and SYK. Moreover, using the quantitative chemical proteomics approach devised in the first part of that work revealed SFKs and BTK, but not SYK, as direct cellular targets of both erlotinib and gefitinib in KG-1 cell extracts. Taken together, these data suggest that cellular perturbation of SFKs and/or BTK translates into rather specific signal transduction inhibition, which in turn contributes to the antileukemic activity of erlotinib and gefitinib in AML.

VI References

1   Clamp, M. *et al.* Distinguishing protein-coding and noncoding genes in the human genome. *Proc Natl Acad Sci U S A* **104**, 19428-19433, doi:0709013104 [pii]
10.1073/pnas.0709013104 (2007).

2   Jungblut, P. R., Holzhutter, H. G., Apweiler, R. & Schluter, H. The speciation of the proteome. *Chem Cent J* **2**, 16, doi:1752-153X-2-16 [pii]
10.1186/1752-153X-2-16 (2008).

3   Zhao, Y. & Jensen, O. N. Modification-specific proteomics: strategies for characterization of post-translational modifications using enrichment techniques. *Proteomics* **9**, 4632-4641, doi:10.1002/pmic.200900398 (2009).

4   Eisenhaber, B. & Eisenhaber, F. Prediction of posttranslational modification of proteins from their amino acid sequence. *Methods Mol Biol* **609**, 365-384, doi:10.1007/978-1-60327-241-4_21 (2010).

5   Walsh, C. T. *Posttranslational Modifications of Proteins: Expanding Nature's Inventory*. (Roberts and Company Publishers, 2006).

6   Nolen, B., Taylor, S. & Ghosh, G. Regulation of protein kinases; controlling activity through activation segment conformation. *Molecular cell* **15**, 661-675 (2004).

7   Yang, Y. *et al.* SIRT1 sumoylation regulates its deacetylase activity and cellular response to genotoxic stress. *Nat Cell Biol* **9**, 1253-1262, doi:ncb1645 [pii]
10.1038/ncb1645 (2007).

8   Guo, X., Williams, J. G., Schug, T. T. & Li, X. DYRK1A and DYRK3 promote cell survival through phosphorylation and activation of SIRT1. *J Biol Chem* **285**, 13223-13232, doi:M110.102574 [pii]
10.1074/jbc.M110.102574 (2010).

9   Bertos, N., Sangwan, V., Yang, X.-J. & Park, M. in *Post-Translational Modifications in Health and Disease* Vol. 13 *Protein Reviews* (ed Cecilio J. Vidal) Ch. 11, 259-279 (Springer New York, 2011).

10   Seet, B. T., Dikic, I., Zhou, M. M. & Pawson, T. Reading protein modifications with interaction domains. *Nat Rev Mol Cell Biol* **7**, 473-483, doi:nrm1960 [pii]
10.1038/nrm1960 (2006).

11   Deribe, Y. L., Pawson, T. & Dikic, I. Post-translational modifications in signal integration. *Nat Struct Mol Biol* **17**, 666-672, doi:nsmb.1842 [pii]
10.1038/nsmb.1842 (2010).

12   Ullrich, A. & Schlessinger, J. Signal transduction by receptors with tyrosine kinase activity. *Cell* **61**, 203-212, doi:0092-8674(90)90801-K [pii] (1990).

13   Schulze, A., Lehmann, K., Jefferies, H. B., McMahon, M. & Downward, J. Analysis of the transcriptional program induced by Raf in epithelial cells. *Genes Dev* **15**, 981-994, doi:10.1101/gad.191101 (2001).

14   Zehorai, E., Yao, Z., Plotnikov, A. & Seger, R. The subcellular localization of MEK and ERK--a novel nuclear translocation signal (NTS) paves a way to the nucleus. *Mol Cell Endocrinol* **314**, 213-220, doi:S0303-7207(09)00260-3 [pii]
10.1016/j.mce.2009.04.008 (2010).

15   Haglund, K. *et al.* Multiple monoubiquitination of RTKs is sufficient for their endocytosis and degradation. *Nat Cell Biol* **5**, 461-466, doi:10.1038/ncb983
ncb983 [pii] (2003).

16   Kholodenko, B. N. Cell-signalling dynamics in time and space. *Nat Rev Mol Cell Biol* **7**, 165-176, doi:nrm1838 [pii]
10.1038/nrm1838 (2006).

17   Andreu-Perez, P. *et al.* Protein arginine methyltransferase 5 regulates ERK1/2 signal transduction amplitude and cell fate through CRAF. *Sci Signal* **4**, ra58, doi:4/190/ra58 [pii] 10.1126/scisignal.2001936 (2011).

18   Hunter, T. Signaling--2000 and beyond. *Cell* **100**, 113-127, doi:S0092-8674(00)81688-8 [pii] (2000).

19   Levene, P. A. & Alsberg, C. L. The cleavage products of vitellin. *J Biol Chem* **2**, 127–133 (1906).

20   Lipmann, F. A. & Levene, P. A. Serinephosphoric acid obtained on hydrolysis of vitellinic acid. *J Biol Chem* **98**, 109-114 (1932).

21   Posternak, S. & Posternak, T. *C.R. Acad.* **184**, 909 (1927).

22   Eckhart, W., Hutchinson, M. A. & Hunter, T. An activity phosphorylating tyrosine in polyoma T antigen immunoprecipitates. *Cell* **18**, 925-933, doi:0092-8674(79)90205-8 [pii] (1979).

23   Burnett, G. & Kennedy, E. P. The enzymatic phosphorylation of proteins. *J Biol Chem* **211**, 969-980 (1954).

24   Fischer, E. H. & Krebs, E. G. Conversion of phosphorylase b to phosphorylase a in muscle extracts. *J Biol Chem* **216**, 121-132 (1955).

25   Li, S., Iakoucheva, L. M., Mooney, S. D. & Radivojac, P. Loss of post-translational modification sites in disease. *Pac Symp Biocomput*, 337-347, doi:9789814295291_0036 [pii] (2010).

26   Ahearn, I. M., Haigis, K., Bar-Sagi, D. & Philips, M. R. Regulating the regulator: post-translational modification of RAS. *Nat Rev Mol Cell Biol* **13**, 39-51, doi:nrm3255 [pii] 10.1038/nrm3255 (2012).

27   Ataullakhanov, F. I. & Vitvitsky, V. M. What determines the intracellular ATP concentration. *Bioscience reports* **22**, 501-511 (2002).

28   Gribble, F. M. *et al.* A novel method for measurement of submembrane ATP concentration. *J Biol Chem* **275**, 30046-30049, doi:10.1074/jbc.M001010200 M001010200 [pii] (2000).

29   Kammermeier, H. in *Advances in Organ Biology* Vol. Volume 4 (eds Ruth A. Altschuld E. Edward Bittar & A. Haworth Robert) 159-169 (Elsevier, 1998).

30   Berg, J., Tymoczko, J. & Stryer, L. *Biochemistry, Fifth Edition: International Version (hardcover)*. (W. H. Freeman, 2002).

31   Lad, C., Williams, N. H. & Wolfenden, R. The rate of hydrolysis of phosphomonoester dianions and the exceptional catalytic proficiencies of protein and inositol phosphatases. *Proc Natl Acad Sci U S A* **100**, 5607-5610, doi:10.1073/pnas.0631607100 0631607100 [pii] (2003).

32   Westheimer, F. H. Why nature chose phosphates. *Science* **235**, 1173-1178 (1987).

33   Schwartz, P. A. & Murray, B. W. Protein kinase biochemistry and drug discovery. *Bioorg Chem* **39**, 192-210, doi:S0045-2068(11)00047-2 [pii] 10.1016/j.bioorg.2011.07.004 (2011).

34   Manning, G., Whyte, D. B., Martinez, R., Hunter, T. & Sudarsanam, S. The protein kinase complement of the human genome. *Science* **298**, 1912-1934 (2002).

35   Brognard, J. & Hunter, T. Protein kinase signaling networks in cancer. *Curr Opin Genet Dev* **21**, 4-11, doi:S0959-437X(10)00190-5 [pii] 10.1016/j.gde.2010.10.012 (2011).

36   Dhanasekaran, N. & Premkumar Reddy, E. Signaling by dual specificity kinases. *Oncogene* **17**, 1447-1455, doi:10.1038/sj.onc.1202251 (1998).

37   Crovello, C. S., Furie, B. C. & Furie, B. Histidine phosphorylation of P-selectin upon stimulation of human platelets: a novel pathway for activation-dependent signal transduction. *Cell* **82**, 279-286, doi:0092-8674(95)90315-1 [pii] (1995).

38   Ciesla, J., Fraczyk, T. & Rode, W. Phosphorylation of basic amino acid residues in proteins: important but easily missed. *Acta Biochim Pol* **58**, 137-148, doi:201114789 [pii] (2011).

39   Kowalewska, K. *et al.* Electron capture dissociation mass spectrometric analysis of lysine-phosphorylated peptides. *Biosci Rep* **30**, 433-443, doi:BSR20090167 [pii] 10.1042/BSR20090167 (2010).

40   Westbrook, J., Feng, Z., Chen, L., Yang, H. & Berman, H. M. The Protein Data Bank and structural genomics. *Nucleic Acids Res* **31**, 489-491 (2003).

41   Knighton, D. R. *et al.* Crystal structure of the catalytic subunit of cyclic adenosine monophosphate-dependent protein kinase. *Science* **253**, 407-414 (1991).

42   Johnson, L. N. & Lewis, R. J. Structural basis for control by phosphorylation. *Chem Rev* **101**, 2209-2242, doi:cr000225s [pii] (2001).

43   Lochhead, P. A. Protein kinase activation loop autophosphorylation in cis: overcoming a Catch-22 situation. *Sci Signal* **2**, pe4, doi:scisignal.254pe4 [pii]
10.1126/scisignal.254pe4 (2009).

44   Huse, M. & Kuriyan, J. The conformational plasticity of protein kinases. *Cell* **109**, 275-282, doi:S0092867402007419 [pii] (2002).

45   Jura, N. *et al.* Mechanism for activation of the EGF receptor catalytic domain by the juxtamembrane segment. *Cell* **137**, 1293-1307, doi:S0092-8674(09)00450-4 [pii]
10.1016/j.cell.2009.04.025 (2009).

46   Rabiller, M. *et al.* Proteus in the world of proteins: conformational changes in protein kinases. *Arch Pharm (Weinheim)* **343**, 193-206, doi:10.1002/ardp.201000028 (2010).

47   Kornev, A. P. & Taylor, S. S. Defining the conserved internal architecture of a protein kinase. *Biochim Biophys Acta* **1804**, 440-444, doi:S1570-9639(09)00306-9 [pii]
10.1016/j.bbapap.2009.10.017 (2010).

48   Leahy, J. L. Pathogenesis of type 2 diabetes mellitus. *Arch Med Res* **36**, 197-209, doi:S0188-4409(05)00004-4 [pii]
10.1016/j.arcmed.2005.01.003 (2005).

49   Notarangelo, L. D. Immunodeficiencies caused by genetic defects in protein kinases. *Curr Opin Immunol* **8**, 448-453, doi:S0952-7915(96)80028-8 [pii] (1996).

50   Hanahan, D. & Weinberg, R. A. The hallmarks of cancer. *Cell* **100**, 57-70, doi:S0092-8674(00)81683-9 [pii] (2000).

51   Hanahan, D. & Weinberg, R. A. Hallmarks of cancer: the next generation. *Cell* **144**, 646-674, doi:S0092-8674(11)00127-9 [pii]
10.1016/j.cell.2011.02.013 (2011).

52   Collett, M. S. & Erikson, R. L. Protein kinase activity associated with the avian sarcoma virus src gene product. *Proc Natl Acad Sci U S A* **75**, 2021-2024 (1978).

53   Castagna, M. *et al.* Direct activation of calcium-activated, phospholipid-dependent protein kinase by tumor-promoting phorbol esters. *J Biol Chem* **257**, 7847-7851 (1982).

54   Hunter, T. & Sefton, B. M. Transforming gene product of Rous sarcoma virus phosphorylates tyrosine. *Proc Natl Acad Sci U S A* **77**, 1311-1315 (1980).

55   Ullrich, A. *et al.* Human epidermal growth factor receptor cDNA sequence and aberrant expression of the amplified gene in A431 epidermoid carcinoma cells. *Nature* **309**, 418-425 (1984).

56   Witte, O. N., Dasgupta, A. & Baltimore, D. Abelson murine leukaemia virus protein is phosphorylated in vitro to form phosphotyrosine. *Nature* **283**, 826-831 (1980).

57   Blume-Jensen, P. & Hunter, T. Oncogenic kinase signalling. *Nature* **411**, 355-365 (2001).

58   Downward, J. *et al.* Close similarity of epidermal growth factor receptor and v-erb-B oncogene protein sequences. *Nature* **307**, 521-527 (1984).

59   Croce, C. M. Oncogenes and cancer. *N Engl J Med* **358**, 502-511, doi:358/5/502 [pii]
10.1056/NEJMra072367 (2008).

60   da Cunha Santos, G., Shepherd, F. A. & Tsao, M. S. EGFR mutations and lung cancer. *Annu Rev Pathol* **6**, 49-69, doi:10.1146/annurev-pathol-011110-130206 (2011).

61   Hunter, T. Treatment for chronic myelogenous leukemia: the long road to imatinib. *J Clin Invest* **117**, 2036-2043, doi:10.1172/JCI31691 (2007).

62   Hidaka, H., Inagaki, M., Kawamoto, S. & Sasaki, Y. Isoquinolinesulfonamides, novel and potent inhibitors of cyclic nucleotide dependent protein kinase and protein kinase C. *Biochemistry* **23**, 5036-5041 (1984).

63   Graziani, Y., Erikson, E. & Erikson, R. L. The effect of quercetin on the phosphorylation activity of the Rous sarcoma virus transforming gene product in vitro and in vivo. *Eur J Biochem* **135**, 583-589 (1983).

64   Uehara, Y., Hori, M., Takeuchi, T. & Umezawa, H. Phenotypic change from transformed to normal induced by benzoquinonoid ansamycins accompanies inactivation of p60src in rat kidney cells infected with Rous sarcoma virus. *Mol Cell Biol* **6**, 2198-2206 (1986).

65   Akiyama, T. *et al.* Genistein, a specific inhibitor of tyrosine-specific protein kinases. *J Biol Chem* **262**, 5592-5595 (1987).

66   Yaish, P., Gazit, A., Gilon, C. & Levitzki, A. Blocking of EGF-dependent cell proliferation by EGF receptor kinase inhibitors. *Science* **242**, 933-935 (1988).

67   Umezawa, H. *et al.* Studies on a new epidermal growth factor-receptor kinase inhibitor, erbstatin, produced by MH435-hF3. *J Antibiot (Tokyo)* **39**, 170-173 (1986).

68   Gazit, A., Yaish, P., Gilon, C. & Levitzki, A. Tyrphostins I: synthesis and biological activity of protein tyrosine kinase inhibitors. *J Med Chem* **32**, 2344-2352 (1989).

69   Tamaoki, T. *et al.* Staurosporine, a potent inhibitor of phospholipid/Ca++dependent protein kinase. *Biochem Biophys Res Commun* **135**, 397-402, doi:0006-291X(86)90008-2 [pii] (1986).

70   Gschwendt, M., Horn, F., Kittstein, W. & Marks, F. Inhibition of the calcium- and phospholipid-dependent protein kinase activity from mouse brain cytosol by quercetin. *Biochem Biophys Res Commun* **117**, 444-447, doi:0006-291X(83)91220-2 [pii] (1983).

71   Yarden, Y. & Ullrich, A. Growth factor receptor tyrosine kinases. *Annu Rev Biochem* **57**, 443-478, doi:10.1146/annurev.bi.57.070188.002303 (1988).

72   Osherov, N., Gazit, A., Gilon, C. & Levitzki, A. Selective inhibition of the epidermal growth factor and HER2/neu receptors by tyrphostins. *J Biol Chem* **268**, 11134-11142 (1993).

73   Tong, L. *et al.* A highly specific inhibitor of human p38 MAP kinase binds in the ATP pocket. *Nat Struct Biol* **4**, 311-316 (1997).

74   Eyers, P. A., Craxton, M., Morrice, N., Cohen, P. & Goedert, M. Conversion of SB 203580-insensitive MAP kinase family members to drug-sensitive forms by a single amino-acid substitution. *Chem Biol* **5**, 321-328 (1998).

75   Levitzki, A. & Mishani, E. Tyrphostins and other tyrosine kinase inhibitors. *Annu Rev Biochem* **75**, 93-109, doi:10.1146/annurev.biochem.75.103004.142657 (2006).

76   Wakeling, A. E. Epidermal growth factor receptor tyrosine kinase inhibitors. *Curr Opin Pharmacol* **2**, 382-387, doi:S1471489202001832 [pii] (2002).

77   Moyer, J. D. *et al.* Induction of apoptosis and cell cycle arrest by CP-358,774, an inhibitor of epidermal growth factor receptor tyrosine kinase. *Cancer Res* **57**, 4838-4848 (1997).

78   Muhsin, M., Graham, J. & Kirkpatrick, P. Gefitinib. *Nat Rev Drug Discov* **2**, 515-516, doi:10.1038/nrd1136 (2003).

79   Dowell, J., Minna, J. D. & Kirkpatrick, P. Erlotinib hydrochloride. *Nat Rev Drug Discov* **4**, 13-14, doi:10.1038/nrd1612 (2005).

80   Johnson, J. R. *et al.* Accelerated approval of oncology products: the food and drug administration experience. *J Natl Cancer Inst* **103**, 636-644, doi:djr062 [pii] 10.1093/jnci/djr062 (2011).

81   Carroll, M. *et al.* CGP 57148, a tyrosine kinase inhibitor, inhibits the growth of cells expressing BCR-ABL, TEL-ABL, and TEL-PDGFR fusion proteins. *Blood* **90**, 4947-4952 (1997).

82   Druker, B. J. Translation of the Philadelphia chromosome into therapy for CML. *Blood* **112**, 4808-4817, doi:112/13/4808 [pii] 10.1182/blood-2008-07-077958 (2008).

83   Schindler, T. *et al.* Structural mechanism for STI-571 inhibition of abelson tyrosine kinase. *Science* **289**, 1938-1942 (2000).

84   Zuccotto, F., Ardini, E., Casale, E. & Angiolini, M. Through the "gatekeeper door": exploiting the active kinase conformation. *J Med Chem* **53**, 2681-2694, doi:10.1021/jm901443h (2010).

85   Druker, B. J. *et al.* Effects of a selective inhibitor of the Abl tyrosine kinase on the growth of Bcr-Abl positive cells. *Nat Med* **2**, 561-566 (1996).

86   Kirkland, L. O. & McInnes, C. Non-ATP competitive protein kinase inhibitors as anti-tumor therapeutics. *Biochem Pharmacol* **77**, 1561-1571, doi:S0006-2952(08)00901-5 [pii] 10.1016/j.bcp.2008.12.022 (2009).

87   Szakacs, G., Paterson, J. K., Ludwig, J. A., Booth-Genthe, C. & Gottesman, M. M. Targeting multidrug resistance in cancer. *Nat Rev Drug Discov* **5**, 219-234, doi:nrd1984 [pii] 10.1038/nrd1984 (2006).

88   Daub, H., Specht, K. & Ullrich, A. Strategies to overcome resistance to targeted protein kinase inhibitors. *Nat Rev Drug Discov* **3**, 1001-1010, doi:nrd1579 [pii] 10.1038/nrd1579 (2004).

89   Blencke, S. *et al.* Characterization of a conserved structural determinant controlling protein kinase sensitivity to selective inhibitors. *Chem Biol* **11**, 691-701 (2004).

90   Fabbro, D. *et al.* Inhibitors of the Abl kinase directed at either the ATP- or myristate-binding site. *Biochim Biophys Acta* **1804**, 454-462, doi:S1570-9639(09)00367-7 [pii] 10.1016/j.bbapap.2009.12.009 (2010).

91 Gumireddy, K. *et al.* ON01910, a non-ATP-competitive small molecule inhibitor of Plk1, is a potent anticancer agent. *Cancer Cell* **7**, 275-286, doi:S1535-6108(05)00062-0 [pii] 10.1016/j.ccr.2005.02.009 (2005).

92 Zhang, J., Yang, P. L. & Gray, N. S. Targeting cancer with small molecule kinase inhibitors. *Nature reviews* **9**, 28-39 (2009).

93 Kwak, E. L. *et al.* Irreversible inhibitors of the EGF receptor may circumvent acquired resistance to gefitinib. *Proc Natl Acad Sci U S A* **102**, 7665-7670, doi:0502860102 [pii] 10.1073/pnas.0502860102 (2005).

94 Adjei, A. A. *et al.* Phase I pharmacokinetic and pharmacodynamic study of the oral, small-molecule mitogen-activated protein kinase kinase 1/2 inhibitor AZD6244 (ARRY-142886) in patients with advanced cancers. *J Clin Oncol* **26**, 2139-2146, doi:JCO.2007.14.4956 [pii] 10.1200/JCO.2007.14.4956 (2008).

95 Wilkins, M. R. *et al.* From proteins to proteomes: large scale protein identification by two-dimensional electrophoresis and amino acid analysis. *Biotechnology (N Y)* **14**, 61-65 (1996).

96 Cox, J. & Mann, M. Quantitative, high-resolution proteomics for data-driven systems biology. *Annu Rev Biochem* **80**, 273-299, doi:10.1146/annurev-biochem-061308-093216 (2011).

97 Cox, J. & Mann, M. Is proteomics the new genomics? *Cell* **130**, 395-398 (2007).

98 Angel, T. E. *et al.* Mass spectrometry-based proteomics: existing capabilities and future directions. *Chem Soc Rev* **41**, 3912-3928, doi:10.1039/c2cs15331a (2012).

99 Aebersold, R. & Mann, M. Mass spectrometry-based proteomics. *Nature* **422**, 198-207, doi:10.1038/nature01511 nature01511 [pii] (2003).

100 Nilsson, T. *et al.* Mass spectrometry in high-throughput proteomics: ready for the big time. *Nat Methods* **7**, 681-685, doi:nmeth0910-681 [pii] 10.1038/nmeth0910-681 (2010).

101 Andersson, C. O. Mass Spectrometric Studies on Amino Acid and Peptide Derivatives. *Acta Chem Scand* **12**, 1353-1353 (1958).

102 Karas, M. & Hillenkamp, F. Laser desorption ionization of proteins with molecular masses exceeding 10,000 daltons. *Anal Chem* **60**, 2299-2301 (1988).

103 Fenn, J. B., Mann, M., Meng, C. K., Wong, S. F. & Whitehouse, C. M. Electrospray ionization for mass spectrometry of large biomolecules. *Science* **246**, 64-71 (1989).

104 Iribarne, J. V. & Thomson, B. A. Evaporation of Small Ions from Charged Droplets. *J Chem Phys* **64**, 2287-2294 (1976).

105 Dole, M., Mack, L. L. & Hines, R. L. Molecular Beams of Macroions. *J Chem Phys* **49**, 2240-& (1968).

106 Steen, H. & Mann, M. The ABC's (and XYZ's) of peptide sequencing. *Nat Rev Mol Cell Biol* **5**, 699-711 (2004).

107 Schirle, M., Heurtier, M. A. & Kuster, B. Profiling core proteomes of human cell lines by one-dimensional PAGE and liquid chromatography-tandem mass spectrometry. *Mol Cell Proteomics* **2**, 1297-1305, doi:10.1074/mcp.M300087-MCP200 M300087-MCP200 [pii] (2003).

108 Olsen, J. V., Ong, S. E. & Mann, M. Trypsin cleaves exclusively C-terminal to arginine and lysine residues. *Mol Cell Proteomics* **3**, 608-614, doi:10.1074/mcp.T400003-MCP200 T400003-MCP200 [pii] (2004).

109 Scigelova, M. & Makarov, A. Orbitrap mass analyzer--overview and applications in proteomics. *Proteomics* **6 Suppl 2**, 16-21, doi:10.1002/pmic.200600528 (2006).

110 Olsen, J. V. *et al.* Parts per million mass accuracy on an Orbitrap mass spectrometer via lock mass injection into a C-trap. *Mol Cell Proteomics* **4**, 2010-2021 (2005).

111 Douglas, D. J., Frank, A. J. & Mao, D. Linear ion traps in mass spectrometry. *Mass Spectrom Rev* **24**, 1-29, doi:10.1002/mas.20004 (2005).

112 Sadygov, R. G., Cociorva, D. & Yates, J. R. Large-scale database searching using tandem mass spectra: Looking up the answer in the back of the book. *Nature Methods* **1**, 195-202, doi:Doi 10.1038/Nmeth725 (2004).

113 Colinge, J. & Bennett, K. L. Introduction to computational proteomics. *Plos Comput Biol* **3**, 1151-1160 (2007).

114 Perkins, D. N., Pappin, D. J. C., Creasy, D. M. & Cottrell, J. S. Probability-based protein identification by searching sequence databases using mass spectrometry data. *Electrophoresis* **20**, 3551-3567 (1999).

115   Elias, J. E. & Gygi, S. P. Target-decoy search strategy for increased confidence in large-scale protein identifications by mass spectrometry. *Nat Methods* **4**, 207-214, doi:nmeth1019 [pii]
10.1038/nmeth1019 (2007).

116   Nesvizhskii, A. I., Vitek, O. & Aebersold, R. Analysis and validation of proteomic data generated by tandem mass spectrometry. *Nat Methods* **4**, 787-797, doi:nmeth1088 [pii]
10.1038/nmeth1088 (2007).

117   Ong, S. E. & Mann, M. Mass spectrometry-based proteomics turns quantitative. *Nat Chem Biol* **1**, 252-262, doi:nchembio736 [pii]
10.1038/nchembio736 (2005).

118   Allet, N. *et al.* In vitro and in silico processes to identify differentially expressed proteins. *Proteomics* **4**, 2333-2351, doi:10.1002/pmic.200300840 (2004).

119   Andersen, J. S. *et al.* Proteomic characterization of the human centrosome by protein correlation profiling. *Nature* **426**, 570-574, doi:10.1038/nature02166
nature02166 [pii] (2003).

120   Ishihama, Y. *et al.* Exponentially modified protein abundance index (emPAI) for estimation of absolute protein amount in proteomics by the number of sequenced peptides per protein. *Mol Cell Proteomics* **4**, 1265-1272, doi:M500061-MCP200 [pii]
10.1074/mcp.M500061-MCP200 (2005).

121   Rappsilber, J., Ryder, U., Lamond, A. I. & Mann, M. Large-scale proteomic analysis of the human spliceosome. *Genome Res* **12**, 1231-1245, doi:10.1101/gr.473902 (2002).

122   Oda, Y., Huang, K., Cross, F. R., Cowburn, D. & Chait, B. T. Accurate quantitation of protein expression and site-specific phosphorylation. *Proc Natl Acad Sci U S A* **96**, 6591-6596 (1999).

123   Washburn, M. P., Ulaszek, R., Deciu, C., Schieltz, D. M. & Yates, J. R., 3rd. Analysis of quantitative proteomic data generated via multidimensional protein identification technology. *Anal Chem* **74**, 1650-1657 (2002).

124   Ong, S. E., Foster, L. J. & Mann, M. Mass spectrometric-based approaches in quantitative proteomics. *Methods* **29**, 124-130, doi:S1046202302003031 [pii] (2003).

125   Beynon, R. J. & Pratt, J. M. Metabolic labeling of proteins for proteomics. *Mol Cell Proteomics* **4**, 857-872, doi:R400010-MCP200 [pii]
10.1074/mcp.R400010-MCP200 (2005).

126   Ong, S. E. *et al.* Stable isotope labeling by amino acids in cell culture, SILAC, as a simple and accurate approach to expression proteomics. *Mol Cell Proteomics* **1**, 376-386 (2002).

127   Ong, S. E. The expanding field of SILAC. *Anal Bioanal Chem* **404**, 967-976, doi:10.1007/s00216-012-5998-3 (2012).

128   Bantscheff, M., Lemeer, S., Savitski, M. M. & Kuster, B. Quantitative mass spectrometry in proteomics: critical review update from 2007 to the present. *Anal Bioanal Chem* **404**, 939-965, doi:10.1007/s00216-012-6203-4 (2012).

129   Zhang, R., Sioma, C. S., Wang, S. & Regnier, F. E. Fractionation of isotopically labeled peptides in quantitative proteomics. *Anal Chem* **73**, 5142-5149 (2001).

130   Olsen, J. V. *et al.* Global, in vivo, and site-specific phosphorylation dynamics in signaling networks. *Cell* **127**, 635-648, doi:S0092-8674(06)01274-8 [pii]
10.1016/j.cell.2006.09.026 (2006).

131   Schreiber, T. B., Mausbacher, N., Breitkopf, S. B., Grundner-Culemann, K. & Daub, H. Quantitative phosphoproteomics--an emerging key technology in signal-transduction research. *Proteomics* **8**, 4416-4432, doi:10.1002/pmic.200800132 (2008).

132   Neher, S. B. *et al.* Proteomic profiling of ClpXP substrates after DNA damage reveals extensive instability within SOS regulon. *Molecular cell* **22**, 193-204, doi:S1097-2765(06)00168-7 [pii]
10.1016/j.molcel.2006.03.007 (2006).

133   Gruhler, A. *et al.* Quantitative phosphoproteomics applied to the yeast pheromone signaling pathway. *Mol Cell Proteomics* **4**, 310-327, doi:M400219-MCP200 [pii]
10.1074/mcp.M400219-MCP200 (2005).

134   Ong, S. E., Kratchmarova, I. & Mann, M. Properties of 13C-substituted arginine in stable isotope labeling by amino acids in cell culture (SILAC). *J Proteome Res* **2**, 173-181 (2003).

135   Van Hoof, D. *et al.* An experimental correction for arginine-to-proline conversion artifacts in SILAC-based quantitative proteomics. *Nat Methods* **4**, 677-678, doi:nmeth0907-677 [pii]
10.1038/nmeth0907-677 (2007).

136   Lossner, C., Warnken, U., Pscherer, A. & Schnolzer, M. Preventing arginine-to-proline conversion in a cell-line-independent manner during cell cultivation under stable isotope labeling by amino acids in cell culture (SILAC) conditions. *Anal Biochem* **412**, 123-125, doi:S0003-2697(11)00025-X [pii] 10.1016/j.ab.2011.01.011 (2011).

137   Kruger, M. *et al.* SILAC mouse for quantitative proteomics uncovers kindlin-3 as an essential factor for red blood cell function. *Cell* **134**, 353-364 (2008).

138   Geiger, T., Cox, J., Ostasiewicz, P., Wisniewski, J. R. & Mann, M. Super-SILAC mix for quantitative proteomics of human tumor tissue. *Nat Methods* **7**, 383-385, doi:nmeth.1446 [pii] 10.1038/nmeth.1446 (2010).

139   DeSouza, L. *et al.* Search for cancer markers from endometrial tissues using differentially labeled tags iTRAQ and cICAT with multidimensional liquid chromatography and tandem mass spectrometry. *J Proteome Res* **4**, 377-386, doi:10.1021/pr049821j (2005).

140   Keshamouni, V. G. *et al.* Differential protein expression profiling by iTRAQ-2DLC-MS/MS of lung cancer cells undergoing epithelial-mesenchymal transition reveals a migratory/invasive phenotype. *J Proteome Res* **5**, 1143-1154, doi:10.1021/pr050455t (2006).

141   Ross, P. L. *et al.* Multiplexed protein quantitation in Saccharomyces cerevisiae using amine-reactive isobaric tagging reagents. *Mol Cell Proteomics* **3**, 1154-1169, doi:10.1074/mcp.M400129-MCP200 M400129-MCP200 [pii] (2004).

142   Thompson, A. *et al.* Tandem mass tags: a novel quantification strategy for comparative analysis of complex protein mixtures by MS/MS. *Anal Chem* **75**, 1895-1904 (2003).

143   Karp, N. A. *et al.* Addressing accuracy and precision issues in iTRAQ quantitation. *Mol Cell Proteomics* **9**, 1885-1897, doi:M900628-MCP200 [pii] 10.1074/mcp.M900628-MCP200 (2010).

144   Wenger, C. D. *et al.* Gas-phase purification enables accurate, multiplexed proteome quantification with isobaric tagging. *Nat Methods* **8**, 933-935, doi:nmeth.1716 [pii] 10.1038/nmeth.1716 (2011).

145   Li, N., Overkleeft, H. S. & Florea, B. I. Activity-based protein profiling: an enabling technology in chemical biology research. *Curr Opin Chem Biol* **16**, 227-233, doi:S1367-5931(12)00003-8 [pii] 10.1016/j.cbpa.2012.01.008 (2012).

146   Rix, U. & Superti-Furga, G. Target profiling of small molecules by chemical proteomics. *Nat Chem Biol* **5**, 616-624 (2009).

147   Daub, H. Characterisation of kinase-selective inhibitors by chemical proteomics. *Biochim Biophys Acta* **1754**, 183-190 (2005).

148   Brehmer, D. *et al.* Cellular targets of gefitinib. *Cancer Res* **65**, 379-382 (2005).

149   Lerman, L. S. A Biochemically Specific Method for Enzyme Isolation. *Proc Natl Acad Sci U S A* **39**, 232-236 (1953).

150   Arsenis, C. & McCormick, D. B. Purification of Liver Flavokinase by Column Chromatography on Flavin-Cellulose Compounds. *J Biol Chem* **239**, 3093-3097 (1964).

151   Cuatrecasas, P., Wilchek, M. & Anfinsen, C. B. Selective enzyme purification by affinity chromatography. *Proc Natl Acad Sci U S A* **61**, 636-643 (1968).

152   Borisy, G. G. & Taylor, E. W. The mechanism of action of colchicine. Binding of colchincine-3H to cellular protein. *J Cell Biol* **34**, 525-533 (1967).

153   Inagaki, M., Watanabe, M. & Hidaka, H. N-(2-Aminoethyl)-5-isoquinolinesulfonamide, a newly synthesized protein kinase inhibitor, functions as a ligand in affinity chromatography. Purification of Ca2+-activated, phospholipid-dependent and other protein kinases. *J Biol Chem* **260**, 2922-2925 (1985).

154   Raida, M. Drug target deconvolution by chemical proteomics. *Curr Opin Chem Biol* **15**, 570-575, doi:S1367-5931(11)00103-7 [pii] 10.1016/j.cbpa.2011.06.016 (2011).

155   Godl, K. *et al.* An efficient proteomics method to identify the cellular targets of protein kinase inhibitors. *Proc Natl Acad Sci U S A* **100**, 15434-15439 (2003).

156   Brehmer, D., Godl, K., Zech, B., Wissing, J. & Daub, H. Proteome-wide identification of cellular targets affected by bisindolylmaleimide-type protein kinase C inhibitors. *Mol Cell Proteomics* **3**, 490-500, doi:10.1074/mcp.M300139-MCP200 M300139-MCP200 [pii] (2004).

157   Terstappen, G. C., Schlupen, C., Raggiaschi, R. & Gaviraghi, G. Target deconvolution strategies in drug discovery. *Nat Rev Drug Discov* **6**, 891-903, doi:nrd2410 [pii]

10.1038/nrd2410 (2007).

158   Karaman, M. W. *et al.* A quantitative analysis of kinase inhibitor selectivity. *Nat Biotechnol* **26**, 127-132 (2008).

159   Fabian, M. A. *et al.* A small molecule-kinase interaction map for clinical kinase inhibitors. *Nat Biotechnol* **23**, 329-336, doi:nbt1068 [pii]
10.1038/nbt1068 (2005).

160   Bantscheff, M. *et al.* Quantitative chemical proteomics reveals mechanisms of action of clinical ABL kinase inhibitors. *Nat Biotechnol* **25**, 1035-1044 (2007).

161   Kocher, T. & Superti-Furga, G. Mass spectrometry-based functional proteomics: from molecular machines to protein networks. *Nat Methods* **4**, 807-815, doi:nmeth1093 [pii]
10.1038/nmeth1093 (2007).

162   Zhu, H. & Snyder, M. Protein chip technology. *Curr Opin Chem Biol* **7**, 55-63, doi:S1367593102000054 [pii] (2003).

163   Bruckner, A., Polge, C., Lentze, N., Auerbach, D. & Schlattner, U. Yeast two-hybrid, a powerful tool for systems biology. *Int J Mol Sci* **10**, 2763-2788, doi:10.3390/ijms10062763 (2009).

164   Vermeulen, M., Hubner, N. C. & Mann, M. High confidence determination of specific protein-protein interactions using quantitative mass spectrometry. *Curr Opin Biotechnol* **19**, 331-337, doi:S0958-1669(08)00069-4 [pii]
10.1016/j.copbio.2008.06.001 (2008).

165   Puig, O. *et al.* The tandem affinity purification (TAP) method: a general procedure of protein complex purification. *Methods* **24**, 218-229, doi:10.1006/meth.2001.1183
S1046-2023(01)91183-1 [pii] (2001).

166   Burckstummer, T. *et al.* An efficient tandem affinity purification procedure for interaction proteomics in mammalian cells. *Nat Methods* **3**, 1013-1019, doi:nmeth968 [pii]
10.1038/nmeth968 (2006).

167   Bouwmeester, T. *et al.* A physical and functional map of the human TNF-alpha/NF-kappa B signal transduction pathway. *Nat Cell Biol* **6**, 97-105, doi:10.1038/ncb1086
ncb1086 [pii] (2004).

168   Brand, M. *et al.* Dynamic changes in transcription factor complexes during erythroid differentiation revealed by quantitative proteomics. *Nat Struct Mol Biol* **11**, 73-80, doi:10.1038/nsmb713
nsmb713 [pii] (2004).

169   Foster, L. J. *et al.* Insulin-dependent interactions of proteins with GLUT4 revealed through stable isotope labeling by amino acids in cell culture (SILAC). *J Proteome Res* **5**, 64-75, doi:10.1021/pr0502626 (2006).

170   Selbach, M. & Mann, M. Protein interaction screening by quantitative immunoprecipitation combined with knockdown (QUICK). *Nat Methods* **3**, 981-983, doi:nmeth972 [pii]
10.1038/nmeth972 (2006).

171   Schulze, W. X. & Mann, M. A novel proteomic screen for peptide-protein interactions. *J Biol Chem* **279**, 10756-10764, doi:10.1074/jbc.M309909200
M309909200 [pii] (2004).

172   Vermeulen, M. *et al.* Selective anchoring of TFIID to nucleosomes by trimethylation of histone H3 lysine 4. *Cell* **131**, 58-69, doi:S0092-8674(07)01079-3 [pii]
10.1016/j.cell.2007.08.016 (2007).

173   Johnson, S. A. & Hunter, T. Kinomics: methods for deciphering the kinome. *Nat Methods* **2**, 17-25, doi:nmeth731 [pii]
10.1038/nmeth731 (2005).

174   Cutillas, P. R. & Jorgensen, C. Biological signalling activity measurements using mass spectrometry. *Biochem J* **434**, 189-199, doi:BJ20101974 [pii]
10.1042/BJ20101974 (2011).

175   Lauffenburger, D. A. Cell signaling pathways as control modules: complexity for simplicity? *Proc Natl Acad Sci U S A* **97**, 5031-5033, doi:97/10/5031 [pii] (2000).

176   Macek, B., Mann, M. & Olsen, J. V. Global and site-specific quantitative phosphoproteomics: principles and applications. *Annu Rev Pharmacol Toxicol* **49**, 199-221, doi:10.1146/annurev.pharmtox.011008.145606 (2009).

177   Salih, E. Phosphoproteomics by mass spectrometry and classical protein chemistry approaches. *Mass Spectrom Rev* **24**, 828-846, doi:10.1002/mas.20042 (2005).

178   Mertins, P. *et al.* Investigation of protein-tyrosine phosphatase 1B function by quantitative proteomics. *Mol Cell Proteomics* **7**, 1763-1777, doi:M800196-MCP200 [pii]
10.1074/mcp.M800196-MCP200 (2008).

179   Hinsby, A. M., Olsen, J. V., Bennett, K. L. & Mann, M. Signaling initiated by overexpression of the fibroblast growth factor receptor-1 investigated by mass spectrometry. *Mol Cell Proteomics* **2**, 29-36 (2003).

180   Rikova, K. *et al.* Global survey of phosphotyrosine signaling identifies oncogenic kinases in lung cancer. *Cell* **131**, 1190-1203, doi:S0092-8674(07)01522-X [pii]
10.1016/j.cell.2007.11.025 (2007).

181   Rush, J. *et al.* Immunoaffinity profiling of tyrosine phosphorylation in cancer cells. *Nat Biotechnol* **23**, 94-101, doi:nbt1046 [pii]
10.1038/nbt1046 (2005).

182   Andersson, L. & Porath, J. Isolation of phosphoproteins by immobilized metal (Fe3+) affinity chromatography. *Anal Biochem* **154**, 250-254, doi:0003-2697(86)90523-3 [pii] (1986).

183   Posewitz, M. C. & Tempst, P. Immobilized gallium(III) affinity chromatography of phosphopeptides. *Anal Chem* **71**, 2883-2892 (1999).

184   Feng, S. *et al.* Immobilized zirconium ion affinity chromatography for specific enrichment of phosphopeptides in phosphoproteome analysis. *Mol Cell Proteomics* **6**, 1656-1665, doi:T600071-MCP200 [pii]
10.1074/mcp.T600071-MCP200 (2007).

185   Larsen, M. R., Thingholm, T. E., Jensen, O. N., Roepstorff, P. & Jorgensen, T. J. Highly selective enrichment of phosphorylated peptides from peptide mixtures using titanium dioxide microcolumns. *Mol Cell Proteomics* **4**, 873-886, doi:T500007-MCP200 [pii]
10.1074/mcp.T500007-MCP200 (2005).

186   Pinkse, M. W., Uitto, P. M., Hilhorst, M. J., Ooms, B. & Heck, A. J. Selective isolation at the femtomole level of phosphopeptides from proteolytic digests using 2D-NanoLC-ESI-MS/MS and titanium oxide precolumns. *Anal Chem* **76**, 3935-3943, doi:10.1021/ac0498617 (2004).

187   Ficarro, S. B. *et al.* Phosphoproteome analysis by mass spectrometry and its application to Saccharomyces cerevisiae. *Nat Biotechnol* **20**, 301-305, doi:10.1038/nbt0302-301
nbt0302-301 [pii] (2002).

188   Leitner, A., Sturm, M. & Lindner, W. Tools for analyzing the phosphoproteome and other phosphorylated biomolecules: a review. *Anal Chim Acta* **703**, 19-30, doi:S0003-2670(11)00953-6 [pii]
10.1016/j.aca.2011.07.012 (2011).

189   Zhou, H. *et al.* Specific phosphopeptide enrichment with immobilized titanium ion affinity chromatography adsorbent for phosphoproteome analysis. *J Proteome Res* **7**, 3957-3967, doi:10.1021/pr800223m (2008).

190   Shevchenko, A., Tomas, H., Havlis, J., Olsen, J. V. & Mann, M. In-gel digestion for mass spectrometric characterization of proteins and proteomes. *Nat Protoc* **1**, 2856-2860, doi:nprot.2006.468 [pii]
10.1038/nprot.2006.468 (2006).

191   Beausoleil, S. A. *et al.* Large-scale characterization of HeLa cell nuclear phosphoproteins. *Proc Natl Acad Sci U S A* **101**, 12130-12135, doi:10.1073/pnas.0404720101
0404720101 [pii] (2004).

192   Villen, J. & Gygi, S. P. The SCX/IMAC enrichment approach for global phosphorylation analysis by mass spectrometry. *Nat Protoc* **3**, 1630-1638, doi:nprot.2008.150 [pii]
10.1038/nprot.2008.150 (2008).

193   Schroeder, M. J., Shabanowitz, J., Schwartz, J. C., Hunt, D. F. & Coon, J. J. A neutral loss activation method for improved phosphopeptide sequence analysis by quadrupole ion trap mass spectrometry. *Anal Chem* **76**, 3590-3598, doi:10.1021/ac0497104 (2004).

194   Olsen, J. V. *et al.* Higher-energy C-trap dissociation for peptide modification analysis. *Nat Methods* **4**, 709-712, doi:nmeth1060 [pii]
10.1038/nmeth1060 (2007).

195   Nagaraj, N., D'Souza, R. C., Cox, J., Olsen, J. V. & Mann, M. Feasibility of large-scale phosphoproteomics with higher energy collisional dissociation fragmentation. *J Proteome Res* **9**, 6786-6794, doi:10.1021/pr100637q (2010).

196   Olsen, J. V. *et al.* A dual pressure linear ion trap Orbitrap instrument with very high sequencing speed. *Mol Cell Proteomics* **8**, 2759-2769, doi:M900375-MCP200 [pii]
10.1074/mcp.M900375-MCP200 (2009).

197   Syka, J. E., Coon, J. J., Schroeder, M. J., Shabanowitz, J. & Hunt, D. F. Peptide and protein sequence analysis by electron transfer dissociation mass spectrometry. *Proc Natl Acad Sci U S A* **101**, 9528-9533, doi:10.1073/pnas.0402700101
0402700101 [pii] (2004).

198   Zubarev, R. A. *et al.* Electron capture dissociation for structural characterization of multiply charged protein cations. *Anal Chem* **72**, 563-573 (2000).

199   Beck, F. *et al.* The good, the bad, the ugly: validating the mass spectrometric analysis of modified peptides. *Proteomics* **11**, 1099-1109, doi:10.1002/pmic.201000562 (2011).

200   Choudhary, C. & Mann, M. Decoding signalling networks by mass spectrometry-based proteomics. *Nat Rev Mol Cell Biol* **11**, 427-439, doi:nrm2900 [pii]
10.1038/nrm2900 (2010).

201   Thingholm, T. E., Palmisano, G., Kjeldsen, F. & Larsen, M. R. Undesirable charge-enhancement of isobaric tagged phosphopeptides leads to reduced identification efficiency. *J Proteome Res* **9**, 4045-4052, doi:10.1021/pr100230q (2010).

202   Olsen, J. V. & Mann, M. Improved peptide identification in proteomics by two consecutive stages of mass spectrometric fragmentation. *Proc Natl Acad Sci U S A* **101**, 13417-13422, doi:10.1073/pnas.0405549101
0405549101 [pii] (2004).

203   Dick, J. E. Stem cell concepts renew cancer research. *Blood* **112**, 4793-4807 (2008).

204   Dash, A. & Gilliland, D. G. Molecular genetics of acute myeloid leukaemia. *Best Pract Res Clin Haematol* **14**, 49-64 (2001).

205   Frohling, S., Scholl, C., Gilliland, D. G. & Levine, R. L. Genetics of myeloid malignancies: pathogenetic and clinical implications. *Journal of clinical oncology : official journal of the American Society of Clinical Oncology* **23**, 6285-6295 (2005).

206   Kelly, L. M. & Gilliland, D. G. Genetics of myeloid leukemias. *Annu Rev Genomics Hum Genet* **3**, 179-198 (2002).

207   Downing, J. R. The core-binding factor leukemias: lessons learned from murine models. *Current opinion in genetics & development* **13**, 48-54 (2003).

208   Estey, E. & Dohner, H. Acute myeloid leukaemia. *Lancet* **368**, 1894-1907 (2006).

209   Chen, J., Odenike, O. & Rowley, J. D. Leukaemogenesis: more than mutant genes. *Nature reviews* **10**, 23-36 (2010).

210   Renneville, A. *et al.* Cooperating gene mutations in acute myeloid leukemia: a review of the literature. *Leukemia* **22**, 915-931 (2008).

211   Tallman, M. S., Gilliland, D. G. & Rowe, J. M. Drug therapy for acute myeloid leukemia. *Blood* **106**, 1154-1163, doi:2005-01-0178 [pii]
10.1182/blood-2005-01-0178 (2005).

212   Robak, T. & Wierzbowska, A. Current and emerging therapies for acute myeloid leukemia. *Clin Ther* **31 Pt 2**, 2349-2370 (2009).

213   Hamilton, A., Gallipoli, P., Nicholson, E. & Holyoake, T. L. Targeted therapy in haematological malignancies. *J Pathol* **220**, 404-418 (2010).

214   Strebhardt, K. & Ullrich, A. Paul Ehrlich's magic bullet concept: 100 years of progress. *Nature reviews* **8**, 473-480 (2008).

215   Ross, J. S. *et al.* Targeted therapies for cancer 2004. *Am J Clin Pathol* **122**, 598-609 (2004).

216   Kindler, T., Lipka, D. B. & Fischer, T. FLT3 as a therapeutic target in AML: still challenging after all these years. *Blood* **116**, 5089-5102, doi:blood-2010-04-261867 [pii]
10.1182/blood-2010-04-261867 (2010).

217   Zarrinkar, P. P. *et al.* AC220 is a uniquely potent and selective inhibitor of FLT3 for the treatment of acute myeloid leukemia (AML). *Blood* **114**, 2984-2992, doi:blood-2009-05-222034 [pii]
10.1182/blood-2009-05-222034 (2009).

218   Levis, M. J. Will newer tyrosine kinase inhibitors have an impact in AML? *Best Pract Res Clin Haematol* **23**, 489-494, doi:S1521-6926(10)00069-1 [pii]
10.1016/j.beha.2010.09.008 (2010).

219   Pao, W. & Chmielecki, J. Rational, biologically based treatment of EGFR-mutant non-small-cell lung cancer. *Nature reviews* **10**, 760-774, doi:nrc2947 [pii]
10.1038/nrc2947 (2010).

220   Boehrer, S. *et al.* Erlotinib exhibits antineoplastic off-target effects in AML and MDS: a preclinical study. *Blood* **111**, 2170-2180, doi:blood-2007-07-100362 [pii]

10.1182/blood-2007-07-100362 (2008).

221   Boehrer, S. *et al.* Erlotinib and gefitinib for the treatment of myelodysplastic syndrome and acute myeloid leukemia: a preclinical comparison. *Biochem Pharmacol* **76**, 1417-1425 (2008).

222   Hahn, C. K. *et al.* Proteomic and genetic approaches identify Syk as an AML target. *Cancer Cell* **16**, 281-294 (2009).

223   Stegmaier, K. *et al.* Gefitinib induces myeloid differentiation of acute myeloid leukemia. *Blood* **106**, 2841-2848 (2005).

224   Stegmeier, F., Warmuth, M., Sellers, W. R. & Dorsch, M. Targeted cancer therapies in the twenty-first century: lessons from imatinib. *Clin Pharmacol Ther* **87**, 543-552 (2010).

225   Chan, G. & Pilichowska, M. Complete remission in a patient with acute myelogenous leukemia treated with erlotinib for non small-cell lung cancer. *Blood* **110**, 1079-1080 (2007).

226   Pitini, V., Arrigo, C. & Altavilla, G. Erlotinib in a patient with acute myelogenous leukemia and concomitant non-small-cell lung cancer. *J Clin Oncol* **26**, 3645-3646 (2008).

227   Blencke, S., Ullrich, A. & Daub, H. Mutation of threonine 766 in the epidermal growth factor receptor reveals a hotspot for resistance formation against selective tyrosine kinase inhibitors. *J Biol Chem* **278**, 15435-15440, doi:10.1074/jbc.M211158200
M211158200 [pii] (2003).

228   Hibi, M., Lin, A., Smeal, T., Minden, A. & Karin, M. Identification of an oncoprotein- and UV-responsive protein kinase that binds and potentiates the c-Jun activation domain. *Genes Dev* **7**, 2135-2148 (1993).

229   Hinsby, A. M., Olsen, J. V. & Mann, M. Tyrosine phosphoproteomics of fibroblast growth factor signaling: a role for insulin receptor substrate-4. *J Biol Chem* **279**, 46438-46447 (2004).

230   Sambrook, J., Fritsch, E. & Maniatis, T. *Molecular Cloning: A Laboratory Manual*. (Cold Spring Harbor Laboratory Press, 1990).

231   Gershoni, J. M. & Palade, G. E. Protein blotting: principles and applications. *Anal Biochem* **131**, 1-15, doi:0003-2697(83)90128-8 [pii] (1983).

232   Rappsilber, J., Mann, M. & Ishihama, Y. Protocol for micro-purification, enrichment, pre-fractionation and storage of peptides for proteomics using StageTips. *Nat Protoc* **2**, 1896-1906, doi:nprot.2007.261 [pii] 10.1038/nprot.2007.261 (2007).

233   Knight, Z. A. & Shokat, K. M. Features of selective kinase inhibitors. *Chem Biol* **12**, 621-637, doi:S1074-5521(05)00123-7 [pii]
10.1016/j.chembiol.2005.04.011 (2005).

234   Berridge, M. V., Herst, P. M. & Tan, A. S. Tetrazolium dyes as tools in cell biology: new insights into their cellular reduction. *Biotechnol Annu Rev* **11**, 127-152, doi:S1387-2656(05)11004-7 [pii] 10.1016/S1387-2656(05)11004-7 (2005).

235   Daub, H. *et al.* Kinase-selective enrichment enables quantitative phosphoproteomics of the kinome across the cell cycle. *Molecular cell* **31**, 438-448, doi:S1097-2765(08)00493-0 [pii] 10.1016/j.molcel.2008.07.007 (2008).

236   Cox, J. & Mann, M. MaxQuant enables high peptide identification rates, individualized p.p.b.-range mass accuracies and proteome-wide protein quantification. *Nat Biotechnol* (2008).

237   Breitling, R., Armengaud, P., Amtmann, A. & Herzyk, P. Rank products: a simple, yet powerful, new method to detect differentially regulated genes in replicated microarray experiments. *FEBS Lett* **573**, 83-92, doi:10.1016/j.febslet.2004.07.055
S0014579304009354 [pii] (2004).

238   Huang da, W., Sherman, B. T. & Lempicki, R. A. Systematic and integrative analysis of large gene lists using DAVID bioinformatics resources. *Nat Protoc* **4**, 44-57, doi:nprot.2008.211 [pii] 10.1038/nprot.2008.211 (2009).

239   Dennis, G., Jr. *et al.* DAVID: Database for Annotation, Visualization, and Integrated Discovery. *Genome Biol* **4**, P3 (2003).

240   Jensen, L. J. *et al.* STRING 8--a global view on proteins and their functional interactions in 630 organisms. *Nucleic Acids Res* **37**, D412-416, doi:gkn760 [pii]
10.1093/nar/gkn760 (2009).

241   Schwartz, D. & Gygi, S. P. An iterative statistical approach to the identification of protein phosphorylation motifs from large-scale data sets. *Nat Biotechnol* **23**, 1391-1398 (2005).

242   Cheng, Y. & Prusoff, W. H. Relationship between the inhibition constant (K1) and the concentration of inhibitor which causes 50 per cent inhibition (I50) of an enzymatic reaction. *Biochem Pharmacol* **22**, 3099-3108 (1973).

243   Maere, S., Heymans, K. & Kuiper, M. BiNGO: a Cytoscape plugin to assess overrepresentation of gene ontology categories in biological networks. *Bioinformatics* **21**, 3448-3449, doi:bti551 [pii] 10.1093/bioinformatics/bti551 (2005).

244   Shannon, P. *et al.* Cytoscape: a software environment for integrated models of biomolecular interaction networks. *Genome Res* **13**, 2498-2504, doi:10.1101/gr.1239303 13/11/2498 [pii] (2003).

245   Adachi, J., Kumar, C., Zhang, Y., Olsen, J. V. & Mann, M. The human urinary proteome contains more than 1500 proteins, including a large proportion of membrane proteins. *Genome Biol* **7**, R80, doi:gb-2006-7-9-R80 [pii] 10.1186/gb-2006-7-9-R80 (2006).

246   Drewes, G. Chemical proteomics in drug discovery. *Methods Mol Biol* **803**, 15-21, doi:10.1007/978-1-61779-364-6_2 (2012).

247   Barouch-Bentov, R. & Sauer, K. Mechanisms of drug resistance in kinases. *Expert Opin Investig Drugs* **20**, 153-208, doi:10.1517/13543784.2011.546344 (2011).

248   Galli, M., Van Gool, F., Rongvaux, A., Andris, F. & Leo, O. The nicotinamide phosphoribosyltransferase: a molecular link between metabolism, inflammation, and cancer. *Cancer research* **70**, 8-11 (2010).

249   Martin, P. R., Shea, R. J. & Mulks, M. H. Identification of a plasmid-encoded gene from Haemophilus ducreyi which confers NAD independence. *J Bacteriol* **183**, 1168-1174 (2001).

250   Wissing, J. *et al.* Chemical proteomic analysis reveals alternative modes of action for pyrido[2,3-d]pyrimidine kinase inhibitors. *Mol Cell Proteomics* **3**, 1181-1193 (2004).

251   Ramotar, D. & Wang, H. Protective mechanisms against the antitumor agent bleomycin: lessons from Saccharomyces cerevisiae. *Current genetics* **43**, 213-224 (2003).

252   Abdelraheim, S. R., Spiller, D. G. & McLennan, A. G. Mammalian NADH diphosphatases of the Nudix family: cloning and characterization of the human peroxisomal NUDT12 protein. *Biochem J* **374**, 329-335 (2003).

253   Hermann, H. *et al.* snRNP Sm proteins share two evolutionarily conserved sequence motifs which are involved in Sm protein-protein interactions. *Embo J* **14**, 2076-2088 (1995).

254   Ye, X. *et al.* Cloning and characterization of a human cDNA ACAD10 mapped to chromosome 12q24.1. *Mol Biol Rep* **31**, 191-195 (2004).

255   Oppermann, F. S. *et al.* Large-scale proteomics analysis of the human kinome. *Mol Cell Proteomics* **8**, 1751-1764 (2009).

256   Barvian, M. *et al.* Pyrido[2,3-d]pyrimidin-7-one inhibitors of cyclin-dependent kinases. *J Med Chem* **43**, 4606-4616 (2000).

257   Cohen, P. The search for physiological substrates of MAP and SAP kinases in mammalian cells. *Trends Cell Biol* **7**, 353-361, doi:S0962-8924(97)01105-7 [pii] 10.1016/S0962-8924(97)01105-7 (1997).

258   Badger, A. M. *et al.* Pharmacological profile of SB 203580, a selective inhibitor of cytokine suppressive binding protein/p38 kinase, in animal models of arthritis, bone resorption, endotoxin shock and immune function. *J Pharmacol Exp Ther* **279**, 1453-1461 (1996).

259   Godl, K. & Daub, H. Proteomic analysis of kinase inhibitor selectivity and function. *Cell Cycle* **3**, 393-395 (2004).

260   Ashburner, M. *et al.* Gene ontology: tool for the unification of biology. The Gene Ontology Consortium. *Nat Genet* **25**, 25-29, doi:10.1038/75556 (2000).

261   Rix, U. *et al.* Chemical proteomic profiles of the BCR-ABL inhibitors imatinib, nilotinib, and dasatinib reveal novel kinase and nonkinase targets. *Blood* **110**, 4055-4063 (2007).

262   Ong, S. E. *et al.* Identifying the proteins to which small-molecule probes and drugs bind in cells. *Proc Natl Acad Sci U S A* **106**, 4617-4622 (2009).

263   Pawson, T. & Scott, J. D. Signaling through scaffold, anchoring, and adaptor proteins. *Science* **278**, 2075-2080 (1997).

264   Drake, A. W., Myszka, D. G. & Klakamp, S. L. Characterizing high-affinity antigen/antibody complexes by kinetic- and equilibrium-based methods. *Anal Biochem* **328**, 35-43, doi:10.1016/j.ab.2003.12.025 S0003269704000673 [pii] (2004).

265   Lurje, G. & Lenz, H. J. EGFR signaling and drug discovery. *Oncology* **77**, 400-410, doi:000279388 [pii] 10.1159/000279388 (2009).

266   Huang, F., Kirkpatrick, D., Jiang, X., Gygi, S. & Sorkin, A. Differential regulation of EGF receptor internalization and degradation by multiubiquitination within the kinase domain. *Molecular cell* **21**, 737-748, doi:S1097-2765(06)00120-1 [pii]
       10.1016/j.molcel.2006.02.018 (2006).

267   Jiang, X. & Sorkin, A. Epidermal growth factor receptor internalization through clathrin-coated pits requires Cbl RING finger and proline-rich domains but not receptor polyubiquitylation. *Traffic* **4**, 529-543, doi:109 [pii] (2003).

268   Choudhary, C. *et al.* Mislocalized activation of oncogenic RTKs switches downstream signaling outcomes. *Molecular cell* **36**, 326-339 (2009).

269   St-Denis, N. A., Derksen, D. R. & Litchfield, D. W. Evidence for regulation of mitotic progression through temporal phosphorylation and dephosphorylation of CK2alpha. *Mol Cell Biol* **29**, 2068-2081, doi:MCB.01563-08 [pii]
       10.1128/MCB.01563-08 (2009).

270   Crooks, G. E., Hon, G., Chandonia, J. M. & Brenner, S. E. WebLogo: a sequence logo generator. *Genome Res* **14**, 1188-1190 (2004).

271   Hassig, C. A. & Schreiber, S. L. Nuclear histone acetylases and deacetylases and transcriptional regulation: HATs off to HDACs. *Curr Opin Chem Biol* **1**, 300-308, doi:S1367-5931(97)80066-X [pii] (1997).

272   Yang, X. J. & Gregoire, S. Metabolism, cytoskeleton and cellular signalling in the grip of protein Nepsilon - and O-acetylation. *EMBO Rep* **8**, 556-562, doi:7400977 [pii]
       10.1038/sj.embor.7400977 (2007).

273   Atadja, P. W. HDAC inhibitors and cancer therapy. *Prog Drug Res* **67**, 175-195 (2011).

274   Copeland, R. A., Olhava, E. J. & Scott, M. P. Targeting epigenetic enzymes for drug discovery. *Curr Opin Chem Biol* **14**, 505-510, doi:S1367-5931(10)00076-1 [pii]
       10.1016/j.cbpa.2010.06.174 (2010).

275   Pflum, M. K., Tong, J. K., Lane, W. S. & Schreiber, S. L. Histone deacetylase 1 phosphorylation promotes enzymatic activity and complex formation. *J Biol Chem* **276**, 47733-47741, doi:10.1074/jbc.M105590200
       M105590200 [pii] (2001).

276   Tsai, S. C. & Seto, E. Regulation of histone deacetylase 2 by protein kinase CK2. *J Biol Chem* **277**, 31826-31833, doi:10.1074/jbc.M204149200
       M204149200 [pii] (2002).

277   Adenuga, D. & Rahman, I. Protein kinase CK2-mediated phosphorylation of HDAC2 regulates co-repressor formation, deacetylase activity and acetylation of HDAC2 by cigarette smoke and aldehydes. *Arch Biochem Biophys* **498**, 62-73, doi:10.1016/j.abb.2010.04.002
       S0003-9861(10)00124-4 [pii] (2010).

278   Moritz, A. *et al.* Akt-RSK-S6 kinase signaling networks activated by oncogenic receptor tyrosine kinases. *Sci Signal* **3**, ra64, doi:10.1126/scisignal.2000998
       3/136/ra64 [pii] (2010).

279   Chen, R. Q. *et al.* CDC25B mediates rapamycin-induced oncogenic responses in cancer cells. *Cancer Res* **69**, 2663-2668, doi:10.1158/0008-5472.CAN-08-3222
       0008-5472.CAN-08-3222 [pii] (2009).

280   Wang, S. *et al.* Control of endothelial cell proliferation and migration by VEGF signaling to histone deacetylase 7. *Proc Natl Acad Sci U S A* **105**, 7738-7743, doi:10.1073/pnas.0802857105
       0802857105 [pii] (2008).

281   Ha, C. H., Jhun, B. S., Kao, H. Y. & Jin, Z. G. VEGF stimulates HDAC7 phosphorylation and cytoplasmic accumulation modulating matrix metalloproteinase expression and angiogenesis. *Arterioscler Thromb Vasc Biol* **28**, 1782-1788, doi:10.1161/ATVBAHA.108.172528
       ATVBAHA.108.172528 [pii] (2008).

282   McKinsey, T. A., Zhang, C. L., Lu, J. & Olson, E. N. Signal-dependent nuclear export of a histone deacetylase regulates muscle differentiation. *Nature* **408**, 106-111, doi:10.1038/35040593 (2000).

283   Rybin, V. O., Guo, J., Harleton, E., Feinmark, S. J. & Steinberg, S. F. Regulatory autophosphorylation sites on protein kinase C-delta at threonine-141 and threonine-295. *Biochemistry* **48**, 4642-4651, doi:10.1021/bi802171c (2009).

284   Rawlings, D. J. *et al.* Activation of BTK by a phosphorylation mechanism initiated by SRC family kinases. *Science* **271**, 822-825 (1996).

285   Tsang, E. *et al.* Molecular Mechanism of the Syk Activation Switch. *Journal of Biological Chemistry* **283**, 32650-32659, doi:DOI 10.1074/jbc.M806340200 (2008).

286   Baba, Y. *et al.* BLNK mediates Syk-dependent Btk activation. *Proc Natl Acad Sci U S A* **98**, 2582-2586, doi:10.1073/pnas.051626198
051626198 [pii] (2001).

287   Dinh, M. *et al.* Activation mechanism and steady state kinetics of Bruton's tyrosine kinase. *J Biol Chem* **282**, 8768-8776, doi:M609920200 [pii]
10.1074/jbc.M609920200 (2007).

288   Wahl, M. I. *et al.* Phosphorylation of two regulatory tyrosine residues in the activation of Bruton's tyrosine kinase via alternative receptors. *Proc Natl Acad Sci U S A* **94**, 11526-11533 (1997).

289   Walchli, S. *et al.* Characterization of clathrin and Syk interaction upon Shiga toxin binding. *Cell Signal* **21**, 1161-1168, doi:S0898-6568(09)00107-7 [pii]
10.1016/j.cellsig.2009.03.005 (2009).

290   Murugappan, S. *et al.* Molecular mechanism and functional implications of thrombin-mediated tyrosine phosphorylation of PKCdelta in platelets. *Blood* **106**, 550-557 (2005).

291   Hall, K. J., Jones, M. L. & Poole, A. W. Coincident regulation of PKCdelta in human platelets by phosphorylation of Tyr311 and Tyr565 and phospholipase C signalling. *Biochem J* **406**, 501-509, doi:BJ20070244 [pii]
10.1042/BJ20070244 (2007).

292   Lal, L. *et al.* Activation of the p70 S6 kinase by all-trans-retinoic acid in acute promyelocytic leukemia cells. *Blood* **105**, 1669-1677, doi:2004-06-2078 [pii]
10.1182/blood-2004-06-2078 (2005).

293   Brdicka, T. *et al.* Phosphoprotein associated with glycosphingolipid-enriched microdomains (PAG), a novel ubiquitously expressed transmembrane adaptor protein, binds the protein tyrosine kinase csk and is involved in regulation of T cell activation. *The Journal of experimental medicine* **191**, 1591-1604 (2000).

294   Kales, S. C., Ryan, P. E., Nau, M. M. & Lipkowitz, S. Cbl and human myeloid neoplasms: the Cbl oncogene comes of age. *Cancer Res* **70**, 4789-4794, doi:0008-5472.CAN-10-0610 [pii]
10.1158/0008-5472.CAN-10-0610 (2010).

295   Larive, R. M. *et al.* Phosphoproteomic analysis of Syk kinase signaling in human cancer cells reveals its role in cell-cell adhesion. *Oncogene* **28**, 2337-2347, doi:onc200999 [pii]
10.1038/onc.2009.99 (2009).

296   Lorenz, U. *et al.* Lck-dependent tyrosyl phosphorylation of the phosphotyrosine phosphatase SH-PTP1 in murine T cells. *Mol Cell Biol* **14**, 1824-1834 (1994).

297   Lu, W. *et al.* Tyrosine 311 is phosphorylated by c-Abl and promotes the apoptotic effect of PKCdelta in glioma cells. *Biochem Biophys Res Commun* **352**, 431-436 (2007).

298   Sada, K., Takano, T., Yanagi, S. & Yamamura, H. Structure and function of Syk protein-tyrosine kinase. *J Biochem* **130**, 177-186 (2001).

299   Shi, Y. Serine/threonine phosphatases: mechanism through structure. *Cell* **139**, 468-484 (2009).

300   van Dijk, T. B. *et al.* Stem cell factor induces phosphatidylinositol 3'-kinase-dependent Lyn/Tec/Dok-1 complex formation in hematopoietic cells. *Blood* **96**, 3406-3413 (2000).

301   Mohamed, A. J. *et al.* Bruton's tyrosine kinase (Btk): function, regulation, and transformation with special emphasis on the PH domain. *Immunol Rev* **228**, 58-73, doi:IMR741 [pii]
10.1111/j.1600-065X.2008.00741.x (2009).

302   Jo, O. D. *et al.* Heterogeneous nuclear ribonucleoprotein A1 regulates cyclin D1 and c-myc internal ribosome entry site function through Akt signaling. *J Biol Chem* **283**, 23274-23287, doi:M801185200 [pii]
10.1074/jbc.M801185200 (2008).

303   Mann, M. Functional and quantitative proteomics using SILAC. *Nat Rev Mol Cell Biol* **7**, 952-958 (2006).

304   Yamamoto, K., Yamazaki, A., Takeuchi, M. & Tanaka, A. A versatile method of identifying specific binding proteins on affinity resins. *Anal Biochem* **352**, 15-23, doi:S0003-2697(06)00109-6 [pii]
10.1016/j.ab.2006.02.008 (2006).

305   Bantscheff, M. *et al.* Chemoproteomics profiling of HDAC inhibitors reveals selective targeting of HDAC complexes. *Nat Biotechnol*, doi:nbt.1759 [pii]
10.1038/nbt.1759 (2011).

306   Hanoulle, X. *et al.* A new functional, chemical proteomics technology to identify purine nucleotide binding sites in complex proteomes. *J Proteome Res* **5**, 3438-3445 (2006).

307   Wakeling, A. E. *et al.* ZD1839 (Iressa): an orally active inhibitor of epidermal growth factor signaling with potential for cancer therapy. *Cancer Res* **62**, 5749-5754 (2002).

308   Atienza, J. M. *et al.* Dynamic and label-free cell-based assays using the real-time cell electronic sensing system. *Assay Drug Dev Technol* **4**, 597-607, doi:10.1089/adt.2006.4.597 (2006).

309   Bromme, D., Rossi, A. B., Smeekens, S. P., Anderson, D. C. & Payan, D. G. Human bleomycin hydrolase: molecular cloning, sequencing, functional expression, and enzymatic characterization. *Biochemistry* **35**, 6706-6714, doi:10.1021/bi960092y
bi960092y [pii] (1996).

310   Prince, J. A. *et al.* Lack of replication of association findings in complex disease: an analysis of 15 polymorphisms in prior candidate genes for sporadic Alzheimer's disease. *Eur J Hum Genet* **9**, 437-444, doi:10.1038/sj.ejhg.5200651 (2001).

311   Su, A. I. *et al.* Large-scale analysis of the human and mouse transcriptomes. *Proc Natl Acad Sci U S A* **99**, 4465-4470 (2002).

312   Leenders, F. *et al.* PKN3 is required for malignant prostate cell growth downstream of activated PI 3-kinase. *Embo J* **23**, 3303-3313, doi:10.1038/sj.emboj.7600345
7600345 [pii] (2004).

313   Fantin, V. R. *et al.* Characterization of insulin receptor substrate 4 in human embryonic kidney 293 cells. *J Biol Chem* **273**, 10726-10732 (1998).

314   Qu, B. H., Karas, M., Koval, A. & LeRoith, D. Insulin receptor substrate-4 enhances insulin-like growth factor-I-induced cell proliferation. *J Biol Chem* **274**, 31179-31184 (1999).

315   Wu, C. *et al.* Systematic identification of SH3 domain-mediated human protein-protein interactions by peptide array target screening. *Proteomics* **7**, 1775-1785, doi:10.1002/pmic.200601006 (2007).

316   Chardin, P. *et al.* Human Sos1: a guanine nucleotide exchange factor for Ras that binds to GRB2. *Science* **260**, 1338-1343 (1993).

317   Jones, R. B., Gordus, A., Krall, J. A. & MacBeath, G. A quantitative protein interaction network for the ErbB receptors using protein microarrays. *Nature* **439**, 168-174 (2006).

318   Gavin, A. C. & Superti-Furga, G. Protein complexes and proteome organization from yeast to man. *Curr Opin Chem Biol* **7**, 21-27, doi:S1367593102000078 [pii] (2003).

319   Rinner, O. *et al.* An integrated mass spectrometric and computational framework for the analysis of protein interaction networks. *Nat Biotechnol* **25**, 345-352, doi:nbt1289 [pii]
10.1038/nbt1289 (2007).

320   Terpe, K. Overview of tag protein fusions: from molecular and biochemical fundamentals to commercial systems. *Appl Microbiol Biotechnol* **60**, 523-533, doi:10.1007/s00253-002-1158-6 (2003).

321   Hidalgo, M. *et al.* Phase I and pharmacologic study of OSI-774, an epidermal growth factor receptor tyrosine kinase inhibitor, in patients with advanced solid malignancies. *J Clin Oncol* **19**, 3267-3279 (2001).

322   Baselga, J. *et al.* Phase I safety, pharmacokinetic, and pharmacodynamic trial of ZD1839, a selective oral epidermal growth factor receptor tyrosine kinase inhibitor, in patients with five selected solid tumor types. *J Clin Oncol* **20**, 4292-4302 (2002).

323   Ogawa, S. *et al.* Deregulated Intracellular Signaling by Mutated c-CBL in Myeloid Neoplasms. *Clin Cancer Res* **16**, 3825-3831, doi:Doi 10.1158/1078-0432.Ccr-09-2341 (2010).

324   Kanou, T. *et al.* The Transmembrane Adaptor Cbp/PAG1 Controls the Malignant Potential of Human Non-Small Cell Lung Cancers That Have c-Src Upregulation. *Mol Cancer Res* **9**, 103-114, doi:Doi 10.1158/1541-7786.Mcr-10-0340 (2011).

325   Brodie, C. & Blumberg, P. M. Regulation of cell apoptosis by protein kinase c delta. *Apoptosis* **8**, 19-27 (2003).

326   Chen, L. F. *et al.* SYK-dependent tonic B-cell receptor signaling is a rational treatment target in diffuse large B-cell lymphoma. *Blood* **111**, 2230-2237, doi:DOI 10.1182/blood-2007-07-100115 (2008).

327   Kurosaki, T. & Kurosaki, M. Transphosphorylation of Bruton's tyrosine kinase on tyrosine 551 is critical for B cell antigen receptor function. *Journal of Biological Chemistry* **272**, 15595-15598 (1997).

328   Mocsai, A., Ruland, J. & Tybulewicz, V. L. J. The SYK tyrosine kinase: a crucial player in diverse biological functions. *Nat Rev Immunol* **10**, 387-402, doi:Doi 10.1038/Nri2765 (2010).

329   Siraganian, R. P., Zhang, J., Suzuki, K. & Sada, K. Protein tyrosine kinase Syk in mast cell signaling. *Mol Immunol* **38**, 1229-1233, doi:S0161589002000688 [pii] (2002).

330   Berton, G., Mocsai, A. & Lowell, C. A. Src and Syk kinases: key regulators of phagocytic cell activation. *Trends Immunol* **26**, 208-214, doi:S1471-4906(05)00026-8 [pii]
10.1016/j.it.2005.02.002 (2005).

331   Lewis, C. M., Broussard, C., Czar, M. J. & Schwartzberg, P. L. Tec kinases: modulators of lymphocyte signaling and development. *Curr Opin Immunol* **13**, 317-325 (2001).

332   Feldman, A. L. *et al.* Syk tyrosine kinase is overexpressed in the majority of peripheral T- and NK-cell lymphomas, and represents a potential therapeutic target. *Blood* **110**, 212a-212a (2007).

333   Rinaldi, A. *et al.* Genomic and expression profiling identifies the B-cell associated tyrosine kinase Syk as a possible therapeutic target in mantle cell lymphoma. *Brit J Haematol* **132**, 303-316, doi:DOI 10.1111/j.1365-2141.2005.05883.x (2006).

334   Honigberg, L. A. *et al.* The Bruton tyrosine kinase inhibitor PCI-32765 blocks B-cell activation and is efficacious in models of autoimmune disease and B-cell malignancy. *P Natl Acad Sci USA* **107**, 13075-13080, doi:DOI 10.1073/pnas.1004594107 (2010).

335   Davis, R. E. *et al.* Chronic active B-cell-receptor signalling in diffuse large B-cell lymphoma. *Nature* **463**, 88-U97, doi:Doi 10.1038/Nature08638 (2010).

336   Nguyen, V. *et al.* A New Approach for Quantitative Phosphoproteomic Dissection of Signaling Pathways Applied to T Cell Receptor Activation. *Molecular & Cellular Proteomics* **8**, 2418-2431, doi:DOI 10.1074/mcp.M800307-MCP200 (2009).

337   Au-Yeung, B. B. *et al.* The structure, regulation, and function of ZAP-70. *Immunological Reviews* **228**, 41-57, doi:DOI 10.1111/j.1600-065X.2008.00753.x (2009).

338   Feshchenko, E. A., Langdon, W. Y. & Tsygankov, A. Y. Fyn, Yes, and Syk phosphorylation sites in c-Cbl map to the same tyrosine residues that become phosphorylated in activated T cells. *J Biol Chem* **273**, 8323-8331 (1998).

339   Lupher, M. L. *et al.* Cbl-mediated negative regulation of the Syk tyrosine kinase - A critical role for Cbl phosphotyrosine-binding domain binding to Syk phosphotyrosine 323. *Journal of Biological Chemistry* **273**, 35273-35281 (1998).

340   Law, C. L., Chandran, K. A., Sidorenko, S. P. & Clark, E. A. Phospholipase C-gamma1 interacts with conserved phosphotyrosyl residues in the linker region of Syk and is a substrate for Syk. *Mol Cell Biol* **16**, 1305-1315 (1996).

341   Poulin, B., Sekiya, F. & Rhee, S. G. Intramolecular interaction between phosphorylated tyrosine-783 and the C-terminal Src homology 2 domain activates phospholipase C-gamma 1. *P Natl Acad Sci USA* **102**, 4276-4281, doi:DOI 10.1073/pnas.0409590102 (2005).

342   Choi, J. H., Ryu, S. H. & Suh, P. G. On/Off-regulation of phospholipase C-gamma 1-mediated signal transduction. *Adv Enzyme Regul* **47**, 104-116 339, doi:DOI 10.1016/j.advenzreg.2006.12.010 (2007).

343   Lee, Y. H. *et al.* Down-Regulation of Phospholipase C-Gamma-1 during the Differentiation of U937 Cells. *Febs Letters* **358**, 105-108 (1995).

344   Schmidt, U., Boucheron, N., Unger, B. & Ellmeier, W. The role of Tec family kinases in myeloid cells. *Int Arch Allergy Imm* **134**, 65-78, doi:Doi 10.1159/000078339 (2004).

345   Ellmeier, W., Abramova, A. & Schebesta, A. Tec family kinases: Regulation of FcεRI-mediated mast cell activation. *FEBS Journal*, no-no, doi:10.1111/j.1742-4658.2011.08073.x (2011).

346   Li, Z. *et al.* Erlotinib effectively inhibits JAK2V617F activity and polycythemia vera cell growth. *J Biol Chem* **282**, 3428-3432, doi:C600277200 [pii] 10.1074/jbc.C600277200 (2007).

347   Dos Santos, C. *et al.* A critical role for Lyn in acute myeloid leukemia. *Blood* **111**, 2269-2279, doi:blood-2007-04-082099 [pii] 10.1182/blood-2007-04-082099 (2008).

348   Scapini, P., Pereira, S., Zhang, H. & Lowell, C. A. Multiple roles of Lyn kinase in myeloid cell signaling and function. *Immunol Rev* **228**, 23-40, doi:IMR758 [pii] 10.1111/j.1600-065X.2008.00758.x (2009).

349   Mocsai, A., Ruland, J. & Tybulewicz, V. L. The SYK tyrosine kinase: a crucial player in diverse biological functions. *Nat Rev Immunol* **10**, 387-402, doi:nri2765 [pii] 10.1038/nri2765 (2010).

350   Ingley, E. Src family kinases: regulation of their activities, levels and identification of new pathways. *Biochim Biophys Acta* **1784**, 56-65, doi:S1570-9639(07)00199-9 [pii] 10.1016/j.bbapap.2007.08.012 (2008).

351   Zhang, S. Q. *et al.* Shp2 regulates SRC family kinase activity and Ras/Erk activation by controlling Csk recruitment. *Molecular cell* **13**, 341-355, doi:S1097276504000504 [pii] (2004).

352   Li, L. *et al.* A critical role for SHP2 in STAT5 activation and growth factor-mediated proliferation, survival, and differentiation of human CD34+ cells. *Blood* **118**, 1504-1515, doi:blood-2010-06-288910 [pii]

10.1182/blood-2010-06-288910 (2011).

353   Scott, L. M., Lawrence, H. R., Sebti, S. M., Lawrence, N. J. & Wu, J. Targeting protein tyrosine phosphatases for anticancer drug discovery. *Curr Pharm Des* **16**, 1843-1862, doi:BSP/CPD/E-Pub/00076 [pii] (2010).

354   Chong, Z. Z. & Maiese, K. The Src homology 2 domain tyrosine phosphatases SHP-1 and SHP-2: diversified control of cell growth, inflammation, and injury. *Histol Histopathol* **22**, 1251-1267 (2007).

355   Perrotti, D., Jamieson, C., Goldman, J. & Skorski, T. Chronic myeloid leukemia: mechanisms of blastic transformation. *J Clin Invest* **120**, 2254-2264, doi:10.1172/JCI41246
41246 [pii] (2010).

356   Chen, P. *et al.* FLT3/ITD mutation signaling includes suppression of SHP-1. *J Biol Chem* **280**, 5361-5369, doi:M411974200 [pii]
10.1074/jbc.M411974200 (2005).

357   Wu, C., Sun, M., Liu, L. & Zhou, G. W. The function of the protein tyrosine phosphatase SHP-1 in cancer. *Gene* **306**, 1-12, doi:S0378111903004001 [pii] (2003).

358   Mashima, R., Hishida, Y., Tezuka, T. & Yamanashi, Y. The roles of Dok family adapters in immunoreceptor signaling. *Immunol Rev* **232**, 273-285, doi:IMR844 [pii]
10.1111/j.1600-065X.2009.00844.x (2009).

359   Liang, X. *et al.* Phosphatidylinositol 3-kinase and Src family kinases are required for phosphorylation and membrane recruitment of Dok-1 in c-Kit signaling. *J Biol Chem* **277**, 13732-13738, doi:10.1074/jbc.M200277200
M200277200 [pii] (2002).

360   Guo, C. Y., Brautigan, D. L. & Larner, J. M. Ionizing radiation activates nuclear protein phosphatase-1 by ATM-dependent dephosphorylation. *J Biol Chem* **277**, 41756-41761, doi:10.1074/jbc.M207519200
M207519200 [pii] (2002).

361   Colon-Gonzalez, F. & Kazanietz, M. G. C1 domains exposed: from diacylglycerol binding to protein-protein interactions. *Biochim Biophys Acta* **1761**, 827-837, doi:S1388-1981(06)00126-0 [pii]
10.1016/j.bbalip.2006.05.001 (2006).

362   Reyland, M. E. Protein kinase C isoforms: Multi-functional regulators of cell life and death. *Front Biosci* **14**, 2386-2399, doi:3385 [pii] (2009).

363   Hampson, P. *et al.* PEP005, a selective small-molecule activator of protein kinase C, has potent antileukemic activity mediated via the delta isoform of PKC. *Blood* **106**, 1362-1368, doi:2004-10-4117 [pii]
10.1182/blood-2004-10-4117 (2005).

364   Roux, P. P. *et al.* RAS/ERK signaling promotes site-specific ribosomal protein S6 phosphorylation via RSK and stimulates cap-dependent translation. *J Biol Chem* **282**, 14056-14064, doi:M700906200 [pii]
10.1074/jbc.M700906200 (2007).

365   Scheper, G. C. & Proud, C. G. Does phosphorylation of the cap-binding protein eIF4E play a role in translation initiation? *Eur J Biochem* **269**, 5350-5359, doi:3291 [pii] (2002).

366   Lekmine, F. *et al.* Interferon-gamma engages the p70 S6 kinase to regulate phosphorylation of the 40S S6 ribosomal protein. *Exp Cell Res* **295**, 173-182, doi:10.1016/j.yexcr.2003.12.021
S0014482704000114 [pii] (2004).

367   Komar, A. A. & Hatzoglou, M. Cellular IRES-mediated translation: the war of ITAFs in pathophysiological states. *Cell Cycle* **10**, 229-240, doi:14472 [pii] (2011).

368   Sharma, S. V. & Settleman, J. Oncogene addiction: setting the stage for molecularly targeted cancer therapy. *Genes Dev* **21**, 3214-3231, doi:21/24/3214 [pii]
10.1101/gad.1609907 (2007).

369   Hendriks, R. W. Drug discovery: New Btk inhibitor holds promise. *Nat Chem Biol* **7**, 4-5, doi:nchembio.502 [pii]
10.1038/nchembio.502 (2011).

370   Kim, L. C., Song, L. & Haura, E. B. Src kinases as therapeutic targets for cancer. *Nat Rev Clin Oncol* **6**, 587-595, doi:nrclinonc.2009.129 [pii]
10.1038/nrclinonc.2009.129 (2009).

371   Guerrouahen, B. S. *et al.* Dasatinib inhibits the growth of molecularly heterogeneous myeloid leukemias. *Clin Cancer Res* **16**, 1149-1158, doi:1078-0432.CCR-09-2416 [pii]
10.1158/1078-0432.CCR-09-2416 (2010).

VII Appendix

1. Abbreviations

°C	degree celsius
μ	micro
Å	ångström
ABL	abelson murine leukemia viral oncogene homolog 1
ABPP	activity-based probe profiling
ADP	adenosine diphosphate
ALL	acute lymphoblastic leukemia
AML	acute myeloid leukemia
Arg	arginine
ASM	aggressive systemic mastocytosis
ATP	adenosine-5'-triphosphate
BC	breast cancer
BCR	breakpoint cluster region
BiNGO	biological networks gene ontology
BLMH	bleomycin hydrolase
BRK	breast tumor kinase
BTK	bruton tyrosine kinase
CBL	casitas B-lineage lymphoma
CCCP	compound-centric chemical proteomic
CDK	cyclin-dependent kinase
CHED	cell division cycle 2-like protein kinase
CEL	chronic eosinophilic leukemia
CID	collision-induced dissociation
CK1	casein kinase 1
CK2	casein kinase II
CML	chronic myeloid leukemia
Da	dalton
DDR1	discoidin domain receptor 1
DNA	deoxyribonucleic acid

DOK1	docking protein 1
EASE score	expression analysis systematic explorer score
ECD	electron capture dissociation
EGFR	epidermal growth factor receptor
ESI	electrospray ionization
ETD	electron transfer dissociation
FDA	Food and Drug Administration
FDR	false discovery rate
FGF	fibroblast growth factor
FGFR	FGF receptor
FLT3	fms-like tyrosine kinase 3
GAK	cyclin G–associated kinase
GIST	gastrointestinal stromal tumors
GO	gene ontology
GRB	growth factor receptor-bound protein
GSK3β	glycogen synthase kinase 3β
GST	glutathione S-transferase
h	hour
HA	human influenza hemagglutinin
HAT	histone acetyltransferase
HCC	hepatocellular carcinoma
HCD	higher-energy C-trap dissociation
HDAC	histone deacetylase
HES	hypereosinophilic syndrome
hnRNP A1	heterogeneous nuclear ribonucleoprotein A1
(HP)LC-MS	(high-performance) liquid-based chromatography MS
IC_{50}	half maximal inhibitory concentration
IP	immunoprecipitation
IRS4	insulin receptor substrate 4
iTRAQ	isobaric tags for absolute and relative quantification
JAK	janus kinase
JNK	c-jun N-terminal kinase
k	kilo
Leu	leucine
LSC	Leukemic Stem Cells (LSC
Lys	lysine
m	milli/mass
M	molar
MALDI	matrix-assisted laser desorption/ionization
MAPK	mitogen-activated protein kinase
MAPKK	MAPK kinase
MAPKKK	MAPK kinase kinase
MDS	myelodysplastic syndrome

min	minute
MPD	myeloproliferative diseases
mRNA	messenger ribonucleic acid
MS	mass spectrometry
mTOR	mammalian target of rapamycin protein kinase
n	nano
NAMPT	nicotinamide phosphoribosyltransferase
NET	neuroendocrine tumor
NSCLC	non-small-cell lung cancer
PC	pancreatic carcinoma
PEP	posterior error probability
Ph+	philadelphia chromosome positive
PIK3C	p110 catalytical subunit of PI3K
PIK3R	p85 regulatory subunits of phosphatidylinositol 3 kinase
PKA	protein kinase A
PKD3	protein kinase D3
PLCG	phospholipase C γ
ppm	parts per million
PPP1CA	serine/threonine-protein phosphatase PP1-α catalytic subunit
PRMT5	protein arginine N-methyltransferase 5
PTM	posttranslational modification
RAF	rapidly accelerated fibrosarcoma
RCC	renal cell carcinoma
RIPK2	receptor-interacting serine/threonine-protein kinase 2
RP	rank product
RPLC	reversed phase liquid chromatography
rpm	rounds per minute
RSK	ribosomal protein S6 Kinase
RT	room temperature
s	second
SAR	structure-activity relationship
SCX	strong cation exchange chromatography
SEGA	subependymal giant cell astrocytoma
Ser	serine
SFK	SRC-family kinase
SH2	src homology 2
SHP	SRC homology region 2 domain-containing phosphatase
SILAC	stable isotope labeling by amino acids in cell culture
siRNA	short interfering RNA
SNRPG	small nuclear ribonucleoprotein G
SOCS6	suppressor of cytokine signaling 6
SOS1	son of sevenless homolog 1
STAGEtips	stopandgoextraction tips

STAT5A	signal transducer and activator of transcription 5A
STRING	search tool for the retrieval of interacting genes/proteins
STS	soft tissue sarcoma
SYK	spleen tyrosine kinase
TAP	tandem affinity purification
TC	thyroid cancer
Thr	threonine
TMT	tandem mass tag
Tyr	tyrosine
Uv/Vis	ultraviolet–visible
V	volt
v/v	volume/volume
w/w	weight/weight
z	charge

2. Additional table

Table A 1: Quantitative chemical proteomic target analysis of immobilized VI16742 and SB203580

Protein Names	Protein Kinase	r (2. inc/1. inc)	K_d(VI16742) [M]	Specificity ratio (control/1. inc)	Ratio 3 mg/1 mg lysate	Ratio 5 h/2.5 h incubation time	IC_{50}(SB203580) [nM]	$K_{d,average}$ (SB203580) [nM]	$IC_{50} \sim K_d$ [nM], kinase assay (SB203580)
Receptor-interacting ser-ine/threonine-protein kinase 2	RIPK2	0.09	5.06	0.02	3.62	1.04	10.5	0.83	2.16
Serine/threonine-protein kinase N3	PKN3	0.37	30.94	0.06		1.48	51.4	17.65	
Cyclin G-associated kinase	GAK	0.35	28.55	0.04	2.88	1.05	335.4	109.20	35.24
Casein kinase I isoform delta	CK1d	0.13	7.74	0.02	3.10	1.00	1508	174.52	150.9
Casein kinase I isoform epsilon	CK1e	0.21	14.18	0.03	3.31		3356	648.90	415.05
Discoidin domain receptor family, member 1	DDR1	0.44	40.77	0.07			1972	804.64	
Mitogen-activated protein kinase 9	JNK2	0.06	3.43	0.05	3.19	0.91	16760	918.88	727.55
Glycogen synthase kinase-3 beta	GSK3B	0.09	5.21	0.02	3.57	0.97	14340	1161.76	3117
CSNK1A1 protein		0.27	19.51	0.03	2.78	0.94	7254	1799.34	
Mitotic checkpoint serine/threonine-protein kinase BUB1	BUB1	0.76	161.39	0.05			3708	2713.51	
Serine/threonine-protein kinase D2	PKD2	0.06	3.56	0.02	3.08	1.11	54930	3117.67	
Tyrosine-protein kinase JAK1	JAK1	0.09	5.35	0.04	3.65	0.98	47640	3952.36	
Mitogen-activated protein kinase 8	JNK1	0.05	3.01	0.04	3.21	0.94	93140	4505.40	
Non-receptor tyrosine-protein kinase TYK2	TYK2	0.10	5.77	0.06	4.59	0.73	56630	5036.01	
Serine/threonine-protein kinase D3	PKD3	0.07	4.01	0.05	2.91	1.02	93530	5933.54	
Glycogen synthase kinase-3 alpha	GSK3A	0.19	12.54	0.01	2.82	1.07	37870	6626.13	
Putative myosin light chain kinase 3	caMLCK/skMLCK/SgK085	0.07	3.66	0.01		0.91	140700	8200.91	
Putative uncharacterized protein MAP4K4	HGK/ZC1	0.59	75.73	0.05			16630	9337.35	
Ephrin type-B receptor 2 precursor	EphB2	0.44	41.46	0.10	3.40	0.94	24800	10220.41	
Basic fibroblast growth factor receptor 1 precursor	FGFR1	0.31	23.18	0.05			41100	11570.71	
Ephrin type-B receptor 4 precursor	EphB4	0.45	41.91	0.06	2.78	0.97	33650	13955.00	37714.5
Ephrin type-A receptor 2 precursor	EphA2	0.51	54.03	0.11	2.42	1.03	31460	15018.40	
TRAF2 and NCK-interacting protein kinase	TNIK/ZC2	0.67	107.87	0.19		1.27	26770	17289.25	
cAMP-specific 3',5'-cyclic phosphodiesterase 4D		0.66	102.20	0.05	2.48	1.09	33530	21237.74	
Proto-oncogene tyrosine-protein kinase Yes	YES	0.40	34.23	0.03			58830	21566.34	4379
Ribosomal protein S6 kinase alpha-1	RSK3	0.27	19.24	0.02	2.91	1.01	88220	21653.19	
Rho-associated protein kinase 2	ROCK2	0.83	254.87	0.08	3.18	1.74	27210	22084.64	
Bromodomain-containing protein 3	BRD3	0.36	29.36	0.04	3.42	1.27	72820	24154.87	

Description	Symbol							
STE20-like serine/threonine-protein kinase	SLK	0.81	216.99	0.05	3.22	1.87	40510	31832.71
Dual specificity mitogen-activated protein kinase kinase 2	MAP2K2	0.77	177.14	0.03		2.03	44100	33060.62
Proto-oncogene tyrosine-protein kinase ABL1	ABL	0.58	72.63	0.06	3.23		61610	33956.99
Tyrosine-protein kinase ABL2	ARG	0.55	64.46	0.09	2.82	1.30	67460	35180.12
LYN protein	LYN	0.47	45.38	0.08	2.67	1.61	97000	42111.05
Bromodomain-containing protein 4	BRD4	0.46	44.49	0.03	3.79	0.96	105500	45286.04
Serine/threonine-protein kinase MRCK beta	MRCKb	0.85	301.21	0.06	2.35	1.34	73260	61234.91
5'-nucleotidase domain-containing protein 1		0.65	94.76	0.07			114500	70496.23
Serine/threonine-protein kinase MST4	MST4	0.59	73.31	0.13			129600	71728.33
Dual specificity mitogen-activated protein kinase kinase 1	MAP2K1	0.78	179.85	0.07		1.68	96960	72963.18
Adenosine kinase		0.64	94.23	0.05		1.63	146600	90064.19
Calcium/calmodulin-dependent protein kinase type II gamma chain	CaMK2g	0.03	1.60	0.06	2.90	0.88		
Calcium/calmodulin-dependent protein kinase type II delta chain	CaMK2d	0.04	1.90	0.02		0.82		
Serine/threonine-protein kinase Nek9	NEK9	0.04	2.30	0.02	2.91	0.92		
cAMP and cAMP-inhibited cGMP 3',5'-cyclic phosphodiesterase 10A		0.05	2.58	0.03		0.98		
Serine/threonine-protein kinase 6	AurA	0.06	3.23	0.03	3.71	1.16		
Serine/threonine-protein kinase ULK3	ULK3	0.06	3.48	0.03	1.52	0.95		
Acyl-CoA dehydrogenase family member 11		0.06	3.50	0.05	3.26	1.01		
Cell division protein kinase 2	CDK2	0.07	3.69	0.04	2.93	0.97		
Serine/threonine-protein kinase TBK1	TBK1	0.07	3.74	0.03	3.37	1.00		
Cell division protein kinase 5	CDK5	0.07	3.75	0.03	2.92	0.96		
Serine/threonine-protein kinase 17B	DRAK2	0.07	3.75	0.01	4.20	0.79		
Non-receptor tyrosine-protein kinase TNK1	TNK1	0.07	3.81	0.02	3.16	1.01		
Mitogen-activated protein kinase kinase kinase MLT	ZAK	0.07	4.07	0.09	3.74	0.99		
Ribosyldihydronicotinamide dehydrogenase [quinone]		0.07	4.13	0.14	2.68	0.91		
Pyridoxal kinase		0.08	4.65	0.08	2.97	0.96		
Serine/threonine-protein kinase PCTAIRE-1	PCTAIRE1	0.10	5.99	0.02	2.88	0.89		
Cyclin-T2		0.11	6.11	0.10				
Proto-oncogene tyrosine-protein kinase FER	FER	0.11	6.26	0.05	2.83	0.98		
Dual specificity protein kinase CLK2	CLK2	0.11	6.31	0.01		0.96		
Mitogen-activated protein kinase kinase kinase MLT	ZAK	0.11	6.34	0.04	3.14	0.93		
Serine/threonine-protein kinase PFTAIRE-1	PFTAIRE1	0.11	6.52	0.01	2.59			
Casein kinase II subunit alpha'	CK2a2	0.11	6.59	0.04	2.69	0.91		
Serine/threonine-protein kinase PCTAIRE-2	PCTAIRE2	0.12	6.79	0.02	2.61	0.97		
Delta(3,5)-Delta(2,4)-dienoyl-CoA isomerase, mitochondrial precursor		0.12	7.17	0.07	3.14	0.96		
AP2-associated protein kinase 1	AAK1	0.12	7.18	0.03	3.58	1.13		

cDNA FLJ75960, highly similar to Homo sapiens serine/threonine kinase 16 (STK16), transcript variant 2, mRNA	MPSK1	0.13	7.45	0.11	2.40	0.86
Serine/threonine-protein kinase MARK1	MARK1	0.13	7.45	0.07		0.95
Cell division protein kinase 9	CDK9	0.13	7.48	0.02	2.77	1.00
MAP/microtubule affinity-regulating kinase 3	MARK3	0.13	7.71	0.04	3.38	1.04
CDNA FLJ45252 fis, clone BRHIP2011199		0.13	7.92	0.03	3.51	1.01
5-azacytidine-induced protein 2		0.14	8.57	0.12	2.83	1.01
Serine/threonine-protein kinase 12	AurB	0.14	8.59	0.02	3.77	1.20
Maternal embryonic leucine zipper kinase	MELK	0.14	8.73	0.05		0.93
Cyclin-T1		0.15	9.22	0.08	2.91	1.00
BMP-2-inducible protein kinase	BIKE	0.16	9.92	0.04	2.88	0.95
Peroxisomal D3,D2-enoyl-CoA isomerase isoform 1 variant		0.17	10.36	0.03	3.20	0.86
LIM domain kinase 2	LIMK2	0.17	10.85	0.04		1.08
Interleukin-1 receptor-associated kinase 1	IRAK1	0.17	10.90	0.06		
Casein kinase 2, beta polypeptide		0.17	10.90	0.06	2.81	0.93
LIM domain kinase 1	LIMK1	0.17	10.96	0.06		1.45
Serine/threonine-protein kinase 17A	DRAK1	0.18	11.75	0.03		
Cyclin-A2		0.18	11.80	0.07	3.48	1.10
PCTAIRE protein kinase 3	PCTAIRE3	0.19	12.47	0.05		
Similar to poly (ADP-ribose) polymerase family, member 10		0.20	12.68	0.08	3.20	1.27
Cytidine deaminase		0.20	12.70	0.06		1.02
Serine/threonine-protein kinase ULK1	ULK1	0.20	13.00	0.10	2.68	0.91
Poly [ADP-ribose] polymerase 10		0.20	13.23	0.04	3.10	1.19
Ribosomal protein S6 kinase alpha-4	MSK2	0.21	14.01	0.03	2.83	1.01
Probable O-sialoglycoprotein endopeptidase		0.21	14.04	0.08	7.41	0.99
Serine/threonine-protein kinase Nek3	NEK3	0.22	14.35	0.05		0.99
Phosphatidylinositol-5-phosphate 4-kinase type-2 gamma		0.23	15.26	0.04	3.21	0.88
Receptor-interacting serine/threonine-protein kinase 5	SgK496	0.23	15.78	0.05		
Serine/threonine-protein kinase LATS1	LATS1	0.24	16.57	0.09		
Mitogen-activated protein kinase kinase kinase kinase 3	KHS2	0.24	16.61	0.04	3.24	1.76
Serine/threonine-protein kinase MARK2	MARK2	0.25	17.00	0.04	2.90	1.03
Serine/threonine-protein kinase MRCK alpha	MRCKa	0.25	17.25	0.07		
Dual specificity mitogen-activated protein kinase kinase 5	MAP2K5	0.25	17.62	0.03		0.90
Serine/threonine-protein kinase Sgk3	SGK3	0.25	17.65	0.03		
Protein kinase, AMP-activated, alpha 1 catalytic subunit	AMPKa1	0.26	17.80	0.03	2.67	0.93
5'-AMP-activated protein kinase catalytic subunit alpha-2	AMPKa2	0.26	17.84	0.02	0.21	0.86

5'-AMP-activated protein kinase subunit gamma-1		0.26	17.93	0.03	2.61	0.93
5'-AMP-activated protein kinase subunit beta-2		0.26	18.11	0.10	2.85	1.02
Dual specificity protein kinase TTK	TTK	0.26	18.42	0.03	4.35	1.21
5'-AMP-activated protein kinase subunit beta-1		0.26	18.47	0.04	2.82	0.93
Inositol polyphosphate multikinase		0.26	18.59	0.07		
TP53RK-binding protein		0.27	18.95	0.05	2.41	1.04
TP53-regulating kinase	PRPK	0.27	19.05	0.04	2.63	1.05
Mitogen-activated protein kinase kinase kinase 11	MLK3	0.27	19.08	0.08		
Insulin-degrading enzyme		0.29	20.74	0.12		
Putative uncharacterized protein DKFZp666O0110	FAK	0.29	21.04	0.04	2.67	1.06
CSNK2A1 protein	CK2a1	0.29	21.69	0.03	2.79	0.93
Mitogen-activated protein kinase kinase kinase 1	MAP3K1	0.30	21.95	0.05	3.92	1.45
Mitogen-activated protein kinase 1	Erk2	0.31	23.18	0.05	2.58	1.00
Serum/glucocorticoid regulated kinase	SGK	0.31	23.70	0.03	2.08	0.97
Serine/threonine-protein kinase Nek6	NEK6/NEK7	0.32	24.63	0.04		
PTK2 protein tyrosine kinase 2 isoform b variant	PYK2	0.33	25.68	0.03	4.29	1.40
Ketohexokinase		0.33	25.71	0.05		
Protein tyrosine kinase 2 beta	PYK2	0.34	26.66	0.04	3.26	1.12
Similar to choline kinase alpha isoform b		0.35	27.48	0.02		
Acidic fibroblast growth factor intracellular-binding protein		0.35	27.94	0.05	3.00	0.98
Cell division control protein 2 homolog	CDC2	0.35	27.99	0.05	2.92	1.09
3-phosphoinositide-dependent protein kinase 1	PDK1	0.35	28.08	0.03		1.06
14-3-3 protein epsilon		0.35	28.17	0.11	4.07	1.15
14-3-3 protein eta		0.36	28.86	0.09	4.09	
Serine/threonine-protein kinase 4	MST1	0.36	28.88	0.05		1.06
Choline kinase alpha		0.36	29.16	0.03		
Uncharacterized protein KIAA0528		0.36	29.87	0.10	3.48	1.14
14-3-3 protein beta/alpha		0.38	31.30	0.20	4.05	1.24
G2/mitotic-specific cyclin-B1		0.38	31.75	0.03	3.15	1.58
14-3-3 protein sigma		0.39	33.23	0.16		1.30
Phosphatidylinositol-5-phosphate 4-kinase type-2 alpha		0.40	35.21	0.02	3.49	1.03
14-3-3 protein zeta/delta		0.41	36.26	0.13	4.24	1.12
Microtubule-associated ser-ine/threonine-protein kinase 3	MAST3	0.42	38.26	0.07		
Serine/threonine-protein kinase tousled-like 2	TLK2	0.43	38.91	0.05	2.55	1.15
Phosphatidylinositol-5-phosphate 4-kinase type-2 beta		0.43	39.25	0.04	3.37	0.98
Nicotinamide phosphoribosyltransferase		0.44	40.59	0.06		

Calcium/calmodulin-dependent protein kinase kinase 1	CaMKK1	0.44	41.19	0.04		1.57
STE20/SPS1-related proline-alanine-rich protein kinase	STLK3	0.45	42.16	0.08		
Mitogen-activated protein kinase kinase kinase 2	MAP3K2	0.45	42.16	0.12	2.14	1.17
Poly [ADP-ribose] polymerase 14		0.45	42.53	0.04	2.79	1.10
Mitogen-activated protein kinase 3	Erk1	0.45	42.90	0.05	2.69	1.08
Cell division protein kinase 7	CDK7	0.47	46.17	0.08	2.61	0.88
Serine/threonine-protein kinase PAK 4	PAK4	0.47	46.26	0.02	3.63	1.16
Serine/threonine-protein kinase 3	MST2	0.47	46.61	0.04		
Serine/threonine-protein kinase RIO2	RIOK2	0.48	48.32	0.05	2.94	0.99
Serine/threonine-protein kinase tousled-like 1	TLK1	0.49	49.30	0.08		
Serine/threonine-protein kinase Pim-2	PIM2	0.49	49.39	0.09		
Testis expressed sequence 264 variant		0.50	52.86	0.07		
3-hydroxyacyl-CoA dehydrogenase type-2		0.51	54.48	0.08		
Phosphatidylinositol-4-phosphate 5-kinase type-1 alpha		0.52	55.77	0.06		1.41
Cyclin-C		0.52	57.00	0.06	2.35	1.18
Deoxycytidine kinase		0.53	57.77	0.05	2.33	1.05
Phosphatidylinositol-4-phosphate 5-kinase type-1 gamma		0.54	60.39	0.19		
SNF-related serine/threonine-protein kinase	SNRK	0.54	60.69	0.05		
Ribosomal protein S6 kinase alpha-3	RSK2	0.54	62.17	0.03	2.35	0.97
Isoform of serine/threonine-protein kinase/endoribonuclease IRE1	IRE1	0.56	66.65	0.06		
PITSLRE serine/threonine-protein kinase CDC2L1	PITSLRE	0.57	68.38	0.05	2.94	
Programmed cell death protein 10		0.57	69.80	0.04	3.34	1.55
Sepiapterin reductase		0.58	70.80	0.06	2.73	1.87
Isochorismatase domain-containing protein 2, mitochondrial precursor		0.59	75.14	0.10		
Serine/threonine-protein kinase 38	NDR1	0.60	78.33	0.01		
Tyrosine-protein kinase CSK	CSK	0.60	79.47	0.02		1.51
Dual specificity tyrosine-phosphorylation-regulated kinase 1A	DYRK1A	0.62	83.84	0.08		
Cell division cycle 2-like protein kinase 5	CHED	0.62	84.63	0.05	5.31	1.42
Serine/threonine-protein kinase 24	MST3	0.63	89.84	0.06		1.41
Cell division cycle 2-related protein kinase 7	CRK7	0.64	90.68	0.07	3.21	1.04
FKBP12-rapamycin complex-associated protein	FRAP	0.64	91.64	0.10		
Mitogen-activated protein kinase 14	p38a	0.64	92.82	0.10		2.16
Hepatocyte growth factor receptor precursor	MET	0.65	94.80	0.08		
Cyclin-H		0.65	96.92	0.05		
2'-phosphodiesterase		0.66	100.10	0.03		

Phosphatidylinositol-4-phosphate 3-kinase C2 domain-containing alpha polypeptide		0.67	104.01	0.18		
Microtubule-associated ser-ine/threonine-protein kinase-like	MASTL	0.68	109.31	0.09		
Serine/threonine-protein kinase N2	PKN2	0.69	114.53	0.03	2.87	1.35
Serine/threonine-protein kinase TAO3	TAO3	0.69	116.38	0.09	2.95	
Ketosamine-3-kinase		0.69	116.78	0.07	2.02	0.95
TFIIH basal transcription factor complex helicase subunit		0.69	117.61	0.17		
Cell division protein kinase 6	CDK6	0.70	118.79	0.10		0.75
CS0DA006YC23 variant		0.70	119.73	0.12	3.84	1.27
Squamous cell carcinoma antigen recognized by T-cells 3		0.71	126.21	0.05	2.07	0.90
MAP2K4 protein	MAP2K4	0.71	127.45	0.06		
Lactoylglutathione lyase		0.72	133.18	0.07		1.39
LIM and senescent cell antigen-like-containing domain protein 1		0.73	143.22	0.04		
Dual specificity mitogen-activated protein kinase kinase 3	MAP2K3	0.74	149.96	0.05		1.60
Alpha-parvin		0.75	155.43	0.06		
XTP3-transactivated gene A protein		0.75	159.12	0.08	3.39	1.04
ATP-citrate synthase		0.76	161.61	0.06	3.59	1.98
Serine/threonine-protein kinase TAO1	TAO1	0.76	162.43	0.06	2.64	1.02
Serine/threonine-protein kinase 10	LOK	0.76	163.64	0.07		
Death-associated protein kinase 2	DAPK2	0.77	171.44	0.11		
Integrin-linked protein kinase	ILK	0.77	171.70	0.03		1.47
Dual specificity mitogen-activated protein kinase kinase 6	MAP2K6	0.77	178.30	0.05	2.41	1.36
Ribosomal protein SA		0.78	184.56	0.11	3.92	2.26
Inhibitor of nuclear factor kappa-B kinase subunit beta	IKKb	0.79	200.75	0.06		
Serine/threonine-protein kinase OSR1	OSR1	0.80	206.63	0.05		
Diphthine synthase		0.80	211.15	0.03		2.72
RSU1 protein		0.81	216.45	0.07		1.34
Ribosomal protein S6 kinase alpha-5	MSK1	0.81	216.73	0.03		
Amylo-1,6-glucosidase, 4-alpha-glucanotransferase isoform 1 variant		0.81	217.79	0.08		
Adenine phosphoribosyltransferase		0.81	222.93	0.05	1.04	1.40
3,2-trans-enoyl-CoA isomerase, mitochondrial precursor		0.82	236.25	0.04	3.25	1.68
WD repeat-containing protein 68		0.83	249.46	0.17	2.58	1.31
Phosphorylase b kinase gamma catalytic chain, testis/liver isoform	PHKg2	0.85	295.80	0.10	2.14	1.33
cAMP-dependent protein kinase, alpha-catalytic subunit	PKACa	0.85	305.35	0.04	2.18	1.76
cAMP-dependent protein kinase, beta-catalytic subunit	PKACb	0.88	389.53	0.01		
Cell division protein kinase 4	CDK4	0.91	511.13	0.07	1.77	1.03

3. **List of figures**

4. List of tables

5. Publications

Sharma, K.*, Weber, C.*, Bairlein, M.*, Greff, Z., Keri, G., Cox, J., Olsen, J.V. & Daub, H. Proteomics strategy for quantitative protein interaction profiling in cell extracts. *Nature Methods* **6**, 741-4 (2009).

Weber, C., Schreiber, TB., Daub, H.
Dual phosphoproteomics and chemical proteomics analysis of erlotinib and gefitinib interference in acute myeloid leukemia cells. *Journal of Proteomics* **4**, 1343-56 (2012)

* equal contribution

6. Acknowledgments

I would like to express my gratitude especially to Dr. Henrik Daub, who instigated my fascinating projects of my dissertation. He provided me enormous scientific support at all times during all phases of my thesis and he enabled an outstanding working climate as a fruitful base.

I also want to thank Prof. Dr. Axel Ullrich for granting optimal working conditions in his Department of Molecular Biology at the Max-Planck-Institute of Biochemistry. I am also very grateful to Prof. Dr. Johannes Buchner for reviewing my thesis and Prof. Dr. Michael Groll for chairing the examining board. The results of my work owe a lot to Prof. Dr. Mathias Mann and his coworkers, who were of great assistance in running the mass spectrometer.

Furthermore, my special thanks go to Dr. Pavlos Stampolidis for revising my thesis. He and other members of the Department of Molecular Biology, namely Felix, Thiemo, Susan, Verena, Nina, Kirti, Kathrin, Pawan, Torsten, Philipp, Markus, Nina, Renate H., Renate G., Susanne, Martin, Thomas, Michaela, Simone, Robert, Stephan… created a very pleasant and friendly atmosphere, I have always enjoyed. In that context, I would like to say also thank you to Bianca, not only for keeping my physical constitution at a reasonable level, but also for her friendship.

I am particularly grateful to my parents for their continuous and loving support and Assol for all her love and back up.